Master's thesis

NTNU
Norwegian University of Science and Technology
Faculty of Natural Sciences
Department of Physics

Mojahed, Martin Aria

Two-flavor chiral perturbation theory at finite isospin density beyond leading order

Master's thesis in Applied Physics and Mathematics
Supervisor: Andersen, Jens Oluf
July 2020

NTNU
Norwegian University of
Science and Technology

Mojahed, Martin Aria

Two-flavor chiral perturbation theory at finite isospin density beyond leading order

Master's thesis in Applied Physics and Mathematics
Supervisor: Andersen, Jens Oluf
July 2020

Norwegian University of Science and Technology
Faculty of Natural Sciences
Department of Physics

NTNU
Norwegian University of
Science and Technology

Abstract

In this master's thesis, we consider two-flavor QCD at finite isospin chemical potential within chiral perturbation theory to next-to-leading order in the low-energy expansion. We calculate the pion condensate and the chiral condensate at zero temperature with both vanishing and finite pionic source. We compare our results at finite pionic source with recent $(2+1)$-flavor lattice QCD results and find that they are in good agreement. We also calculate the free energy and the pion condensate at finite temperature and use the results to generate the phase-transition curve between the normal phase and the pion-condensed phase. The phase-transition curve exhibits a significant temperature dependence and is in poor agreement with the recent lattice QCD simulations as well as various effective-model results in the QCD literature. The poor agreement on the phase-transition curve between χPT and LQCD carries into poor agreements on the pion condensate as well. Finally, we calculate the chiral condensate at finite temperature and use the result to investigate the chiral crossover at small values of the isospin chemical potential. We find that χPT to next-to-leading order predicts a pseudo-critical temperature that is much higher than on the lattice.

As we increase the temperature, we find a new type of behavior in the density evolution of the ground-state configuration. Instead of rotating smoothly on the Goldstone manifold, the ground-state evolution changes discontinuously at some value of the isospin chemical potential in the pion-condensed phase at high temperatures. We discuss how the discontinuity arises by studying the renormalized free energy at finite temperature.

Finally, this thesis also provides a detailed discussion of how to renormalize the density-dependent pion masses in the pion-condensed phase, and we show that one of the branches is a massless Goldstone boson.

Samandrag

I denne avhandlinga studerer me two-flavor QCD ved endeleg isospin kjemisk potensial ved å bruke kiral perturbasjonsteori forbi leiande orden i lågenergi ekspansjonen. Me reknar ut pionkondensatet og det kirale kondensatet ved null temperatur både med og utan pionkilde. Me samanliknar resultata med pionkilde opp mot nylege $(2 + 1)$-flavor QCD simuleringar på gitteret, og finn godt samsvar. Me brukar imaginær-tid formalismen for kvantefeltteoriar til å rekne ut den frie energien og pionkondensatet ved endeleg temperatur. Uttrykka me kjem fram til blir brukt til å generera faseovergangskurva som separerer den normale fasen frå den pionkondenserte fasen. Kurva er tydeleg påverka av temperatureffektar og gir eit dårleg samsvar med simuleringar på gitteret og effektive modell berekningar i litteraturen. Det dårlege samsvaret mellom faseovergangskurvene medfører at samsvaret mellom pionkondensata ved endeleg temperatur også vert dårlege.

Vidare reknar me ut det kirale kondensatet ved endeleg temperatur, og brukar resultatet til å studere den kirale faseovergangen for låge verdiar av isospinpotensialet. Det viser seg at kiral perturbasjonsteori til leiande orden anslår ein pseudokritisk temperatur som er mykje høgare enn det som er observert på gitteret.

Me observerer ei ny type oppførsel i isospintetthetsutviklinga til grunntilstanden på Goldstone-mangfoldigheita ved moderat til høge temperaturar. Grunntilstandskonfigurasjonen endrar seg diskontinuerleg ved ein temperaturavhengig verdi for isospinpotensialet i den pionkondeserte fasen, før han held fram med å rotere på ein glatt måte. Me diskuterer utviklinga til grunntilstanden ved å sjå på den frie energien.

Denne avhandlinga inneheld også ein grundig diskusjon om korleis ein skal renormalisere dei isospinavhengige massane i den kondenserte fasen. Me visar også at ein av eksitasjonane i den pionkondenserte fasen er eit masselaust Goldstone boson.

Preface

This master's thesis investigates quantum effects and finite-temperature effects in the pion-condensed phase within two-flavor chiral perturbation theory. It represents 20 weeks of work and was carried out during the spring semester of 2020 at the Norwegian University of Science and Technology (NTNU) under the supervision of Professor Jens Oluf Andersen. This thesis is a continuation of a project on thermodynamics in the pion-condensed phase carried out during the fall of 2019.

I am indebted to the people who have supported me through this work. I would like to thank Professor Jens Oluf Andersen for outstanding supervision, numerous helpful discussions, and for allowing me to participate in his research group. I would also like to thank Dr. Prabal Adhikari for many interesting discussions along the way and for always being willing to help me. Lastly, I want to thank my friends and family in Sandnes, California, and Trondheim for always supporting me.

از بابا به خاطر همه ی زحمات و حمایت هایشان متشکرم.

Martin Aria Mojahed
Trondheim, Norway
July, 2020

Contents

Chapter 1

Introduction

Quantum chromodynamics[1], or QCD for short, is the gauge field theory describing the strong interaction in the celebrated Standard Model (SM) of particle physics. It has had huge success in explaining and predicting a range of different phenomena through almost 50 years of experiments and observations. Although QCD is formulated using only a few ingredients it gives rise to an extremely rich theory, containing a variety of phases, chiral symmetry breaking, confinement, asymptotic freedom, etc. Unfortunately, many of the properties of the theory are not directly computable from currently available ab-initio predictive methods. Thus, QCD remains an active research area that we continue to learn from almost half a century after its discovery.

In the following, we provide a somewhat non-technical overview of some properties of QCD. The goal is to provide a reader that is not an expert in the field with a basic understanding of the motivation underlying the work in this thesis. A more technical treatment is postponed to chapters two and three, where we revisit some of the ideas in a more mathematical manner.

Introduction to QCD

To provide a rough overview of quantum chromodynamics, we compare it with quantum electrodynamics (QED), the quantum theory of electromagnetism. QED describes the interaction of electrically charged elementary particles; QCD describes the interactions of colored elementary particles. Electromagnetic interactions are mediated by massless spin-1 particles called *photons*, strong interactions by massless spin-1 particles called *gluons*. There is only one type of electric charge, while the color charge comes in three different varieties; red (r), green (g), and blue (b). Each of the colors have a corresponding anticolor; antired ($\bar{r}$), antigreen ($\bar{g}$) and antiblue ($\bar{b}$).[1]

Quarks are massive elementary spin $\frac{1}{2}$ particles carrying one unit of color charge. For each type of quark there is an antiquark carrying one unit of anticolor, analogously to the electron and anti-electron (positron) in QED, which have identical intrinsic properties except that they carry opposite electric charge. The color of a quark can be changed in an interaction with a gluon, as shown diagrammatically in the figure at the top of the next page. In this diagram, a blue quark turns into a red quark emitting a blue-antired ($b\bar{r}$) gluon. This process conserves color charge, like all other QCD processes.

[1] Similarly to the electric charge q, which has an opposite charge $-q$.

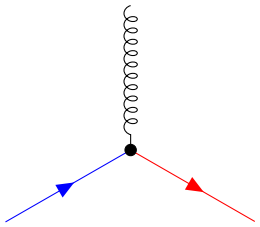

The diagram above illustrates an important feature of QCD; gluons carry one unit of color and one unit of anticolor. This means that unlike photons, gluons carry the charge of the interaction and therefore interact among themselves, giving rise to additional vertices on the following form:

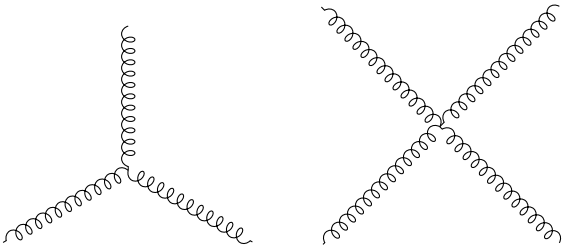

The fact that gluons carry color causes the strength of the strong interaction to become increasingly weaker at high energies. This effect is known as *asymptotic freedom* and was first discovered by Gross, Wilczek [2] and Politzer[3] in 1973. In 2004 they shared the Nobel prize for their discovery. Asymptotic freedom implies that the theory becomes increasingly strongly interacting at lower energies, and causes perturbation theory to break down at energies below ~ 1 GeV. Studying QCD below this energy scale is notoriously hard, and requires non-perturbative techniques. We will elaborate further on this issue in the next sections.

Quarks and gluons are not observed as free particles in our low-energy, everyday world. Instead, they form bound states, referred to as *hadrons*. This property is known as *color confinement*. QCD describes color confinement by imposing that only color-neutral states can be observed in nature at low energies. Confinement has not been proven analytically yet, but its existence is well supported by numerical simulations known as lattice QCD (LQCD), where QCD is defined on a discretized spacetime.

Color confinement prevents physicists from performing experiments on bare quarks and gluons. They must therefore rely on experimental studies of hadrons to better their understanding of how QCD is realized in nature. An example is given by spectroscopy experiments of hadrons, which have shown that there are six different types of quarks in nature.[2] The different quarks are distinguished by a new quantum number, called flavor. In this work, we will only deal with the two lightest quark flavors, the up (u) quark and down (d) quark, whose masses are only a few MeV.

Phase diagram of nuclear matter I

In the following, we consider QCD in thermal equilibrium and introduce the phase structure of the theory. We begin by considering the grand-canonical[3] phase diagram for hadronic matter as a function of the temperature T and the baryonic chemical potential μ_B. The baryon chemical potential is related to the quark chemical potential μ_q as

[2]Theoretical studies have shown it to be very unlikely that there exist new types of quarks that have not already been discovered.

[3]The grand canonical ensemble is the natural statistical ensemble to work within relativistic theories, where particles may be created and annihilated.

$\mu_B = 3\mu_q$. It is the conjugate parameter to the baryon number density $n_B = \frac{1}{3}(n_q - n_{\bar{q}})$ in the grand canonical ensemble. Therefore, one may think intuitively about μ_B as a parameter that determines the baryon density, i.e. the excess of quarks over antiquarks in the system.

It turns out that QCD has an extremely rich phase structure[4, 5], as shown by the conjectured QCD phase diagram in Fig.1.1. We say conjectured, because only parts of the phase diagram have been explored through first-principle calculations. For example, at very high temperatures, where QCD is perturbative due to asymptotic freedom, we know that there is a state of matter where quarks and gluons are no longer confined, referred to as a quark-gluon plasma (QGP). The phase transition from hadronic matter to QGP is referred to as the deconfinement transition, and LQCD simulations suggest that it occurs at a temperature around 160 MeV[6]. Experiments have confirmed the existence of a quark-gluon plasma, and the first direct observation of QGP was announced at the Relativistic Heavy Ion Collider (RHIC) in 2005[7–9].

Asymptotic freedom also implies that the theory becomes perturbative at asymptotically large values for μ_I, where the system enters a color superconducting phase referred to as the color-flavor-locked (CFL) phase[5, 10–12].[4] The remaining parts of the phase diagram, i.e. essentially all of Fig.1.1, is inaccessible to perturbative calculations. This is not completely disastrous since we still have LQCD, which is also a first-principle calculation method. It turns out, however, that LQCD is (currently[5]) useless in regions of the phase diagram where the value of the baryon chemical potential is not very small. This is due to the notorious fermion sign problem, which we briefly review in the following.

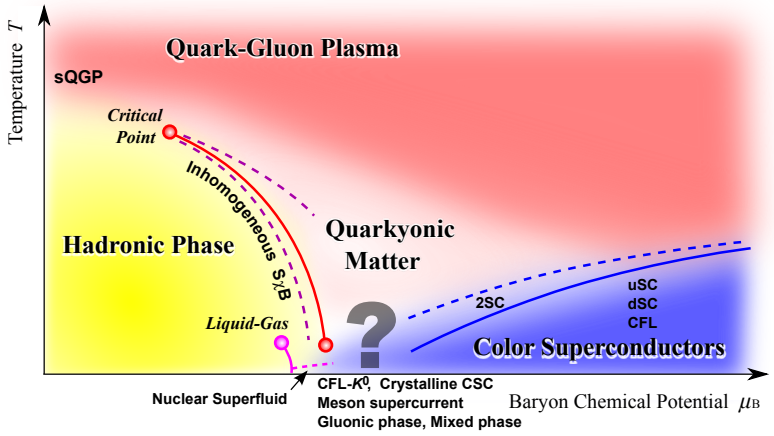

Figure 1.1: Conjectured QCD phase diagram in the $\mu_B - T$ plane. The figure is taken from Ref.[4] with permission from the authors.

Fermion sign problem

In LQCD calculations the QCD partition function $\mathcal{Z}$ is written as a Euclidean path integral,

$$\mathcal{Z} = \int DAD\bar{q}Dq e^{-S}. \tag{1.1}$$

[4] As we will see in great detail in chapter 2, QCD is (approximately) invariant under something called flavor symmetry transformations, and color symmetry transformation. The CFL phase gets its name from the fact that color symmetry transformations are locked to flavor symmetry transformations in this phase.

[5] It may be possible to solve QCD at finite baryon density with for example quantum computers in the future since the sign problem is absent in quantum algorithms[13].

Here A denotes the gluon fields, $\bar{q}, q$ the quark fields, and S the QCD action, which can be written on the following schematic form,

$$S = S_{\mathrm{YM}} + \int d^4x \bar{q} M q. \tag{1.2}$$

S_{YM} is the Yang-Mills action depending purely on gauge fields (the gluons), and M denotes the Euclidean Dirac operator, which depends on gauge fields and the baryon chemical potential. The quark fields can be integrated out of the path integral in Eq.(1.1) to yield the following expression (where we have ignored unimportant constants),

$$\mathcal{Z} = \int DA e^{-S_{\mathrm{YM}}} \det M(\mu_B). \tag{1.3}$$

In numerical lattice calculations the integrand in the path integral,

$$\rho(A) \sim e^{-S_{\mathrm{YM}}} \det M(\mu_B), \tag{1.4}$$

is interpreted as a probability weight for configurations of gauge fields, and should therefore be positive and real[14]. However, it turns out that the Dirac determinant becomes complex at nonzero (real-valued) baryonic chemical potential,

$$[\det M(\mu_B)]^* = \det M(-\mu_B^*) \in \mathbb{C}. \tag{1.5}$$

This results in a complex probability weight $\rho(A)$, so standard Monte-Carlo importance sampling methods are no longer applicable. For this reason, alternative methods have been proposed to gain insight into the phase diagram at small μ_B. These include analytic continuation from an imaginary μ_B[15], and Taylor expansion around $\mu_B = 0$[16]. However, none of the proposed methods have seen much success beyond small values for μ_B.

We note that the fermion sign problem has nothing to do with the Grassmannian nature of fermions, but only the complexity of the determinant M, and it is therefore also present in bosonic theories.

Effective theories and modeling

The absence of applicable first-principle-calculation methods has forced physicists to approach the phase diagram of dense QCD in more pragmatic ways. One way to go is to simplify QCD by taking certain limits of the parameters of the theory, and use the simplified results to gain insights about real QCD. Two well-known examples include taking the number limit of colors N_c to infinity, and changing the number of spacetime dimensions from $(3+1)$ to $(1+1)$.

Another, and so far more successful approach, is to resort to QCD models and effective theories. Effective models are constructed in a way that correctly describes a specific feature of QCD. Examples include the Nambu-Jona-Lasinio (NJL) model[17] and the Quark Meson (QM) model[18, 19], which have the same dynamical chiral symmetry breaking pattern as QCD and are commonly used to model the so-called *chiral transition*.[6] On the other hand we have effective theories, which are based on more sophisticated principles. Unlike effective models, which are often constructed with the single purpose of understanding a specific phenomenon, effective theories attempt to describe the full behavior of QCD at some energy scale. The most famous example is Chiral Perturbation theory (χPT)[21–23], which is used to study the low-energy dynamics of QCD. χPT is only based

[6] There are also Polyakov loop extended versions of the NJL and QM models[20], referred to as PNJL and PQM models, which are used to model the deconfinement transition in QCD.

on the low-energy degrees of freedom and symmetries of QCD and has successfully predicted a variety of low-energy QCD phenomena to high levels of accuracy. We will discuss χPT in much greater detail in chapters two and three.

A question that arises in the context of dense strongly-interacting matter is how accurate the effective modeling- and theory predictions are. Since LQCD is unavailable, we have no ab-initio results to compare model predictions with. Luckily, there are regimes of QCD that can provide useful insights about the level of agreement we may expect between model results and *actual* QCD at finite values for μ_B. We elaborate further on this in the following section.

Phase diagram of nuclear matter II

There is nothing stopping us from adding more axes (i.e. external parameters) to Fig.1.1, to construct a higher-dimensional phase diagram. For instance, instead of having a common chemical potential $\mu_q = \frac{1}{3}\mu_B$ for all quark flavors, we can associate a chemical potential μ_f to each of them. Since we consider QCD with two flavors, we may include μ_u and μ_d, or equivalently $\mu_B = \frac{3}{2}(\mu_u + \mu_d)$ and $\mu_I = \frac{1}{2}(\mu_u - \mu_d)$. The subscript I is short for isospin, and μ_I determines the excess of up quarks over down quarks in the system. There are many physical settings where $\mu_I \neq 0$, for example; in the evolution of the early universe, inside compact stellar objects like neutron stars, and in certain heavy-ion collisions. Such systems are typically characterized by nonzero values for μ_B, μ_I, and T. However, we will forget about realistic physical systems for now and only consider the QCD phase diagram in the (μ_I, T) plane at $\mu_B = 0$. Something wonderful happens here; the Dirac determinant becomes positive, $\det M(\mu_I) \geq 0$,[24] i.e there is no fermion sign problem anymore. The absence of the fermion sign problem means that the entire (μ_I, T) plane is accessible to standard lattice Monte Carlo simulations, at least in principle.

The QCD phase diagram in the (μ_I, T) plane was conjectured in a seminal paper by Stephanov and Son [25] in 2001. A possible scenario for the phase diagram is displayed in Fig.1.2. The lower-left corner shows a hadronic phase, similar to the QCD phase that we experience in our low-energy everyday world. As we increase the temperature, we encounter a deconfinement transition (red dashed line) to a quark-gluon plasma. By moving along the μ_I-axis, we reach the blue phase in the figure, which is a Bose-Einstein condensate (BEC) of electrically charged pions, referred to as the *pion-condensed phase*. The blue line indicates the phase transition to the BEC phase. For very large values of μ_I, there is a transition to a Bardeen-Cooper-Schrieffer (BCS)[26] state of weakly bound Cooper pairs. Perturbative calculations have confirmed the existence of the BCS and the QGP phases.

The (μ_I, T) phase plane is an interesting playground where one can compare effective theory and model results with LQCD simulations. It helps us check consistency, and estimate the accuracy of various effective approaches in different phases of strongly interacting matter. Although the (μ_I, T) diagram is of limited usefulness in direct applications when $\mu_B = 0$, it provides insight to the (μ_B, T) phase diagram, both on the conceptual and on the technical level. Broadly speaking, this summarizes a lot of the motivation behind the efforts that have been put into the (μ_I, T) phase diagram in the past 20 years.

Various regions of the (μ_I, T) diagram have now been studied through a number of approaches. This includes χPT[25, 28–30], hard thermal loop perturbation theory[31], the functional renormalization group[32], and a number of effective descriptions like; the NJL model[33–36], the QM model[37], the linear sigma model[38], random matrix models[39], the holographic principle[40], and many more. More recently, Brandt et al. published high-precision lattice QCD simulations[27, 41–43], where they computed the BEC-transition curve (the blue line in Fig.1.2), the deconfinement-transition curve(the red line in Fig.1.2),

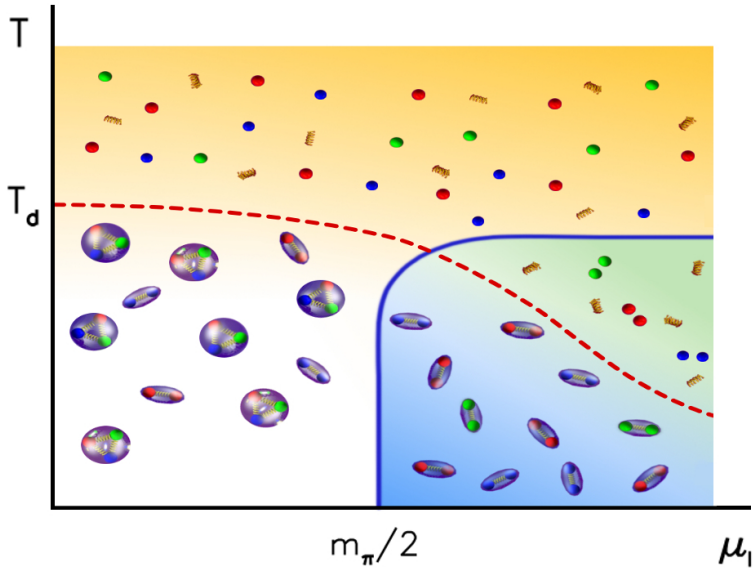

Figure 1.2: Conjectured QCD phase diagram in the $\mu_I - T$ plane at $\mu_B = 0$. The figure is taken from Ref.[27] with permission from the authors.

and various thermodynamical quantities.[7] Their results at vanishing temperature have been compared to χPT at next-to-leading order by Adhikari and Andersen in a series of very recent papers[44–47]. Their work show a generally good agreement between LQCD and χPT in the pion-condensed phase at zero temperature. The work in this thesis is a continuation of the study of χPT in the pion-condensed phase beyond leading order.

Thesis outline

This thesis is organized as follows. Chapter 2 reviews some useful background material on QCD and two-flavor χPT at zero temperature. It also includes a discussion of low-energy QCD at finite isospin chemical potential. In chapter 3, we review renormalization in χPT and demonstrate the procedure by renormalizing the parameters of the Lagrangian to one loop. In chapter 4, we present the ansatz for the ground state configuration in the pion-condensed phase, along with the χPT Lagrangian written in terms of pion fields. We also present some useful tree-level relations and a derivation of the free energy to one loop. In chapter 5, we provide a detailed discussion of how to renormalize the neutral pion mass m_{π^0} to next-to-leading order in the pion-condensed phase. Chapter 6 discusses the two remaining quasi-particle modes in the pion-condensed phase, and we show that one of them is massless to next-to-leading order in the low-energy expansion. In chapter 7, we calculate the free energy, the chiral condensate, and the pion condensate at finite isospin density with both vanishing and non-vanishing (pseudoscalar) pionic source. We compare our finite pionic source results with recent lattice data, and discuss the results. Chapter 8 starts with a brief review of thermal and statistical field theory and a derivation of Splittorff et al.'s analytical low-temperature approximation of the BEC phase-transition curve[48]. We proceed to calculate the free energy and the pion condensate at finite temperature and use the results to generate the BEC-transition curve numerically. We discuss our result for the phase-transition curve and compare it with NJL-model and recent lattice QCD results. We also calculate the chiral condensate at finite temperature and briefly discuss

[7] This work was motivated by the possibility of a new class of compact stars called *pion stars*, whose main constituent is a Bose-Einstein condensate of charged pions.

the chiral transition. We summarize our results in chapter 9 and discuss some possible improvements and extensions of our work. Details about calculations and derivations are found in Appendices B-E.

Part I

Introduction and preliminaries

Chapter 2

Symmetry breaking and effective theories

In this chapter, we first summarize the basic properties of the QCD Lagrangian, emphasizing its global symmetries. We proceed to introduce the concept of effective field theories (EFTs) and discuss chiral Perturbation theory as an effective field theory for QCD. We then discuss the transformation properties of the degrees of freedom in χPT and outline the construction of the chiral Lagrangian. In the final section, we discuss two-flavor QCD at nonzero chemical potentials. Conclusively, we show how the isospin chemical potential enters the chiral Lagrangian.

2.1 QCD and symmetries

QCD is the non-abelian gauge theory [1]for the strong interaction in nature, with color $SU(3)$ [2]as the underlying gauge group[1, 2, 50, 51]. The theory contains eight gauge bosons, i.e one gauge boson for each generator of the gauge group, and they are called gluons. The matter fields of QCD are color-carrying spin $\frac{1}{2}$ fermions called quarks. In chapter 1 we mentioned that there are six types of quarks known to exist, and we distinguish them with a quantum number called flavor. The six flavors of quark have different masses, but similar properties with respect to the gluon fields. The QCD Lagrangian, which is obtained from the gauge principle, reads[52],

$$\mathcal{L}_{\text{QCD}} = \sum_f \bar{q}_f \left(i\not{D} - m_f \right) q_f - \frac{1}{4} F^a_{\mu\nu} F^{a\mu\nu}, \tag{2.1}$$

$$\not{D} \equiv \gamma^\mu D_\mu, \tag{2.2}$$

$$D_\mu = \partial_\mu + i g_s \lambda_a A^a_\mu, \tag{2.3}$$

$$F^a_{\mu\nu} = \partial_\mu A^a_\nu - \partial_\nu A^a_\mu - g_s f_{abc} A^b_\mu A^c_v. \tag{2.4}$$

Here λ_a denotes the a'th Gell-Mann matrix,[3] A_a denotes the a'th gluon field, $F^a_{\mu\nu}$ is the non-abelian field strength tensor and g_s denotes the QCD coupling constant. γ^μ are the Dirac matrices, and D^μ is the covariant derivative. $\not{D}$ acts on color and Dirac indices only, which means that it is independent of flavor. For each quark flavor f the quark field q_f

[1]For the reader unfamiliar with non-abelian gauge theory we recommend the treatment of the subject in Ref.[49] as a good introduction and reference.

[2]Thereby making up the $SU(3)$ component of the $SU(3) \times SU(2) \times U(1)$ Standard Model of particle physics.

[3]The Gell-Mann matrices are the generators of $SU(3)$ in the fundamental representation.

consists of a color triplet (subscripts r, g, and b standing for "red," "green," and "blue", respectively),

$$q_f = \begin{pmatrix} q_{f,r} \\ q_{f,g} \\ q_{f,b} \end{pmatrix}. \tag{2.5}$$

This object transforms in the fundamental representation **3** of the gauge group (and the antiquarks transform in the anti-fundamental representation $\bar{\mathbf{3}}$ of the gauge group). Gluons on the other hand, transform in the adjoint representation **8** of the gauge group, and thereby also carry color charge.

In the present work, we focus on the dynamics of the lightest bound states of quarks and gluons, called *pions*. The starting point of our current theoretical understanding of pions is the (approximate) global symmetries of QCD, which we proceed to discuss in the following.

Accidental, global symmetries of QCD

The six quarks are commonly divided into three light flavors up, down, and strange (u, t and s), and three heavy flavors charm, bottom, and top (c, b and t),

$$\begin{pmatrix} m_u = 0.005\text{GeV} \\ m_d = 0.009\text{GeV} \\ m_s = 0.175\text{GeV} \end{pmatrix} \ll 1\text{GeV} < \begin{pmatrix} m_c = (1.15 - 1.35)\text{GeV} \\ m_b = (4.0 - 4.4)\text{GeV} \\ m_t = 174\text{GeV} \end{pmatrix}. \tag{2.6}$$

Here the scale of 1 GeV is associated with the masses of the lightest hadrons containing light quarks [53]. If the six quark masses had been equal, then the QCD Lagrangian in Eq.(2.1) would have been manifestly $SU(6)$-flavor symmetric. However, since the mass difference between the two categories of quarks is large > 1GeV we only expect an approximate symmetry to hold between the three, or to a larger extent, the two lightest quark flavors. We are only interested in hadron physics at energies below ~ 1GeV in the current work, and we will proceed to approximate the full QCD Lagrangian by its light-flavor version, i.e., ignore the effects of the three heavy quark flavors.[4]

If we use the approximation $m_u = m_d = m_s \neq 0$, then we obtain a manifestly $U(3)$-flavor symmetric theory. The smallness of the quark masses are commonly used to extend the approximation to the following,

$$m_u = m_d = m_s = 0, \tag{2.7}$$

which is referred to as the *chiral* limit. We will see that this approximation gives rise to a larger flavor-symmetry group than $U(3)$. However, to understand *why* these approximations are justifiable in the first place we first have to introduce the concept of QCD scale.

If we had computed the QCD β function and solved the renormalization group equation for the running coupling g_s, we would have seen that it becomes infinite at some finite value of the $\overline{\text{MS}}$ parameter Λ. This value is referred to as the QCD scale Λ_{QCD}[54]. More specifically, the QCD analogue of the fine structure constant to one loop reads[49],

$$\alpha_s(\Lambda) = \frac{2\pi}{b_0 \log\left(\frac{\Lambda}{\Lambda_{\text{QCD}}}\right)}, \tag{2.8}$$

where $b_0 = 11 - \frac{2}{3}N_f$, N_f is the number of flavors in the theory, and Λ is the energy scale that the coupling is evaluated at. Since $b_0 > 0$ the coupling becomes weaker at higher

[4] When we eventually get to the effective theory, we will learn that the effects of (virtual) heavier quarks are included in the theory's low-energy constants, which are again determined from experiments.

energies, which is the phenomenon known as asymptotic freedom. The value of $\Lambda_{\rm QCD}$ quoted in the literature varies due to differences in the approximation schemes used to calculate $\alpha_s(\Lambda)$, but it is typically of order $\Lambda_{\rm QCD} \sim 0.2$GeV[49, 54, 55].

To summarize, the QCD scale $\Lambda_{\rm QCD}$ is introduced through quantum corrections and supplants the dimensionless coupling constant in the theory.[5] Thus, the theory gains a dimensionful quantity, which allows us to discuss the smallness of QCD parameters in a meaningful way.

The masses of the up and down quarks are much smaller than the QCD scale $\Lambda_{\rm QCD}$. Consequently, the approximation $m_u = m_d = 0$ is clearly justified. The strange-quark mass is also (somewhat) smaller than the QCD scale. It is sometimes useful (though less justified) to treat the strange quark as massless[54] and employ the approximation in Eq.(2.8). In the present work we ignore the strange quark, and employ the so called two-flavor chiral limit $m_u, m_d \to 0$ as the starting point for our discussion of QCD at low energies. The two-flavor chiral Lagrangian follows directly from Eq.(2.1), and reads

$$\mathcal{L}_{QCD^0} = \sum_{f=u,d} \bar{q}_f \left(i\not{D}\right) q_f - \frac{1}{4} F^a_{\mu\nu} F^{a\mu\nu}. \tag{2.9}$$

The following discussion and equations generalize straightforwardly to the three flavor case.

The full global symmetry group of two-flavor QCD in the chiral limit can be made manifest in the Lagrangian in Eq.(2.9) by projecting the Dirac field variables q onto their chiral components (Weyl field variables). The projection operators are defined as follows,

$$P_R \equiv \frac{1+\gamma^5}{2}, \tag{2.10}$$

$$P_L \equiv \frac{1-\gamma^5}{2}, \tag{2.11}$$

$$P_R + P_L = 1, \tag{2.12}$$

with subscripts R and L standing for right and left, respectively. The relation between the Dirac field q and its right and left-handed field components q_R and q_L can now be written as,

$$q_R = P_R q, \quad q_L = P_L q, \quad \bar{q}_R = \bar{q} P_L, \quad \bar{q}_L = \bar{q} P_R. \tag{2.13}$$

We use the relations in Eqs.(2.10)-(2.13) to write,

$$\bar{q}\gamma^\mu q = \bar{q}(P_R + P_L)\gamma^\mu(P_R + P_L)q = \bar{q}_R \gamma^\mu q_R + \bar{q}_L \gamma^\mu q_L, \tag{2.14}$$

where the last equality is obtained by using $\{\gamma^5, \gamma^\mu\} = 0$ and $(\gamma^5)^2 = 0$. The equation above shows that the matter sector of the chiral QCD Lagrangian can be decoupled into a sum of left-handed quarks coupled to left-handed quarks, and a sum of right-handed quarks coupled to right-handed quarks;

$$\mathcal{L}_{QCD^0} = \sum_{f=u,d} \bar{q}_{R,f} \left(i\not{D}\right) q_{R,f} + \bar{q}_{L,f} \left(i\not{D}\right) q_{L,f} - \frac{1}{4} F^a_{\mu\nu} F^{a\mu\nu}. \tag{2.15}$$

This Lagrangian is manifestly invariant under the following transformations,

$$\begin{pmatrix} u_R \\ d_R \end{pmatrix} \to R \begin{pmatrix} u_R \\ d_R \end{pmatrix} = \exp\left(-i\theta^R - i \sum_{a=1}^{3} \frac{\tau^a}{2} \theta^R_a \right), \tag{2.16}$$

$$\begin{pmatrix} u_L \\ d_L \end{pmatrix} \to L \begin{pmatrix} u_L \\ d_L \end{pmatrix} = \exp\left(-i\theta^L - i \sum_{a=1}^{3} \frac{\tau^a}{2} \theta^L_a \right), \tag{2.17}$$

[5] The process in which a dimensionless constant such as g_s is replaced by a dimensionful one, such as $\Lambda_{\rm QCD}$, is called *dimensional transmutation*.

due to the flavor independence of the covariant derivative. Here R and L denote unitary 2×2 matrices, τ^a denotes the a'th Pauli matrix acting in flavor space, and the thetas are transformation parameters. In the the three-flavor case one replaces the Pauli matrices with Gell-Mann matrices.

The invariance of $\mathcal{L}_{QCD^0}$ under Eqs.(2.16)-(2.17) imply that the *classical* theory admits global $U(2) \times U(2) = SU(2)_R \times SU(2)_L \times U(1)_R \times U(1)_L$ symmetry transformations. Consequently, Noether's theorem[56] gives rise to $(3+1) \times 2 = 8$ (classically) conserved currents,

$$L^{\mu,a} = \bar{q}_L \gamma^\mu \frac{\tau^a}{2} q_L, \qquad L^\mu = \bar{q}_L \gamma^\mu q_L, \tag{2.18}$$

$$R^{\mu,a} = \bar{q}_R \gamma^\mu \frac{\tau^a}{2} q_R, \qquad R^\mu = \bar{q}_R \gamma^\mu q_R, \tag{2.19}$$

where $L^{\mu,a}$ and $R^{\mu,a}$ denote left and right-handed $SU(2)$ currents, and L^μ and R^μ denote left and right-handed $U(1)$ currents, respectively. It is common, and useful, to construct the following linear combinations of left and right-handed currents,

$$V^{\mu,a} = R^{\mu,a} + L^{\mu,a} = \bar{q} \gamma^\mu \frac{\tau^a}{2} q, \qquad V^\mu = R^\mu + L^\mu = \bar{q} \gamma^\mu q, \tag{2.20}$$

$$A^{\mu,a} = R^{\mu,a} - L^{\mu,a} = \bar{q} \gamma^\mu \gamma^5 \frac{\tau^a}{2} q, \qquad A^\mu = R^\mu - L^\mu = \bar{q} \gamma^\mu \gamma^5 q, \tag{2.21}$$

where the combinations in the first line and the second line transform as vector densities and axial-vector densities under Parity transformations, respectively.

It turns out that the path-integral measure $\mathcal{D}\bar{q}\mathcal{D}q$ is *not* invariant under axial $U(1)$ symmetry transformations[57, 58]. Consequently, the singlet axial current A^μ in Eq.(2.21) is only conserved at the classical level and broken upon quantization. The symmetry group at the quantum level is therefore reduced to $G \equiv SU(2)_V \times SU(2)_A \times U(1)_V$. It is worth pointing out that the remaining $U(1)$ charge conserves quark number $N_q - N_{\bar{q}} = \frac{1}{3} N_B$, which is equivalent to conservation of Baryon number N_B.

We now proceed to include a quark-mass matrix with equal non-zero diagonal entries $m_u = m_d \neq 0$. This approximation is commonly referred to as the *isospin limit*. Non-zero quark masses give rise to a new term in the Lagrangian,

$$\mathcal{L}_M = -\bar{q} M q = -(\bar{q}_L M q_R + \bar{q}_R M q_L), \tag{2.22}$$

which mixes left and right-handed fields. The mass term transforms under $SU(2)_R \times SU(2)_L$ transformations as follows,

$$-\bar{q}_{i,L} M_{ij} q_{j,R} + (L \leftrightarrow R) \longrightarrow - \left(U^L_{ik}\right)^\dagger U^R_{jl} \bar{q}_{k,L} M_{ij} q_{l,R} + (L \leftrightarrow R), \tag{2.23}$$

where $(U^L,\, U^R) \in SU(2)_L \times SU(2)_R$. We observe that the mass term is only invariant under transformations where the $SU(2)_L$ parameters are set equal to the $SU(2)_R$ parameters. This set of transformations is *exactly* equal to the set of elements in $SU(2)_V$, which elucidate why $SU(2)_V$ is referred to as the isospin symmetry group.

Finally, if we set $m_u \neq m_d$, then the remaining symmetry group breaks explicitly as follows, $SU(2)_V \times U(1)_V \to U(1)_{I_3} \times U(1)_V = U(1)_u \times U(1)_d$, where I_3 denotes the diagonal $SU(2)$ generator. The conservation of baryon number is a consequence of the fact that individual flavor currents $\bar{u}\gamma^\mu u$ and $\bar{d}\gamma^\mu d$ are always conserved in strong interactions, because of the diagonality of the quark mass matrix, and the flavor independence of the strong coupling. The conserved $U(1)_{I_3}$ symmetry will be of great importance to us later when we proceed to consider QCD at nonzero isospin density.

$\boldsymbol{U(2)_V \times SU(2)_A \to U(2)_V}$

So far, we have specified that the conserved $U(1)_V$ symmetry classifies hadrons by their baryon numbers. However, we have not addressed how the remaining (approximate) $SU(2)_V \times SU(2)_A$ symmetry is realized in nature. The latter is very important to our current understanding of QCD and is discussed in the following.

It is a well known experimental fact that the two lightest baryons, the proton and the neutron, form a **2** representation of $SU(2)_V$, and that the three lightest mesons, i.e. the pions, form a **3** representation of $SU(2)_V$.[6] However, there is no evidence (that the author is aware of) for a classification that distinguishes right- and left-handed components of spin-one-half hadrons. These observations can only be reconciled with the $U(2)_V \times SU(2)_A$ symmetry of the underlying Lagrangian if the axial generators are spontaneously broken [54]. This is in fact believed to be the case,[7] and the three pions (which have odd parity) are identified as the corresponding pseudo-Goldstone bosons.

To spontaneously break a non-supersymmetric symmetry, we need an operator transforming non-trivially under it to acquire a nonzero vacuum expectation value (vev). To respect the Lorentz, the $SU(3)$-color and the isospin symmetries, the operator has to be a Lorentz scalar, a color singlet, and invariant under $SU(2)_V$, respectively. These conditions can only be satisfied by a composite operator. The simplest candidate is $\bar{q}q$. Indeed, the QCD vacuum is expected to contain a condensate of quark-antiquark pairs,[8]

$$\langle 0|\bar{q}q|0\rangle = \langle 0|\bar{q}_L q_R + \bar{q}_R q_L|0\rangle \neq 0. \tag{2.24}$$

The formation of this condensate is analogous[17] to the appearance of a condensate of electron pairs in the ground state of a metal in BCS theory[26, 49].

It is easily seen that Eq.(2.24) transforms non-trivially when $R \neq L$, while it is left unchanged by flavor-locked transformations $R = L$, and therefore does the job of breaking the axial generators. Since the quark fields have a mass dimension of 3/2, it is expected that the condensate scale as $\langle 0|\bar{q}q|0\rangle \sim \Lambda^3_{\rm QCD}$, since $\Lambda_{\rm QCD}$ is the only energy scale in massless QCD.

2.2 EFTs with spontaneously broken symmetries

In the first chapter, we stated that QCD has become widely accepted as the fundamental gauge theory of the strong interaction. Despite this, we still lack an ab-initio description of the low-energy dynamics of the theory and therefore have to utilize effective descriptions. Current algebra methods[61, 62] played an important role in the theoretical understanding of low-energy hadron physics[63–65] already in the early 1960s. The central idea was that even without exact knowledge about the Lagrangian of the underlying theory, it remains possible to make physical predictions purely based on symmetry properties of Greens functions. Nowadays, effective field theories (EFTs) have become the state-of-the-art tool for analyzing theories containing several widely separated energy or momentum scales. The most famous EFT describing the low-energy dynamics of the lightest hadrons is χPT, whose degrees of freedom (DoF) are the Goldstone fields associated with the

[6] Historically, the quark model was motivated by observations that groups of particles, more specifically the lightest mesons, were related to each other in a way that matched the representation theory of $SU(3)$[59], (where the pions formed an $SU(2)$ subgroup).

[7] Actually, there is a theorem [60] that states that the QCD ground state (in vacuum) is invariant under $SU(2)_V \times U(1)_V$ in the chiral limit, which implies that the spectrum of physical states in QCD with massless quarks can be organized according to irreducible representations of $SU(2)_V \times U(1)_V$.

[8] Although this has not been derived from first principles yet, there are compelling theoretical and phenomenological arguments that the QCD vacuum breaks the chiral symmetry.

spontaneously broken axial generators. The framework of χPT has allowed us to extend and systematically explore corrections to results from the current-algebra days[53].

In the following, we briefly present some basic properties of EFTs, focusing on the conceptuals. We do this to set the stage for a more technical discussion in section 2.3, and to provide a reader unfamiliar with EFTs and χPT a gentle overview of the underlying philosophy. The informed reader may skim through this part, or skip it altogether. The interested reader is referred to Refs.[66–71] and references therein for further introductory literature about EFTs.

Interlude: The philosophy of effective field theories

Many theoretical physicists share a common dream about a theory of everything, which unifies all the fundamental interactions and provides an understanding of all observed phenomena in terms of some fundamental dynamics among the basic constituents of nature. However, even with such a marvelous theory at hand, quantitative analysis at the most elementary level will still be of little use for a comprehensive description of nature at all physical scales[66]. A less dramatic example is provided by the interplay between quantum electrodynamics (QED) and chemistry. Although the laws of chemistry have their origin in the electromagnetic interaction, it does not seem very appropriate to describe phenomena in chemistry quantitatively in terms of the fundamental QED interactions among quarks and leptons. The point is that to obtain a simple description of some physical phenomena, one has to isolate the most relevant elements from the rest. The first and most important step is to choose variables that capture the physics that is most relevant to the problem of interest.

In terms of more technical jargon, some theories involve widely separated energy scales, which allows us to study low-energy dynamics without detailed knowledge about the dynamics occurring at higher energy scales. The fundamental idea is to identify parameters that are very large (or small) compared to the relevant energy scale and send them to infinity (or zero)[66]. An effective field theory is a tool that describes the low-energy physics in terms of the relevant degrees of freedom at that energy scale.

A procedure for coming up with EFTs is through so-called matching calculations[71]. One starts at a high energy scale, where the physics is described by a set of heavy fields Φ with mass M and a set of light particle fields ϕ. The Lagrangian then takes the general form,

$$\mathcal{L}_H(\Phi, \phi) + \mathcal{L}(\phi), \tag{2.25}$$

where $\mathcal{L}(\phi)$ contains all the terms that are independent of the heavy fields, and $\mathcal{L}_H(\Phi, \phi)$ is everything else. For energy scales $\Lambda > M$, the evolution of the theory from one energy scale to another is described by the renormalization group (RG). However, once Λ goes below the mass of the heavy fields M, one changes the effective theory to a new theory without the heavy fields in it. This is what distinguishes effective theories from Wilsonian renormalization, where the theory is left untouched. In the EFT-approach a tower of operators constructed with the light fields $\delta\mathcal{L}(\phi)$ is put in by hand to construct the Lagrangian for the new EFT, which takes the form,

$$\mathcal{L}(\phi) + \delta\mathcal{L}(\phi). \tag{2.26}$$

The matching between the high-energy theory and the low-energy theory at the scale $\Lambda = M$ determines the coefficients of the new field interactions, which encode the dynamics of the heavy fields Φ. The coefficients in $\mathcal{L}(\phi)$ are different in the two theories[66], and the new coefficients are also found from matching conditions. Once the matching has been performed, one may evolve to lower energy scales by using the RG equations of the new

EFT Eq.(2.26), until a new particle threshold is reached. Then we have to match to a new EFT without the heavy mode(s), and the procedure repeats itself.

One way to classify EFTs is related to the status of their coupling constants[69]. In the case of low-energy QCD, the matching cannot be performed perturbatively. This is the general case for EFTs where the transition to the new theory occurs via a phase transition due to spontaneous symmetry breaking[69]. This means that we cannot use the matching procedure outlined above to create a low-energy effective field theory for hadronic QCD.

Why chiral perturbation theory works

Luckily for us, it is possible to construct predictive low-energy effective field theories for nonperturbative theories as well. Historically, the starting point for χPT as an effective field theory for QCD at very low energies was the assumption that Goldstone bosons from the spontaneously broken chiral symmetry are the appropriate degrees of freedom, and what Weinberg refers to as a folk theorem[21, 72]:

Theorem 1. *If one writes down the most general Lagrangian possible, including all terms consistent with the assumed symmetry principles, and then calculates matrix elements with this Lagrangian to any given order of perturbation theory, the result will simply be the most general possible S-matrix consistent with analyticity, perturbative unitarity, cluster decomposition, and the assumed symmetry properties.*

The proof of the theorem relies on Lorentz invariance, the absence of anomalies, and that the Ward identities satisfied by the Green functions of the symmetry currents are equivalent to the invariance of the generating functional under local transformations[53, 73, 74]. If the Ward identities contain anomalies (in our case there is the axial $U(1)$ anomaly), they show up as a modification of the generating functional, which can be incorporated through so-called Wess-Zumino-Witten (WZW) terms[75, 76].

In the case of χPT, there is an infinite number of terms that satisfy Weinberg's theorem, and therefore an infinite number of couplings in the theory. If the theory is going to be of phenomenological usefulness, then there must be a way to systematize and limit the number of couplings that are present. Making Weinberg's theorem useful for phenomenological applications requires two tools[21, 53]:

- A scheme to organize the terms in the effective Lagrangian.
- A systematic method to access the importance of diagrams generated by the interaction terms of the effective Lagrangian when computing physical processes.

In χPT, the terms in the Lagrangian are organized by a derivative expansion, or equivalently by powers of momentum. The momentum of pions on shell $p^2 = m_\pi^2$ is of the same order as the mass. m_π^2 is proportional to the sum of the quarks masses $m_u + m_d$ and it is therefore convenient to count m_u and m_d as $O(p^2)$[77]. The terms with the lowest powers of momentum will be most important in the low-energy EFT.

Weinberg's power-counting scheme[21] analyzes the behavior of a given diagram under a linear rescaling of all the external momenta, $p_i \to tp_i$, and a quadratic rescaling of the light quark masses, $m_q \to t^2 m_q$ (which is equivalent to a linear rescaling of the GB masses). The chiral dimension D of a given diagram with amplitude $\mathcal{M}(p_i, m_q)$ is defined by $M(tp_i, t^2 m_q) = t^D \mathcal{M}(p_i, m_q)$[53]. D is a measure for the importance of diagrams, where diagrams with lower chiral dimensions are more important. Simple dimensional analysis, similar to the methods used in standard QFT textbooks[49, 78] to determine superficial degree of divergence, can be employed to obtain D for any given diagram[53, 77]. The

result is,

$$D = 2 + 2N_L + \sum_{n=1}^{\infty} N_{2n}(2n-2). \tag{2.27}$$

Here N_L denotes the number of independent loops, and N_{2n} denotes the number of vertices originating from terms with chiral dimension $2n$.

Weinberg's framework is sufficient to construct a Lagrangian that is of phenomenological usefulness at low energies. We have so far been very vague about what exactly we mean by "low energies". In the following, we make this notion more explicit by discussing perturbative convergence in χPT.

The chiral symmetry breaking scale Λ_{CSB} is the dimensional parameter that characterizes the convergence of the momentum power expansion[79, 80]. A "naive" dimensional analysis of loop diagrams suggests that this scale is given by $\Lambda_{\text{CSB}} \approx 4\pi f_\pi$. Here $f_\pi \approx 93\text{MeV}$ denotes the pion-decay constant in the chiral limit, and the factor of 4π originates from the calculation of integrals in four-dimensional Minkowski space[80]. An alternative dimensional scale is provided by the lightest excitations that are not included in the theory as explicit degrees of freedom. Those are the lightest hadrons that are not Goldstone bosons for three-flavor χPT, and the lightest hadrons containing a strange quark for two-flavor χPT. The exchange of such a hadron yield a propagator on the form $(k^2 - M^2)^{-1} \approx -M^{-2}(1 + \frac{k^2}{M^2} + ...)$, where M denotes the mass of the excitation. This converges when $\left|k^2\right| < M^2$, which provides a mass scale that is consistent with $4\pi f_\pi$[53]. If we assume reasonable coefficients, the momentum expansion leads to the expectation that χPT converges for center-of-mass (CoM) energies sufficiently below the ρ-meson mass for three-flavor, and the Kaon mass for two-flavor χPT. This approximation is of course very primitive, and its validity highly dependent on the process under consideration. However, there is no doubt that an expansion in p/Λ_{CSB} will converge sufficiently fast at sufficiently low energies, which makes χPT tremendously efficient at very low energies.

2.3 The chiral Lagrangian

In this section, we outline the technical principles that are used to construct the two-flavor χPT Lagrangian. Our treatment will follow that in Ref.[53], and the reader is referred to Refs.[22, 81] for details.

We will first state how Ward identities are related to the invariance of the generating functional under local gauge transformations, and use this to derive the χPT Lagrangian to leading order. We will then explain how to derive the χPT Lagrangian to order $O(p^4)$, and present the most relevant parts of the result.

In section 2.1, we learned that the two-flavor QCD Lagrangian is invariant under $G = SU(2)_L \times SU(2)_R \times U(1)_V$ and we wrote down the corresponding Noether currents. Following the procedure of Gasser and Leutwyler [22], we extend the massless two-flavor QCD Lagrangian in Eq.(2.1) by introducing couplings of the four vector currents, the three axial-vector currents and the scalar and pseudoscalar quark densities to external complex-valued fields $v^\mu(x), v_c, a^\mu(x), p$ and s[53],

$$\mathcal{L} = \mathcal{L}^0_{\text{QCD}} + \mathcal{L}_{ext} = \mathcal{L}^0_{\text{QCD}} + \bar{q}\gamma_\mu(v^\mu + v_c + \gamma^5 a^\mu)q - \bar{q}(s - i\gamma^5 p)q. \tag{2.28}$$

The external fields are Hermitian and color-neutral 2×2 matrices,

$$v^\mu = \sum_{i=1}^{3} \frac{\tau^i}{2} v_i^\mu, \quad a^\mu = \sum_{i=1}^{3} \frac{\tau^i}{2} a_i^\mu, \quad v_c = \mathbb{1} v_c, \quad p = \sum_{i=0}^{3} \tau^i p_i, \quad s = \sum_{i=0}^{3} \tau^i s_i. \tag{2.29}$$

The ordinary massive two-flavor QCD Lagrangian is obtained by setting $v^\mu(x) = v_c = a^\mu(x) = p = 0$ and $s_0 = \mathrm{diag}(m_u, m_d)$.

It is convenient to introduce the generating functional $W(v^\mu, v_c, a^\mu, p, s)$ at this point, which is defined as,

$$\exp[iW(v^\mu, v_c, a^\mu, p, s)] = \exp[iW\{f\}] = \langle 0|T\exp\left[i\int d^4x\mathcal{L}\right]|0\rangle = \langle 0|T\exp\left[iS\right]|0\rangle\,. \tag{2.30}$$

Here T denotes the time ordering operator, f is the collection of external fields, and $\mathcal{L}$ is the Lagrangian given in Eq.(2.28). The rationale behind this is that, in the absence of anomalies, the chiral Ward identities obeyed by the Greens functions are equivalent to the invariance of the generating functional under gauge transformations of the external fields[74],

$$W[f] \to W[R(g)f] = W[f]. \tag{2.31}$$

Here g is a gauge transformation,

$$g : \mathcal{M}_4 \to SU(2)_V \times SU(2)_A, \tag{2.32}$$

where $\mathcal{M}_4$ denotes four-dimensional Minkowski space and R denotes the representation of the symmetry generators. In the present case R is just the fundamental representation of G, as we can see from Eq.(2.29).

We have so far ignored the anomalous terms entering the Ward identities, which spoil the gauge invariance of the generating functional. If we take them into account, then the generating functional undergoes the following change under infinitesimal chiral transformations[74],

$$\delta W\{f\} = -\int d^4x\,\mathrm{Tr}\{\beta(x)\Omega[f]\}, \tag{2.33}$$

where $\Omega[f]$ is a local function of order $O(p^4)$, and $\beta(x)$ is an infinitesimal transformation,

$$\beta : \mathcal{M}_4 \to SU(2)_A. \tag{2.34}$$

The point is that anomalies do not spoil the symmetry of the theory with respect to gauge transformations of the external fields. Instead, they modify the transformation law of the generating functional by replacing the condition in (2.31) by the condition in (2.33), which is equally strong[74].

In the low energy effective theory of QCD we have to construct a sequence of generating functionals,

$$W^{(2)}_{eff}(v^\mu, v_c, a^\mu, p, s) + W^{(4)}_{eff}(v^\mu, v_c, a^\mu, p, s) + ..., \tag{2.35}$$

which characterizes the true generating functional $W_{\mathrm{QCD}}(v^\mu, v_c, a^\mu, p, s)$ of the full theory[74]. This means that the global symmetries of the effective theory have to be gauged, and that couplings to the *same* external fields v, a, p, s as in QCD have to be introduced. But before we proceed to outline the explicit construction of these generating functionals, we need to know how the Goldstone bosons are realized in the chiral effective theory.

Realization of the Goldstone bosons

The χPT Lagrangian is commonly written in terms of a nonlinear realization of the symmetry group $G = SU(N_f)_R \times SU(N_f)_L$[82, 83], with N_f equal to two or three. In this section, we outline how this realization is constructed and justified.

We have seen that although the Lagrangian is invariant under G, the ground state only remains invariant under the subgroup $H = SU(N_f)_V$, giving rise to $n = n_G - n_H$[9] Goldstone bosons. Each of the Goldstone modes are described by an independent field variable π_i, which is a continuous real function on $\mathcal{M}_4$. We collect these field variables in a vector Π, and define the following vector space[53];

$$M_1 \equiv \{\Pi : \mathcal{M}_4 \to R^n\}, \tag{2.36}$$

The idea is to find a map ϕ that uniquely associates with each pair $(g, \Pi) \in G \times M_1$ an element in M_1 such that,

$$\phi(e, \Pi) = \Pi, \quad \forall \Pi \in M_1, \tag{2.37}$$

$$\phi(g_1, \phi(g_2, \Pi)) = \phi(g_1 g_2, \Pi), \quad \forall g_1, g_2 \in G \quad \forall \Pi \in M_1. \tag{2.38}$$

The map ϕ defines an operation of G on M_1, but it is in general not a representation because we do not require linearity $\phi(g, \lambda\Pi) \neq \lambda\phi(g, \Pi)$. ϕ is used to establish a relationship between the GB fields and the quotient space G/H, which allows us to discuss the transformation properties of the Goldstone bosons under G. In order to give a qualitative description of this relationship we need the following remarks and terminology;

- The quotient G/H is the set of all left cosets $\{gH | g \in G\}$ of H in G.[10] Elements of the quotient are sets of group elements, and these sets are completely disjoint.
- We will let $\Pi = 0$ denote the "origin" of M_1, which loosely speaking can be thought of as the ground state (GS) in the normal phase of the effective theory. Since the GS is invariant under the subgroup H, we require that $\phi(h, 0) = 0$ for every $h \in H$.[11]

It follows from the group-homomorphism property in Eq.(2.38) that ϕ maps the origin onto the same element in R^n for all elements of a coset, i.e

$$\phi(gh, 0) = \phi(g, 0) \tag{2.39}$$

for any $g \in G$ and all $h \in H$. We can now prove that the mapping of the origin is injective with respect to the cosets; Let $g, g' \in G$ where $g' \notin gH$, and assume that $\phi(g, 0) = \phi(g', 0)$, then

$$0 = \phi(e, 0) = \phi(g^{-1}, \phi(g, 0)) = \phi(g^{-1}g', 0). \tag{2.40}$$

The first equality follows from Eq.(2.37), the second equality is obtained by using the homomorphism property, and the last equality follows from the assumption $\phi(g, 0) = \phi(g', 0)$ and homomorphism. Thus, we have showed that $0 = \phi(g^{-1}g', 0)$, which implies $g'g^{-1} \in H$ in contradiction to the assumption. Hence the mapping ϕ can be inverted on the image $\phi(g, 0)$, so ϕ is injective with respect to the left cosets. This means that there is an isomorphism between G/H and the Goldstone boson fields M_1, so they are isomorphic.

The isomorphism between the GB fields and the quotient G/H is no lucky coincidence, but guaranteed by the isomorphism theorems[12] of abstract algebra. Specifically, the image of G under a homomorphism ϕ is isomorphic to $G/\ker\phi$, where ker denotes the kernel of ϕ. Hence by requiring the kernel to be identical to the subgroup H, we make the image $\phi(g, 0)$ isomorphic to the quotient G/H.

[9] Here n_G and n_H denotes the number of group generators in G and H respectively.
[10] This definition assumes that H is a normal subgroup of G
[11] In more technical terms this means that H is the little group of $\Pi = 0$.
[12] Also known as Noether's isomorphism theorems.

Now that we have established the isomorphism, we may discuss the transformation properties of the GB fields under an element $g \in G$. To each vector of Goldstone fields Π there is a unique coset $\tilde{g}H$, $\tilde{g} \in G$, such that $\phi(\tilde{g}H, 0) = \Pi$. Let $f \equiv \tilde{g}h \in \tilde{g}H$ be a representative of this coset, and apply the mapping $\phi(g)$ to Π;

$$\phi(g, \Pi) = \phi(g, \phi(f, 0)) = \phi(gf, 0) = \phi(f', 0) \equiv \Pi', \quad f' \in g(\tilde{g}H). \tag{2.41}$$

Hence we obtain the transformed field Π' from Π by multiplying the coset representing Π by g, which gives the coset representing Π'. This procedure uniquely determines how the Goldstone bosons transforms up to an appropriate choice of variables parametrizing G/H[53].

While the considerations above are quite general we now make the discussion more spesific to QCD by explicitly considering $G = \{(L, R)|R \in SU(N_f)_R, L \in SU(N_f)_L\}$ and $H = \{(V, V)|V \in SU(N_f)_V\}$, which is isomorphic to $SU(N_f)$. If we define $\tilde{g} = (\tilde{L}, \tilde{R})$, then we may uniquely characterize the left coset $\tilde{g}H = \{(\tilde{L}V, \tilde{R}V)|V \in SU(N)_V\}$ by the matrix $\Sigma = \tilde{R}\tilde{L}^\dagger$[53, 84],

$$(\tilde{L}V, \tilde{R}V) = (\tilde{L}V, \tilde{R}\tilde{L}^\dagger\tilde{L}V) = (1, \tilde{R}\tilde{L}^\dagger)(\tilde{L}V, \tilde{L}V), \tag{2.42}$$

which implies that $\tilde{g}H = (1, \tilde{R}\tilde{L}^\dagger)H$. To obtain the transformation properties of the Π vector isomorphic to Σ under $g = (L, R) \in G$, we multiply g into the left coset,

$$g\tilde{g}H = (L, R\tilde{R}\tilde{L}^\dagger)H = (1, R(\tilde{R}\tilde{L}^\dagger)L^\dagger), \tag{2.43}$$

i.e

$$\Sigma \to \tilde{R}\Sigma L^\dagger. \tag{2.44}$$

If we allow the cosets to also depend on x this relation extends into,

$$\Sigma(x) \to \tilde{R}\Sigma(x)L^\dagger. \tag{2.45}$$

We now specialize to two flavors $N_f = 2$, where there are three Goldstone bosons $n = 3$. Let $\mathcal{H}_2$ denote the set of all 2×2 traceless and Hermitian matrices, which under addition of matrices defines a vector space. We define a second set[53],

$$M_2 \equiv \{\pi : M_4 \to \mathcal{H}_2\}, \tag{2.46}$$

where the entries in π are continous functions. Elements in M_1 and M_2 are related accordingly;

$$\pi(x) = \sum_{i=1}^{3} \tau_i \pi_i(x) = \begin{pmatrix} \pi_3(x) & \pi_1(x) - i\pi_2(x) \\ \pi_1(x) + i\pi_2(x) & -\pi_3(x) \end{pmatrix} \equiv \begin{pmatrix} \pi^0(x) & \sqrt{2}\pi^+ \\ \sqrt{2}\pi^- & -\pi^0(x) \end{pmatrix}, \tag{2.47}$$

where $\pi_i(x) = \frac{1}{2}\,\mathrm{Tr}[\pi\tau_i]$. Finally, let us define a set M_3 as,

$$M_3 = \{\Sigma : \mathcal{M}^4 \to SU(2)|\Sigma(x) = \exp\left[i\frac{\pi(x)}{f}\right], \pi(x) \in M_2\}, \tag{2.48}$$

where $f \approx 93$ MeV is a parameter in the theory. This entire construction ensures that the homomorphic property is inherited from M_1 down to M_3;

$$\phi : G \times M_3 \to M_3, \tag{2.49}$$

$$\phi[(L, R), \Sigma(x)] = R\Sigma(x)L^\dagger. \tag{2.50}$$

Furthermore, ϕ defines an operation of G on M_3:

- $R\Sigma(x)L^\dagger \in M_3$,
- $\phi[(\mathbb{1},\mathbb{1}),\Sigma(x)] = \Sigma(x)$,
- Let $g_i = (L_i, R_i)$, then $\phi[g_1, \phi(g_2,\Sigma(x))] = R_1R_2\Sigma(x)L_2^\dagger L_1^\dagger = \phi[g_1g_2,\Sigma(x)]$.

Since M_3 is *not* a vector space under matrix addition, the map ϕ is called a nonlinear realization.

Notice from Eq.(2.48) that the Goldstone bosons parametrizes the group manifold $SU(2)$, which is generalized to $SU(N_f)$ for QCD with N_f flavors. The group manifold is isomorphic to $G/H = SU(N_f)_R \times SU(N_f)_L/SU(N_f)_V$. For this reason, the Goldstone bosons in QCD are often referred to as coordinate functions on the G/H manifold, and G/H is commonly referred to as the Goldstone manifold.[13]

The configuration that we referred to as "the origin" is given by $U_0 = \mathbb{1}$. The origin remains invariant under the action of the subgroup $SU(2)_V$, but *not* under the action of $SU(2)_A$,

$$\phi[(V,V),U_0] = VV^\dagger = U_0, \tag{2.51}$$

$$\phi[(A,A^\dagger),U_0] = A^\dagger A^\dagger \neq U_0. \tag{2.52}$$

This is consistent with the transformation properties we expect from the ground state in QCD, and we conclude that U_0 is in fact the real ground state of the system.

Finally, by expanding Eq.(2.50) in the fields one may explore the transformation properties of $\Sigma(x)$ under H, and its transformation properties under axial transformations $(A, A^\dagger)$. The well known result[82] is that the fields π_i transforms as a triplet under H, while they transform non-trivially under axial transformations.

Now that we know how to handle the degrees of freedom in the χPT Lagrangian properly, we return to the explicit construction of the lowest order terms in the theory. The following will serve as a handy reference when we need to determine the transformation properties of external fields and sources later in this thesis.

Gauging the effective theory

In order to construct the sequence of effective generating functionals in Eq.(2.35), which is invariant under the gauged symmetry group, we first need to introduce the covariant derivative D_μ. The covariant derivative ensures that $D_\mu\Sigma(x)$ transforms in the same way as $\Sigma(x)$, see Eq.(2.45).

We start with the external vector and axial fields in Eqs.(2.28)-(2.29), which we use to define new external fields $r_\mu^a(x)$ and $l_\mu^a(x)$ as follows,

$$v_\mu^a \equiv \frac{1}{2}(r_\mu^a + l_\mu^a), \qquad a_\mu^a \equiv \frac{1}{2}(r_\mu^a - l_\mu^a). \tag{2.53}$$

Here $r_\mu^a(x)$ and $l_\mu^a(x)$ corresponds to Θ_R^a and Θ_L^a respectively, where

$$R = \exp\left[i\frac{\tau^a}{2}\Theta_R^a\right], \qquad L = \exp\left[i\frac{\tau^a}{2}\Theta_L^a\right]. \tag{2.54}$$

The transformation properties of the new field variables are obtained by requiring Eq.(2.35) to be invariant under local $SU(2)_R \times SU(2)_L$ transformations,

$$r_\mu \to Rr_\mu R^\dagger + iR\partial_\mu R^\dagger, \tag{2.55}$$

$$l_\mu \to Ll_\mu L^\dagger + iL\partial_\mu L^\dagger. \tag{2.56}$$

[13] The quotient space G/H is generally not a manifold by construction, but because of the symmetry and symmetry breaking patterns of QCD it "accidentally" obtains the additional structure of a manifold.

We write the covariant derivative in terms of the new field variables as,

$$D_\mu\Sigma \equiv \partial_\mu\Sigma - ir_\mu\Sigma + i\Sigma l_\mu \to \partial_\mu(R\Sigma L^\dagger) - iRr_\mu\Sigma(x)L^\dagger + R(\partial_\mu R^\dagger)R\Sigma(x)L^\dagger$$
$$+ iR\Sigma(x)l_\mu L^\dagger - R\Sigma(x)(\partial_\mu L^\dagger) = R(\partial_\mu\Sigma - ir_\mu\Sigma + i\Sigma l_\mu)L^\dagger = RD_\mu\Sigma L^\dagger, \tag{2.57}$$

where we have used that $R(\partial_\mu R^\dagger) = \partial_\mu(RR^\dagger) - (\partial_\mu R)R^\dagger = -(\partial_\mu R)R^\dagger$. We observe that the construction of $D_\mu\Sigma$ in Eq.(2.57) transforms in the required way.

The field strength tensors associated with r_μ and l_μ reads,

$$f^R_{\mu\nu} = \partial_\mu r_\nu - \partial_\nu r_\mu - i[r_\mu, r_\nu], \tag{2.58}$$
$$f^L_{\mu\nu} = \partial_\mu l_\nu - \partial_\nu l_\mu - i[l_\mu, l_\nu], \tag{2.59}$$
$$\mathrm{Tr}\{f^R_{\mu\nu}\} = \mathrm{Tr}\{f^L_{\mu\nu}\} = 0, \tag{2.60}$$

and they transform as $Rf^R_{\mu\nu}R^\dagger$ and $Lf^L_{\mu\nu}L^\dagger$ under the gauged symmetry group, respectively.

Following the original work of Ref.[22] we introduce a new field χ, which is defined as,

$$\chi \equiv 2B_0(s + ip). \tag{2.61}$$

The constant B_0 on the right hand side is related to the quark condensate through $3B_0f^2 = \langle 0|\bar{q}q|0\rangle$. Furthermore, in the isospin limit $m_u = m_d$ we have the Gell-Mann-Oakes-Renner relations[85] relating B_0 to the lightest quark masses and the pion mass as follows,

$$m_\pi^2 = 2B_0m_u. \tag{2.62}$$

We will revisit these relations in part III of this thesis, where we discuss the quark and pion condensates at finite isospin density.

We have now formally introduced all the building blocks that are used to construct the chiral Lagrangian,[14] namely Σ, $D_\mu\Sigma$, r_μ, l_μ, $f^R_{\mu\nu}$, $f^L_{\mu\nu}$, χ and higher order (covariant) derivatives of Σ and χ. These are counted as follows in Weinberg's power-counting scheme;

$$\Sigma = O(p^0), \quad D_\mu\Sigma = O(p), \quad r_\mu = l_\mu = O(p), \quad f^R_{\mu\nu} = f^L_{\mu\nu} = O(p^2), \quad \chi = O(p^2). \tag{2.63}$$

Each additional covariant derivative operator D_μ contributes with an extra momentum power p. The transformation properties of the building blocks, including the higher order covariant derivative terms, under C (charge conjugation), P (parity transformations) and the gauge group is nicely summarized in table 4.2 in Ref.[53].

One way to proceed with the construction of the chiral Lagrangian[81] in terms of the building blocks in Eq.(2.63) is to consider operators $A_1, A_2, ...$that transform in the same way as Σ under the gauge group. It is possible to form invariant terms by tracing[15] products of the type $A_iA_j^\dagger$;

$$\mathrm{Tr}\Big[A_iA_j^\dagger\Big] \to \mathrm{Tr}\Big[RA_iL^\dagger(RA_jL^\dagger)^\dagger\Big] = \mathrm{Tr}\Big[A_iA_j^\dagger\Big]. \tag{2.64}$$

The generalization to higher products is obvious,

$$\mathrm{Tr}\Big[A_iA_j^\dagger A_kA_l^\dagger\Big], \qquad \mathrm{Tr}\Big[A_iA_j^\dagger\Big]\,\mathrm{Tr}\Big[A_kA_l^\dagger\Big], ... \tag{2.65}$$

The operators to order $O(p^2)$, which transform like $R...L^\dagger$, are constructed from the operators in Eq.(2.63) and their covariant derivatives,

$$\Sigma, \qquad D_\mu\Sigma, \qquad D_\mu D_\nu\Sigma, \qquad \chi, \qquad f^R_{\mu\nu}\Sigma, \qquad \Sigma f^L_{\mu\nu}. \tag{2.66}$$

[14] This is no longer true if we introduce chemical potentials.

[15] The trace is with respect to flavor indices of course.

The invariant operators at order $O(p^0)$ and $O(p)$ are constants, so the leading order (LO) non-constant Lagrangian is order $O(p^2)$[22]. The non-constant invariant operators at order p^2 are[53],

$$\begin{aligned}&\mathrm{Tr}\Big[D_\mu D_\nu \Sigma\Sigma^\dagger\Big] = -\,\mathrm{Tr}\Big[D_\mu\Sigma(D_\nu\Sigma)^\dagger\Big] = \mathrm{Tr}\Big[\Sigma(D_\nu D_\mu\Sigma)^\dagger\Big],\\ &\mathrm{Tr}\Big[\chi\Sigma^\dagger\Big], \qquad \mathrm{Tr}\Big[\Sigma\chi^\dagger\Big].\end{aligned} \tag{2.67}$$

Imposing Lorentz invariance leaves us with three terms,

$$\mathrm{Tr}\Big[D_\mu\Sigma(D^\mu\Sigma)^\dagger\Big], \qquad \mathrm{Tr}\Big[\chi\Sigma^\dagger \pm \Sigma\chi^\dagger\Big]. \tag{2.68}$$

The remaining symmetries to check are parity and charge invariance.[16] Parity constraints the sign in the second term in Eq.(2.68) to be positive. This leaves us with the most general effective Lagrangian to order p^2 that is consistent with Weinberg's theorem[22],

$$\mathcal{L}_2 = \frac{f^2}{4}\,\mathrm{Tr}\Big[D_\mu\Sigma(D^\mu\Sigma)^\dagger\Big] + \frac{f^2}{4}\,\mathrm{Tr}\Big[\chi\Sigma^\dagger + \Sigma\chi^\dagger\Big]. \tag{2.69}$$

This Lagrangian contains two free parameters, f and B_0. Notice that Eq.(2.69) is just the non-linear sigma model coupled to external fields. The purpose of the multiplicative constant $\frac{f^2}{4}$ is to generate the standard form of the kinetic term and the mass term; $\frac{1}{2}\partial_\mu\pi_a\partial^\mu\pi_a + \frac{1}{2}m^2\pi^2$ in the expanded Lagrangian (m is introduced in the proceeding paragraph).

For two-flavor QCD in the isospin limit and absence of external fields[17]we have that $\chi = m_\pi^2$. This is easily verified by substituting Eq.(2.62) into the definition of χ. The result is only correct to leading order in χPT, and χ is in general replaced by a new parameter that is referred to as m. In this notation, which is the notation we will use in this thesis, the leading-order Lagrangian reads,

$$\mathcal{L}_2 = \frac{f^2}{4}\,\mathrm{Tr}\Big[D_\mu\Sigma(D^\mu\Sigma)^\dagger\Big] + \frac{f^2m^2}{4}\,\mathrm{Tr}\Big[\Sigma + \Sigma^\dagger\Big]. \tag{2.70}$$

By following the procedure that we outlined above, one may also derive the χPT Lagrangian to next-to-leading order. Thus, if the set of all locally invariant operators to order $O(p^4)$ is obtained, and then reduced by throwing away all operators that are either constant, inconsistent with Lorentz, P or C- invariance, or equivalent to another operator in the set, one obtains $\mathcal{L}_4$.[18] However, the result will contain some redundant structures[19] which can be eliminated to obtain the minimal number of independent terms. The elimination is done by using the equations of motion associated with $\mathcal{L}_2$, and the interested reader is referred to Refs.[81, 86–88] to see how it works. The interested reader is also referred to the original work in Ref.[22] for the full Lagrangian at NLO.[20] We will only need a subset of the full two-flavor Lagrangian at NLO, which in the notation of

[16]It is sufficient to consider P and C, only, because the time inversal symmetry T is then automatically incorporated by the CPT theorem.

[17]We saw earlier that this limit is obtained by setting $v^\mu(x) = v_c = a^\mu(x) = p = 0$ and $s = \mathrm{diag}(m_u, m_d)$ where s reduces to $s_0 = \mathrm{diag}(m_u, m_u)$ in the isospin limit.

[18]One must also include a coupling constant for each of the terms in the Lagrangian.

[19]This did not happen at leading order, and is a new phenomena once we go beyond the leading order.

[20]The original action S_{ext} in Ref.[22] does not account for the axial anomaly. However, the Wess-Zumino-Witten action S_{wzw}[89] transforms exactly as Eq.(2.33), and therefore the difference $S_{ext} - S_{wzw}$ yields a gauge invariant action. We will from now on ignore S_{wzw} as it does not enter any of the calculations in this thesis.

Ref.[90] reads,

$$\mathcal{L}_4 = \frac{1}{4}l_1(\mathrm{Tr}[D_\mu\Sigma^\dagger D^\mu\Sigma])^2 + \frac{1}{4}l_2\mathrm{Tr}[D_\mu\Sigma^\dagger D_\nu\Sigma]\mathrm{Tr}[D^\mu\Sigma^\dagger D^\nu\Sigma] + \frac{1}{16}(l_3+l_4)m^4(\mathrm{Tr}[\Sigma+\Sigma^\dagger])^2 + \frac{1}{8}l_4m^2\mathrm{Tr}[D_\mu\Sigma^\dagger D^\mu\Sigma]\mathrm{Tr}[\Sigma+\Sigma^\dagger] + h_1\,\mathrm{tr}\left[m^4\right]. \quad (2.71)$$

Here $l_1 - l_4$ denote bare low-energy couplings constants (LECs). The complete chiral Lagrangian in Ref.[22] contains ten terms, with LECs $l_1 - l_7$ and $h_1 - h_3$.[21] We will revisit the low-energy couplings in chapter 3.

2.4 QCD and Chemical potentials

In this section, we discuss two-flavor QCD and χPT at nonzero chemical potentials. More precisely, we review how the inclusion of chemical potentials affect the global symmetries of QCD, and how sufficiently high values of the isospin chemical potential triggers the formation of a pion condensate. We do not address QCD with three-flavors, which has a richer structure of meson condensation than two-flavor QCD due to the additional strange chemical potential. The interested reader is referred to Refs.[91, 92] for details about meson condensation in three-flavor χPT.

Chemical potentials, symmetry breaking and the pion condensed phase

In the grand canonical ensemble, we need to introduce terms on the form $\mu_i Q_i$ in the Hamiltonian $\mathcal{H}$, where Q_i denotes the conserved Noether charge,

$$Q = \int d^3x J_i^0(x), \quad (2.72)$$

associated with the conserved current $J_i^\mu(x)$. Thus, chemical potentials couple minimally to the zeroth component of conserved currents and are therefore treated as zeroth components of gauge fields. Consequently, by including one chemical potential for each of the QCD flavors f_i we have to modify the covariant derivative in Eq.(2.1) for QCD with N flavors as follows,

$$D_\mu = \partial_\mu + ig_s\lambda_a A_\mu^a - i\delta_{\mu 0}\mu, \quad (2.73)$$

where $\mu = \mathrm{diag}(\mu_{f_1}, \mu_{f_2}, ...\mu_{f_N})$. When $N_f = 2$, we may write this matrix in terms of a different basis (μ_B, μ_I) as shown below,

$$\mathrm{diag}(\mu_u, \mu_d) = \frac{\mu_B}{3} + \mu_I\frac{\tau_3}{2}. \quad (2.74)$$

This definition ensures that μ_B is nonzero in baryonic matter, while it vanishes completely when we only consider mesons. Consequently, μ_B drops completely out of the mesonic chiral Lagrangian[93].

The three pions $\pi^0(u\bar{u},\ d\bar{d})$, $\pi^+(u\bar{d})$, and $\pi^-(d\bar{u})$ constitutes an isospin triplet with third-components $I_3 = 0$, $I_3 = \frac{1}{2}$, and $I_3 = -\frac{1}{2}$, respectively. Neglecting all non-QCD effects and setting the isospin chemical potential to zero leads to a mass degeneracy between the pions, i.e the three pions have equal mass m_π. However, the presence of a nonzero

[21] The terms proprtional to the h_i's, are so called contact terms. The definition of h_1 in Eq.(2.71) is *not* the same as that in Ref.[22]

isospin chemical potential induces a Zeeman-like energy splitting;[22]

$$E_{\pi^0} = \sqrt{p^2 + m_\pi^2}, \tag{2.75}$$

$$E_{\pi^-} = \mu_I + \sqrt{p^2 + m_\pi^2}, \tag{2.76}$$

$$E_{\pi^+} = -\mu_I + \sqrt{p^2 + m_\pi^2}, \tag{2.77}$$

where p denotes spatial momentum. Eqs.(2.76)-(2.77) suggest that one pion mode becomes massless at $|\mu_I| = m_\pi$, which is an indication of a spontaneously broken symmetry. In order to consider the possibility of spontaneous symmetry breaking (SSB) we first need to know how nonzero isospin affects the symmetries of QCD. Introducing the isospin chemical potential in the Hamiltonian yields,

$$[\mathcal{H}, \tau_3] = 0, \qquad [\mathcal{H}, \tau_1] \neq 0, \qquad [\mathcal{H}, \tau_2] \neq 0, \tag{2.78}$$

since τ_3 does not commute with the remaining two $SU(2)$ generators. Hence, $\mu_I \neq 0$ explicitly breaks $SU(2)_V \times U(1)_B \to U(1)_{I_3} \times U(1)_B = U(1)_u \times U(1)_d \equiv N$. This result is also true when $m_u \neq m_d$. The remaining symmetry group N generates independent phase rotations of the two flavor fields. This residual symmetry is extremely important, because it proves that SSB is possible, and that we can have a phase transition from a normal phase with symmetry group N, to a superfluid phase with a reduced symmetry group[91]. It turns out that $U(1)_{I_3}$ is in fact spontaneously broken[25] at high values of the isospin chemical potential. Furthermore, the generator of electric charge $Q \equiv \frac{1}{6}\mathbb{1} + \frac{1}{2}\tau_3$ [23] is also broken in this phase as a direct consequence of the broken I_3 generator. We note that the spontaneously broken electric charge generator makes the system an electric *superconductor* in the second phase.

The massless mode in Eq.(2.76)-(2.77) condenses to form a Bose-Einstein condensate (BEC) for temperatures below the relevant critical temperature. We will only consider non-negative values for the isospin potential $\mu_I \geq 0$ in this thesis, where the positively charged pion π^+ becomes massless at $\mu_I = m_\pi$ at vanishing temperature. The phase transition from the normal phase to the pion-condensed phase at zero temperature is second order[44, 93]. This is not surprising due to the fact that the chiral condensate and the meson condensate can coexist, because the condensation mechanisms are independent[91, 93].

The final question we address before we move on with renormalization is how finite isospin chemical potential is incorporated into the effective framework. The isospin chemical potential corresponds to the zeroth component of the gauge field v_i^μ associated with vector transformations generated by τ_3, see Eq.(2.29) for details. Thus, gauge invariance fixes the way μ_I is allowed to enter the chiral Lagrangian[25]. We have seen that the external gauge field v_i^μ enters the effective construction through the covariant derivative in Eq.(2.57). We use the definition in Eq.(2.53) to write,

$$r_\mu = l_\mu = \frac{\tau_3}{2}\mu_I \delta_{\mu 0}, \tag{2.79}$$

which we substitute into the expression for the covariant derivative in Eq.(2.57) to obtain,

$$D_\mu \Sigma \equiv \nabla_\mu \Sigma = \partial_\mu \Sigma - i\frac{\mu_I \delta_{0\mu}}{2}[\tau_3, \Sigma], \tag{2.80}$$

$$D_\mu \Sigma^\dagger \equiv \nabla_\mu \Sigma^\dagger = \partial_\mu \Sigma^\dagger - i\frac{\mu_I \delta_{0\mu}}{2}[\tau_3, \Sigma]^\dagger. \tag{2.81}$$

[22] The validity of the following relations can only be assumed to hold for sufficiently low μ_I, and in fact they break down for $\mu_I > m_\pi$.

[23] This equality follows from the Gell-Mann–Nishijima formula $Q = I_3 + \frac{1}{2}Y$, where Q and Y are the generators of electric charge and hypercharge respectively.

The relevant terms in the chiral Lagrangian at next-to-leading order in vacuum given in Eq.(2.71) are then modified to the following,

$$\mathcal{L}_4 = \frac{1}{4}l_1(\mathrm{Tr}[\nabla_\mu\Sigma^\dagger\nabla^\mu\Sigma])^2 + \frac{1}{4}l_2\mathrm{Tr}[\nabla_\mu\Sigma^\dagger\nabla_\nu\Sigma]\mathrm{Tr}[\nabla^\mu\Sigma^\dagger\nabla^\nu\Sigma] + \frac{1}{16}(l_3+l_4)(\mathrm{Tr}[\chi^\dagger\Sigma+\Sigma^\dagger\chi])^2 + \frac{1}{8}l_4\mathrm{Tr}[\nabla_\mu\Sigma^\dagger\nabla^\mu\Sigma]\mathrm{Tr}[\chi^\dagger\Sigma+\Sigma^\dagger\chi] + h_1\,\mathrm{Tr}\left[\chi^\dagger\chi\right], \quad (2.82)$$

at nonzero isospin chemical potential.

Chapter 3

χPT at one loop

The main focus of this thesis is to compute quantum corrections to tree-level results in χPT. To obtain well-defined and finite results for observables, we need to employ a suitable renormalization scheme. In this chapter, we provide an overview of how the renormalization procedure in two-flavor χPT is implemented at next-to-leading order. We begin by reviewing dimensional regularization before we proceed to discuss renormalization in χPT. We demonstrate the procedure by renormalizing m and f in the normal phase to one loop.[1] The interested reader is referred to the original work in Ref.[22] for details about χPT to one loop, and Ref.[95] for renormalization of χPT to higher orders.

3.1 Dimensional Regularization

In this section, we briefly review the method of dimensional regularization (dimreg). A standard textbook[49, 53, 55] way of introducing dimensional regularization is to discuss Wick rotation, derive the surface area of the unit sphere in arbitrary dimensions, and highlight some relations between Beta and Gamma functions. We will follow an alternative route in the following, where we highlight some of the fundamental ideas and principles underlying the regularization of well-behaved scalar integrals in the absence of infrared divergences.

In dimensional regularization, the dimension of spacetime is analytically continued to an arbitrary spacetime dimension d [96]. Dimreg preserves gauge invariance and many dimension-independent symmetries, and it has become the most popular regularization method for (non-supersymmetric) gauge theories. Notably, dimensional regularization preserves translational invariance in momentum-space[2] and thereby avoids the problem with anomalies occurring in more primitive schemes which violate this symmetry. Dimensional regularization also preserves chiral symmetries and has become the conventional regularization scheme in the context of χPT.

A drawback with dimreg is its inability to handle dimensionally dependent quantities, such as the γ^5 matrix and the antisymmetric tensor $\epsilon_{\alpha\beta\gamma\delta}$, which can lead to complications in theories where these quantities are necessary to prove Ward identities.

Mathematical tools

The principle of dimensional continuation is important to understand dimensional regularization, and is expressed by the following theorem[97];

[1] The renormalization of m was also performed in Ref.[94].

[2] This is a consequence of the fact that dimensional continuation does not spoil the translational invariance of the relevant integrals.

Theorem 2. *Let an analytic function $g_1(z)$ be defined in a region[3] $\mathcal{D}_1$, and let $\mathcal{D}_2$ be another region which has a certain subregion $\mathcal{R}$, but only this one, in common with $\mathcal{D}_1$. Then if a function $g_2(z)$ exists which is analytic in $\mathcal{D}_2$ and coincides with $g_1(z)$ in $\mathcal{R}$, there can only be one such function. We call $g_1(z)$ and $g_2(z)$ analytic continuations of each other.*

The theorem above states that $g_2(z)$ is *unique*, provided that $\mathcal{R}$ is not the empty set, and implies that the representations of $g_1(z)$ and $g_2(z)$ are equal in $\mathcal{R}$.

The Gamma function $\Gamma(z)$ arises naturally in dimreg. There are many representations of $\Gamma(z)$ to be found in the literature, but only two appear suitable in the current context[98]. The first one is Euler's representation,

$$\Gamma_E(z) \equiv \int_0^\infty t^{z-1}e^{-t}dt, \quad \mathrm{Re(z)} > 0. \tag{3.1}$$

The second one is Weierstrass's partial fraction series expansion,

$$\Gamma_W(z) = \sum_{n=0}^{\infty} \frac{(-1)^n}{n!\,(n+z)} + \int_1^\infty t^{z-1}e^{-t}dt, \tag{3.2}$$

which is analytic at all points in the complex plane, except from the negative integers. $\Gamma_W(z)$ is in fact a unique analytic continuation of $\Gamma_E(z)$, because $\mathrm{Re}(z) > 0$ is a subset of its region of validity and $\Gamma_W(z) = \Gamma_E(z)$ here.

Prescription

In this subsection we review how regularization of massive fields[98, 99] in a scalar field theory is carried out in the MS (read: minimal subtraction) scheme.[4] There is an algorithmic procedure, due to Passarino and Veltman[100], the so-called Passarino Veltman reduction, which successively reduces integrals that show up in amplitude calculations in QFT into scalar integrals[101]. The following procedure is therefore readily generalized to quantum field theories with more exotic fields.

Assume that the following four-dimensional integral

$$I(p) = \int \frac{d^4k}{(2\pi)^4} J(k^2, k\cdot p), \tag{3.3}$$

is ultravioletly divergent. We outline how to regularize this integral in dimreg through a number of steps below[98] (where we work in Euclidean space, which is always possible by Wick rotating);

- Define the inner product between vectors over a complex d-dimensional vector space.
- Parametrize all momentum-space propagators with the following transformation,

$$\frac{1}{k^2+m^2} = \int_0^\infty d\alpha e^{-\alpha(k^2+m^2)}. \tag{3.4}$$

- Change the integration measure from $\frac{d^4k}{(2\pi)^4}$ to $\Lambda^{4-d}\frac{d^dk}{(2\pi)^d}$, where d is a complex number and Λ is the renormalization scale which makes the dimension of the integral independent of the spacetime-dimension d.

[3] A non-empty open subset of the complex plane.

[4] The "minimal" in minimal subtraction refers to the fact that no additional finite factors are subtracted in this scheme.

- Use the following generalized Gaussian integral to integrate over momentum space,

$$\int \Lambda^{4-d} \frac{d^d k}{(2\pi)^d} e^{-xk^2+2k\cdot b} = \left(\frac{\pi}{x}\right)^{\frac{d}{2}} \frac{1}{(2\pi)^d} e^{\frac{b^2}{x}}. \tag{3.5}$$

  The formula in Eq.(3.5) reduces to the standard Gaussian integral for integer values of d. For complex values of d the right hand side has to be taken as the definition of the integral to the left.

- The resulting amplitude is now well defined in a finite domain of the complex plane.[5] The amplitude outside this domain has to be taken as the analytic continuation of the amplitude inside the domain.

- Feynman parametrization[49, 102] can be employed to rewrite scalar loop integrals into a form suitable for the outlined procedure. Integration over Feynman parameters leads to Gamma functions in the domains where the integrals exist. The analytic continuation defined in Eq.(3.5) can then be implemented by using the Weierstrass representation of the Gamma function[98].

- Expand all d-dependent terms in Laurent series around $d = 4$, so $I(p)$ takes the form,

$$I(p) = \frac{A}{(d-4)} + B + O(d-4), \tag{3.6}$$

  where A and B are momentum dependent. Ultraviolet divergences now manifest themselves as poles at $d = 4$.

- The divergent term in Eq.(3.6) has to be canceled by a counterterm. Once this is achieved we take the limit $d \to 4$, and $I(p)$ can be analytically continued back to Minkowski space.

We illustrate the outlined procedure by calculating the following standard integral,

$$I = \Lambda^{4-d} \int \frac{d^d k}{(2\pi)^d} \frac{1}{k^2+m^2} = \Lambda^{4-d} \frac{m^{d-2}}{(2\pi)^d} \int \frac{d^d k}{k^2+1}. \tag{3.7}$$

First, we have to rewrite the integral into Gaussian form, which we subsequently evaluate using Eq.(3.5);

$$\begin{aligned} I &= \Lambda^{4-d} \frac{m^{d-2}}{(2\pi)^d} \int d^d k \int_0^\infty d\alpha e^{-\alpha(k^2+1)} = \Lambda^{4-d} \frac{m^{d-2}}{(4\pi)^{d/2}} \int_0^\infty \alpha^{-\frac{d}{2}} e^{-\alpha} d\alpha \\ &= \Lambda^{4-d} \frac{m^{d-2}}{(4\pi)^{\frac{d}{2}}} \Gamma\left(1 - \frac{d}{2}\right). \end{aligned} \tag{3.8}$$

The Gamma function in the second line of the equation above is understood to be in the Weierstrass representation. Since $\Gamma_W(z)$ has isolated poles at $z = 0, -1, -2, ...$, the integral I obtains isolated poles at $d = 4, 6, 8, ...$ To analyze the behavior near $d = 4$ we define $d = 4 - 2\epsilon$, and subsequently expand around $d = 4$ to obtain,

$$I = -\frac{m^2}{(4\pi)^2} (4\pi)^\epsilon \left(\frac{\Lambda^2}{m^2}\right)^\epsilon \left[\frac{1}{\epsilon} + 1 - \gamma + O(\epsilon)\right], \tag{3.9}$$

where γ denotes the Euler-Mascheroni constant $\gamma \approx 0.5772$[49].

[5] We are currently ignoring the possibility of having infrared problems, where the domain may shrink to the empty set.

The renormalization scheme outlined above only absorbs the divergent part of the loop integral. In this thesis we employ the $\overline{\text{MS}}$ (read: modified minimal subtraction) scheme, which absorbs the divergent part of the loop integral plus a constant that always arises as a part of the regularization. The $\overline{\text{MS}}$ scheme is implemented by rescaling the renormalization scale as shown below,

$$\Lambda^2 \to \Lambda^2 \left(\frac{e^\gamma}{4\pi}\right)^\epsilon. \tag{3.10}$$

The integral in Eq.(3.9) reduces nicely to the following expression,

$$I = -\frac{m^2}{(4\pi)^2}\left[\frac{1}{\epsilon} + 1 + \log\frac{\Lambda^2}{m^2} + O(\epsilon)\right] \tag{3.11}$$

in the $\overline{\text{MS}}$ scheme.

The prescription discussed so far is sufficient to regularize integrals associated with massive scalar fields[6] in the absence of infrared divergences. There are techniques to handle infrared divergences in consistent ways[96], but we will not discuss them here. Instead, we briefly review some results for loop integrals with massless particles, which we will make active use of later in this thesis.

If we had attempted to solve the integral associated with a massless scalar propagator by following the prescription above,

$$I = \int \frac{d^dk}{(2\pi)^d}\frac{1}{k^2} = \int \frac{d^dk}{(2\pi)^d}\frac{p^2 - 2p\cdot k}{k^2(k^2-p^2)} + \int \frac{d^dk}{(2\pi)^d}\frac{k^2}{k^2(k^2-p^2)}, \quad p^2 \neq 0, \tag{3.12}$$

and naively added the two integrals on the right hand side, we would have obtained $I = 0$. However, the regions where the two integrals on the right hand side of Eq.(3.12) are defined does not overlap, so we cannot add their analytic continuations[98]. Leibrandt regularizes massless loop integrals by extending the definition of the Gaussian integral in Eq.(3.5), see Ref.[98] for details. In Ref.[103] the authors use Leibrandts extension to prove the so called t'Hooft Veltman conjecture for *massless* particles, which states that

$$\int \frac{d^dk}{(2\pi)^d}(k^2)^{\beta-1} = 0, \tag{3.13}$$

for $\beta = 1, 2, ...$ and complex d, and $\beta = 0$ when $d > 2$.[7] In particular, this implies that Eq.(3.12) is zero in four dimensions, and that $\int \frac{d^4k}{(2\pi)^4}(k^2)^n = 0$, $n = -1, 0, 1, 2....$ These results will be used to simplify some of our calculations later on.

Loosely speaking, dimreg allows us to isolate the divergences appearing in loop integrals. However, we have to lose the divergences completely in expressions for observables. This is what renormalization does for us, as we will see in the following.

3.2 Renormalization in χPT

In chapter 2, we saw that the χPT Lagrangian contains an infinite number of terms and that it is non-renormalizable in the conventional sense of the word. This means that a calculation at some given order n in the power-counting scheme requires higher-order terms to cancel the divergences that arise at order n. Consequently, one needs more and

[6] Here we assume that there are no emerging anomalies or appearance of Dirac matrices, which makes things trickier.

[7] Eq.(3.12) is undefined in $d = 2$ dimensions, which is consistent with the fact that Goldstone bosons are forbidden in $d = 2$ dimensions[104].

more couplings l_i as one goes to higher loop orders (or equivalently higher orders in the power-counting scheme). If we use a regularization scheme that preserves the symmetries of the Lagrangian, such as dimreg, then the counterterms have to be invariant under the same symmetries as the Lagrangian. Since the full effective Lagrangian is constructed to contain all terms compatible with the symmetries of the theory, the divergences can always be canceled by renormalizing coupling constants in the Lagrangian appropriately.

If we calculate one-loop corrections using $\mathcal{L}_2$, then the divergences become order $O(p^4)$. Since $\mathcal{L}_4$ contains all inequivalent terms permitted by the underlying symmetry principles, it must be possible to absorb the one-loop divergences from $\mathcal{L}_2$ into the LECs $l_1 - l_7$ and $h_1 - h_3$. In Ref.[22] Gasser and Leutwyler calculate the one-loop generating functional and obtain the renormalized LECs that cancel the one loop divergences in the MS scheme. They write the renormalized LECs on the following form,

$$l_i = l_i^r + \gamma_i \lambda, \qquad h_i = h_i^r + \gamma_i \lambda, \tag{3.14}$$

$$\lambda = \frac{\Lambda^{-2\epsilon}}{2(4\pi)^2}\left[-\frac{1}{\epsilon} - (4\pi - \gamma + 1)\right], \tag{3.15}$$

where l_i^r denotes a renormalized coupling. In the $\overline{\text{MS}}$ scheme, the couplings take the following form,

$$l_i = l_i^r - \frac{\gamma_i \Lambda^{-2\epsilon}}{2(4\pi)^2}\left[\frac{1}{\epsilon} + 1\right], \tag{3.16}$$

$$h_i = h_i^r - \frac{\delta_i \Lambda^{-2\epsilon}}{2(4\pi)^2}\left[\frac{1}{\epsilon} + 1\right], \tag{3.17}$$

where the numerical values for the coefficients γ_i read[22],

$$\gamma_1 = \frac{1}{3}, \quad \gamma_2 = \frac{2}{3}, \quad \gamma_3 = -\frac{1}{2}, \quad \gamma_4 = 2, \quad \gamma_5 = -\frac{1}{6}, \quad \gamma_6 = -\frac{1}{3}, \quad \gamma_7 = 0, \tag{3.18}$$

$$\delta_1 = 2, \quad \delta_2 = \frac{1}{12}, \quad \delta_3 = 0. \tag{3.19}$$

We do not use the same operators as Ref.[22] in this thesis. We will call one of our coupling constants h_1, see Eq.(2.71), and it will *not* be the same LEC as the one in the equations above. The constant that we will denote by h_1 is *not* running, i.e $\delta_1 = 0$ and $h_1 = h_1^r$.

The renormalized LECs, l_i^r and h_i^r, are running coupling constants that satisfy renormalization group (RG) equations.[8] These are obtained by differentiating both sides of Eq.(3.16) and Eq.(3.17), respectively, with respect to the renormalization scale Λ. Since the bare couplings are independent of Λ we immediately obtain,

$$\Lambda \frac{dl_i^r}{d\Lambda} = -\frac{\gamma_i}{2(4\pi)^2}, \tag{3.20}$$

$$\Lambda \frac{dh_i^r}{d\Lambda} = -\frac{\delta_i}{2(4\pi)^2}. \tag{3.21}$$

A set of low-energy constants $\bar{l}_i$ and $\bar{h}_i$ are defined via the solutions of the RG equations as,

$$l_i^r = \frac{\gamma_i}{2(4\pi)^2}\left[\bar{l}_i - \log\frac{\Lambda^2}{m^2}\right], \tag{3.22}$$

$$h_i^r = \frac{\delta_i}{2(4\pi)^2}\left[\bar{h}_i - \log\frac{\Lambda^2}{m^2}\right]. \tag{3.23}$$

[8] For LECs with $\gamma_i = 0$ or $\delta_i = 0$ the renormalized couplings simply equal the bare couplings, which are scale independent. The equations (3.20-3.23) does not apply to such couplings.

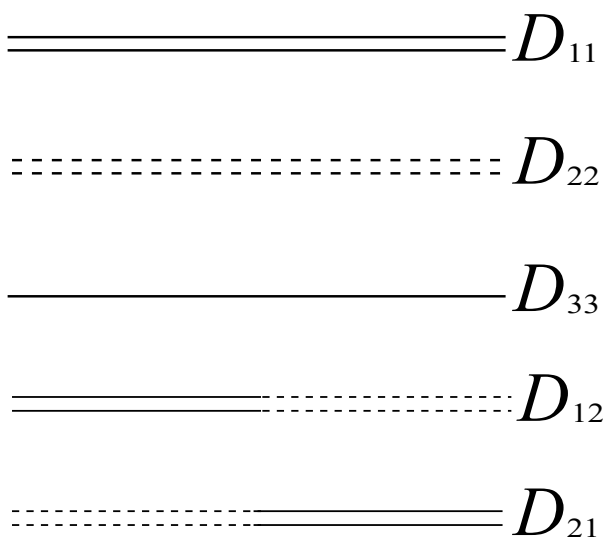

Figure 3.1: Bare pion propagators in the $\{\pi_1, \pi_2, \pi_3\}$ basis. D_{11} denotes the bare $\langle\pi_1\pi_1\rangle$ propagator, D_{22} denotes the bare $\langle\pi_2\pi_2\rangle$ propagator, D_{33} denotes the bare $\langle\pi_3\pi_3\rangle$ propagator, D_{12} denotes the bare $\langle\pi_1\pi_2\rangle$ propagator and D_{21} denotes the bare $\langle\pi_2\pi_1\rangle$ propagator.

Numerical values for the low-energy constants $\bar{l}_i$ and $\bar{h}_i$ are obtained from phenomenological evaluations based on experimental data[22]. The only running LECs of relevance in this thesis are $l_1^r - l_4^r$, see Eq.(2.82). Numerical values for $\bar{l}_1 - \bar{l}_4$ were estimated by Colangelo, Gasser and Leutwyler in Ref.[105], where they obtained,

$$\bar{l}_1 = -0.4 \pm 0.6, \qquad \bar{l}_2 = 4.3 \pm 0.1, \tag{3.24}$$

$$\bar{l}_3 = 2.9 \pm 2.4, \qquad \bar{l}_4 = 4.4 \pm 0.2. \tag{3.25}$$

3.3 Renormalizing the parameters of the Lagrangian

We are now in a position to renormalize the parameters of the Lagrangian m and f to one loop. Next-to-leading order relations for m and f are necessary in consistent calculations within χPT to next-to-leading order. Although these relations are well known in the literature[22, 106] we include their derivations as a warm-up, and because the author was unable to find a detailed derivation of the next-to-leading order correction to the tree-level relation $f_\pi = f$ in the χPT literature.

We use the parametrization in Eq.(2.48) to expand the leading-order Lagrangian in Eq.(2.70) to quartic order in the pion fields and the next-to-leading order Lagrangian in Eq.(2.71) to quadratic order in the pion fields. The terms in the result that are relevant to the present calculation read,[9]

$$\mathcal{L} = \frac{1}{2}\partial^\mu\pi_a\partial_\mu\pi_a - \frac{m^2}{2}\pi_a\pi_a + \frac{1}{6f^2}[\partial^\mu\pi_a\pi_a\partial_\mu\pi_b\pi_b - \partial^\mu\pi_a\partial_\mu\pi_a\pi_b\pi_b] + \frac{m^2}{24f^2}(\pi_a\pi_a)^2$$
$$- m^4(l_3 + l_4)\frac{\pi_a\pi_a}{f^2} + \frac{l_4 m^2}{f^2}\partial_\mu\pi_a\partial^\mu\pi_a. \tag{3.26}$$

We notice that there are no cubic interactions present in Eq.(3.26).

[9] The static contribution is omitted.

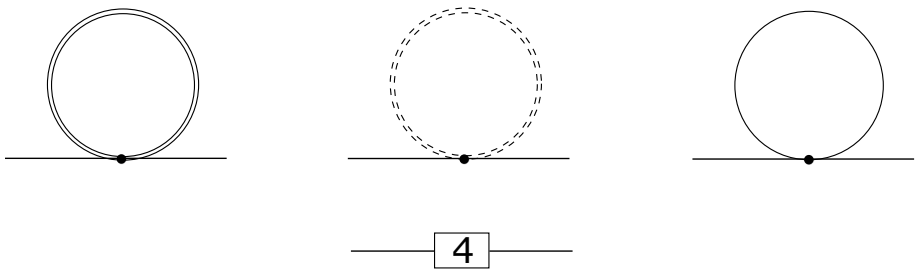

Figure 3.2: Self-energy diagrams at next-to-leading order in the low-energy expansion. The first three diagrams are one-loop corrections derived from $\mathcal{L}_2$, while the last diagram is derived from $\mathcal{L}_4$.

3.3.1 Renormalizing m

The three pion masses are degenerate at zero external fields, so it is sufficient only to consider π_3, which is what we do in the following.

The physical pion mass m_π is determined by the location of the pole in the pion propagator. We notice that the kinetic term and the mass term in Eq.(3.26) takes the canonical form $\frac{1}{2}\partial^\mu\pi_a\partial_\mu\pi_a - \frac{m^2}{2}\pi_a\pi_a$. It follows that the renormalized pion propagators can be written on the form shown below,

$$\frac{i}{k^2 - m^2 - \Sigma(k^2)}, \tag{3.27}$$

at any given order in the momentum expansion. Here $\Sigma(k^2)$ denotes the renormalized self energy at the given order in the expansion. The self energy at $O(p^2)$ is zero, so the propagator has a simple pole at $k^2 = m^2$, which yields the leading-order relation $m = m_\pi$.

The remaining terms in Eq.(3.26) are used to determine the self-energy $\Sigma(k^2)$ to next-to-leading order. The result can be represented diagrammatically as the sum of the four Feynman diagrams in Fig.3.2, where the different lines are explained in the caption of Fig.3.1.

The vertex factors in the loop diagrams are determined by the quartic terms in Eq.(3.26). Explicitly, the Feynman rule for $\pi_a(p_1)\pi_b(p_2) \to \pi_c(p_3)\pi_d(p_4)$ reads,

$$\begin{aligned}&\frac{i}{3f^2}[\delta_{ab}\delta_{cd}(s + m^2 + 2(p_1p_2 + p_3p_4)) + \delta_{ac}\delta_{bd}(t + m^2 - 2(p_1p_3 + p_2p_4))\\ &+ \delta_{ad}\delta_{bc}(u + m^2 - 2(p_1p_4 + p_2p_3))],\end{aligned} \tag{3.28}$$

where $s = (p_1+p_2)^2 = (p_3+p_4)^2$, $t = (p_1-p_3)^2 = (p_4-p_2)^2$, and $u = (p_1-p_4)^2 = (p_2-p_3)^2$ are the Mandelstam variables. The sum of the loop diagrams in Fig.3.2 is easily determined from the Feynman rules in Eq.(3.28), and the result reads,

$$-i\Sigma(p^2)_{\text{loop}} = \frac{1}{2}\frac{i}{3f^2}\int_k \frac{i(5m^2 - 4p^2 - 4k^2)}{k^2 - m^2}, \tag{3.29}$$

where the factor of $\frac{1}{2}$ originates from the symmetry of the loop diagrams. We use Eq.(3.13) to rewrite the result as follows,

$$-i\Sigma(p^2)_{\text{loop}} = i\frac{m^2 - 4p^2}{6f^2}\int_k \frac{i}{k^2 - m^2}. \tag{3.30}$$

We add the contribution from $\mathcal{L}_4$, which can be read directly from Eq.(3.26), to the one-loop contribution in Eq.(3.30) and obtain the complete self energy to next-to-leading order;

$$\Sigma(p^2) = \frac{4p^2 - m^2}{6f^2}\frac{m^2}{(4\pi)^2}\Big[-\frac{1}{\epsilon} - 1 + \log\frac{m^2}{\mu^2}\Big] - \frac{2l_4 m^2 p^2}{f^2} + \frac{2m^4}{f^2}(l_3 + l_4). \tag{3.31}$$

Eq.(3.31) can be rewritten as $\Sigma(p^2) = A + Bp^2$, where

$$A = \frac{m^4}{f^2}\Big\{2(l_3 + l_4) - \frac{1}{6(4\pi)^2}\Big[-\frac{1}{\epsilon} - 1 + \log\frac{m^2}{\mu^2}\Big]\Big\}, \tag{3.32}$$

$$B = \frac{m^2}{f^2}\Big\{-2l_4 + \frac{2m^2}{3(4\pi)^2}\Big[-\frac{1}{\epsilon} - 1 + \log\frac{m^2}{\mu^2}\Big]\Big\}. \tag{3.33}$$

Notice that $A = O(p^4)$ and $B = O(p^2)$. The defining equation for the pion mass $m_\pi^2 - m^2 - \Sigma(m_\pi^2) = 0$ can be written in terms of the new variables A and B as,

$$m_\pi^2 = \frac{m^2 + A}{1 - B} = (m^2 + A)(1 + B + B^2 + ...). \tag{3.34}$$

Since our calculation is to next-to-leading order, we ignore terms of higher order (i.e. NNLO and higher) to be self-consistent. This leads to the final result

$$m_\pi^2 = m^2 + A + Bm^2 = m^2\left(1 - \frac{m^2}{2f^2(4\pi)^2}\bar{l}_3\right), \tag{3.35}$$

which is in agreement with the original result in Ref.[22].

3.3.2 Renormalizing f

The pion decay constant f_π can be determined through the correlator of two axial currents[22, 23, 107],

$$\int d^4x e^{ipx}\,\langle 0|TA^{a\mu}A^{b\nu}|0\rangle = \delta^{ab}\frac{p^\mu p^\nu f_\pi^2}{p^2 - m_\pi^2}, \tag{3.36}$$

or through the matrix element,

$$\Big\langle 0\Big|A^{a\mu}\Big|\pi^b(p)\Big\rangle = ip^\mu\delta^{ab}f_\pi. \tag{3.37}$$

We will use the latter to determine the next-to-leading order relation for f in the following. The matrix element $\langle 0|A^{a\mu}|\pi^a(p)\rangle$ (no summation over a intended) is the same for $a = 1$, 2, 3, so it is once again sufficient to only consider $a = 3$.

The axial current $A^{i\mu}$ couples minimally to the external field $a_{i\mu}$ in the QCD Lagrangian in Eq.(2.28). The axial currents in the effective theory can therefore be obtained by varying the χPT action S_{eff} with respect to the external fields $a_{i\mu}$, which yields the following relation,

$$A^{i\mu} = \frac{\partial\mathcal{L}_{\text{eff}}}{\partial a_{i\mu}}\Big|_{a_\mu=0}. \tag{3.38}$$

The axial currents can also be obtained from Noether's theorem[56] through the relations,

$$L^{a\mu} = \frac{\partial\delta\mathcal{L}_{\text{eff}}}{\partial(\partial_\mu\Theta_a^L)}, \qquad R^{a\mu} = \frac{\partial\delta\mathcal{L}_{\text{eff}}}{\partial(\partial_\mu\Theta_a^R)}, \qquad A^{a\mu} = R^{a\mu} - L^{a\mu}, \tag{3.39}$$

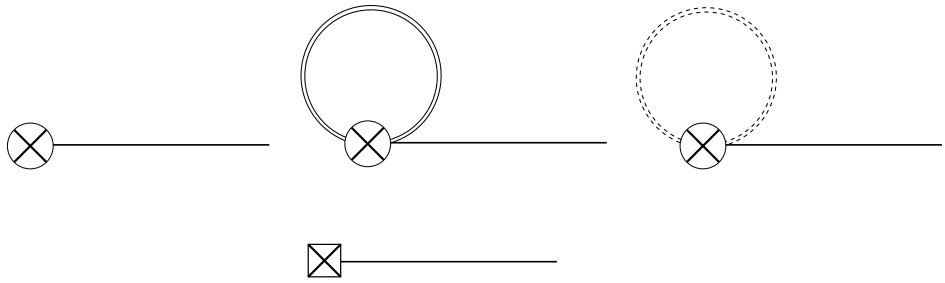

Figure 3.3: The diagrams that contribute to $\langle 0|A^{3\mu}|\pi^3(p_\mu)\rangle$ to next-to-leading order in the low-energy expansion. The first diagram is the leading-order contribution, the next two are one-loop corrections derived from $\mathcal{L}_2$, while the last diagram is derived from $\mathcal{L}_4$.

where $\delta\mathcal{L}_{\text{eff}}$ denotes the change in the effective Lagrangian under the relevant infinitesimal transformation. Either way, the contributions from $\mathcal{L}_2$ and $\mathcal{L}_4$ to $A^{3\mu}$ reads,

$$A_2^{3\mu} = -i\frac{f^2}{4}\,\mathrm{Tr}\Big[\tau_3\{\Sigma,\partial^\mu\Sigma^\dagger\}\Big], \tag{3.40}$$

$$A_4^{3\mu} = -il_4\frac{m^2f^2}{2}\,\mathrm{Tr}\Big[\tau_3\{\Sigma,\partial^\mu\Sigma^\dagger\}\Big] + ..., \tag{3.41}$$

respectively, where we have omitted the contributions from the terms proportional to l_1 and l_2 in Eq.(2.71), whose lowest order contributions are $O(p^6)$.[10] Expanding the right hand sides of the equations above in the pion fields we obtain,

$$A_2^{3\mu} = -f\partial^\mu\pi_3 + \frac{2}{3f}(\phi_a\phi_a\partial^\mu\phi_3 - \phi_3\phi_a\partial^\mu\phi_a) + ..., \tag{3.42}$$

$$A_4^{3\mu} = -l_4\frac{2m^2}{f}\partial^\mu\pi_3 + ..., \tag{3.43}$$

where the omitted terms are of higher order in the fields.

The terms in Eq.(3.42) and (3.43) are represented diagrammatically by the Feynman diagrams in Fig.3.3. We will denote the first diagram, the sum of the two following diagrams and the last diagram by A_1, A_2, and A_3, respectively.[11] The relationship between the diagrams in Fig3.3 and the matrix element of interest is obtained through the LSZ reduction formula[108], see for example Ref.[49] for details. The LSZ formula leads to the following defining equation for the pion decay constant[106],

$$ip_\mu f_\pi = \sqrt{Z}(A_1 + A_2 + A_3), \tag{3.44}$$

where Z denotes the wave function renormalization, which is defined as the residue of the propagator in Eq.(3.27);

$$Z = \left(1 - \frac{\partial\Sigma}{\partial p^2}\right)^{-1}. \tag{3.45}$$

This implies that we can express Z as $Z = 1 + B + B^2 + ...$, which lets us write Eq.(3.44) consistently to $O(p^4)$ as,

$$ip_\mu f_\pi = \left(1 + \frac{B}{2}\right)A_1 + A_2 + A_3. \tag{3.46}$$

[10] The only terms proportional to l_1 or l_2 in the current are of cubic and higher order in the fields. Such terms give one loop and higher corrections to the matrix elements, i.e corrections of order $O(p^4+p^2) = O(p^6)$ and higher.

[11] With this definition $A_1 = O(p^2)$, while A_2 and A_3 are $O(p^4)$

Thus, to order $O(p^2)$ we obtain,

$$\langle 0|A^{3\mu}|\pi^3(p)\rangle = \langle 0|-f\partial^\mu\pi^3|\pi^3(p)\rangle = ip^\mu f. \tag{3.47}$$

By comparing Eq.(3.37) with Eq.(3.47) we recover the tree-level result $f = f_\pi$.

The next-to-leading order contributions to the matrix element read,

$$\frac{B}{2}A_1 = -ip_\mu f\left[l_4\frac{m^2}{f^2} + \frac{m^2}{3f^2(4\pi)^2}\left(\frac{1}{\epsilon}+1+\log\frac{\Lambda^2}{m^2}\right)\right], \tag{3.48}$$

$$A_2 = ip_\mu f\left[\frac{4m^2}{3f^2(4\pi)^2}\left(\frac{1}{\epsilon}+1+\log\frac{\Lambda^2}{m^2}\right)\right], \tag{3.49}$$

$$A_3 = ip_\mu f\left[2l_4\frac{m^2}{f^2}\right]. \tag{3.50}$$

When we add Eqs.(3.48)-(3.50) together, all the divergences and scale dependent terms cancel out nicely in the sum. Finally, by combining Eqs.(3.46)-(3.50) we obtain,

$$f_\pi = f\left[1 + \frac{m^2}{f^2(4\pi)^2}\bar{l}_4 + O\left(\frac{m^4}{f^4}\right)\right], \tag{3.51}$$

which is consistent with the original result in Ref.[22]. By squaring the result we obtain an expression that is more convenient for later use,

$$f_\pi^2 = f^2\left[1 + \frac{2m^2}{f^2(4\pi)^2}\bar{l}_4 + O\left(\frac{m^4}{f^4}\right)\right]. \tag{3.52}$$

Part II

Quasi-particle masses in the pion-condensed phase

Chapter 4

χPT in the pion-condensed phase

In this part of the thesis, we discuss how to calculate the quasi-particle masses to next-to-leading order in the pion-condensed phase. The discussion requires knowledge about relevant terms in the Lagrangian and the tree-level dispersion relations. To make this thesis as self-contained as possible, we use this chapter to review some results of χPT at finite isospin, which will be useful later. We start by reviewing the ground state configuration in the pion-condensed phase and express the Lagrangian in terms of pion fields. Tree-level relations for the medium-dependent pion masses and pion-decay constants are obtained, and the renormalized free energy to next-to-leading order is derived. The leading-order terms in the Lagrangian up to quadratic order in the fields, as well as the renormalized free energy, are also found in Ref.[94]. Details about the derivation of the Lagrangian are found in Appendix B.

In Ref.[94] we reviewed how to obtain the ground state configuration (GS) at finite values of the isospin chemical potential, and how to describe fluctuations around the ground state configuration in the two phases. Our starting point was the following completely general parametrization Σ_α of the Goldstone-manifold $SU(2)_R \times SU(2)_L/SU(2)_V \sim SU(2)_A$,

$$\Sigma_\alpha = e^{i\alpha\hat{\pi}_i\tau_i} = \cos\alpha + i\hat{\pi}_i\tau_i \sin\alpha, \tag{4.1}$$

$$\hat{\pi}_i\hat{\pi}_i = 1. \tag{4.2}$$

The parameters $\hat{\pi}_i$ and α are determined by minimizing the static Hamiltonian $\mathcal{H}_{\text{static}}$[28], which to leading order reads,

$$\mathcal{H}_{\text{static}} = \frac{f^2\mu_I^2}{8}\,\text{Tr}\Big(\tau_3\Sigma\tau_3\Sigma^\dagger - \mathbb{1}\Big) - \frac{m^2f^2}{4}\text{Tr}[\Sigma + \Sigma^\dagger]. \tag{4.3}$$

Substituting the representation in Eq.(4.1) into $\mathcal{H}_{\text{static}}$ yields,

$$\mathcal{H}_{\text{static}} = -\frac{f^2\mu_I^2}{2}(\hat{\pi}_1\hat{\pi}_1 + \hat{\pi}_2\hat{\pi}_2)\sin^2\alpha - m^2f^2\cos\alpha, \tag{4.4}$$

which is minimized when $\hat{\pi}_3 = 0$. Minimizing the static energy with respect to α yields the well-known results,

$$\alpha = 0, \quad m_\pi < \mu_I, \qquad\qquad \cos\alpha = \frac{m_\pi^2}{\mu_I^2}, \quad m_\pi \geq \mu_I. \tag{4.5}$$

We recover the standard ansatz for the ground state in Refs.[25, 109][1] by substituting the

[1]The expression in the references can be obtained by defining a new variable π as follows; $\hat{\pi}_1 \equiv \cos\pi$ and $\hat{\pi}_2 \equiv \sin\pi$.

expressions for α in Eq.(4.5) into Eq.(4.1);

$$\Sigma_\alpha = \mathbb{1}, \qquad \mu_I < m_\pi, \tag{4.6}$$

$$\Sigma_\alpha = \cos\alpha + i(\hat{\pi}_1\tau_1 + \hat{\pi}_2\tau_2)\sin\alpha, \qquad \cos\alpha = \frac{m_\pi^2}{\mu_I^2}, \qquad \mu_I \geq m_\pi. \tag{4.7}$$

Notice that the ground-state energy in Eq.(4.4) is degenerate with respect to $\hat{\pi}_1$ and $\hat{\pi}_2$. More precisely, there is a residual $O(2)$ symmetry between $\hat{\pi}_1$ and $\hat{\pi}_2$. The subgroup of continuous transformations $SO(2)$ is exactly equal to $U(1)_{I_3}$,[2] which signals that the symmetry generated by I_3 is spontaneously broken when $\mu_I \geq m$. The ground state for $\mu_I > m_\pi$ is a pion (electromagnetic) superconductor[110] with one Goldstone mode, as noted in chapter 2.

Following Ref.[44] we set $\hat{\pi}_1 = 1$ and $\hat{\pi}_2 = 0$ in the parametrization of the ground state in Eq.(4.4). This choice was also employed in Ref.[94], where we showed that the following expression represents a consistent parametrization of fluctuations around the GS[28, 44],

$$\Sigma = A_\alpha(U\Sigma_0 U)A_\alpha. \tag{4.8}$$

The quantities on the right hand side of Eq.(4.8) are defined as follows,

$$A_\alpha = \cos\frac{\alpha}{2} + i\tau_1\sin\frac{\alpha}{2}, \tag{4.9}$$

$$\Sigma_0 = \mathbb{1}, \tag{4.10}$$

$$U = \exp\left(i\frac{\pi_a\tau_a}{2f}\right). \tag{4.11}$$

The parametrization in Eq.(4.8) rotates the (broken) $SU(2)_A$ generators appropriately as the ground state is tilted with the angle α. In Appendix B, we use this parametrization to derive the terms in the χPT Lagrangian that are needed in the calculations of the quasi-particle masses.

4.1 Tree-level analysis

The leading-order Lagrangian in χPT at non-zero isospin chemical potential reads,

$$\mathcal{L}_2 = \frac{f^2}{4}\,\mathrm{Tr}\left[\nabla^\mu\Sigma^\dagger\nabla_\mu\Sigma\right] + \frac{f^2m^2}{4}\,\mathrm{Tr}\left[\Sigma + \Sigma^\dagger\right]. \tag{4.12}$$

At the end of chapter 2 we showed that the covariant derivatives are given by,

$$\nabla_\mu\Sigma = \partial_\mu\Sigma - i[v_\mu, \Sigma], \tag{4.13}$$

$$\nabla_\mu\Sigma^\dagger = \partial_\mu\Sigma^\dagger - i[v_\mu, \Sigma^\dagger], \tag{4.14}$$

where $v_\mu = \delta_{\mu 0}\mu_I\frac{\tau_3}{2}$.

We use the parameterization in Eq.(4.8) to derive the leading-order Lagrangian in terms of the pion fields π_a (see Appendix B for technical details). The result can be written as,

$$\mathcal{L}_2 = \mathcal{L}_2^{\text{static}} + \mathcal{L}_2^{\text{linear}} + \mathcal{L}_2^{\text{quadratic}} + \mathcal{L}_2^{\text{cubic}} + \mathcal{L}_2^{\text{quartic}} + ... \tag{4.15}$$

where,

$$\mathcal{L}_2^{\text{static}} = f^2m^2\cos\alpha + \frac{1}{2}f^2\mu_I^2\sin^2\alpha, \tag{4.16}$$

[2] The well known isomorphism between the two groups $U(1)$ and $SO(2)$ is $e^{i\theta} \to \begin{pmatrix}\cos\theta & -\sin\theta \\ \sin\theta & \cos\theta\end{pmatrix}$.

$$\mathcal{L}_2^{\text{linear}} = f(-m^2 \sin\alpha + \mu_I^2 \cos\alpha \sin\alpha)\pi_1 + f\mu_I \sin\alpha \partial_0 \pi_2, \tag{4.17}$$

$$\begin{aligned}\mathcal{L}_2^{\text{quadratic}} &= \frac{1}{2}\partial^\mu \pi_a \partial_\mu \pi_a + \mu_I \cos\alpha(\pi_1 \partial_0 \pi_2 - \pi_2 \partial_0 \pi_1) - \frac{1}{2}[m^2 \cos\alpha - \mu_I^2 \cos(2\alpha)]\pi_1^2 \\ &- \frac{1}{2}[m^2 \cos\alpha - \mu_I^2 \cos^2\alpha]\pi_2^2 - \frac{1}{2}[m^2 \cos\alpha + \mu_I^2 \sin^2\alpha]\pi_3^2,\end{aligned} \tag{4.18}$$

$$\mathcal{L}_2^{\text{cubic}} = \frac{(m^2 - 4\mu_I^2 \cos\alpha)\sin\alpha}{6f}\pi_1\pi_a\pi_a - \frac{\mu_I \sin\alpha}{f}[\pi_1^2 \partial_0 \pi_2 + \pi_3^2 \partial_0 \pi_2], \tag{4.19}$$

$$\begin{aligned}\mathcal{L}_2^{\text{quartic}} &= \frac{1}{24f^2}\pi_a\pi_a[(m^2 \cos\alpha - 4\mu_I^2 \cos 2\alpha)\pi_1^2 + (m^2 \cos\alpha - 4\mu_I^2 \cos^2\alpha)\pi_2^2 \\ &+ (m^2 \cos\alpha + 4\mu_I^2 \sin^2\alpha)\pi_3^2] - \frac{\mu_I \cos\alpha}{3f^2}\pi_a\pi_a(\pi_1\partial_0\pi_2 - \pi_2\partial_0\pi_1) \\ &+ \frac{1}{6f^2}\left[\pi_a\pi_b\partial^\mu\pi_a\partial_\mu\pi_b - \pi_a\pi_a\partial^\mu\pi_b\partial_\mu\pi_b\right].\end{aligned} \tag{4.20}$$

There are several things to notice about $\mathcal{L}_2$. The occurrence of ∂_0 explicitly breaks the Lorentz-boost invariance and leaves the frame in which particles are at rest with the medium as the privileged frame. Spatial rotations and translations are left unaffected because the considered medium is isotropic and homogeneous[91]. By taking the chemical potential to zero, we recover full Lorentz invariance, as we should.

We notice that $\mathcal{L}_2^{\text{cubic}}$ vanishes in the normal phase, and must therefore also vanish at the second-order phase transition between the vacuum- and the pion-condensed phase.[3] In the limit $\alpha = \mu_I = 0$ we recover the well-known vacuum result for $\mathcal{L}_2$, see for example Ref.[53] for details.

The inverse propagator in the π_a basis can be read directly from Eq.(4.18). The result is

$$D^{-1} = \begin{pmatrix} D_{12}^{-1} & 0 \\ 0 & P^2 - m_3^2 \end{pmatrix}, \tag{4.21}$$

$$D_{12}^{-1} = \begin{pmatrix} P^2 - m_1^2 & ip^0 m_{12} \\ -ip^0 m_{12} & P^2 - m_2^2 \end{pmatrix}, \tag{4.22}$$

where $P = (p_0, p)$ denotes the four-momentum, and we have defined the mass parameters as

$$m_1^2 = m^2 \cos\alpha - \mu_I^2 \cos(2\alpha), \tag{4.23}$$

$$m_2^2 = m^2 \cos\alpha - \mu_I^2 \cos^2\alpha, \tag{4.24}$$

$$m_3^2 = m^2 \cos\alpha + \mu_I^2 \sin^2\alpha, \tag{4.25}$$

$$m_{12} = 2\mu_I \cos\alpha. \tag{4.26}$$

The dispersion relations for the mass eigenstates are found from the poles of the propagator, i.e by solving $\det\big(D^{-1}\big) = 0$ for p_0^2. The results are,

$$\begin{aligned}E_{\pi^\pm}^2 &= p^2 + \frac{1}{2}\Big(m_1^2 + m_2^2 + m_{12}^2 \\ &\pm \sqrt{4p^2 m_{12}^2 + (m_1^2 + m_2^2 + m_{12}^2)^2 - 4m_1^2 m_2^2}\Big),\end{aligned} \tag{4.27}$$

$$E_{\pi^0}^2 = p^2 + m_3^2, \tag{4.28}$$

[3] This observation is what makes the renormalization of self-energies at the phase transition point $\mu_I = m_\pi$ much easier than in the bulk $\mu_I > m_\pi$.

where π^0 is identical to π_3, and $\pi^\pm$ are linear combinations of π_1 and π_2.[4] $\pi^\pm$ are just the usual charge eigenstates in the normal phase, but turn into complicated functions of π_1 and π_2 in the pion-condensed phase, as we will see later in chapter 6.[5]

Using Eqs.(4.21)-(4.22) we may finally write the full propagator in terms of the dispersion relations in Eq.(4.27) as,

$$D = \begin{pmatrix} D_{12} & 0 \\ 0 & (P^2 - m_3^2)^{-1} \end{pmatrix}, \tag{4.29}$$

$$D_{12} = \frac{1}{(p_0^2 - E_{\pi^+}^2)(p_0^2 - E_{\pi^-}^2)} \begin{pmatrix} P^2 - m_1^2 & -ip^0 m_{12} \\ ip^0 m_{12} & P^2 - m_2^2 \end{pmatrix}. \tag{4.30}$$

Masses

The tree-level (quasi-particle) masses are obtained by setting $p = 0$ in Eqs.(4.27)-(4.28),

$$m_{\pi^\pm}^2 = \frac{1}{2}\Big(m_1^2 + m_2^2 + m_{12}^2 \pm \sqrt{(m_1^2 + m_2^2 + m_{12}^2)^2 - 4m_1^2 m_2^2}\Big), \tag{4.31}$$

$$m_{\pi^0}^2 = m_3^2. \tag{4.32}$$

The variables on the right hand sides of Eqs.(4.31)-(4.32) are evaluated at the leading-order minimum of the free energy $\cos\alpha = \frac{m_\pi}{\mu_I}$. The results are displayed in Fig.4.1 as functions of the normalized isospin chemical potential, for values $0 \leq \mu_I \leq 2.5 m_\pi$.

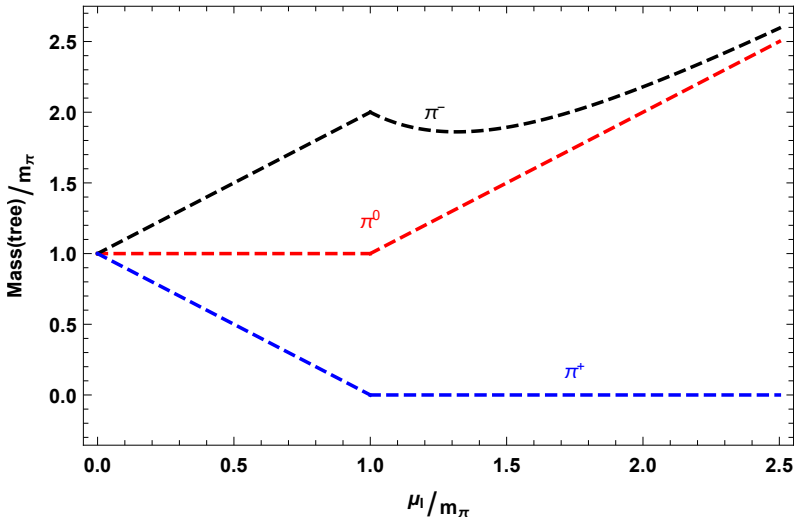

Figure 4.1: Tree-level masses normalized to the mass of the neutral pion in the vacuum, as a function of the normalized isospin chemical potential.

We expect one of the charged branches to be the Goldstone boson associated with the spontaneusly broken I_3 generator. Since m_2 vanishes in the pion-condensed phase, Eq.(4.31) simplifies to

$$m_{\pi^\pm}^2 = \frac{1}{2}\left[m_1^2 + m_{12}^2 \pm (m_1^2 + m_{12}^2)\right]. \tag{4.33}$$

This equation verifies that one of the modes becomes massless at $\mu_I = m_\pi$, as indicated by the blue line in Fig.4.1.

[4] This implies that π^0 is electrically neutral, while π^+ and π^- carry electric charge.

[5] Some authors use $\pi^\pm$ to denote the charge eigenstates and $\tilde{\pi}^\pm$ to denote the charged mass eigenstates. However, since we are mainly concerned with mass eigenstates in this thesis we use the simpler notation $\pi^\pm$ to denote the charged mass eigenstates.

Decay constants

The pion-decay constants at finite isospin chemical potential and temperature were first studied by Loewe and Villavicencio in Ref.[29], where they focused on the normal phase $\mu_I < m_\pi$. However, to the best of our knowledge, there has not been published any studies of the medium-dependent decay constants in the second phase yet. The pion-decay constants in the BEC phase are one of the topics that are being addressed in our ongoing study of χPT at finite isospin density. In this subsection, we present the tree-level results.

By differentiating the effective Lagrangian with respect to the external field $a_{i\mu}$ we obtain,

$$A_{i\mu} = -i\frac{f^2}{4}\,\mathrm{Tr}\Big[\tau_i\{\Sigma,\partial_\mu\Sigma^\dagger\}\Big] + \frac{f^2}{4}\,\mathrm{Tr}\left[\tau_i\left(\Sigma^\dagger v_\mu\Sigma - \Sigma v_\mu\Sigma^\dagger\right)\right]. \tag{4.34}$$

Substituting the parametrization in Eq.(4.8) into Eq.(4.34) and subsequently expand the result to linear order in the pion fields lets us express the axial currents as follows,

$$A_{1\mu} = -f\partial_\mu\pi_1 + f\mu_I\delta_{\mu 0}\cos\alpha\pi_2, \tag{4.35}$$

$$A_{2\mu} = -f\partial_\mu\cos\alpha\pi_2 - \mu_I f\delta_{\mu 0}\left(\pi_1\cos 2\alpha + \frac{f\sin 2\alpha}{2}\right), \tag{4.36}$$

$$A_{3\mu} = -f\partial_\mu\cos\alpha\pi_3. \tag{4.37}$$

In the vacuum limit $\mu_I = \alpha = 0$ we recover the tree-level result $A_{i\mu} = -f\partial_\mu\pi_i$, as we should.

It is easily seen from Eq.(4.4) that in the chiral limit $m = 0$ we obtain a ground state that is characterized by $\alpha = \frac{\pi}{2}$. In this case $\{\pi_1, \pi_2, \pi_3\}$ become the mass eigenstates, which can be verified by substituting $\alpha = \frac{\pi}{2}$ into the dispersion relations in Eqs.(4.27)-(4.28). Substituting Eqs.(4.35)-(4.37) into (3.37) we obtain the following leading-order results for the chiral decay constants in the pion-condensed phase,

$$f_{\pi_1} = f_\pi, \tag{4.38}$$

$$f_{\pi_2} = f_{\pi_3} = 0. \tag{4.39}$$

The result $f_{\pi_2} = 0$ is consistent with π_2 being the Goldstone boson, which cannot decay (because it is massless). The neutral pion does not have any leptonic decays in this limit,[6] while the result for π_1 is the same as at vanishing chemical potential.

4.2 Next-to-leading-order analysis

We are going to need $\mathcal{L}_4^{\text{static}}$, $\mathcal{L}_4^{\text{linear}}$ and $\mathcal{L}_4^{\text{quadratic}}$ to renormalize the free energy, the one-point function and the self energies to one loop, respectively. In Appendix B we write the next-to-leading order Lagrangian in terms of the pion fields, and the result is given below,

$$\mathcal{L}_4^{\text{static}} = (l_1+l_2)\mu_I^4\sin^4\alpha + l_4 m^2\mu_I^2\cos\alpha\sin^2\alpha + (l_3+l_4)m^4\cos^2\alpha, \tag{4.40}$$

$$\mathcal{L}_4^{\text{linear}} = \left[4\,(l_1+l_2)\,\frac{\mu_I^4}{f}\sin^3\alpha\cos\alpha + l_4\frac{m^2\mu_I^2}{f}\left(2\sin\alpha - 3\sin^3\alpha\right) - (l_3+l_4)\,\frac{m^4}{f}\sin 2\alpha\right]\pi_1$$
$$+\left[4\,(l_1+l_2)\,\frac{\mu_I^3}{f}\sin^3\alpha + l_4\frac{m^2\mu_I}{f}\sin 2\alpha\right]\partial_0\pi_2, \tag{4.41}$$

[6] The matrix element $\langle 0|A^{3\mu}|\pi^3\rangle$ only controls weak decays of the neutral pion, and not the anomalous process $\pi^0 \to \gamma\gamma$

$$\mathcal{L}_4^{\text{quadratic}} = (l_1+l_2)\frac{2\mu_I^4\sin^2\alpha}{f^2}\left[(1+2\cos(2\alpha))\pi_1^2+\cos^2\alpha\pi_2^2-\sin^2\alpha\pi_3^2\right]$$
$$+ l_1\frac{4\mu_I^2\sin^2\alpha}{f^2}(\partial_0\pi_2)^2 + l_2\frac{2\mu_I^2\sin^2\alpha}{f^2}(\partial_0\pi_2)^2 + (l_1+l_2)\frac{4\mu_I^3\sin\alpha\sin(2\alpha)}{f^2}\left[\pi_1\partial_0\pi_2-\pi_2\partial_0\pi_1\right]$$
$$+ l_1\frac{2\mu_I^2}{f^2}\sin^2\alpha(\partial_\mu\pi_a)(\partial^\mu\pi_a) + l_2\frac{2\mu_I^2}{f^2}\sin^2\alpha(\partial_0\pi_a)^2 + l_2\frac{2\mu_I^2}{f^2}\sin^2\alpha(\partial_\mu\pi_2)(\partial^\mu\pi_2)$$
$$- (l_3+l_4)\frac{m^4}{f^2}\left[\cos(2\alpha)\pi_1^2+\cos^2\alpha(\pi_2^2+\pi_3^2)\right] - l_4\frac{m^2\mu_I}{f^2}(\cos^2\alpha+\cos(2\alpha))(\pi_2\partial_0\pi_1-\pi_1\partial_0\pi_2)$$
$$+ l_4\frac{m^2\mu_I^2\cos\alpha}{f^2}\left[(-5+9\cos(2\alpha))\pi_1^2+(1+3\cos(2\alpha))\pi_2^2-6\sin^2\alpha\pi_3^2\right]$$
$$+ l_4\frac{m^2\cos\alpha}{f^2}(\partial_\mu\pi_a)(\partial^\mu\pi_a). \tag{4.42}$$

Free energy at finite isospin

We have so far seen that the mass parameter m and the isospin chemical potential μ_I have formal interpretations as external source fields. We are interested in various physical quantities as functions of μ_I and it would be wonderful if there was a functional of the external fields from which we could obtain the observables of interest. In chapter 2, we saw that the generating functional $W[\{f\}]$ is precisely what we are looking for. However, obtaining W exactly would require us to solve the path integral altogether, which we are not able to do (analytically at least). What we *can* do, is to find a perturbative extension of the generating functional, starting with its functional integral definition.

Since W is the generator of all connected diagrams[49], a perturbative expansion amounts to calculating loops. We are interested in χPT to next-to-leading order where the partition function contains three different contributions: the tree-level contribution from $\mathcal{L}_2$, the one-loop contribution from $\mathcal{L}_2$, and the tree-level contribution from $\mathcal{L}_4$. Therefore, it is sufficient only to consider $\mathcal{L}_2$ as we expand W beyond the mean-field approximation.

In chapter 3, we saw that one-loop integrals in χPT are UV divergent. According to Weinberg's theorem, the divergences should be canceled exactly by terms in $\mathcal{L}_4$ by renormalizing the LECs appropriately. Moreover, the values of the counterterms must be independent of μ_I and m, and the constants γ_i must be identical in the two phases[111].

Finally, the generating functional of a scalar field theory is the same as minus one times Helmholtz free energy Ω. We will use the terminology free energy from now on when we refer to Ω, and reserve the term "generating functional" for the QCD generating functional given in Eq.(2.30). Once we have renormalized Ω, the thermodynamic functions that measure bulk properties of matter can be obtained, as we will see examples of in Part III.

Perturbative expansion

The fields π_i are excitations around the (rotated) ground state configuration, so their expectation values $\langle\pi_i\rangle$ have to vanish. We can therefore use the following leading-order mean-field approximation for the free energy,[7]

$$e^{-i\Omega} = \int D\pi \exp\left\{ i\int d^4x\mathcal{L}_2[\pi_i=0]\right\}, \tag{4.43}$$

[7]We use π to denote all three pions in the path-integral measure.

which is equivalent to $\Omega_0 = \mathcal{H}^{\text{static}}$. Minimizing the free energy with respect to α yields,

$$\frac{\partial \Omega_0}{\partial \alpha} = -m^2 \sin\alpha + \mu_I^2 \cos\alpha \sin\alpha = 0. \tag{4.44}$$

Comparing Eqs.(4.17) and (4.44) we see that,

$$\frac{\delta \mathcal{L}_2}{\delta \pi_i}\Big|_{\pi=0} = 0. \tag{4.45}$$

We proceed to expand the fields in the path-integral action around $\pi = 0$,

$$\begin{aligned} e^{-i\Omega} = \int D\pi \exp\Big\{ i \int d^4x \left(\mathcal{L}_2[\pi_i = 0] + \mathcal{L}_4[\pi_i = 0]\right)\Big\} \times \\ \exp\Big\{ i \int d^4x \frac{\delta \mathcal{L}_2}{\delta \pi_i}\pi_i + \frac{i}{2}\int d^4x \frac{\delta^2 \mathcal{L}_2}{\delta\pi_i \delta\pi_j}\pi_i\pi_j + ...\Big\}, \end{aligned} \tag{4.46}$$

All functional derivatives are evaluated at $\pi = 0$, and the omitted terms give higher order corrections. The terms linear in π_i vanishes by Eq.(4.45), which leaves us with a Gaussian approximation of the path-integral. The Gaussian approximation is exactly solvable and can be written as a functional determinant[49],

$$\begin{aligned} e^{-i\Omega} &\approx \int D\pi \exp\Big\{ i \int d^4x (\mathcal{L}_2[\pi_i = 0] + \mathcal{L}_4[\pi_i = 0]) + \frac{i}{2}\int d^4x \frac{\delta^2 \mathcal{L}_2}{\delta\pi_j \delta\pi_i}\pi_i\pi_j \Big\} \\ &= \exp\Big\{ i \int d^4x \left(\mathcal{L}_2[\pi_i = 0] + \mathcal{L}_4[\pi_i = 0]\right)\Big\} \left(\det\left[-\frac{\delta^2 \mathcal{L}_2}{\delta\pi_i \delta\pi_j}\Big|_{\pi=0}\right]\right)^{-\frac{1}{2}}. \end{aligned} \tag{4.47}$$

Taking the logarithm of the equations above we obtain,

$$\Omega = -\int d^4x \left(\mathcal{L}_2^{\text{static}} + \mathcal{L}_4^{\text{static}}\right) - \frac{i}{2VT}\log\det\left[-\frac{\delta^2 \mathcal{L}_2^{\text{quadratic}}}{\delta\pi_i \delta\pi_j}\right] + ..., \tag{4.48}$$

where V and T denotes the spatial and temporal volumes that are integrated over in the action, respectively.

Derivation

We will denote the three contributions to the free energy in Eq.(4.48) by Ω_0, Ω_1^{static} and Ω_1^{loop}, where,

$$\Omega_0 = -f^2 m^2 \cos\alpha - \frac{1}{2} f^2 \mu_I^2 \sin^2\alpha, \tag{4.49}$$

$$\Omega_1^{\text{static}} = -(l_1 + l_2)\mu_I^4 \sin^4\alpha - l_4 m^2 \mu_I^2 \cos\alpha \sin^2\alpha - (l_3 + l_4) m^4 \cos^2\alpha, \tag{4.50}$$

$$\Omega_1^{\text{loop}} = -\frac{i}{2VT}\,\text{Tr}\log\left[-\frac{\delta^2 \mathcal{L}_2^{\text{quadratic}}}{\delta\pi_i \delta\pi_j}\right]. \tag{4.51}$$

Here, we used the identity $\log\det(A) = \text{Tr}\log(A)$ to obtain Eq.(4.51). The trace is a sum over discrete quantum numbers and an integral over continuous quantum numbers. In the case of a scalar theory we do not have any discrete quantum numbers, and all we have to do is integrate $\langle x| -\frac{\delta^2 \mathcal{L}_2^{\text{quadratic}}}{\delta\pi_i \delta\pi_j} |x\rangle$ over spacetime[112], which yields,

$$\begin{aligned} \log\det\Big(-\frac{\delta^2 \mathcal{L}_2^{\text{quadratic}}}{\delta\pi_i \delta\pi_j}\Big) = (VT)\int_P \big[\log\left(-P^2 + m_3^2\right) + \\ \log\left(-P^2 + (E_{\pi^+}^2 - p^2)\right) + \log\left(-P^2 + (E_{\pi^-}^2 - p^2)\right)\big]. \end{aligned} \tag{4.52}$$

The integral on the right hand side of the equation is over $d = 4 - 2\epsilon$ dimensions. To obtain Eq.(4.52) we used the following well known relation,

$$\begin{aligned}\mathrm{Tr}\log\left(\partial^2 + m^2\right) &= \int d^4x \,\langle x|\log\left(\partial^2 + m^2\right)|x\rangle = \int d^4x \int \frac{d^4k}{(2\pi)^4}\,\langle x|\log\left(\partial^2 + m^2\right)|k\rangle\,\langle k|x\rangle \\ &= \int d^4x \int \frac{d^4k}{(2\pi)^4}\log\left(-k^2 + m^2\right)\langle x|k\rangle\,\langle k|x\rangle = VT\int \frac{d^4k}{(2\pi)^4}\log\left(-k^2 + m^2\right), \qquad (4.53)\end{aligned}$$

where the second equality follows by inserting a complete set of plane waves.

The integrals in Eq.(4.52) can be written in a better way by first Wick rotating,

$$\int_P \log\left[-P^2 + m^2\right] = i\int_p\int_{p_0}\log\left[p_0^2 + (p^2 + m^2)\right], \qquad (4.54)$$

where the integrals over p and p_0 are evaluated in $d = 3 - 2\epsilon$ and $d = 1 - 2\epsilon$ dimensions respectively, and then use the following trick,

$$\begin{aligned}\int_{p_0}\log\left(p_0^2 + \Delta^2\right) &= -\frac{\partial}{\partial\alpha}\int_{p_0}\frac{1}{(p_0^2 + \Delta^2)}\Big|_{\alpha=0} \\ &= -\frac{\partial}{\partial\alpha}\left[\frac{1}{(4\pi)^{\frac{d}{2}}}\frac{\Gamma(\alpha - \frac{d}{2})}{\Gamma(\alpha)}\Big(\frac{1}{\Delta}\Big)^{\alpha-\frac{d}{2}}\right]\Big|_{\alpha=0} = \Delta, \qquad (4.55)\end{aligned}$$

where $\Delta \equiv \sqrt{p^2 + m^2}$. The relations above lets us rewrite Eq.(4.51) as,

$$\Omega_1^{\mathrm{loop}} = \frac{1}{2}\int_p E_{\pi^0} + \frac{1}{2}\int_p (E_{\pi^+} + E_{\pi^-}) \equiv \Omega_{1,\pi^0} + \Omega_{1,\pi^+} + \Omega_{1,\pi^-}. \qquad (4.56)$$

The contribution to Ω_1^{loop} from the neutral pion π^0 can be determined analytically in the $\overline{\mathrm{MS}}$ scheme by using Eq.(E.14),

$$\Omega_{1,\pi^0} = \frac{1}{2}\int_p \sqrt{p^2 + m_3^2} = -\frac{m_3^4}{4(4\pi)^2}\left[\frac{1}{\epsilon} + \frac{3}{2} + \frac{\Lambda^2}{m^2}\right]. \qquad (4.57)$$

The contribution from the charged pions are harder to obtain because of their complicated dispersion relations. In order to isolate the ultraviolet divergent parts of $\Omega_{1,\pi^+} + \Omega_{1,\pi^-}$ we expand the dispersion relations in powers of inverse momenta $\frac{1}{p}$ as,

$$\begin{aligned}E_{\pi^+} + E_{\pi^-} &= 2p + \frac{2(m_1^2 + m_2^2) + m_{12}^2}{4p} \\ &- \frac{8(m_1^4 + m_2^4) + 4(m_1^2 + m_2^2)m_{12}^2 + m_{12}^4}{64p^3} + ... \qquad (4.58)\end{aligned}$$

where the remaining terms generate finite contributions to Ω_1^{loop}.

The ultraviolet behaviour of $E_{\pi^+} + E_{\pi^-}$ is the same as that of $E_1 + E_2$, where $E_{1,2} = \sqrt{p^2 + m_{1,2}^2 + \frac{1}{4}m_{12}^2} = \sqrt{p^2 + \tilde{m}_{1,2}^2}$, $\tilde{m}_1^2 = m_3^2$ and $\tilde{m}_2^2 = m^2\cos\alpha$. This observation lets us write the contributions from the charged modes as,

$$\Omega_{1,\pi^+} + \Omega_{1,\pi^-} = \Omega_{1,\pi^+}^{\mathrm{div}} + \Omega_{1,\pi^-}^{\mathrm{div}} + \Omega_{1,\pi^+}^{\mathrm{fin}} + \Omega_{1,\pi^-}^{\mathrm{fin}}, \qquad (4.59)$$

where

$$\Omega_{1,\pi^+}^{\mathrm{div}} + \Omega_{1,\pi^-}^{\mathrm{div}} = \frac{1}{2}\int_p (E_1 + E_2), \qquad (4.60)$$

$$\Omega_{1,\pi^+}^{\mathrm{fin}} + \Omega_{1,\pi^-}^{\mathrm{fin}} = \frac{1}{2}\int_p (E_{\pi^+} + E_{\pi^-} - E_1 - E_2). \qquad (4.61)$$

The subtraction integral in Eq.(4.61) is finite, and can be computed numerically. The evaluation of the divergent integral in Eq.(4.60) can be carried out analytically in the $\overline{\text{MS}}$ scheme, and we use Eq.(E.14) from Appendix E to obtain,

$$\Omega^{\text{div}}_{1,\pi^+} + \Omega^{\text{div}}_{1,\pi^-} = -\frac{\tilde{m}_1^4}{4(4\pi)^2}\left[\frac{1}{\epsilon} + \frac{3}{2} + \log\frac{\Lambda^2}{\tilde{m}_1^2}\right] - \frac{\tilde{m}_2^4}{4(4\pi)^2}\left[\frac{1}{\epsilon} + \frac{3}{2} + \log\frac{\Lambda^2}{\tilde{m}_1^2}\right]. \tag{4.62}$$

Using Eqs.(3.16)-(3.22), we find that the divergent and scale-dependent terms from Ω_1^{static} are exactly cancelled by the divergent and scale dependent terms from Ω_1^{loop} in the sum $\Omega_1^{\text{static}} + \Omega_1^{\text{loop}}$. Thus, $\Omega_1^{\text{loop}} + \Omega_1^{\text{static}}$ is finite and scale independent.

Putting it all together we find that the renormalized free energy $\Omega = \Omega_0 + \Omega_1^{\text{loop}} + \Omega_1^{\text{static}}$ to next-to-leading order reads,

$$\begin{aligned}\Omega = &-m^2 f^2 \cos\alpha - \frac{f^2\mu_I^2}{2}\sin^2\alpha - \frac{\mu_I^4 \sin^4\alpha}{4(4\pi^2)}\left[1 + \frac{2}{3}\bar{l}_1 + \frac{4}{3}\bar{l}_2 + 2\log\frac{m^2}{m_3^2}\right] \\ &- \frac{m^4\cos^2\alpha}{4(4\pi^2)}\left[\frac{3}{2} - \bar{l}_3 + 4\bar{l}_4 + \log\frac{m^2}{\tilde{m}_2^2} + \log\frac{m^2}{m_3^2}\right] - \frac{m^2\mu_I^2\sin^2\alpha\cos\alpha}{2(4\pi^2)}\left[1 + 2\bar{l}_4 + 2\log\frac{m^2}{m_3^2}\right] \\ &+ \Omega^{\text{fin}}_{1,\pi^+} + \Omega^{\text{fin}}_{1,\pi^-}.\end{aligned} \tag{4.63}$$

In the limit $\alpha = 0$ we recover the free energy in the normal phase $\mu_I < m_\pi$,

$$\Omega = -f^2 m^2 - \frac{3m^4}{4(4\pi)^2}\left[\frac{1}{2} - \frac{1}{3}\bar{l}_3 + \frac{4}{3}\bar{l}_4\right]. \tag{4.64}$$

Notice that the result does not depend on μ_I all the way up to the phase transition, which is the Silver-Blaze property[44, 113].[8]

The defining equation for the ground state parameter α is obtained by minimizing the vacuum energy, which at zero temperature is equal to Ω,

$$\frac{\partial\Omega}{\partial\alpha} = 0. \tag{4.65}$$

We will refer to this equation as the equation of motion (EoM) for Ω in the remainder of this thesis.

In Fig.4.2 we display the solution to Eq.(4.65) as a function of the normalized isospin chemical potential. The red curve shows the leading-order result, while the blue curve shows the next-to-leading-order result. The difference between the curves is increasing with higher isospin chemical potential. There is also a noticeable difference between the curves in a domain very close to the phase transition.

[8] The name Silver-Blaze originates from an Arthur Conan Doyle story with the same name.

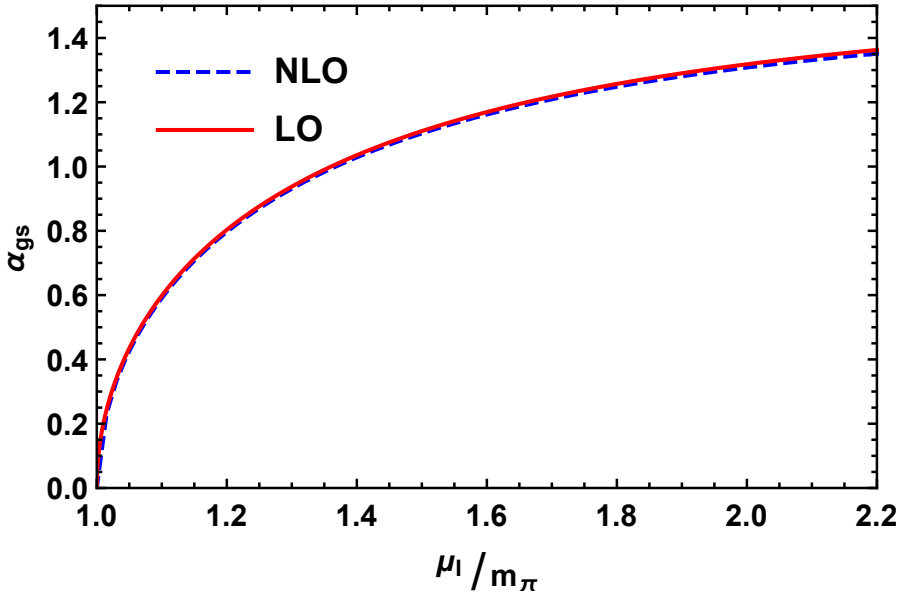

Figure 4.2: The figure shows α that minimizes the effective potential as a function of the normalized isospin chemical potential μ_I/m_π. The red curve shows the leading-order result, while the blue dashed curve shows the next-to-leading-order result.

Chapter 5

The neutral pion

The leading-order results for the quasi-particle masses have been known since the early days of χPT at finite isospin density[92], which was almost 20 years ago. However, a complete next-to-leading order calculation of the quasi-particle masses in the second phase has not yet been carried out. A next-to-leading-order result for one of the two massive quasi-particles would provide another opportunity to compare χPT beyond the leading order in the pion-condensed phase with lattice calculations. In this chapter, we discuss how to calculate the neutral-pion mass m_{π^0} to next-to-leading order in the pion-condensed phase.

This chapter is structured as follows; In the first section we present the Feynman diagrams contributing to the self-energy of the neutral pion. In the second section, we discuss the technical aspects of the renormalization procedure. We proceed to derive an approximation of the next-to-leading-order result, where we evaluate the loop integrals at the leading-order minimum $\cos\alpha = \frac{m_\pi^2}{\mu_I^2}$. This calculation is formally incorrect since the loop-integrals should be evaluated at the next-to-leading-order minimum and not the leading-order minimum. However, we have decided to include the calculation as an illustration of the renormalization procedure. Relevant loop integrals are found in Appendix E.

5.1 Self energy

The self energy $-i\Sigma_{33}$ of the neutral pion π^0 receives one-loop contributions from the cubic and quartic terms in $\mathcal{L}_2$ and corrections from the quadratic terms in $\mathcal{L}_4$ at next-to-leading order. The self energy is represented diagrammatically by the Feynman diagrams in Fig.5.1 shown below. Vertex factors must be evaluated at the tree-level minimum $\cos\alpha = \frac{m_\pi^2}{\mu_I^2}$, in order to work consistently to next-to-leading order[44].

We introduce the following notation to refer to diagrams in Fig.5.1 in a consistent way;

- The 4-vertex diagram with π_i running in the loop is denoted as $-i\Sigma^{\pi_i}_{33(4\pi)}$. The diagram with a mixed loop propagator $\langle\pi_1\pi_2\rangle$ is denoted as $-i\Sigma^{\pi_1\pi_2}_{33(4\pi)}$.

- The 3-vertex diagram with π_i in one branch and π_j in the other branch is denoted as $-i\Sigma^{\pi_i\pi_j}_{33(3\pi)}$. Mixed propagators are denoted in the same way as above.

- The sum of the tadpole diagrams is denoted as $-i\Sigma^{\mathrm{T}}_{33}$.

- The renormalized diagrams are denoted with an additional "R" in the subscript. The sum of all of the renormalized diagrams is denoted as $-i\Sigma_{33R}$.

We use the newly defined notation to write the sum of the diagrams in Fig.5.1 as,

$$-i\Sigma_{33}(P^2,p_0) = -i\left[\Sigma^{\pi_1}_{33(4\pi)}(P^2,p_0) + \Sigma^{\pi_2}_{33(4\pi)}(P^2,p_0) + \Sigma^{\pi_3}_{33(4\pi)}(P^2,p_0) + \Sigma^{\pi_1\pi_2}_{33(4\pi)}(P^2,p_0) + \Sigma^{\pi_1\pi_3}_{33(3\pi)}(P^2,p_0) + \Sigma^{\partial_0\pi_2\pi_3}_{33(3\pi)}(P^2,p_0) + \Sigma^{(\partial_0\pi_2\pi_1)\pi_3}_{33(3\pi)}(P^2,p_0) + \Sigma^{\pi_3\pi_3}_{33(2\pi)}(P^2,p_0) + \Sigma^{\mathrm{T}}_{33}(P^2,p_0)\right], \tag{5.1}$$

where $P = (p_0, \vec{p})$ is the four-momentum of the external pion.

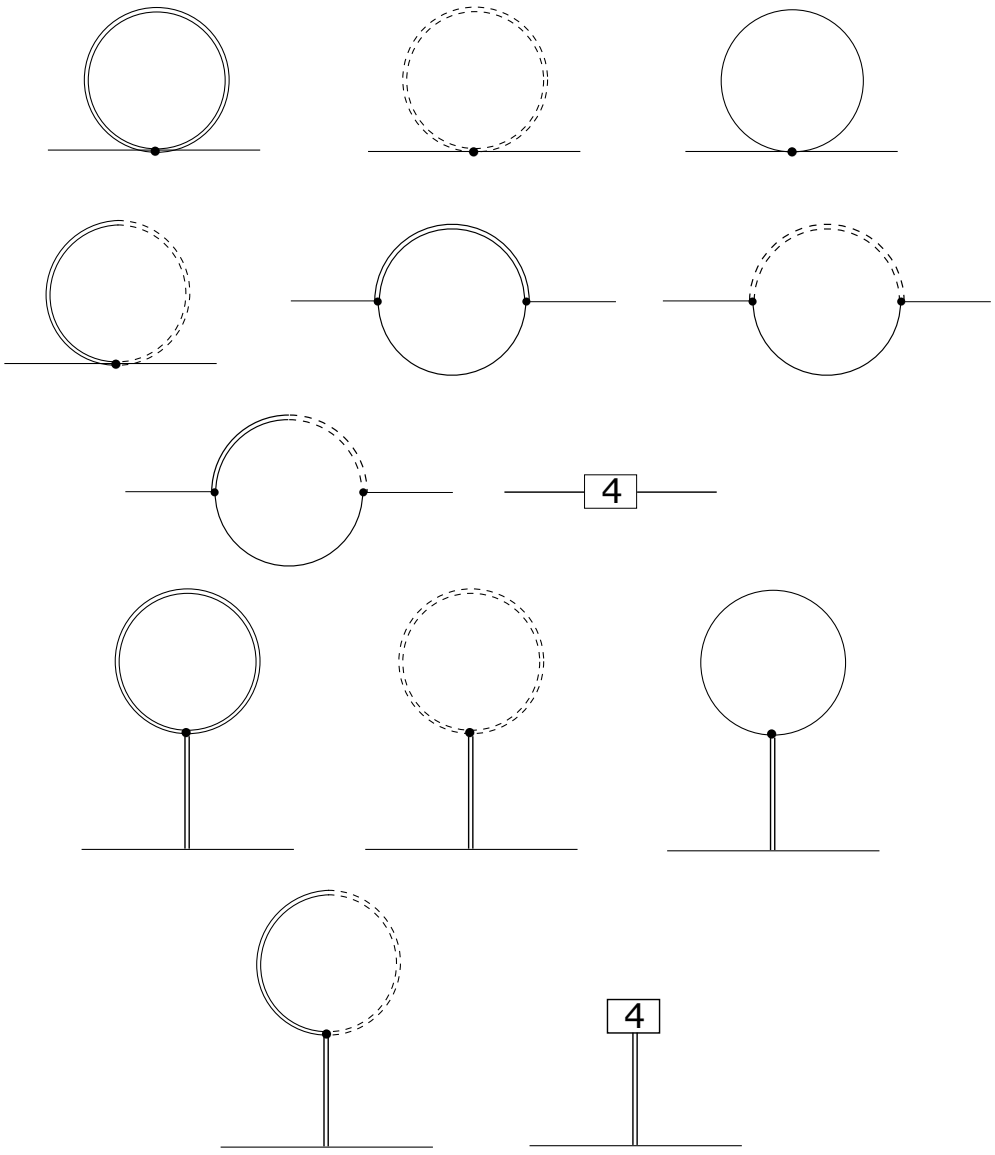

Figure 5.1: π_3 self-energy diagrams at next-to-leading order. The first four diagrams are one-loop corrections derived from $\mathcal{L}_2^{\text{quartic}}$, the next three diagrams are one-loop corrections derived from $\mathcal{L}_2^{\text{cubic}}$, and the last diagram in the third line is derived from $\mathcal{L}_4^{\text{quadratic}}$. The remaining diagrams are referred to as tadpole diagrams, and are derived from $\mathcal{L}_2^{\text{cubic}}$ and $\mathcal{L}_4^{\text{quadratic}}$.

In Appendix C.1 we show that the one-point function Γ^1 vanishes at next-to-leading order, which implies that the tadpole diagrams in Fig.5.1 also vanishes to working order.

At next-to-leading order the inverse propagator D_{33}^{-1} in Eq.(4.21) receives a nonzero

contribution from the self energy;

$$D_{33}^{-1} = P^2 - m_3^2 - \Sigma_{33R}(P^2, p_0). \tag{5.2}$$

The defining equation for the renormalized neutral pion mass m_{π^0} follows immediately,

$$m_{\pi^0}^2 = m_3^2 + \Sigma_{33R}(\vec{p} = 0). \tag{5.3}$$

The renormalized self energy $\Sigma_{33R}(P^2, p_0)$ in Eq.(5.3) is evaluated at the tree-level value for the neutral mass $P^2 = p_0^2 = m_3^2$.

The expressions for the one-point irreducible (1PI) self-energy diagrams shown in Fig.5.1 are listed below.

4-vertex diagrams

$$\Sigma_{33(4\pi)}^{\pi_1} = \left(\frac{2m_1^2}{3f^2} - \frac{m_{12}^2}{24f^2} - \frac{p^2}{3f^2}\right)(-i)\int_k \frac{k^2 - m_2^2}{(k_0^2 - E_{\pi^+}^2)(k_0^2 - E_{\pi^-}^2)} - \frac{1}{3f^2}(-i)\int_k \frac{k^2(k^2 - m_2^2)}{(k_0^2 - E_{\pi^+}^2)(k_0^2 - E_{\pi^-}^2)} \tag{5.4}$$

$$\Sigma_{33(4\pi)}^{\pi_2} = \left(\frac{m_1^2}{3f^2} - \frac{m_{12}^2}{24f^2} - \frac{p^2}{3f^2}\right)(-i)\int_k \frac{k^2 - m_1^2}{(k_0^2 - E_{\pi^+}^2)(k_0^2 - E_{\pi^-}^2)} - \frac{1}{3f^2}(-i)\int_k \frac{k^2(k^2 - m_1^2)}{(k_0^2 - E_{\pi^+}^2)(k_0^2 - E_{\pi^-}^2)} \tag{5.5}$$

$$\Sigma_{33(4\pi)}^{\pi_3} = \left(\frac{m_{12}^2}{8f^2} + \frac{2m_1^2}{f^2}\right)(-i)\int_k \frac{1}{k^2 - m_3^2} \tag{5.6}$$

$$\Sigma_{33(4\pi)}^{\pi_1\pi_2} = \frac{2m_{12}^2}{3f^2}(-i)\int_k \frac{k_0^2}{(k_0^2 - E_{\pi^+}^2)(k_0^2 - E_{\pi^-}^2)} \tag{5.7}$$

The 3-vertex diagrams

$$\Sigma_{33(3\pi)}^{\pi_1\pi_3} = -\frac{m_1^2 m_{12}^2}{4f^2}(-i)\int_k \frac{k^2 - m_2^2}{(k_0^2 - E_{\pi^+}^2)(k_0^2 - E_{\pi^-}^2)(q^2 - m_3^2)} \tag{5.8}$$

$$\Sigma_{33(3\pi)}^{\partial_0\pi_2\pi_3} = -\frac{4m_1^2}{f^2}(-i)\int_k \frac{k_0^2(k^2 - m_1^2)}{(k_0^2 - E_{\pi^+}^2)(k_0^2 - E_{\pi^-}^2)(q^2 - m_3^2)} \tag{5.9}$$

$$\Sigma_{33(3\pi)}^{(\partial_0\pi_2\pi_1)\pi_3} = \frac{2m_1^2 m_{12}^2}{f^2}(-i)\int_k \frac{k_0^2}{(k_0^2 - E_{\pi^+}^2)(k_0^2 - E_{\pi^-}^2)(q^2 - m_3^2)} \tag{5.10}$$

Counterterms

$$\Sigma_{33(2\pi)}^{\pi_3\pi_3} = (l_1 + l_2)\frac{4}{f^2}m_1^4 + l_4\frac{3}{4f^2}m_1^2 m_{12}^2 + (l_3 + l_4)\frac{1}{8f^2}m_{12}^4 - l_1\frac{4}{f^2}m_1^2 p^2 - l_4\frac{1}{2f}m_{12}^2 p^2 - l_2\frac{4}{f^2}m_1^2 p_0^2. \tag{5.11}$$

5.2 Renormalization

In order to renormalize the neutral pion mass we first have to isolate the divergent and scale dependent terms in Σ_{33}. This can be achieved by substituting the following series expansion,

$$\frac{1}{(k_0^2 - E_{\pi^+}^2)(k_0^2 - E_{\pi^-}^2)} = \frac{1}{(k_0^2 - E_1^2)(k_0^2 - E_2^2)} + \frac{m_{12}^2 k_0^2}{(k_0^2 - E_1^2)^2(k_0^2 - E_2^2)^2} + \frac{m_{12}^4 k_0^4}{(k_0^2 - E_1^2)^3(k_0^2 - E_2^2)^3} + ... \tag{5.12}$$

into the loop integrals on the right hand sides of Eqs.(5.4)-(5.5) and Eqs.(5.7)-(5.10). The substitution generates a finite number of divergent integrals in Eqs.(5.4)-(5.5) and Eqs.(5.7)-(5.10) that are rather straightforward to regularize using Feynman parameters.

We know that the sum of all divergent and scale-dependent terms in Σ_{33} has to vanish, since the one-loop generating functional is finite and scale independent[22]. In the following, we discuss how to obtain the contribution that each of the diagrams in Fig.5.1 render to the renormalized self energy. We refer to the contribution from one diagram to Σ_{33R} as "the renormalized diagram".

The contribution from Eq.(5.6) to the renormalized self-energy is obtained by carrying out a standard integral in dimensional regularization, and subsequently eliminate the divergent and scale-dependent terms from the result. The renormalized self-energy contributions associated with Eqs.(5.4)-(5.5) and Eqs.(5.7)-(5.10) can be obtained through the following procedure: Pick one of the diagrams. Use Eq.(5.12) to expand the loop integral that occurs in the expression for the diagram. Remove the divergent integrals that occur in the series expansion of the loop integral from the expression of the diagram. Evaluate the divergent integrals in the $\overline{\text{MS}}$ scheme, and add the finite and scale-independent terms in the results back to the expression for the diagram to obtain the renormalized diagram. Finally, sum all the renormalized diagrams to obtain the renormalized self energy. The result (i.e. the renormalized self energy) is a finite sum of divergent integrals, which formally evaluate to a finite number, plus an additional finite contribution from the regularization procedure and the counterterms in Eq.(5.11). The numerical values of the renormalized self energies are obtained by evaluating the (finite valued) sums of divergent integrals numerically.

Renormalizing Σ_{33} using $\cos\alpha = \frac{m_\pi^2}{\mu_I^2}$ in the loop integrals

A good portion of the time spent on this thesis was devoted to calculating m_{π^0} to next-to-leading order, with the *incorrect* assumption that we could use the tree-level relation $\cos\alpha = \frac{m_\pi^2}{\mu_I^2}$ in the loop-integrals. The loop-integrals should be evaluated at the next-to-leading order minimum for the calculation to be consistent.[1] We have nevertheless decided to include parts of the calculation in the following subsections for a couple of reasons. Firstly, the calculation serves as an illustration of the preceding discussion on how to renormalize the quasi-particle masses. Secondly, the result provides a non-trivial check of the future calculation, where we are going to treat α as a free parameter when we evaluate the loop integrals, as the result of the future calculation should reduce to the result we obtain here in the limit $\cos\alpha = \frac{m_\pi^2}{\mu_I^2}$.

In the subsection below, we present the divergent and scale-dependent terms associated with the 1PI self-energy diagrams. We proceed to present the renormalized diagrams,

[1] The difference between the leading-order minimum (red line) and the next-to-leading order minimum (blue line) can be studied in Fig.4.2.

whose sum Σ_{33R} is the (incorrect) next-to-leading order correction to the neutral medium-dependent pion mass. Details about the (divergent) integrals that are carried out to obtain the results below are found in Appendix E.

The divergent and scale dependent terms using $\cos\alpha = \frac{m_\pi^2}{\mu_I^2}$ in the loop integrals

$$\Sigma_{33(4\pi)}^{\pi_1 div} = \frac{1}{(4\pi f)^2}\left[\frac{m_1^2}{3} - \frac{5m_{12}^4}{96} - \frac{m_1^2 m_{12}^2}{24} - \frac{p^2}{3}\left(m_1^2 + \frac{m_{12}^2}{4}\right)\right]\left(\frac{1}{\epsilon} + \log\Lambda^2\right) \tag{5.13}$$

$$\Sigma_{33(4\pi)}^{\pi_2 div} = \frac{1}{(4\pi f)^2}\left[-\frac{5m_{12}^4}{96} - \frac{m_{12}^2}{12}p^2\right]\left(\frac{1}{\epsilon} + \log\Lambda^2\right) \tag{5.14}$$

$$\Sigma_{33(4\pi)}^{\pi_3 div} = \frac{1}{(4\pi f)^2}\left[m_3^2\left(\frac{m_{12}^2}{8} + 2m_1^2\right)\right]\left(\frac{1}{\epsilon} + \log\Lambda^2\right) \tag{5.15}$$

$$\Sigma_{33(4\pi)}^{\pi_1\pi_2 div} = \frac{1}{(4\pi f)^2}\left[\frac{2m_{12}^2}{3}\left(\frac{m_1^4}{4} + \frac{m_{12}^2}{8}\right)\right]\left(\frac{1}{\epsilon} + \log\Lambda^2\right) \tag{5.16}$$

$$\Sigma_{33(3\pi)}^{\pi_1\pi_3 div} = \frac{1}{(4\pi f)^2}\left[-\frac{m_1^2 m_{12}^2}{4}\right]\left(\frac{1}{\epsilon} + \log\Lambda^2\right) \tag{5.17}$$

$$\Sigma_{33(3\pi)}^{\partial_0\pi_2\pi_3 div} = \frac{1}{(4\pi f)^2}\left[-4m_1^2\left(\frac{m_3^2}{4} - \frac{p^2}{12} + \frac{p_0^2}{3} + \frac{m_{12}^2}{8}\right)\right]\left(\frac{1}{\epsilon} + \log\Lambda^2\right) \tag{5.18}$$

$$\Sigma_{33(3\pi)}^{(\partial_0\pi_2\pi_1)\pi_3 div} = \frac{1}{(4\pi f)^2}\left[\frac{m_1^2 m_{12}^2}{2}\right]\left(\frac{1}{\epsilon} + \log\Lambda^2\right) \tag{5.19}$$

$$\begin{aligned}\Sigma_{33(2\pi)}^{\pi_3\pi_3 div} = \frac{1}{(4\pi f)^2}\Bigg[&-2m_1^4(\gamma_1+\gamma_2) - \frac{3m_1^2 m_{12}^2}{8}\gamma_4 - \frac{m_{12}^4}{16}(\gamma_3+\gamma_4)\\ &+2m_1^2 p^2\gamma_1 + \frac{m_{12}^2 p^2}{4}\gamma_4 + 2m_1^2 p_0^2\gamma_2\Bigg]\left(\frac{1}{\epsilon} + \log\Lambda^2\right)\end{aligned} \tag{5.20}$$

It is easy to verify that the sum of Eqs.(5.13)-(5.20) is zero.

Renormalized self energies using $\cos\alpha = \frac{m_\pi^2}{\mu_I^2}$ in the loop integrals

The following is an overview of the renormalized self energies. They are obtained by following the procedure that we outlined at the beginning of this section. The scale dependence in $\Sigma_{33(2\pi)}^{\pi_3\pi_3}$ cancels the scale-dependence of the remaining self-energy diagrams. We have, for simplicity, added the $\log m^2$ terms, which accompanies the $\log\Lambda^2$ terms in $\Sigma_{33(2\pi)}^{\pi_3\pi_3}$, to the remaining renormalized self energies.

$$\Sigma^{\pi_1}_{33(4\pi)R} = \left(\frac{m_1^2}{3f^2} - \frac{m_{12}^2}{8f^2}\right)(-i)\left[\int_k \frac{k^2}{(k_0^2 - E^2_{\pi^+})(k_0^2 - E^2_{\pi^-})} - \int_k \frac{1}{(k^2 - m_1^2)}\right.$$
$$\left. - \int_k \frac{m_{12}^2 k_0^2}{(k^2 - m_1^2)^2 k^2}\right] - \frac{1}{3f^2}(-i)\left[\int_k \frac{k^4}{(k_0^2 - E^2_{\pi^+})(k_0^2 - E^2_{\pi^-})}\right.$$
$$\left. - \int_k \frac{k^2}{k^2 - m_1^2} - \int_k \frac{m_{12}^2 k_0^2}{(k^2 - m_1^2)^2} - \int_k \frac{m_{12}^4 k_0^4}{(k^2 - m_1^2)^3 k^2}\right]$$
$$- \frac{1}{(4\pi f)^2}\left[\frac{17}{576}m_{12}^4 + \frac{1}{4}m_1^2 m_{12}^2 + \left(\frac{7}{96}m_{12}^4 + \frac{5}{24}m_1^2 m_{12}^2\right)\log\frac{m^2}{m_1^2}\right] \tag{5.21}$$

$$\Sigma^{\pi_2}_{33(4\pi)R} = -\frac{m_{12}^2}{8f^2}(-i)\left[\int_k \frac{(k^2 - m_1^2)}{(k_0^2 - E^2_{\pi^+})(k_0^2 - E^2_{\pi^-})} - \int_k \frac{1}{k^2} - \int_k \frac{m_{12}^2 k_0^2}{(k^2 - m_1^2)k^4}\right]$$
$$- \frac{1}{3f^2}(-i)\left[\int_k \frac{k^2(k^2 - m_1^2)}{(k_0^2 - E^2_{\pi^+})(k_0^2 - E^2_{\pi^-})} - \int_k 1 - \int_k \frac{m_{12}^2 k_0^2}{(k^2 - m_1^2)k^2} - \int_k \frac{m_{12}^4 k_0^4}{(k^2 - m_1^2)^2 k^4}\right]$$
$$- \frac{1}{(4\pi f)^2}\left[\frac{47}{576}m_{12}^4 + \frac{1}{8}m_1^2 m_{12}^2 + \left(\frac{7}{96}m_{12}^4 + \frac{1}{12}m_1^2 m_{12}^2\right)\log\frac{m^2}{m_1^2}\right] \tag{5.22}$$

$$\Sigma^{\pi_3}_{33(4\pi)R} = \frac{1}{(4\pi f)^2}\left(2m_1^4 + \frac{5}{8}m_1^2 m_{12}^2 + \frac{1}{32}m_{12}^4\right)\left(1 + \log\frac{m^2}{m_3^2}\right) \tag{5.23}$$

$$\Sigma^{\pi_1\pi_2}_{33(4\pi)R} = \frac{2m_{12}^2}{3f^2}(-i)\left[\int_k \frac{k_0^2}{(k_0^2 - E^2_{\pi^+})(k_0^2 - E^2_{\pi^-})} - \int_k \frac{k_0^2}{(k^2 - m_1^2)(k^2)} - \int_k \frac{m_{12}^2 k_0^4}{(k^2 - m_1^2)^2 (k^2)^2}\right]$$
$$+ \frac{1}{(4\pi f)^2}\left[\frac{m_1^2 m_{12}^2}{6}\left(\frac{3}{2} + \log\frac{m^2}{m_1^2}\right) + \frac{m_{12}^4}{12}\left(\frac{5}{6} + \log\frac{m^2}{m_1^2}\right)\right] \tag{5.24}$$

$$\Sigma^{\pi_1\pi_3}_{33(3\pi)R} = -\frac{m_1^2 m_{12}^2}{4f^2}(-i)\left[\int_k \frac{k^2}{(k_0^2 - E^2_{\pi^+})(k_0^2 - E^2_{\pi^-})(q^2 - m_3^2)} - \int_k \frac{1}{(k^2 - m_1^2)(q^2 - m_3^2)}\right.$$
$$\left. - \frac{i}{(4\pi)^2}\int_0^1 dx\Theta(1-x)\Theta(x)\log\left[m_1^2(1-x) + m_3^2 x^2\right] + i\frac{\log m^2}{(4\pi)^2}\right] \tag{5.25}$$

$$\Sigma^{\partial_0\pi_2\pi_3}_{33(3\pi)R} = -\frac{4m_1^2}{f^2}(-i)\left[\int_k \frac{k_0^2(k^2 - m_1^2)}{(k_0^2 - E^2_{\pi^+})(k_0^2 - E^2_{\pi^-})(q^2 - m_3^2)} - \int_k \frac{k_0^2}{k^2(q^2 - m_3^2)}\right.$$
$$- \int_k \frac{m_{12}^2 k_0^4}{k^4(k^2 - m_1^2)(q^2 - m_3^2)} - \frac{i m_{12}^2}{2(4\pi)^2}\int_0^1 dx\int_0^{1-x} dy\Theta[1-x-y, x+y]\left(\frac{3y}{2}\log\Delta\right.$$
$$\left.\left. + \frac{6yx^2}{\Delta}p_0^2 - \frac{2yx^4}{\Delta^2}p_0^4\right)\right] - \frac{1}{(4\pi f)^2}\left[\left(\frac{2m_1^4}{3} + \frac{m_1^2 m_{12}^2}{6}\right)\left(\frac{5}{3} + \log\frac{m^2}{m_3^2}\right) + \right.$$
$$\left.\frac{4m_1^2 p_0^2}{3}\left(\frac{2}{3} + \log\frac{m^2}{m_3^2}\right) + \frac{m_1^2 m_{12}^2}{2}\log m^2\right], \quad \text{where} \quad \Delta \equiv m_3^2 x^2 + m_1^2 y. \tag{5.26}$$

$$\Sigma^{(\partial_0\pi_2\pi_1)\pi_3}_{33(3\pi)R} = \frac{2m_1^2 m_{12}^2}{f^2}(-i)\int_k \left[\frac{k_0^2}{(k_0^2 - E^2_{\pi^+})(k_0^2 - E^2_{\pi^-})(q^2 - m_3^2)} - \int_k \frac{k_0^2}{k^2(k^2 - m_1^2)(q^2 - m_3^2)}\right]$$
$$+ \frac{2m_1^2 m_{12}^2}{(4\pi)^2 f^2}\left[\frac{\log m^2}{4} - \frac{1}{2}\int_0^1 dy\int_0^{1-y}\Theta[1-x-y, x+y]\log\left(m_1^2 x + m_3^2 y^2\right)dx\right.$$
$$\left. - \frac{p_0^2}{m_1^2}\int_0^1 x^2\log\left(\frac{m_1^2 - m_1^2 x + m_3^2 x^2}{m_3^2 x^2}\right)dx\right] \tag{5.27}$$

$$\Sigma^{\pi_3\pi_3}_{33(2\pi)R} = \frac{1}{(4\pi f)^2}\left[\frac{m_{12}^4}{32}(1-\bar{l}_3) + \frac{m_1^2 m_{12}^2}{2}\left(\frac{\bar{l}_4}{2} - \frac{\bar{l}_1}{3} - \frac{1}{6}\right) + \frac{4m_1^4}{3}(\bar{l}_2 - 1) - \frac{4m_1^2 p_0^2}{3}(\bar{l}_2 - 1)\right] \tag{5.28}$$

$$\Sigma^{\mathrm{T}}_{33\mathrm{R}} = 0, \tag{5.29}$$

The integrals that occur in the equations above have been Wick rotated to Euclidean space and evaluated numerically with adaptive quadratures. All of the renormalized self energies converge steadily for increasingly larger integration boundaries.

In Fig.5.2, we display the result for m_{π^0} that we have obtained by using $\cos\alpha = \frac{m_\pi^2}{\mu_I^2}$ in the loop integrals. The blue dashed curve shows the next-to-leading-order result, while the red curve shows the tree-level result. We observe that the difference between the two curves is tiny. Finally, we emphasize that this plot does not represent the true χPT result to next-to-leading order, and should not be used to compare χPT with lattice data or effective-model results. However, it should provide a fair indication of the order of magnitude of the next-to-leading-order correction to the neutral pion mass.

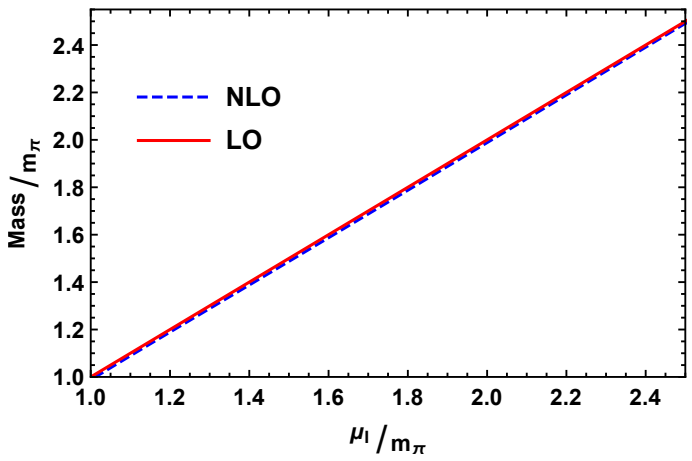

Figure 5.2: The normalized neutral pion mass in the pion-condensed phase as a function of the normalized isospin chemical potential. The red curve shows the leading-order result and the blue dashed curve shows the next-to-leading-order result when the loop integrals are evaluated at $\cos\alpha = \frac{m_\pi^2}{\mu_I^2}$ (which is inconsistent to next-to-leading order).

Chapter 6

The charged quasi-particles

In this chapter, we will focus on the two electrically charged quasi-particle modes $\pi^{\pm}$. It is considerably more challenging to obtain the isospin-dependent masses of the charged quasi-particles compared to the neutral pion, due to the mixing of the charge eigenstates in the pion-condensed phase. In the first section, we start by taking a closer look at the nature of this mixing. We proceed to show that the π^{+}-mode remains massless to next-to-leading order in the low-energy expansion and end the chapter with an outlook of how to proceed with the renormalization of the remaining charged mode. Feynman diagrams, algebraic expressions, and calculations that are relevant to our discussion are found in Appendices C and D.

The inverse propagator in Eq.(4.22) is Hermitian, so there has to exist a unitary matrix U such that $U^{\dagger}D_{12}^{-1}U$ is diagonal.[1] We find that it is useful to define a matrix A as,

$$A = \begin{pmatrix} \frac{i\left(-m_1^2+m_2^2+\sqrt{(m_1^2-m_2^2)^2+4m_{12}^2k_0^2}\right)}{2p_0m_{12}} & \frac{1}{\frac{2p_0m_{12}}{m_1^2-m_2^2+\sqrt{(m_1^2-m_2^2)^2+4m_{12}^2p_0^2}}} \\ -i & \end{pmatrix}, \tag{6.1}$$

to help us write the matrix U as,

$$U = \frac{A}{|\det A|}. \tag{6.2}$$

The matrix U relates the mass-eigenstates to π_1 and π_2 as follows,

$$\begin{pmatrix} \pi^- \\ \pi^+ \end{pmatrix} = U \begin{pmatrix} \pi_2 \\ \pi_1 \end{pmatrix} \tag{6.3}$$

In the normal phase $\alpha = 0$ we have $m_1^2 = m_2^2$, and the relation in Eq.(6.3) reduces to

$$\begin{pmatrix} \pi^- \\ \pi^+ \end{pmatrix} = \begin{pmatrix} \frac{i}{\sqrt{2}} & \frac{1}{\sqrt{2}} \\ -\frac{i}{\sqrt{2}} & \frac{1}{\sqrt{2}} \end{pmatrix} \begin{pmatrix} \pi_2 \\ \pi_1 \end{pmatrix}. \tag{6.4}$$

Thus, we recover that the charged eigenstates are mass eigenstates in the normal phase, as we should.

In the chiral limit $\alpha \to \frac{\pi}{2}$ we see that the matrix element A_{22} vanishes, and by applying L'Hôpital's rule to A_{11} we obtain,

$$\begin{pmatrix} \pi^- \\ \pi^+ \end{pmatrix} = \begin{pmatrix} 0 & 1 \\ -i & 0 \end{pmatrix} \begin{pmatrix} \pi_2 \\ \pi_1 \end{pmatrix}, \tag{6.5}$$

[1] More precisely, the vectors in $U^{\dagger}$ are orthonormal eigenvectors of D_{12}^{-1}.

The result in Eq.(6.5) is consistent with the discussion in chapter 4.1, where we argued that $\{\pi_1, \pi_2, \pi_3\}$ becomes the mass eigenstate basis in the chiral limit.

Multiplying the matrix in Eq.(6.1) with the matrix in Eq.(6.4) gives the relationship between the charge eigenstates and the mass eigenstates. As $\alpha \neq 0$, we see that $m_1^2 \neq m_2^2$, which makes the mixing of charge eigenstates in the pion-condensed phase manifest. It is interesting to see that the mixing angles are energy-dependent, which is a consequence of the broken generators of Lorentz boosts.

The mixing of isospin eigenstates makes it quite challenging to obtain the self energies of the charged quasi-particle modes in the pion-condensed phase. One possible approach to determine the renormalized masses is to use the relation in Eq.(6.3) to rewrite the Lagrangian in the mass-eigenstate basis, which makes the remaining calculation similar to that of the neutral pion. Such a transformation will, however, make the interaction terms much more complicated and most likely increase the number of diagrams that we need to evaluate. A second approach is to calculate the self-energies Σ_{11}, Σ_{22}, and Σ_{12}, and determine the zeros of the inverse propagator in the $\{\pi_i\}$ basis. We will employ the second approach in the following.

The inverse propagator to next-to-leading order reads,

$$D_{12}^{-1} = \begin{pmatrix} P^2 - m_1^2 - \Sigma_{11}(P^2, p_0) & ip^0 m_{12} + \Sigma_{12}(P^2, p_0) \\ -ip^0 m_{12} + \Sigma_{21}(P^2, p_0) & P^2 - m_2^2 - \Sigma_{22}(P^2, p_0) \end{pmatrix}. \tag{6.6}$$

Since the theory is invariant under time-reversal we expect one off-diagonal entry to be the time reversed of the other off-diagonal entry in the matrix above. In other words, if T is the time-reversal operator, then the following must be true,[2]

$$\begin{aligned} T\left(ip^0 m_{12} + \Sigma_{12}\right) &= -ip^0 m_{12} + T(\Sigma_{12}) = -ip^0 m_{12} + \Sigma_{21} \\ \implies \mathrm{Re}(\Sigma_{12}) &= \mathrm{Re}(\Sigma_{21}), \qquad \mathrm{Im}(\Sigma_{12}) = -\mathrm{Im}(\Sigma_{12}). \end{aligned} \tag{6.7}$$

Since Σ_{12} is purely imaginary we may write the inverse propagator as,

$$D_{12}^{-1} = \begin{pmatrix} P^2 - m_1^2 - \Sigma_{11}(P^2, p_0) & ip^0 m_{12} + \Sigma_{12}(P^2, p_0) \\ -ip^0 m_{12} - \Sigma_{12}(P^2, p_0) & P^2 - m_2^2 - \Sigma_{22}(P^2, p_0) \end{pmatrix}, \tag{6.8}$$

which is a Hermitian 2×2 matrix.

The charged quasi-particle masses are obtained by solving

$$\det D_{12}^{-1} = 0, \tag{6.9}$$

at vanishing spatial momentum, with the self energies evaluated at the tree-level masses given in Eq.(4.33). The presence of $\Sigma_{12}(P^2, p_0)$ makes the next-to-leading-order expressions for the quasi-particle masses much more complicated than the tree-level results in Eq.(4.31). However, the complicated solution to Eq.(6.9) simplifies considerably for the π^+ mode, as we will see in the following section.

6.1 Goldstone boson

In chapter 4, we derived the tree-level result $m_\pi^+ = 0$ for $\mu_I \geq m_\pi$. This result should hold to all orders in the low-energy expansion to be consistent with Goldstone's theorem. In this section, we go beyond the leading order and show that the π^+-mode remains massless at next-to-leading order in the low-energy expansion.

[2] T acts on a complex number by complex conjugation, i.e if $c \in \mathbb{C}$, then $Tc = c^*$. Since the operation of complex conjugation is nonlinear T is referred to as an antilinear operator.

We have explicitly checked that all diagrams that may contribute to the off-diagonal entry Σ_{12} in the self-energy matrix vanishes at $P^2 = p_0 = 0$. This property holds to all orders in the momentum expansion, due to time-reversal symmetry. Vanishing off-diagonal entries in the self-energy matrix puts Eq.(6.8) on the same form as Eq.(4.22), which implies that we can write $m^2_{\pi^+}$ as follows,

$$m^2_{\pi^+} = \frac{1}{2}\Big(m_1^2 + \Sigma_{11}(0) + m_2^2 + \Sigma_{22}(0) + m_{12}^2 \\ - \sqrt{\left[m_1^2 + \Sigma_{11}(0) + m_2^2 + \Sigma_{22}(0) + m_{12}^2\right]^2 - 4\left[m_1^2 + \Sigma_{11}(0)\right]\left[m_2^2 + \Sigma_{22}(0)\right]}\Big). \tag{6.10}$$

We introduce the short-hand notation $\Sigma_{ij}(0,0) \equiv \Sigma_{ij}(0)$ in Eq.(6.10), and we will continue to use this notation in the remainder of this thesis.

It is easily seen from Eq.(6.10) that $m_2^2 + \Sigma_{22}(0) = 0$ is a sufficient condition for the mode to be massless. We show that this condition is satisfied in the BEC-phase $\mu_I \geq m_\pi$ in the following. The reader is referred to Appendices C.1 and C.2 for technical details.

Comparing Eq.(4.24) with Eq.(4.44) we see that,

$$m_2^2 = \frac{1}{f^2}\left(\frac{\cos\alpha}{\sin\alpha}\right)\frac{\partial\Omega_0}{\partial\alpha}. \tag{6.11}$$

In Appendix C.2 we show by explicit calculation that,

$$\Sigma_{22}(0) = \frac{1}{f^2}\left(\frac{\cos\alpha}{\sin\alpha}\right)\frac{\partial\Omega_1}{\partial\alpha} + ..., \tag{6.12}$$

where $\Omega_1 \equiv \Omega_1^{\text{loop}} + \Omega_1^{\text{static}}$. The terms we have omitted in Eq.(6.12) can be written on the following form,

$$\frac{C}{f^2}(\mu_I^2\cos\alpha - m^2)X, \tag{6.13}$$

where $\mu_I^2\cos\alpha - m^2$ arise from vertex factors, X is a one-loop integral, and C is a non-vanishing function of m, μ_I and α. This observation lets us write the sum of Eqs.(6.11) and (6.12) as,

$$m_2^2 + \Sigma_{22}(0) = \frac{1}{f^2}\left(\frac{\cos\alpha}{\sin\alpha}\right)\frac{\partial\Omega}{\partial\alpha} + \frac{C}{f^2}(\mu_I^2\cos\alpha - m^2)X. \tag{6.14}$$

The first term on the right-hand-side of the equation above is always zero, due to the condition in Eq.(4.65). The second term can clearly be written on the same form as Eq.(C.13), which we argued only have non-vanishing NNLO contributions in the BEC phase.[3] Thus, to working order we obtain,

$$m_2^2 + \Sigma_{22}(0) = 0, \qquad \mu_I \geq m_\pi. \tag{6.15}$$

The condition in Eq.(6.15) implies that Eq.(6.10) vanishes in the pion-condensed phase, so the theory continues to respect Goldstone's theorem at next-to-leading order in the momentum expansion.

6.2 Outlook

The remaining quasi-particle is, without doubt, the toughest one of the three to handle in the pion-condensed phase. The expression for $m^2_{\pi^-}$ is expected to take a much more

[3] See Appendix C.1 for details.

complicated form than Eq.(6.10), since we have no reason to believe that $\Sigma_{12}(m_1^2 + m_{12}^2)$ is zero. Therefore, it is not reasonable to believe that any of the self energies evaluated at $P^2 = p_0^2 = m_1^2 + m_{12}^2$ should be finite valued. Our only requirement is that the complicated expression for m_{π^-} becomes finite when the self energies are evaluated at the tree-level mass. This condition provides a non-trivial check of our calculations. We have postponed the renormalization of m_{π^-} to next-to-leading order, due to the complexity of the task. However, we will make some remarks on the remaining parts of this work.

In the previous section, we verified that $\Sigma_{22}(0)$ is finite, which indicates that our result for the momentum-independent divergent terms is correct. Similarly, obtaining a finite expression for $\Sigma_{11}(0)$ would strongly indicate that the momentum-independent divergent part of Σ_{11} is likely to be correct. The remaining divergent contributions originate from Σ_{12}, and momentum-dependent terms in Σ_{11} and Σ_{22}. These contributions can be checked by the requirement that m_{π^-} has to be finite valued when the self-energy diagrams are evaluated at the tree-level mass. These observations provide a couple of consistency checks that can become very useful as part of a troubleshooting procedure in future calculations.

Once the divergent terms have been taken care of, the rest of the calculation (i.e. obtaining a numerical result) follows the procedure outlined at the beginning of section 5.2.

Part III

Quark and pion condensates at finite isospin and temperature

Chapter 7

Quark and pion condensates at zero temperature

In this part of the thesis, which consists of chapters 7 and 8, we use two-flavor χPT to next-to-leading order to calculate the chiral and pion condensates. In chapter 7, we consider the zero-temperature limit and calculate the free energy, the chiral condensate, and the pion condensate at finite (pseudoscalar) pionic source. We compare our results for the chiral and pion condensates with recent $(2+1)$-flavor lattice QCD calculations performed by Brandt, Endrodi, and Schmalzbauer in Ref.[27], and find that they are in very good agreement. We also consider the condensates in the absence of a pionic source, where there are no available lattice data to compare with. This limit is currently quite challenging to perform on the lattice, and our results can be used to gauge the quality of future LQCD calculations at vanishing pionic source.

In Ref.[27], Brandt et al. also generate the chiral and pion condensates at finite temperature. Furthermore, they investigate the phase boundary between the normal and pion-condensed phases, as well as the chiral crossover transition. Although low-temperature[111] and low-density[114] approximations of the phase boundary between the normal phase and the BEC phase have previously been obtained within the χPT framework, there are no complete[1] results within χPT at finite temperature to compare Brandt et al.'s results with. In chapter 8, we fill this gap in the QCD literature by extending the analysis in chapter 7 to finite temperature.

7.1 Preliminaries

We start this chapter by discussing how the chiral and pion condensates are generated within full QCD and χPT, before we proceed to introduce the effective pionic-source-dependent Lagrangian.

The pionic source

The formation of a pion-condensate is signaled by a nonzero expectation value of one of the following operators,

$$\bar{q}i\gamma_5\tau_i q \sim (\bar{u}\gamma_5 d - \bar{d}\gamma_5 u) \sim \pi^- - \pi^+, \qquad i = 1, 2. \tag{7.1}$$

We will, without loss of generality, use $i = 1$ in the following. The expectation value of the operator in Eq.(7.1) at finite μ_I in the microscopic theory is obtained by varying the

[1] By complete results we mean results that are obtained without utilizing any additional assumptions or approximations in the calculations.

generating functional in Eq.(2.30) with respect to the external (source) field p_1, and set all external fields (except from s_0 and v_3^μ) to zero.[2] For this reason, p_1 is usually referred to as the *pionic source* and commonly denoted as $j \equiv p_1$[47, 48, 111].

The expectation value of the pion operator π^+ in the effective theory is generated by differentiating the effective free energy with respect to the pionic source. We follow the convention[3] in Ref.[47], and write

$$\langle \pi^+ \rangle = \frac{1}{2} \frac{\partial \Omega}{\partial j}. \tag{7.2}$$

The way j enters the effective theory is dictated by the symmetries of the chiral Lagrangian. In section 2.3 we showed how the field χ enters the effective Lagrangian at leading order in Eq.(2.69), and next-to-leading order in Eq.(2.82), by only invoking symmetry arguments. The pseudoscalar pionic sourcefield p_1 is encoded into the definition of the field χ, as shown in Eq.(2.61). Thus, we obtain the j-dependent chiral Lagrangian to next-to-leading order in the low-energy expansion by substituting $\chi = 2B_0 \left[\mathrm{diag}(m_u, m_d) + i\tau_1 j\right]$ into Eqs.(2.69) and (2.82).

Our primary motivation for calculating the pion condensate is to study the phase diagram to next-to-leading order in χPT, and to compare results with recent lattice simulations. In order to obtain the phase diagram at vanishing external fields and sources, we need to take the limit $j \to 0$ at the end of our calculations. It has been shown that evaluating this limit does not lead to any problems within the effective theory[47].

The situation on the lattice is more complicated for several reasons. The LQCD simulations are performed over a finite volume, where there can be no SSB.[4] However, the presence of $j\bar{q}i\gamma_5\tau_{1,2}q$ in the (Euclidean) QCD Lagrangian explicitly breaks the $U(1)_{I_3}$ symmetry. Such a term is necessary for the SSB to happen on the lattice, and makes the would-be-massless mode a massive pseudo-Goldstone boson. The physical limit $j \to 0$ can be obtained subsequently by extrapolation[27].

A nonzero pionic source is needed to stabilize the lattice algorithms, and the physical limit $j \to 0$ remains technically challenging to perform, see Ref.[27] for details. Consequently, there is a lack of LQCD data for the most interesting case $j = 0$. Comparing χPT results with LQCD data at finite j should nevertheless provide a good indication of the level of agreement that we can expect between the effective theory and the microscopic theory in the physically interesting limit $j = 0$.

Generating $\langle \bar{q}q \rangle$

The quark condensate $\langle \bar{q}q \rangle = \langle \bar{u}u \rangle + \langle \bar{d}d \rangle$ in the microscopic theory is obtained by varying the generating functional in Eq.(2.30) with respect to $s^0 = \mathrm{diag}(m_u, m_d)$,

$$\langle \bar{q}q \rangle = -\frac{\delta W}{\delta s^0}. \tag{7.3}$$

The quark condensate in the effective theory is obtained by differentiating the effective free energy with respect to the quark masses. In the isospin limit $m_u = m_d \equiv m_q$, the up and down quark condensates become equal $\langle \bar{u}u \rangle = \langle \bar{d}d \rangle = \frac{1}{2}\langle \bar{q}q \rangle$. Following Ref.[47], we define $\langle \bar{\psi}\psi \rangle$ to be equal to $\frac{1}{2}\langle \bar{q}q \rangle$,

$$\langle \bar{\psi}\psi \rangle \equiv \frac{1}{2} \frac{\partial \Omega}{\partial m_q}. \tag{7.4}$$

[2] Remember that the external fields s_0 and v_3^μ corresponds to the quark mass and the isospin chemical potential, respectively.

[3] The convention we are referring to is the additional factor of $\frac{1}{2}$.

[4] At finite volume, the transition amplitude from one ground state to another does not necessarily vanish.

7.2 Lagrangian

We derive the relevant terms in the χPT Lagrangian at finite isospin chemical potential and finite (pseudoscalar) pionic source in terms of the pion fields in Appendices B.3 and B.4. In the notation of Ref.[47], the result reads,

$$\mathcal{L}_2^{\text{static}} = 2f^2 B_0 m_j + \frac{1}{2} f^2 \mu_I^2 \sin^2\alpha, \tag{7.5}$$

$$\mathcal{L}_2^{\text{linear}} = f\left(-2B_0\overline{m}_j + \mu_I^2 \sin\alpha\cos\alpha\right)\pi_1 + f\mu_I \sin\alpha\partial_0\pi_2, \tag{7.6}$$

$$\mathcal{L}_2^{\text{quadratic}} = \frac{1}{2}\partial_\mu\pi_a\partial^\mu\pi_a + \frac{1}{2}m_a^2\pi_a^2 + \mu_I\cos\alpha\left(\pi_1\partial_0\pi_2 - \pi_2\partial_0\pi_1\right), \tag{7.7}$$

$$\mathcal{L}_4^{\text{static}} = (l_1+l_2)\mu_I^4\sin^4\alpha + 2l_4B_0m_j\mu_I^2\sin^2\alpha + 4(l_3+l_4)B_0^2m_j^2 + 8h_1B_0^2(m_j^2+\overline{m}_j^2), \tag{7.8}$$

where the source-dependent masses are,

$$m_j = m_q\cos\alpha + j\sin\alpha, \tag{7.9}$$

$$\overline{m}_j = m_q\sin\alpha - j\cos\alpha, \tag{7.10}$$

$$m_1^2 = 2B_0m_j - \mu_I^2\cos 2\alpha, \tag{7.11}$$

$$m_2^2 = 2B_0m_j - \mu_I^2\cos^2\alpha, \tag{7.12}$$

$$m_3^2 = 2B_0m_j + \mu_I^2\sin^2\alpha. \tag{7.13}$$

The definition of m_{12} in Eq.(4.26) is unaltered by finite j. The inverse propagator and dispersion relations at finite j are obtained by substituting Eqs.(7.11)-(7.13) into Eq.(4.21) and (4.27)-(4.28), respectively.

7.3 Tree-level analysis

The leading-order contribution to the free energy Ω_0 is given by $-\mathcal{L}_2^{\text{static}}$,

$$\Omega_0 = -2f^2B_0m_j - \frac{1}{2}f^2\mu_I^2\sin^2\alpha. \tag{7.14}$$

Minimizing the free energy with respect to α yields,

$$\frac{\partial\Omega_0}{\partial\alpha} = 2B_0\overline{m}_j - \mu_I^2\sin\alpha\cos\alpha = 0. \tag{7.15}$$

Comparing Eq.(7.6) with Eq.(7.15) we see that the linear Lagrangian vanishes at the leading-order minimum of the free energy.

We use the free energy in Eq.(7.14) and the definitions in Eqs.(7.2) and (7.4) to obtain the following tree-level results for the condensates[92],

$$\langle\bar\psi\psi\rangle_{\mu_I,0}^{\text{tree}} = -f^2B_0\cos\alpha = \langle\bar\psi\psi\rangle_{0,0}^{\text{tree}}\cos\alpha, \tag{7.16}$$

$$\langle\pi^+\rangle_{\mu_I,0}^{\text{tree}} = -f^2B_0\sin\alpha = \langle\bar\psi\psi\rangle_{0,0}^{\text{tree}}\sin\alpha. \tag{7.17}$$

Here $\langle O\rangle_{\mu_I,T}$ denotes the expectation value of the operator O at isospin chemical potential μ_I and temperature T. The equations above suggest that α can be interpreted as an angle that rotates the chiral condensate into a pion condensate. In particular,

$$\langle\bar\psi\psi\rangle_{\mu_I,0}^2 + \langle\pi^+\rangle_{\mu_I,0}^2 = \langle\bar\psi\psi\rangle_{0,0}^2. \tag{7.18}$$

This interpretation of α does not seem to be very fundamental as it is lost at next-to-leading order in the effective theory[47], and it is not observed either on the lattice[27] or in model-dependent calculations within the Nambu-Jona-Lasinio (NJL) model[115].

To analyze the condensates beyond leading order, we first have to renormalize the free energy in the presence of the pionic source j. In the following section, we renormalize Ω to next-to-leading order, which is a straightforward generalization of the calculation in section 4.2 that includes the effects of finite j.

7.4 Next-to-leading-order analysis

In this section, we calculate the free energy, the quark condensate, and the pion condensate at finite (pseudoscalar) pionic source. We then proceed to introduce and discuss the observables that we will plot in section 7.5.

Free energy at nonzero j

The static contribution Ω_1^{static} to the free energy at next-to-leading order is given by $-\mathcal{L}_4^{\text{static}}$;

$$\Omega_1^{\text{static}} = -(l_1+l_2)\mu_I^4 \sin^4\alpha - 2l_4 B_0 m_j \mu_I^2 \sin^2\alpha - 4(l_3+l_4)B_0^2 m_j^2 - 8h_1 B_0^2(j^2+m_q^2). \tag{7.19}$$

The one-loop contribution from $\mathcal{L}_2$ to the free energy is given by the formula in Eq.(4.51). Comparing Eq.(4.18) with Eq.(7.7) we see that the form of the quadratic Lagrangian at leading order $\mathcal{L}_2^{\text{quadratic}}$ is the same for vanishing and finite pionic source. To be specific, both Eq.(4.18) and Eq.(7.7) can be written as,

$$\mathcal{L}_2^{\text{quadratic}} = \frac{1}{2}\partial_\mu \pi_a \partial^\mu \pi_a + \frac{1}{2} m_a^2 \pi_a^2 + \mu_I \cos\alpha\,(\pi_1 \partial_0 \pi_2 - \pi_2 \partial_0 \pi_1)\,, \tag{7.20}$$

where the parameters m_a are given by Eqs.(4.23)-(4.25) and Eqs.(7.11)-(7.13) for the two cases, respectively. For this reason, the one-loop calculation of the free energy at finite j can be performed by following the one-loop calculation in chapter 4.3 step by step.

The renormalized free energy at finite pionic source can be expressed on the following form,

$$\Omega_1^{\text{loop}} = \Omega_{1,\pi^0} + \Omega_{1,\pi^+}^{\text{div}} + \Omega_{1,\pi^-}^{\text{div}} + \Omega_{1,\pi^+}^{\text{fin}} + \Omega_{1,\pi^-}^{\text{fin}}, \tag{7.21}$$

where the terms on the right-hand side of Eq.(7.21) can be written as,

$$\Omega_{1,\pi^0} + \Omega_{1,\pi^+}^{\text{div}} + \Omega_{1,\pi^-}^{\text{div}} = -\frac{\tilde{m}_1^4}{2(4\pi)^2}\left[\frac{1}{\epsilon} + \frac{3}{2} + \log\frac{\Lambda^2}{\tilde{m}_1^2}\right] - \frac{\tilde{m}_2^4}{4(4\pi)^2}\left[\frac{1}{\epsilon} + \frac{3}{2} + \log\frac{\Lambda^2}{\tilde{m}_2^2}\right], \tag{7.22}$$

$$\Omega_{1,\pi^+}^{\text{fin}} + \Omega_{1,\pi^-}^{\text{fin}} = \frac{1}{2}\int_p (E_{\pi^+} + E_{\pi^-} - E_1 - E_2), \tag{7.23}$$

where,

$$E_i = \sqrt{p^2 + \tilde{m}_i^2}, \qquad \tilde{m}_1^2 = m_3^2, \qquad \tilde{m}_2^2 = 2B_0 m_j. \tag{7.24}$$

Using Eq.(3.16)-(3.23) we find that the sum $\Omega_1^{\text{loop}} + \Omega_1^{\text{static}}$ is finite and scale independent, and obtain the following expression for the renormalized free energy at next-to-leading order in the effective theory[47],

$$\begin{aligned}\Omega_{\text{eff}} = {} & -2f^2 B_0 m_j - \frac{1}{2} f^2 \mu_I^2 \sin^2\alpha - \frac{1}{(4\pi)^2}\left[\frac{3}{2} - \bar{l}_3 + 4\bar{l}_4 + \log\frac{2B_0 m_q}{\tilde{m}_2^2} + 2\log\frac{2B_0 m_q}{m_3^2}\right] B_0^2 m_j^2 \\ & - \frac{1}{(4\pi)^2}\left[1 + 2\bar{l}_4 + 2\log\frac{2B_0 m_q}{m_3^2}\right] B_0 m_j \mu_I^2 \sin^2\alpha - \frac{1}{2(4\pi)^2}\left[\frac{1}{2} + \frac{1}{3}\bar{l}_3 + \frac{2}{3}\bar{l}_2 + \log\frac{2B_0 m_q}{m_3^2}\right] \\ & - 8h_1 B_0^2(j^2 + m_q^2) + \Omega_{1,\pi^+}^{\text{fin}} + \Omega_{1,\pi^-}^{\text{fin}}.\end{aligned} \tag{7.25}$$

In the limit of vanishing pionic source $j = 0$, Eq.(7.25) reduces to the result in Eq.(4.63), plus the constant term proportional to h_1 that we ignored in chapter 4. The h_1-term in Eq.(7.25) is independent of α and does not affect the ground state configuration Σ_α.

Having obtained the renormalized free energy in the presence of the external (pseudoscalar) pionic source j, we proceed to generate algebraic expressions for the pion and quark condensates to next-to-leading order. We will employ the following definition,

$$\bar{h}_1 \equiv 2(4\pi)^2 h_1, \tag{7.26}$$

to express our results in a way that is suitable for comparison with previously obtained results at $\mu_I = 0$.

Pion condensate

The pion condensate to next-to-leading order in the low-energy expansion at finite (pseudoscalar) pionic source j and finite isospin chemical potential μ_I is obtained by differentiating $\frac{1}{2}\Omega$ with respect to j. The result reads,

$$\begin{aligned}\langle \pi^+ \rangle_{\mu_I,0} = -f^2 B_0 \sin\alpha \Bigg\{ 1 + \frac{1}{(4\pi)^2} \Bigg[\left(-\bar{l}_3 + 4\bar{l}_4 + \log\frac{2B_0 m_q}{\tilde{m}_2^2} + 2\log\frac{2B_0 m_q}{m_3^2} \right) \frac{B_0 m_j}{f^2} \\ + \left(\bar{l}_4 + \log\frac{2B_0 m_q}{m_3^2} \right) \frac{\mu_I^2 \sin^2\alpha}{f^2} \Bigg] \Bigg\} - \frac{4}{(4\pi)^2} \bar{h}_1 B_0^2 j + \frac{1}{2} \left(\frac{\partial \Omega^{\rm fin}_{1,\pi^+}}{\partial j} + \frac{\partial \Omega^{\rm fin}_{1,\pi^-}}{\partial j} \right),\end{aligned} \tag{7.27}$$

where the last term on the right-hand side of Eq.(7.27) is given by,

$$\begin{aligned}\frac{\partial \Omega^{\rm fin}_{1,\pi^+}}{\partial j} + \frac{\partial \Omega^{\rm fin}_{1,\pi^-}}{\partial j} = \frac{B_0 \sin\alpha}{2} \Bigg\{ \int_k \frac{1}{E_{\pi^+}} \left[1 + \frac{m_{12}^2}{\sqrt{4k^2 m_{12}^2 + (m_1^2 + m_2^2 + m_{12}^2)^2 - 4m_1^2 m_2^2}} \right] \\ + \int_k \frac{1}{E_{\pi^-}} \left[1 - \frac{m_{12}^2}{\sqrt{4k^2 m_{12}^2 + (m_1^2 + m_2^2 + m_{12}^2)^2 - 4m_1^2 m_2^2}} \right] - \int_k \frac{1}{\sqrt{p^2 + \tilde{m}_1^2}} \\ - \int_k \frac{1}{\sqrt{p^2 + \tilde{m}_2^2}} \Bigg\}.\end{aligned} \tag{7.28}$$

We observe from Eq.(7.27) and Eq.(7.28) that the pion condensate at vanishing temperature $\langle \pi^+ \rangle_{\mu_I,0}$ is proportional to $\sin\alpha$. Consequently, the right-hand side of Eq.(7.27) reduces to zero in the sourceless normal phase $\alpha = j = 0$, as it should.

Quark condensate

The quark condensate to next-to-leading order in the low-energy expansion at finite (pseudoscalar) pionic source j and finite isospin chemical potential μ_I is obtained by differentiating $\frac{1}{2}\Omega$ with respect to the continuum quark mass m_q. The result reads,

$$\begin{aligned}\langle \bar{\psi}\psi \rangle_{\mu_I,0} = -f^2 B_0 \cos\alpha \Bigg\{ 1 + \frac{1}{(4\pi)^2} \Bigg[\left(-\bar{l}_3 + 4\bar{l}_4 + \log\frac{2B_0 m_q}{\tilde{m}_2^2} + 2\log\frac{2B_0 m_q}{m_3^2} \right) \frac{B_0 m_j}{f^2} \\ + \left(\bar{l}_4 + \log\frac{2B_0 m_q}{m_3^2} \right) \frac{\mu_I^2 \sin^2\alpha}{f^2} \Bigg] \Bigg\} - \frac{4}{(4\pi)^2} \bar{h}_1 B_0^2 m_q + \frac{1}{2} \left(\frac{\partial \Omega^{\rm fin}_{1,\pi^+}}{\partial m} + \frac{\partial \Omega^{\rm fin}_{1,\pi^-}}{\partial m} \right),\end{aligned} \tag{7.29}$$

where the last term on the right-hand side of Eq.(7.29) is given by,

$$\frac{\partial\Omega^{\rm fin}_{1,\pi^+}}{\partial m}+\frac{\partial\Omega^{\rm fin}_{1,\pi^-}}{\partial m}=\frac{B_0\cos\alpha}{2}\left\{\int_k\frac{1}{E_{\pi^+}}\left[1+\frac{m_{12}^2}{\sqrt{4k^2m_{12}^2+(m_1^2+m_2^2+m_{12}^2)^2-4m_1^2m_2^2}}\right]\right.$$
$$+\int_k\frac{1}{E_{\pi^-}}\left[1-\frac{m_{12}^2}{\sqrt{4k^2m_{12}^2+(m_1^2+m_2^2+m_{12}^2)^2-4m_1^2m_2^2}}\right]-\int_k\frac{1}{\sqrt{p^2+\tilde{m}_1^2}}$$
$$\left.-\int_k\frac{1}{\sqrt{p^2+\tilde{m}_2^2}}\right\}. \tag{7.30}$$

In the limit of vanishing pionic source and isospin chemical potential $j=\mu_I=0$, Eq.(7.30) vanishes and Eq.(7.29) reduces to,

$$\langle\bar{\psi}\psi\rangle^{\rm vacuum}_{0,0}=-f^2B_0\left[1+\frac{B_0m_q}{(4\pi)^2}\left(4\bar{l}_4+4\bar{h}_1-\bar{l}_3\right)\right]=-f^2B_0\left[1+\frac{m^2}{2(4\pi)^2}\left(4\bar{l}_4+4\bar{h}_1-\bar{l}_3\right)\right]. \tag{7.31}$$

We can compare our result in Eq.(7.31) with expressions obtained by Gasser and Leutwyler in Ref.[22];

$$\left\langle\bar{u}u+\bar{d}d\right\rangle^{\rm GL}_{0,0}=-2f^2B_0\left[1+\frac{m_\pi^2}{2(4\pi)^2}\left(4\bar{h}_1^{\rm GL}-\bar{l}_3\right)+O(m_\pi^4)\right], \tag{7.32}$$

which reduces to the following expression in the isospin limit,

$$\langle\bar{\psi}\psi\rangle^{\rm GL}_{0,0}=-f^2B_0\left[1+\frac{m_\pi^2}{2(4\pi)^2}\left(4\bar{h}_1^{\rm GL}-\bar{l}_3\right)+O(m_\pi^4)\right]. \tag{7.33}$$

The subscript GL is there to remind us that Gasser and Leutwyler use a different set of tensors and coupling constants in their Lagrangian. The coupling that they denote by h_1 is running and has $\delta_1^{\rm GL}=2$, as shown in Eq.(3.19) in section 3.2. The coupling constant that we denote by h_1 can be expressed in terms of Gasser and Leutwylers couplings as $h_1=\frac{1}{2}(h_1^{\rm GL}-l_4)$. It follows from Eqs.(3.18)-(3.19) that $\delta_1=1-1=0$, which is consistent with our calculation of the renormalized (scale-independent) free energy. Using the definition in Eq.(7.26) we obtain the following relation,

$$\bar{h}_1=\bar{h}_1^{\rm GL}-\bar{l}_4, \tag{7.34}$$

which is a convenient relation for later purposes.

We notice that the presence of h_1 in Eq.(7.27) and Eq.(7.29) spoils the tree-level relation $\langle\pi^+\rangle_{\mu_I,0}\cos\alpha=\langle\bar{\psi}\psi\rangle_{\mu_I,0}\sin\alpha$. If we consider the physical limit $j=0$, then the tree-level relation is modified into

$$\langle\bar{\psi}\psi\rangle_{\mu_I,0}=\frac{\cos\alpha}{\sin\alpha}\langle\pi^+\rangle_{\mu_I,0}-16h_1B_0^2m_q, \tag{7.35}$$

at next-to-leading order.

Definitions and choice of parameters

The low-energy constant $\bar{h}_1^{\rm GL}$ enters the full two-flavor χPT Lagrangian of Gasser and Leutwyler[22] as a counterterm needed to renormalize the generating functional to one loop. It does not multiply any of the terms that contain pion fields, so it is not directly measurable and in that sense *unphysical*. As $\bar{h}_1^{\rm GL}$ enters the (j-dependent) expectation value of the pion and quark condensates at next-to-leading order, the results in Eqs.(7.27)

and (7.29) depend on a quantity that is needed for technical reasons, but undeterminable from χPT alone[116].

We notice that the h_1 term in Eq.(7.29) is independent of both μ_I and j. Thus, we may eliminate the constant from the quark sector by considering quark-condensate *deviations*, rather than $\langle\bar{\psi}\psi\rangle_{\mu_I,0}$. As an example, we could choose the deviation of the quark condensate $\langle\bar{\psi}\psi\rangle_{\mu_I,0}$ relative to its vacuum-value $\langle\bar{\psi}\psi\rangle_{0,0}^{j=0}$. This quantity would measure the effects of finite j and finite μ_I, and be independent of the unphysical constant $\bar{h}_1^{\rm GL}$.

The situation for the pion condensate is a little more intricate, due to the j dependence of the h_1 term in Eq.(7.27). Thus, we cannot subtract away the h_1 dependence by considering pion-condensate deviations relative to the expectation value of π^+ in the vacuum. A possible resolution is to consider pion-condensate deviations relative to the source *dependent* vacuum $\langle\pi^+\rangle_{0,0}^{j}$, instead of $\langle\pi^+\rangle_{0,0}^{j=0}$. Such an observable would be independent of the unphysical constant $\bar{h}_1^{\rm GL}$, but it would also come with a setback, as it cannot measure the effects of finite j. Another possible resolution is to just estimate a numerical value for $\bar{h}_1^{\rm GL}$. Estimations of $\bar{h}_1^{\rm GL}$ have previously been performed by utilizing effective models [22], large N_c arguments [90] and constructing effective Lagrangians that include higher resonance fields [117]. In Ref.[90] Gerber and Leutwyler consider the effect of ρ-meson exchange to obtain $\bar{h}_1^{\rm GL} = \bar{l}_3$, which we will utilize as an indication of the magnitude of $\bar{h}_1$ in the next section. It should be mentioned that it is problematic to assume saturation of the unphysical constant $\bar{h}_1^{\rm GL}$ by meson resonances. This is discussed nicely by Jamin within the framework of three-flavor χPT in Ref.[116]. Due to the challenges associated with determining the unphysical low-energy constant $\bar{h}_1^{\rm GL}$, we propose that in future comparisons of χPT with LQCD at finite density one could determine $\bar{h}_1^{\rm GL}$ by fitting χPT to LQCD data in the vacuum $\mu_i = 0$.

On the lattice, the expectation value of the quark condensate $\langle\bar{q}q\rangle$ is obtained by differentiating the logarithm of the path-integral representation of the QCD partition function $\mathcal{Z}$ with respect to the continuum quark mass m_q. The partition function contains ultraviolet divergences (in the lattice spacing) which is inherited by the quark condensate.[5] The lattice-spacing divergences in the quark condensate can be eliminated by considering quark condensate deviations relative to the value of the condensate at fixed values for μ_I and j. The renormalized quantities that the authors in Ref.[27] consider in their LQCD calculations, and that the authors in Ref.[47] adapt in their χPT analysis are,[6]

$$\Sigma_{\bar{\psi}\psi} = -\frac{2m_q}{m_\pi^2 f_\pi^2}\left[\langle\bar{\psi}\psi\rangle_{\mu_I,0} - \langle\bar{\psi}\psi\rangle_{0,0}^{j=0}\right] + 1, \tag{7.36}$$

$$\Sigma_\pi = -\frac{2m_q}{m_\pi^2 f_\pi^2}\langle\pi^+\rangle_{\mu_I,0}\,. \tag{7.37}$$

The normalization factors are set to $\frac{2m_q}{m_\pi^2 f_\pi^2}$, to cancel multiplicative divergences on the lattice. Since our main interest is to compare χPT beyond leading order in the pion-condensed phase with LQCD calculations, we adapt the LQCD observables in Eqs.(7.36) and (7.37) to study the quark and pion condensates in the following.

The definition in Eq.(7.36) is independent of $\bar{h}_1^{\rm GL}$ and is therefore a perfectly fine quantity from the χPT perspective. It ensures that $\Sigma_{\bar{\psi}\psi}$ is equal to one in the sourceless vacuum, while the definition in Eq.(7.37) ensures that Σ_π vanishes in the sourceless

[5] The condensates also have non-trivial renormalization constants, which are taken care of by m_q in Eqs.(7.36)-(7.36), see Ref.[27] and references therein for a more complete discussion of renormalization on the lattice.

[6] Eqs.(7.36)-(7.37) carry an extra factor of 2 compared to Ref.[27], which is exactly compensated by the difference of a factor of $\frac{1}{2}$ each in our definitions of the quark and pion condensates. Our convention is identical to that of Ref.[47].

vacuum. Furthermore, $\Sigma_{\bar{\psi}\psi}$ and Σ_π satisfy the following tree-level relation,

$$\Sigma^2_{\bar{\psi}\psi} + \Sigma^2_\pi = 1, \tag{7.38}$$

for all values of j. The relation in Eq.(7.38) follows from Eq.(7.18) and is no longer satisfied at next-to-leading order, as we will see in the plots presented in section 7.5.

There is a clear drawback with the definition of Σ_π in Eq.(7.37), namely that it is dependent on the unphysical low-energy constant $\bar{h}_1^{\rm GL}$. This forces us to choose a numerical value for $\bar{h}_1^{\rm GL}$ in the following. One possible approach to determine a value for $\bar{h}_1^{\rm GL}$ is to fit χPT and LQCD results for Σ_π at very low values of the isospin chemical potential (or in the vacuum), to facilitate for a fair comparison of χPT with LQCD at higher values of the isospin chemical potential. This approach is not very suitable for our current investigation, due to a limited set of lattice data that we have available at this time. We will therefore employ the crude estimation $\bar{h}_1^{\rm GL} = \bar{l}_3$ as previously discussed, as well as $\bar{h}_1 = 0$. The latter choice is motivated by the fact that we are not even confident about which sign $\bar{h}_1^{\rm GL}$ has, and that by setting $\bar{h}_1$ strictly to zero we see the effects of overlooking the uncertainties associated with $\bar{h}_1^{\rm GL}$ in the results.

We will use the following values and relations for the remaining parameters in the numerical calculations of Eq.(7.36)-(7.37); The next-to-leading order relations for $m^2 = 2B_0 m_q$ and f that we derived in chapter 3.3, the value for α that minimizes the free energy to next-to-leading order, the values for the low-energy-constants $\bar{l}_1 - \bar{l}_4$ in Eq.(3.24), and the following values for m_π and f_π,

$$m_\pi = 131 \pm 3 \text{ MeV}, \qquad f_\pi = \frac{128 \pm 3}{\sqrt{2}} \text{ MeV}. \tag{7.39}$$

The values in Eq.(7.39) are identical to the ones used by Brandt et al. in their lattice calculations in Ref.[27].

Uncertainties in the phenomenological parameters, i.e $\bar{l}_1 - \bar{l}_4$, m_π and f_π, carry into uncertainties in m and f. To estimate the uncertainties in our calculations we define $m_{\rm min}$, $f_{\rm min}$, $m_{\rm cen}$, $f_{\rm cen}$ and $m_{\rm max}$, $f_{\rm max}$ as the values of m and f obtained through Eqs.(3.35) and (3.52) by using the minimum, central and maximum values of the phenomenological parameters , respectively[44]. The results are given below,

$$m_{\rm cen} = 132.4884 \text{ MeV}, \quad f_{\rm cen} = 84.9342 \text{ MeV}, \tag{7.40}$$
$$m_{\rm min} = 128.2409 \text{ MeV}, \quad f_{\rm min} = 83.2928 \text{ MeV}, \tag{7.41}$$
$$m_{\rm max} = 136.9060 \text{ MeV}, \quad f_{\rm max} = 86.5362 \text{ MeV}. \tag{7.42}$$

The continuum quark masses were not calculated in the lattice study in Ref.[27], so we have to choose a value for m_q. Following Ref.[47] we set $m_q = 3.47$ MeV, which is the average of the up and down continuum masses obtained by the Budapest-Marseille-Wuppertal Collaboration in Ref.[118]. With this choice for m_q, we obtain the following values for B_0;

$$B_0^{\rm min} = 2369.70 \text{ MeV}, \quad B_0^{\rm cen} = 2529.28 \text{ MeV}, \quad B_0^{\rm max} = 2700.76 \text{ MeV}. \tag{7.43}$$

We use a blue band obtained by varying m, f, B_0 and $\bar{l}_1$-$\bar{l}_4$ in their respective uncertainty ranges to illustrate how the uncertainties in Eqs.(3.24)-(3.25) and Eqs.(7.40)-(7.43) affect the quantities that we are plotting.[7]

[7]The uncertainty in $\bar{l}_3$ carry into uncertainty in $\bar{h}_1$ in the calculations where we use $\bar{h}_1^{\rm GL} = \bar{l}_3$.

7.5 Results

In this section, we start by analyzing how the nature of the phase transition between the normal phase and the BEC phase is affected by finite j. We proceed to compare our results for the condensates at finite j with lattice data provided by Brandt et al.[27]. We use the insights that we gain from the finite j sector to discuss our results at vanishing pionic source where there are no lattice data to compare with.

7.5.1 Finite pionic source

Firstly, we wish to emphasize that to perform a fair comparison between LQCD and χPT calculations, we need to use the exact same values for all parameters. However, this is not possible as continuum quark masses were not calculated in the LQCD study. We also want to emphasize that there is a significant uncertainty associated with the numerical value of the unphysical low-energy constant $\bar{h}_1^{\mathrm{GL}}$. The comparison performed here is therefore only meant to be suggestive.

The presence of an external pionic source explicitly breaks the $U(1)_{I_3}$ symmetry, as we have already discussed. This implies that there is no sharp phase transition between the normal phase and the BEC phase when $j \neq 0$.[8] The transition is instead a smooth crossover occurring over a range of values for μ_I, where the pion condensate changes significantly, as we will see examples of in Figs.7.2-7.7.

The qualitative difference between having a finite pionic source and not having a pionic source is nicely captured by the panels in Fig.7.1, which display α_{gs} as a function of μ_I at different values of j. In the leftmost panel, we show $\alpha_{gs}(\mu_I)$ in the absence of a pionic source. We observe a sudden change in the curve at $\mu_I = m_\pi$, which signals a second-order phase transition.[9] In the rightmost panel we show α_{gs} for $j = 0.00517054 m_\pi$, which varies smoothly as a function of μ_I. In the lower panel, we show α_{gs} for $j = 0.0129263 m_\pi$, which also varies smoothly as a function of μ_I. We observe that the slope of the curve in the lower panel is significantly flatter in a neighborhood around $\mu_I = m_\pi$ compared to the slope of the curve in the panel to the right. This is a reflection of the fact that the magnitude of the symmetry-breaking parameter j is larger in the former compared to the latter.

Before we proceed to present numerical results for pion and chiral condensate deviations, we want to remind the reader about what type of behavior we expect to observe at high isospin densities, and briefly discuss the underlying physics. The magnitude of the pion condensate is naturally expected to be much larger at high isospin densities than at low isospin densities because it is the order parameter for the transition to the BEC phase. The magnitude of the chiral condensate, on the other hand, is expected to be smaller in the high-density regime compared to the low-density regime. It is a well-established fact, due to asymptotic freedom, that the system enters a BCS state of weakly bound Cooper pairs at asymptotic isospin densities. Furthermore, the transition from the BEC state to the BCS state is believed to be an analytic crossover[25] because the two states break the same symmetries. The conjectured analytic crossover suggests that the magnitude of $\langle \bar{\psi}\psi \rangle$ should be small at very high isospin densities, and we expect this to be reflected in the high-density regime of our results.

[8] By *sharp* we mean that the phase transition occurs at a specific point.

[9] We have already seen that $\alpha_{gs} = 0$ in the normal phase, and that an abrupt change in α_{gs} causes the pion condensate (which is the BEC order parameter) to change abruptly.

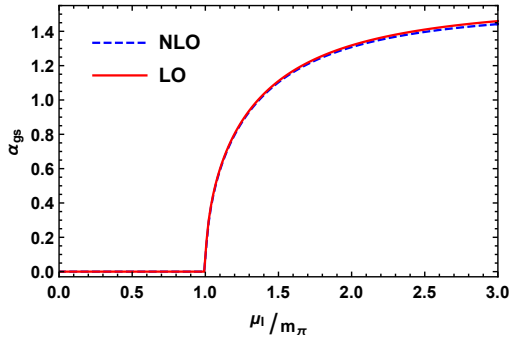

(a) The figure shows α_{gs} as a function of normalized isospin chemical potential in the absence of external pionic sources.

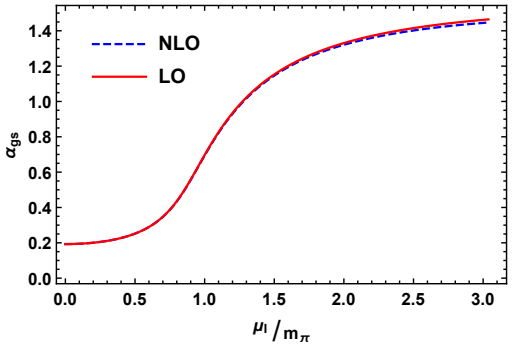

(b) The figure shows α_{gs} as a function of normalized isospin chemical potential for $j = 0.00517054 m_\pi$ and $h_1 = 0$.

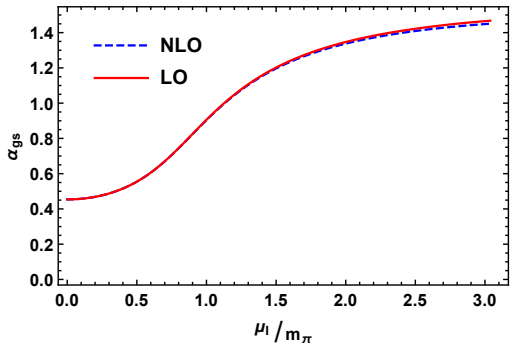

(c) The figure shows α_{gs} as a function of normalized isospin chemical potential for $j = 0.0129263 m_\pi$ and $h_1 = 0$.

Figure 7.1: The figures show the angle α_{gs} that minimizes the free energy Ω as a function of normalized isospin chemical potential for different values for the external pionic source j. The red curves are the LO results, while the blue curves are the NLO results.

Pion condensate at $j = 0.00517054 m_\pi$

In Fig.7.2, we display the normalized pion condensate at $j = 0.00517054 m_\pi$, which is the smallest value of the pionic source for which lattice QCD data are available at zero temperature. The red curve is the leading-order result, the blue dashed curve is the next-to-leading-order result obtained by using $h_1 = 0$, the blue band was explained at the end of the previous section, and the black dots are lattice results.

Firstly, we notice that the magnitude of the normalized pion condensate exceeds one at isospin chemical potential higher than $\sim 1.5 m_\pi$ both on the lattice and in χPT to next-to-leading order. Thus, the tree-level relation in Eq.(7.38) is broken by quantum effects, as we mentioned earlier. We observe that the next-to-leading-order result is a significant improvement of the tree-level result in the same region $\mu_I > 1.5 m_\pi$. While the magnitude of the lattice QCD deviation increases more rapidly than the magnitude of the next-to-leading order χPT result for $\mu_I > m_\pi$, they show similar *qualitative* behavior for all values of the isospin chemical potential. The leading-order, next-to-leading order, and lattice results are in excellent agreement when $\mu_I < m_\pi$.

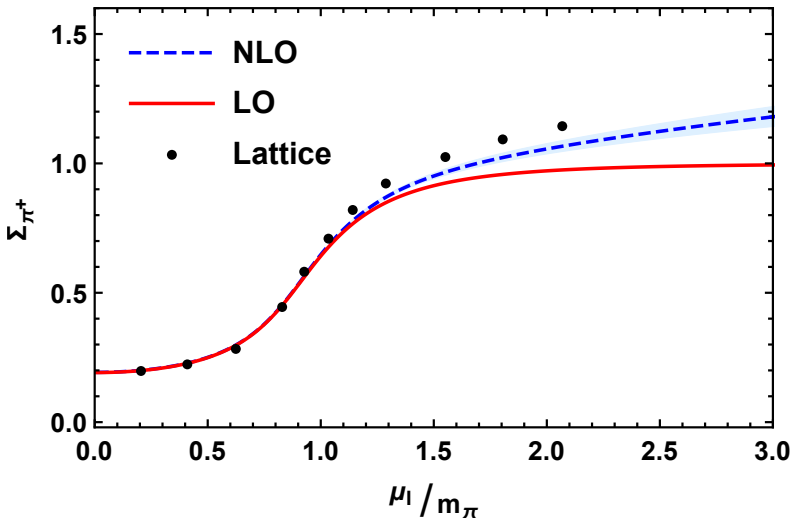

Figure 7.2: Normalized pion condensate Σ_{π^+} as a function of normalized isospin chemical potential at zero temperature, $h_1 = 0$ and $j = 0.00517054 m_\pi$. See text for details.

In Fig.7.3, we show the normalized pion condensate at $j = 0.00517054 m_\pi$, where we have used Gerber and Leutwyler's relation $\bar{h}_1^{\rm GL} = \bar{l}_3$. The result is in good agreement with Fig.7.2 and the lattice data.

We observe that the central values of the next-to-leading-order result for the normalized pion condensate in Fig.7.3 is shifted slightly towards lower values compared to the corresponding curve in Fig.7.2. This is due to $\bar{h}_1^{\rm cen} = \bar{l}_3^{\rm cen} - \bar{l}_4^{\rm cen} < 0$, and illustrates the impact that the choice of $\bar{h}_1$ has on our results. More spesifically, the following term,

$$\frac{4}{(4\pi)^2} \bar{h}_1 B_0^2 j \tag{7.44}$$

in Eq.(7.27) causes a constant shift in results obtained with nonzero values for $\bar{h}_1$, compared to the result where $\bar{h}_1 = 0$. The size of the shift depends on the magnitude and sign of $\bar{h}_1$ as well as the magnitude of the (pseudoscalar) pionic source j.

Finally, we observe that the blue band in Fig.7.3 is wider than the corresponding band in Fig.7.2, due to the uncertainties in $\bar{l}_3$ and $\bar{l}_4$ that translate into uncertainties in $\bar{h}_1 = \bar{l}_3 - \bar{l}_4$.

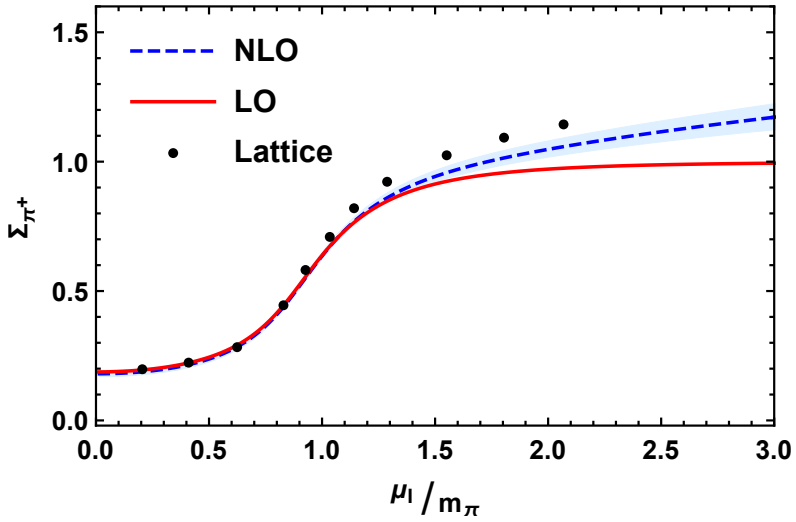

Figure 7.3: Normalized pion condensate Σ_{π^+} as a function of normalized isospin chemical potential at zero temperature, $\bar{h}_1^{\rm GL} = \bar{l}_3$ and $j = 0.00517054 m_\pi$. See text for details.

Chiral condensate at $j = 0.00517054 m_\pi$

In Fig.7.4, we show the normalized quark condensate deviation for $j = 0.00517054 m_\pi$. The leading-order, next-to-leading order, and lattice results are in excellent agreement for values of the isospin chemical potential up to $\sim m_\pi$. The leading-order result is in very good agreement with LQCD data beyond this point, while the next-to-leading-order result is in slightly less good agreement with LQCD. The difference between LQCD and χPT to next-to-leading order in Fig.7.4 is comparable to the difference we observe in Fig.7.2, while this is certainly not the case for the differences between the LQCD and the leading-order χPT results. This indicates that while the differences in the condensate deviations between χPT at NLO and LQCD are significant when $\mu_I > m_\pi$, they show similar qualitative behavior, but with χPT at next-to-leading order consistently under or overshooting compared to LQCD results.

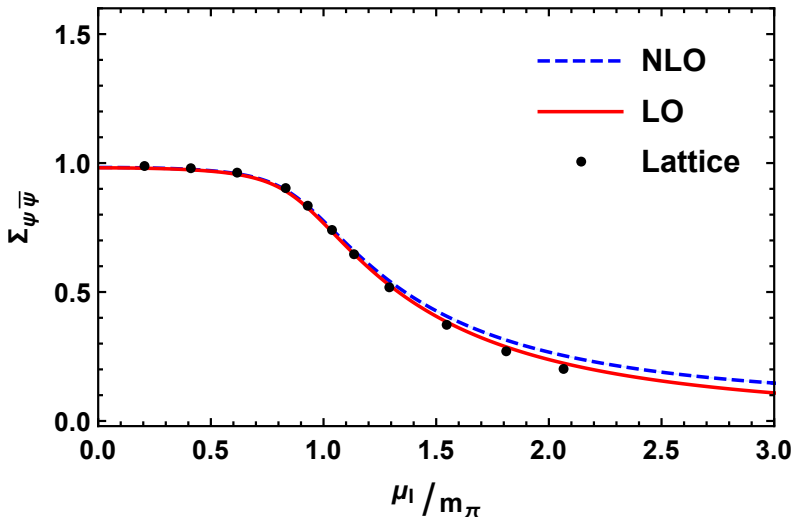

Figure 7.4: Normalized quark condensate deviation $\Sigma_{\bar{\psi}\psi}$ as a function of normalized isospin chemical potential at zero temperature and $j = 0.00517054 m_\pi$. See text for details.

Pion condensate at $j = 0.0129263 m_\pi$

In Fig.7.5, we display the normalized pion condensate with $h_1 = 0$ at $j = 0.0129263 m_\pi$. The difference between the leading-order result and the lattice result becomes significant for smaller values of μ_I than what we observe in Fig.7.2. The agreement between the next-to-leading-order result and the lattice result is very similar to what we observe in Fig.7.2. We also notice that the relation in Eq.(7.38) is broken by the blue curve and the lattice data in Fig.7.5.

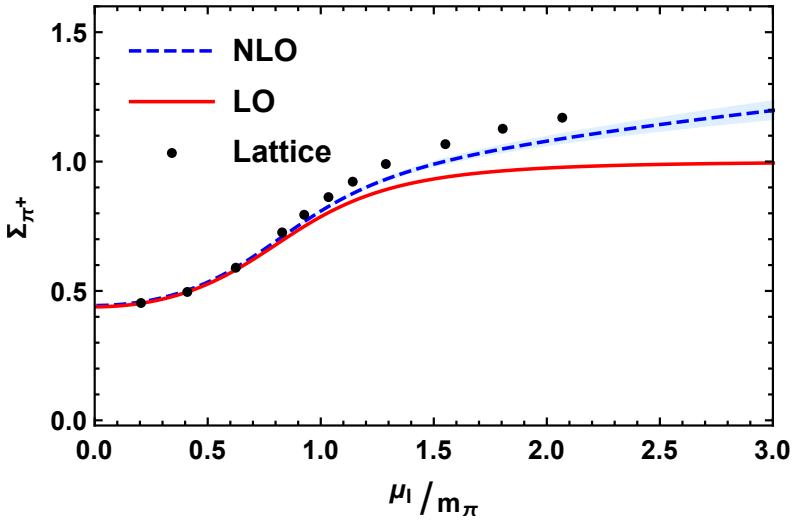

Figure 7.5: Normalized pion condensate Σ_{π^+} as a function of normalized isospin chemical potential at zero temperature, $h_1 = 0$ and $j = 0.0129263 m_\pi$. See text for details.

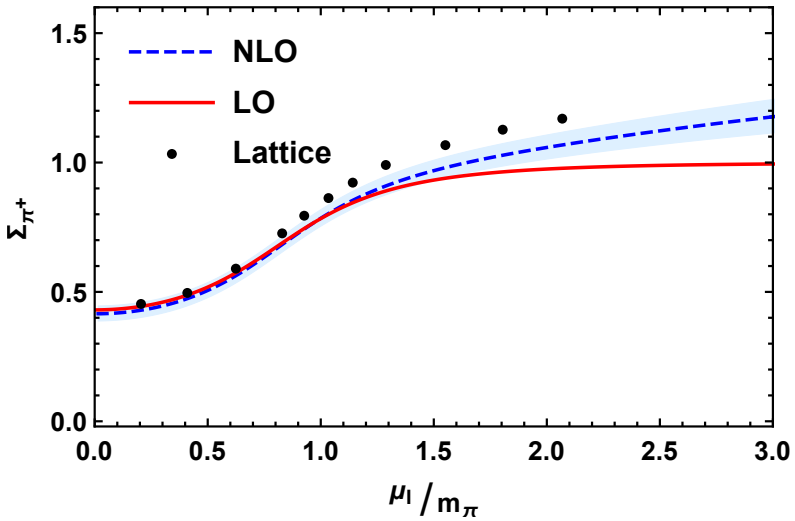

Figure 7.6: Normalized pion condensate Σ_{π^+} as a function of normalized isospin chemical potential at zero temperature, $\bar{h}_1^{\rm GL} = \bar{l}_3$ and $j = 0.0129263 m_\pi$. See text for details.

In Fig.7.6 we show the normalized pion condensate deviation at $j = 0.0129263 m_\pi$, where we use the relation $\bar{h}_1^{\rm GL} = \bar{l}_3$. We observe that the shift in the blue curve in Fig.7.6 relative to the blue curve in Fig.7.5 is larger than the shift between the blue curves in Fig.7.2 and Fig.7.3. We also observe that the blue band in Fig.7.6 is wider than the blue band in Fig.7.3. These observations are direct consequences of the fact that a larger value of j amplifies the effects that h_1 has on the pion condensate, and that the results in Figs.7.5 and 7.6 are generated at a larger value of j than the results in Figs.7.2 and 7.3.

Chiral condensate at $j = 0.0129263 m_\pi$

In Fig.7.7, we show the normalized quark condensate deviation for $j = 0.0129263 m_\pi$. We observe that the lattice result is in noticeably better agreement with χPT to next-to-leading order compared to χPT at leading-order when the isospin chemical potential is smaller than $\sim m_\pi$. Beyond this point, the agreements between the leading order, the next-to-leading order, and the lattice results resemble what we observe in Fig.7.4.

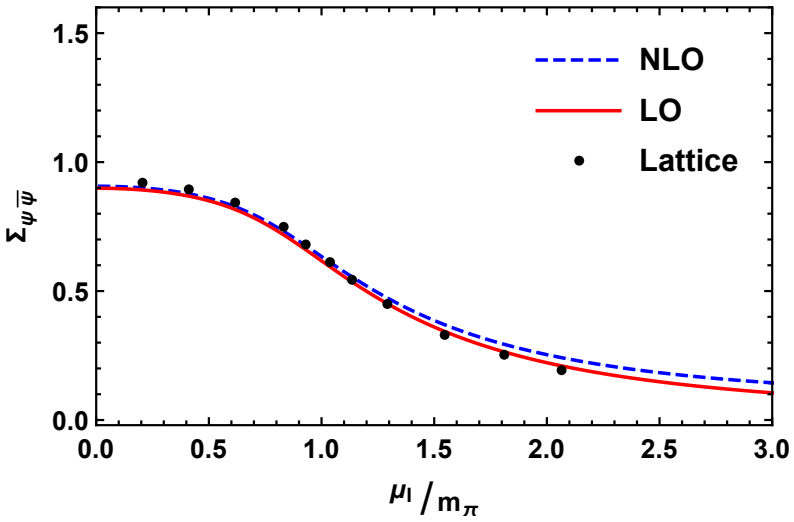

Figure 7.7: Normalized quark condensate deviation $\Sigma_{\bar{\psi}\psi}$ as a function of normalized isospin chemical potential at zero temperature and $j = 0.0129263 m_\pi$. See text for details.

The agreements on the normalized condensate deviations at finite j between χPT and lattice QCD are excellent at low values of the isospin chemical potential. By increasing the isospin chemical potential to higher values, we find a gradually worse agreement between LQCD and χPT. This is consistent with the fact that χPT is a low-energy effective field theory with systematic corrections whose magnitude increase with μ_I.

The improvements in the normalized pion condensates as we go from leading order to next-to-leading order in χPT are highly significant. The asymptotic behavior of the next-to-leading-order results are entirely different from the asymptotic behavior of the leading-order results and clearly violate the tree-level relation in Eq.(7.38). Furthermore, the results for Σ_{π^+} at high values of μ_I show a reasonable qualitative agreement between LQCD and χPT to next-to-leading order, with the magnitude of the next-to-leading-order result being significantly lower than the magnitude of the LQCD result.

We observe that the agreement on the normalized chiral condensate deviations between χPT and LQCD is barely improved at next-to-leading order for low values of the isospin chemical potential. It is, however, a little unexpected that the leading-order result is in slightly better agreement with LQCD for higher values of μ_I. Nevertheless, based on the inconsistencies in the agreement between LQCD and χPT at leading order for normalized chiral and pion condensate deviations, one may suspect this to be a coincidence. The agreement between LQCD and χPT at next-to-leading order is still quite consistent over the set of normalized chiral and pion condensate deviations that we have considered, which signals a more stable performance as we include more systematic corrections. This is consistent with what we expect from an EFT.

7.5.2 Vanishing pionic source

In Fig.7.8, we show the normalized pion condensate in the absence of external pionic sources. We find that the normalized pion condensate to next-to-leading order is signifi-

cantly larger than the tree-level result for $\mu_I > 1.5m_\pi$. We also find that the leading-order result asymptotes to one, while the magnitude of the next-to-leading-order result increases steadily and breaks the tree-level relation in Eq.(7.38).

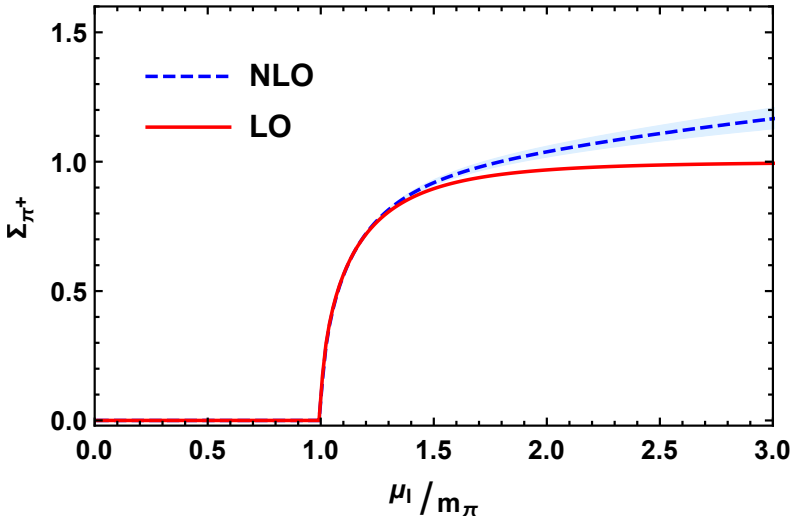

Figure 7.8: Normalized pion condensate Σ_{π^+} as a function of normalized isospin chemical potential at zero temperature and vanishing (pseudoscalar) pionic source. See text for details.

In Fig.7.9, we show the normalized chiral condensate deviation in the absence of external pionic sources. We find that the magnitude of the next-to-leading-order result is larger than the the tree-level result when $\mu_I > 1.5m_\pi$. The difference between the leading-order and the next-to-leading-order result for $\Sigma_{\bar{\psi}\psi}$ is, however, much smaller than the corresponding difference in the result for Σ_{π^+}.

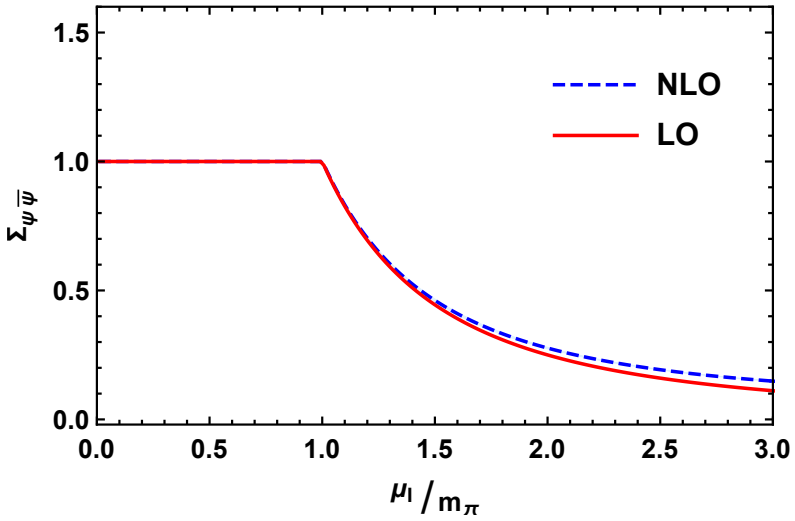

Figure 7.9: Normalized quark condensate deviation $\Sigma_{\bar{\psi}\psi}$ as a function of normalized isospin chemical potential at zero temperature and vanishing (pseudoscalar) pionic source. See text for details.

The difference between the next-to-leading-order and leading-order results at vanishing pionic source closely resembles differences that we find at finite j. If we use LQCD data from Ref.[27] as a benchmark, then we should expect the next-to-leading-order corrections to provide a significant improvement to the leading-order result for Σ_{π^+}. By extrapolating

from the difference between LQCD and χPT at $j = 0.00517054 m_\pi$ and $j = 0.0129263 m_\pi$, we expect the magnitudes of Σ_{π^+} and $\Sigma_{\bar{\psi}\psi}$ at higher values of the isospin chemical potential to be somewhat lower and higher, respectively, than future LQCD results.

The results presented here can be used to gauge the quality of future LQCD calculations of the pion and chiral condensates at vanishing pionic source. However, we emphasize that it is not possible to perform a fully quantitative comparison between χPT and currently available LQCD data or lattice calculations in the future without access to the continuum quark-mass values on the lattice. We also emphasize that the results we obtain for Σ_{π^+} depend on the unphysical low-energy constant $\bar{h}_1^{\rm GL}$, whose numerical value has not been estimated very accurately in our study. Future studies may resolve this issue by either redefining Σ_{π^+} to subtract $\langle \pi^+ \rangle$ evaluated at $j \neq \mu_I = 0$, or by fitting χPT with LQCD lattice data in the (source-dependent) vacuum.

Chapter 8

Quark and pion condensates at finite temperature

In this chapter, we extend the analysis from the previous chapter by including finite-temperature effects. We start by calculating the finite-temperature contribution to the free energy, which we subsequently use to derive Splittorff et al.'s low-temperature Landau functional[111], and their analytical low-temperature approximation of the phase-transition curve between the normal and pion-condensed phases. We then confront Splittorff's low-temperature approximation with a numerical calculation of the phase-transition curve using the complete expression for the free energy to next-to-leading order in χPT. We also compare our numerical calculation with Brandt et al.'s LQCD results in Ref.[27] and $SU(2)$ NJL-model results obtained by He, Jin, and Zhuang in Ref.[36].

We proceed to generate the pion and chiral condensates from the free energy and analyze their temperature dependence. This leads to an interesting observation of how high temperatures give rise to a new type of behavior in the density evolution[1] of the ground-state configuration in the pion-condensed phase. We end our discussion with a short remark on χPT's ability to predict the chiral crossover at low values of the isospin chemical potential.

The following section reviews basic elements of thermal field theory (TFT) and (non-topological) phase transitions. We have included it as a preparation for the calculations that follow in the next sections, and for the sake completeness. The informed reader may skim through this section, or skip it altogether.

8.1 TFT basics

Extending the framework of quantum field theory to include finite-temperature effects is necessary in many areas of research. Relevant examples include the interior of compact stars, and the (μ_B, T) phase diagram of QCD, which finds applications in areas ranging from heavy-ion collisions[119] to the early universe.

There are two well-established frameworks for finite temperature field theory, the imaginary-time formalism, and the real-time formalism. Both of the frameworks have advantages and disadvantages, which make them useful in different types of applications. One main difference between the two is that only the real-time formalism can describe out-of-equilibrium processes.

The main disadvantage with the real-time formalism is related to the technical aspect of the framework, which makes it cumbersome to work with. The imaginary-time formalism, on the other hand, naturally connects the partition function in statistical mechanics

[1] By density evolution, we mean how the ground state evolves as a function of μ_I while we keep all other parameters fixed.

to the path integral in quantum field theory. Many of the perturbative and numerical evaluation techniques in QFT extend nicely into the imaginary-time framework, making most calculations simpler to perform than in the real-time formalism. We will stick to the imaginary-time formalism in this thesis. An introduction to the real-time formalism can be found in Ref.[120], and more information about the imaginary-time formalism can be found in standard textbooks about TFT, like Refs.[121, 122].

Statistical field theory

We begin by recalling some basic notions from statistical field theory. The fundamental object in equilibrium statistical mechanics is the density matrix $\hat{\rho}$, which in the grand canonical ensemble[2] is given by,

$$\hat{\rho} = \exp\left[-\beta(\hat{H} - \mu_i \hat{N}_i)\right]. \tag{8.1}$$

Here β denotes the inverse temperature, $\hat{H}$ is the Hamilton operator, and μ_i denotes the chemical potential that couple to the i'th (conserved) number operator $\hat{N}_i$. The density matrix can be used to calculate the thermal average of any observable O,

$$\langle \hat{O} \rangle = \frac{\operatorname{Tr} \hat{O}\hat{\rho}}{\hat{\rho}}. \tag{8.2}$$

From the denisty matrix we also obtain the grand canonical partition function[121],

$$Z = Z(V, T, \{\mu_i\}) = \operatorname{Tr} \hat{\rho} = \sum_i \langle \phi_i | \hat{\rho} | \phi_i \rangle, \tag{8.3}$$

where the sum is over all eigenstates $|\phi_i\rangle$ of the field operator $\hat{\phi}$.[3] The grand canonical partition function is the single most important function in thermodynamics, and all thermodynamic properties of the theory can be derived from it.

We will proceed to show how the partition function is connected to the path integral in QFT. We will for concreteness only discuss four-dimensional bosonic theories, but the discussion generalizes straightforwardly to different numbers of dimensions. For notational convenience, we stop writing hats on operators and denote $H - \mu_i N_i$ by $\mathcal{H}$ in the following.

Imaginary-time formalism

In the path-integral formulation of QFT one writes the transition amplitude for going from an initial state $|\phi_0\rangle$ at time t_0 to a final state $|\phi_f\rangle$ at time t_f as,

$$\langle \phi_f | e^{-i\mathcal{H}t_f} | \phi_0 \rangle = \mathcal{N} \int \mathcal{D}\pi \mathcal{D}\phi \exp\left[i \int_0^{t_f} dt \int d^3x \dot{\pi}\phi - \mathcal{H} \right]. \tag{8.4}$$

Here $\dot{\pi}$ denotes the conjugate momentum of the field ϕ and $\mathcal{N}$ is a (divergent) normalization factor that drops out of all calculations of physical quantities. The integrals $\int \mathcal{D}\pi$ and $\int \mathcal{D}\phi$ denote the sum over all conjugate momenta and all field configurations respecting the initial and final condition, respectively.

Wick rotating to the Euclidean metric $(\tau, \vec{x}) = (it, \vec{x})$, [4]and identifying $it_1 \equiv \beta$ [5] lets us rewrite the transition amplitude in Eq.(8.4) as,

$$\langle \phi_f | e^{-\beta\mathcal{H}} | \phi_0 \rangle = \mathcal{N} \int \mathcal{D}\pi \mathcal{D}\phi \exp\left[\int_0^{\beta} d\tau \int d^3x i\dot{\pi}\phi - \mathcal{H} \right]. \tag{8.5}$$

[2]The grand canonical ensemble is the natural ensemble to use in relativistic theories, where particles can be created and annihilated.

[3]The field ϕ_i (with no hat) is the eigenvalue corresponding to the state $|\phi_i\rangle$; $\hat{\phi}\,|\phi_i\rangle = \phi_i\,|\phi_i\rangle$.

[4]The new time variable $\tau = it$ explains why the formalism is called imaginary time.

[5]Here we effectively replace time with temperature.

The expression on the left-hand side is remarkably similar to the right-hand side of Eq.(8.3). By restricting the initial state and the final state in Eq.(8.5) to be equal $|\phi_0\rangle = |\phi_f\rangle \equiv |\phi_a\rangle$, and summing over all states $|\phi_a\rangle$ we obtain,

$$Z = \sum_{\phi_i} \langle \phi_i | e^{-\beta \mathcal{H}} | \phi_i \rangle = \mathcal{N} \int \mathcal{D}\pi \int_{\text{periodic}} \mathcal{D}\phi \exp\left[\int_0^\beta d\tau \int d^3x i\dot{\pi}\phi - \mathcal{H} \right]. \tag{8.6}$$

The integration over conjugate momenta is unrestricted as before, while the integration over the field variable $\int_{\text{periodic}} \mathcal{D}\phi$ includes all paths in field-configuration space that respect the periodic condition $|\phi_f\rangle = |\phi_0\rangle$.

If the Hamiltonian is at most quadratic in the conjugate momentum, which is usually the case, then the integral $\int \mathcal{D}\pi$ can be performed analytically by completing the square. Replacing π with ϕ takes us from the Hamiltonian to the Lagrangian description, where the partition function reads,

$$Z = \mathcal{N}' \int_{\text{periodic}} \mathcal{D}\phi \exp\left[\int_0^\beta d\tau \int d^3x \mathcal{L} \right], \tag{8.7}$$

where $\mathcal{N}'$ is a new temperature-dependent normalization constant.

To see what restrictions the periodic boundary conditions puts on the field-operator ϕ we consider the thermal two-point Greens function,

$$G(\tau', \tau, x', x) = \frac{\text{Tr}\{T[e^{-\beta H}\phi(\tau', x')\phi(\tau, x)]\}}{Z}, \tag{8.8}$$

where T denotes the imaginary-time ordering operator,

$$T[e^{-\beta H}\phi(\tau', x')\phi(\tau, x)] = \phi(\tau', x')\phi(\tau, x)\Theta(\tau' - \tau) + \phi(\tau, x)\phi(\tau', x')\Theta(\tau - \tau'). \tag{8.9}$$

Using the Heisenberg equation for the field operator,

$$\phi(\tau + \delta\tau, x) = e^{iH\delta t}\phi(\tau, x)e^{-iH\delta t} = e^{H\delta\tau}\phi(\tau, x)e^{-iH\delta\tau}, \tag{8.10}$$

and the cyclic property of the trace, we obtain,

$$G(\tau', \tau, x', x) = G(\tau' + \beta, \tau, x', x). \tag{8.11}$$

The relation in Eq.(8.11) imposes the following periodicity condition on the field operator,

$$\phi(\tau + \beta, x) = \phi(\tau, x). \tag{8.12}$$

The periodicity in Eq.(8.12) admits us to perform a Fourier expansion in the field,

$$\phi(\tau, x) = \frac{1}{\beta} \sum_{n=-\infty}^{\infty} \phi_n(x) e^{i\omega_n \tau}, \tag{8.13}$$

where

$$\omega_n = \frac{2\pi n}{\beta}, \qquad n \in \mathbb{Z}, \tag{8.14}$$

are the so called bosonic Matsubara frequencies. The full Fourier representation of $\phi(x)$ is obtained by transforming the spatial variables x in the usual way,

$$\phi(\tau, x) = \frac{1}{\beta} \sum_{n=-\infty}^{\infty} \int \frac{d^3p}{(2\pi)^3} \phi_n(\vec{p}) e^{i(\omega_n \tau + \vec{p}\cdot\vec{x})}. \tag{8.15}$$

Topologically speaking "turning on" the temperature in the imaginary-time formalism amounts to a compactification of the "time dimension" from the real line to the unit circle: $\mathbb{R} \times \mathbb{R}^3 \to \mathbb{S}_1 \times \mathbb{R}^3$. From Eq.(8.13) we see that the compactification comes at the price of an infinite tower of operators $\phi_n(x)$. Since ϕ is a scalar field with mass m it satisfies the (Euclidean) Klein-Gordon (KG) equation,

$$(-\partial_0\partial^0 - \nabla^2 + m^2)\phi^2 = 0. \tag{8.16}$$

By substituting Eq.(8.13) into Eq.(8.16) we obtain an infinite number of KG equations for massive 3D fields,

$$\sum_{n=-\infty}^{\infty} (-\nabla^2 + \omega_n^2 + m^2)\phi_n(x) = 0. \tag{8.17}$$

Each Fourier mode ϕ_n can be therefore be interpreted formally as a scalar particle in three-dimensional Euclidean space with mass $m_n^2 = m^2 + \frac{4\pi^2 n^2}{\beta^2}$.[6]

Finally, we are going to need finite-temperature momentum integrals when we calculate one-loop corrections to the free energy. The zero-temperature momentum integral in dimensional regularization is modified into the following sum-integral at finite temperature,

$$\int \frac{d^{d+1}k}{(2\pi)^{d+1}} \to \frac{1}{\beta} \sum_{n=-\infty}^{\infty} \int \frac{d^d k}{(2\pi)^d} \equiv \sum\!\!\!\!\!\!\int_K . \tag{8.18}$$

The short-hand notation on the right hand side is standard in the finite-temperature literature, and will be used in the remainder of this thesis.

Phase transitions

In chapter 2.4, we mentioned that the one-dimensional phase diagram $(\mu_I, T) = (\mu_I, 0)$ has a second-order phase-transition point at $\mu_I = m_\pi$ separating the normal phase from the Bose-Einstein condensate. By turning on the temperature, we access the full two-dimensional (μ_I, T) phase diagram with possibly new phases that do not exist at zero temperature. A natural question to ask is how the phases in the one-dimensional diagram are extended into the two-dimensional phase diagram. Loosely speaking, it is also unclear how "the nature of" the transition is affected by thermal effects. These questions can be addressed in a precise way in Landau's theory for (non-topological) phase transitions[123]. To set the stage for the upcoming calculations in the next section, we review some important notions from the classical theory of phase transitions in the following.

Landau's theory is based on two concepts, free energy, and symmetry. Landau realized that a phase can be associated with a set of symmetries, and he defined a phase transition as a change in that symmetry set. We have already seen that the normal phase is characterized by $U(1)_B \times U(1)_{I_3}$, while the $U(1)_{I_3}$ is broken in the BEC phase. Landau also recognized that it is always possible to identify a so-called *order parameter* M, which is zero in one of the phases and nonzero in the other phase. More specifically, when we consider quantum theories, M becomes the expectation value of some operator. We will refer to the phase where M is nonzero as the ordered or low-temperature phase and the other phase as the unordered or high-temperature phase. A phase transition can, in most cases, be classified according to the behavior of M at the critical temperature T_c separating the two phases. If M as a function of temperature is discontinues at T_c we have a first-order phase transition. A sketch of a first-order transition is shown in the panel to the left in

[6] Notice that the fields ϕ_n with $n \neq 0$ gain extra mass from momentum in the compactified dimension.

Fig. 8.1, where we have plotted the free energy of a system as a function of M at different temperatures. If M increases continuously from zero at T_c we have a second-order phase transition, as shown in the panel to the right in Fig. 8.1.

It is also possible to have so-called crossover transitions. These are characterized by a rapid change in thermodynamic variables as the system evolves from one phase to another, with the two phases being indistinguishable in the crossover region. The transition temperature is then called a pseudocritical temperature, which is not uniquely defined but depends on the choice of the approximate order parameter. In fact, it is well established that the chiral symmetry restoration takes place via a smooth crossover[124–126], and recent LQCD simulations of the crossover can be found in Ref.[127].

Second order phase transitions

The pion condensate, i.e., the expectation value of the π^+ operator, is the order parameter for the phase transition between the normal phase and the BEC phase. While studying the magnitude of the pion condensate as a function of μ_I and T numerically is rather straightforward, it becomes a highly non-trivial task to analyze $\langle\pi^+\rangle$ analytically. Analytical calculations and approximations of the phase-transition curve simplify significantly if we identify the angle α as an effective order parameter[48, 111]. Recall that α is by no means a fundamental quantity, but merely a parameter in the ansatz for the ground-state configuration on the Goldstone manifold, see Eq.(4.8). It would, therefore, be incorrect to acknowledge α as a true order parameter in Landau's theory. However, we have already seen that the phase transition leads to a rotation of the ground state away from the normal configuration at zero temperature. The angle α simply parametrize the rotation[7] of the ground state on the $SU(2)$ manifold. It is zero in the normal phase and nonzero in the pion-condensed phase, which is similar to the behavior of the real order parameter. We will show in a later section that the interpretation of α as an effective order parameter remains valid at finite temperature.

The authors of Refs.[48, 111] obtained the first results for the phase-transition curve in the (μ_I, T)-plane within χPT, by using α as the expansion parameter in a Landau functional. The validity of their approach is by no means obvious. For example, the coefficients of a Landau functional (see the paragraphs below for details) in the true order parameter $\langle\pi^+\rangle$ may be quite different from the coefficients of a Landau functional in α, depending on the details of the relationship between $\langle\pi^+\rangle$ and α. Treating α as a proper order parameter may, therefore, lead to incorrect conclusions about the order of the phase-transition curve. While keeping this in mind, we follow the original work in Refs.[48, 111] in the following, and derive their low-temperature approximation for the phase-transition curve. For the sake of completeness, we begin by summarizing some elementary facts about Landau functionals and some useful results from the χPT literature. We proceed to consider the zero-temperature limit first.

In chapters 4 and 7 we obtained the following tree-level results,

$$\alpha = 0, \qquad \mu_I < m_\pi, \tag{8.19}$$

$$\cos\alpha = \frac{m_\pi}{\mu_I}, \qquad \mu_I \geq m_\pi, \tag{8.20}$$

$$\langle\pi^+\rangle^{\text{tree}}_{\mu_I,0} = -f^2 B_0 \sin\alpha. \tag{8.21}$$

We see from Eqs.(8.19) and (8.20) that α changes continuously from zero to nonzero at the phase-transition point $m_\pi = \mu_I$. It follows that the order parameter in Eq.(8.21) also

[7] Rotation is perhaps not the best expression to use here, as α can change discontinuously as we have already seen in the chiral limit.

changes continuously from zero to nonzero at $m_\pi = \mu_I$, which signals that the phase transition is second order. In order to go beyond tree-level we need to consider the renormalized free energy Ω.

The free energy can be well approximated by the first few terms in a Taylor expansion in α close to the transition point, since α is expected to be small here. Realizing that the terms in $\mathcal{L}_2^{\text{static}}$, $\mathcal{L}_2^{\text{quadratic}}$ and $\mathcal{L}_4^{\text{static}}$ are invariant under $\alpha \to -\alpha$ lets us write the free energy expansion on the following form,[8]

$$\Omega = \Omega(\alpha = 0) + c_2\alpha^2 + c_4\alpha^4 + ... \tag{8.22}$$

Here the coefficients c_i are real-valued functions of μ_I, m and f. The Taylor expansion of the free energy in Eq.(8.22) is often referred to as a Landau- or Ginzburg-Landau functional.

The phase-transition is located at the point where c_2 vanishes, and the transition is first or second-order depending on whether c_4 is negative or positive at the transition, respectively. The relevance of c_4's sign near the phase transition can be appreciated at a qualitative level by studying Fig. 8.1, where $c_4 < 0$ is identified with the behavior in the panel to the left, and $c_4 > 0$ is identified with the behavior in the panel to the right.

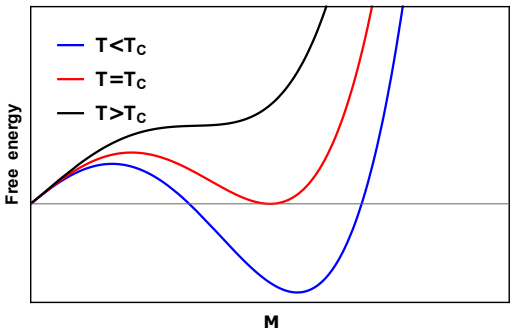

(a) A sketch of the free energy as a function of the order parameter M at different temperatures for a first-order phase transition. Notice that the minimum is degenerate at the critical temperature, where the finite value for M wins when $T < T_c$ and $M = 0$ wins when $T > T_c$.

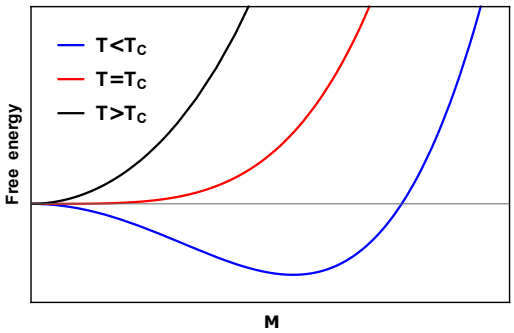

(b) A sketch of the free energy as a function of the order parameter M at different temperatures for a second-order phase transition. The value of M that minimizes the free energy changes continuously from a finite value on the low-temperature side to zero on the high-temperature side of the phase transition.

Figure 8.1: The figures show qualitative sketches of the nature of first and second-order phase transitions. The plot to the left illustrates a first-order phase transition, and the figure to the right illustrates a second-order phase transition.

In Ref.[44] Adhikari and Andersen derive the Landau functional for the free energy given in Eq.(4.63) using α as the effective order parameter. They find that c_2 vanishes at $\mu_I = m_\pi$ and that $c_4(\mu_I = m_\pi) > 0$. This result is identical to what we find at tree-level. If we include finite-temperature effects into the expression for the free energy, then c_2 and c_4 become temperature dependent. We can then extend the analysis into the (μ_I, T) plane, and calculate a phase-transition *curve* $\mu_I^c(T)$. Here we may encounter the possibility of having a point where c_4 and c_2 are both zero. This is referred to as a *tricritical point*[128, 129], and signals that a second order phase transition is turning into a first order phase transition (or vice versa).

As a final remark, we mention that thermal fluctuations due to the presence of a heat bath are expected to weaken the magnitude of the condensate $\langle \pi^+ \rangle$, and therefore drive

[8] We are assuming throughout this thesis that the medium is isotropic, so α is the same in all parts of space. If this is not the case, then the expansion needs to take the energy costs of having α varying into consideration.

the phase transition towards higher values of μ_I as we increase the temperature.

8.2 Free energy at nonzero temperature

The renormalized free energy in Eq.(7.25) is the sum of three contributions; the leading-order contribution to the static energy Ω_0, the next-to-leading order contribution to the static energy $\Omega_1^{\rm static}$, and the one-loop contribution $\Omega_1^{\rm loop}$. Only the latter involves an explicit momentum integration. The temperature dependence of Ω is therefore encoded into $\Omega_1^{\rm loop}$. We now proceed to calculate the thermal sum-integrals in $\Omega_1^{\rm loop}$.

A key integral

The starting point for the one-loop calculation at zero temperature is,[9]

$$\Omega_1^{\rm loop} = \frac{1}{2}\int_K \log\big(k_0^2 + E_{\pi^0}^2\big) + \frac{1}{2}\int_K \log\big(k_0^2 + E_{\pi^+}^2\big) + \frac{1}{2}\int_K \log\big(k_0^2 + E_{\pi^-}^2\big), \tag{8.23}$$

which extends to,

$$\Omega_1^{\rm loop} = \frac{1}{2}\sum\!\!\!\!\!\!\int_K \log\big(\omega_n^2 + E_{\pi^0}^2\big) + \frac{1}{2}\sum\!\!\!\!\!\!\int_K \log\big(\omega_n^2 + E_{\pi^+}^2\big) + \frac{1}{2}\sum\!\!\!\!\!\!\int_K \log\big(\omega_n^2 + E_{\pi^-}^2\big), \tag{8.24}$$

at finite temperature $T \neq 0$. The Matsubara sum

$$v(E) \equiv \sum_{n=-\infty}^{\infty} \log\left(\omega_n^2 + E^2\right), \tag{8.25}$$

that appears in the sum-integral

$$J(T,E) \equiv \sum\!\!\!\!\!\!\int_K \log\big(\omega_n^2 + E^2\big), \tag{8.26}$$

can be evaluated by using the following trick[130]; Differentiate $v(E)$ with respect to E,

$$\frac{\partial v}{\partial E} = \frac{\beta}{\pi}\sum_{n=-\infty}^{\infty} \frac{\left(\frac{\beta E}{2\pi}\right)}{n^2 + \left(\frac{\beta E}{2\pi}\right)^2}, \tag{8.27}$$

and use the following identity,

$$\sum_{n=-\infty}^{\infty} \frac{y}{n^2 + y^2} = \pi\coth(\pi y), \tag{8.28}$$

to obtain,

$$\frac{\partial v}{\partial E} = \beta\left[1 + \frac{2}{e^{\beta E} - 1}\right], \tag{8.29}$$

$$v(E) = \beta\left[E + \frac{2}{\beta}\log\left(1 - e^{-\beta E}\right)\right] + ... \tag{8.30}$$

The omitted terms do not depend on E and will be ignored in the following.

The evaluation of the Matsubara sum in Eq.(8.25) reduces the sum-integral $J(T,E)$ to a regular integral over three-momenta,

$$J(T,E) = J_0(E) + J_T(T,E) = \int_k E + 2T\int_k \log\left(1 - e^{-\beta E}\right), \tag{8.31}$$

where we have separated $J(T,E)$ into a temperature-independent part $J_0(E)$ and a temperature-dependent part $J_T(T,E)$. If we take E to be one of the dispersion relations in Eq.(4.27)-(4.28), then the integrand in the temperature-dependent part $J_T(T,E)$ becomes exponentially damped, which implies that the d^3k-integral in $J_T(T,E)$ is finite.

[9] This follows from Eq.(4.51) in combination with Wick rotating (4.52).

The renormalized free energy

It follows from the analysis on the previous page that we can write the one-loop contribution to the free energy at finite temperature as,

$$\Omega_1^{\text{loop}} = \frac{1}{2}\int_k E_{\pi^0} + \frac{1}{2}\int_k E_{\pi^+} + \frac{1}{2}\int_k E_{\pi^-} + \frac{1}{\beta}\int_k \log\left(1-e^{-\beta E_{\pi^0}}\right) + \frac{1}{\beta}\int_k \log\left(1-e^{-\beta E_{\pi^+}}\right)$$
$$+ \frac{1}{\beta}\int_k \log\left(1-e^{-\beta E_{\pi^-}}\right) \equiv \Omega_{1,\pi^0} + \Omega_{1,\pi^+} + \Omega_{1,\pi^-} + \Omega^T_{1,\pi^0} + \Omega^T_{1,\pi^+} + \Omega^T_{1,\pi^-}. \tag{8.32}$$

The divergences in Ω_1^{loop} are still cancelled by the counterterms in Ω_1^{static}, since the temperature-dependent contributions to the free energy are finite valued. In conclusion, we may write the renormalized free energy at finite temperature as,

$$\Omega = \Omega(T=0) + \Omega^T_{1,\pi^0} + \Omega^T_{1,\pi^+} + \Omega^T_{1,\pi^-} \equiv \Omega_{T=0} + \Omega_T. \tag{8.33}$$

Neither of the integrals Ω^T_{1,π^0}, Ω^T_{1,π^+} and Ω^T_{1,π^-} can be expressed in terms of elementary functions[131], but they can be evaluated numerically without much difficulty.

8.2.1 Expansion in α

The way we represent the thermal contribution to the free energy in Eq.(8.32) is perfectly fine for numerical analysis, and we will employ it as our starting point when we proceed to analyze the chiral and pion condensates at finite temperature. However, the expression for Ω_T in Eq.(8.32) is not a particularly suitable starting point for an analytical expansion of the free energy in α. We will therefore return to Eq.(8.24) and proceed to derive an analytical approximation of the Landau functional in α, by employing techniques presented in Ref.[48]. It is worth noting that this approach requires α to be treated as an independent variable and not as a function of m, f, μ_I, and T[111].

Neutral pion contribution

In Appendix C.3, we show that the neutral-pion contribution $\Omega_{1,\pi^0} + \Omega^T_{1,\pi^0}$ can be written as,

$$\Omega_{1,\pi^0} + \Omega^T_{1,\pi^0} = -\frac{1}{2}\sum_{n\in\mathbb{Z}}\int_0^\infty \frac{dt e^{-tm_3^2}}{(4\pi)^{\frac{d}{2}} t^{\frac{d}{2}+1}} e^{-\frac{n^2}{4T^2 t}}. \tag{8.34}$$

The temperature-independent part Ω_{1,π^0} is given by the $n=0$ term in Eq.(8.34), which agrees with what we found in Eq.(4.57). The temperature-dependent part Ω^T_{1,π^0} is given by the remaining terms, and in Appendix C.3 we show that it can be represented by an infinite sum of modified Bessel functions K_2,[10]

$$\Omega^T_{1,\pi^0} = -\frac{1}{2}\frac{16m_3^2T^2}{(4\pi)^2}\sum_{n=1}^\infty \frac{K_2\left(\frac{m_3 n}{T}\right)}{n^2}. \tag{8.35}$$

The temperature-dependent contribution Ω^T_{1,π^0} is finite valued, as we have already discussed, but it is not known analytically. However, we may use the following asymptotic series for modified Bessel functions $K_v(z)$[132],

$$K_v(z) = \sqrt{\frac{\pi}{2z}}e^{-z}\left(1 + \frac{4v^2-1}{8z} + \frac{(4v^2-1)(4v^2-9)}{2!\,(8z)^2} + O(z^{-3})...\right), \qquad |\arg z| < \frac{3\pi}{2}, \tag{8.36}$$

[10] The same result is obtained if we substitute $k \to Tx$ into $\frac{1}{\beta}\int_k \log\left(1-e^{-\beta E_{\pi^0}}\right)$, then expand the logarithm in powers of the exponential and finally integrate the expansion term by term[121, 131]. However, this method is not suitable for $\Omega^T_{1,\pi^+} + \Omega^T_{1,\pi^-}$, which is why we have adapted the approach in Ref.[48].

to obtain an analytical low-temperature approximation of Eq.(8.35). Thus, in the limit where $T \ll m_\pi, \mu_I$ we obtain the following approximation of Ω^T_{1,π^0},

$$\Omega^T_{1,\pi^0} = -\frac{1}{2}\frac{T^{\frac{5}{2}}}{\sqrt{2}}\left(\frac{m_3}{\pi}\right)^{\frac{3}{2}} e^{-\frac{m_3}{T}}\left[1 + \frac{15}{8}\frac{T}{m_3}\left(\sum_{n=1}^{\infty}\frac{1}{n^3}\right) + O\left(\frac{T^2}{m_3^2}\right)\right]. \tag{8.37}$$

Remaining contribution

The remaining one-loop contribution to the free energy can be written as,

$$\Omega_{1,\pi^\pm} + \Omega^T_{1,\pi^\pm} = \frac{1}{2}\sum\!\!\!\!\!\!\int_K \log\left[(K^2 + m_1^2)(K^2 + m_2^2) + k_0^2 m_{12}^2\right]. \tag{8.38}$$

The prescription we used to separate Ω_{1,π^0} from Ω^T_{1,π^0} is no longer directly applicable here, since the argument of the log on the right hand side of Eq.(8.38) cannot be written on the standard form $\log(p^2 + m^2)$. In chapter 6 we saw that the mixing of electric-charge eigenstates in the pion-condensed phase manifested itself through the nonzero value of $m_1^2 - m_2^2$. It is the same quantity that prevents us from expressing the argument of the log in Eq.(8.38) on the standard Klein-Gordon form in the pion-condensed phase, as we can see from the equation below,

$$\begin{aligned}
&\Omega_{1,\pi^\pm} + \Omega^T_{1,\pi^\pm} = \frac{1}{2}\sum\!\!\!\!\!\!\int_K \log\left\{\left[K^2 + \frac{1}{2}\left(m_1^2 + m_2^2\right)\right]^2 + k_0^2 m_{12}^2 - \frac{1}{4}\left(m_1^2 - m_2^2\right)^2\right\} = \\
&\frac{1}{2}\sum\!\!\!\!\!\!\int_K \log\left\{\left[\left(k_0 + \frac{i}{2}m_{12}\right)^2 + p^2 + \frac{1}{2}\left(m_1^2 + m_2^2 + \frac{1}{2}m_{12}^2\right)\right]\right. \\
&\left.\times\left[\left(k_0 - \frac{i}{2}m_{12}\right)^2 + p^2 + \frac{1}{2}\left(m_1^2 + m_2^2 + \frac{1}{2}m_{12}^2\right)\right] - \frac{1}{4}(m_1^2 - m_2^2)^2\right\}
\end{aligned} \tag{8.39}$$

Expanding in $-\frac{1}{4}(m_1^2 - m_2^2)^2$ is effectively the same as expanding in α^4, since $(m_1^2 - m_2^2)^2 = \mu_I^4 \sin^4\alpha \sim \alpha^4$. We use this observation to write,

$$\begin{aligned}
&\Omega_{1,\pi^\pm} + \Omega^T_{1,\pi^\pm} = \frac{1}{2}\sum\!\!\!\!\!\!\int_K \log\left\{\left[\left(k_0 + \frac{i}{2}m_{12}\right)^2 + p^2 + \frac{1}{2}\left(m_1^2 + m_2^2 + \frac{1}{2}m_{12}^2\right)\right]\right. \\
&\left.\times\left[\left(k_0 - \frac{i}{2}m_{12}\right)^2 + p^2 + \frac{1}{2}\left(m_1^2 + m_2^2 + \frac{1}{2}m_{12}^2\right)\right]\right\} - \frac{1}{8}(m_1^2 - m_2^2)^2\sum\!\!\!\!\!\!\int_K \\
&\left\{\frac{1}{\left[\left(k_0 + \frac{i}{2}m_{12}\right)^2 + p^2 + \frac{1}{2}\left(m_1^2 + m_2^2 + \frac{1}{2}m_{12}^2\right)\right]\left[\left(k_0 - \frac{i}{2}m_{12}\right)^2 + p^2 + \frac{1}{2}\left(m_1^2 + m_2^2 + \frac{1}{2}m_{12}^2\right)\right]}\right\} \\
&+ O(\alpha^8).
\end{aligned} \tag{8.40}$$

In Appendix C.3 we show that the temperature-dependent part of the first term in Eq.(8.40) can be written as,

$$\begin{aligned}
&\mathcal{I}(T) \equiv \frac{1}{2}\sum\!\!\!\!\!\!\int_K \log\left\{\left[\left(k_0 + \frac{i}{2}m_{12}\right)^2 + p^2 + \frac{1}{2}\left(m_1^2 + m_2^2 + \frac{1}{2}m_{12}^2\right)\right]\times\right. \\
&\left.\left[\left(k_0 - \frac{i}{2}m_{12}\right)^2 + p^2 + \frac{1}{2}\left(m_1^2 + m_2^2 + \frac{1}{2}m_{12}^2\right)\right]\right\} = -\frac{b^2T^2}{\pi^2}\sum_{n=1}^{\infty}\frac{K_2\left(\frac{bn}{T}\right)}{n^2}\cosh\left(\frac{an}{T}\right),
\end{aligned} \tag{8.41}$$

where we have ignored temperature-independent terms, and defined new constants a and b as,

$$a \equiv \frac{1}{2}m_{12} = \mu_I \cos\alpha, \qquad b \equiv \sqrt{\frac{1}{2}\left(m_1^2 + m_2^2 + \frac{1}{2}m_{12}^2\right)} = \sqrt{m_\pi^2 \cos\alpha + \frac{1}{2}\mu_I^2 \sin^2\alpha}. \tag{8.42}$$

The temperature-dependent part of the second integral in Eq.(8.40) is finite and can be rewritten as[48],

$$\begin{aligned}
&\not\!\!\int\!\!\!\!\!\sum_K \left\{ \frac{1}{\left[(k_0+ia)^2 + p^2 + b^2\right] \times \left[(k_0-ia)^2 + p^2 + b^2\right]} \right\} = \\
&\frac{1}{8}\not\!\!\int\!\!\!\!\!\sum_K \frac{1}{k_0^2}\left(\frac{1}{a}\frac{\partial}{\partial a} + \frac{1}{b}\frac{\partial}{\partial b}\right) \log\left\{ \left[(k_0+ia)^2 + \vec{k}^2 + b^2\right]\left[(k_0-ia)^2 + \vec{k}^2 + b^2\right] \right\} = \\
&-\frac{b^2T^2}{4\pi^2}\sum_{n=1}^{\infty}\frac{1}{(2\pi nT)^2}\left(\frac{1}{a}\frac{\partial}{\partial a} + \frac{1}{b}\frac{\partial}{\partial b}\right) b^2 \frac{K_2\left(\frac{bn}{T}\right)}{n^2}\cosh\left(\frac{an}{T}\right) = \\
&\frac{1}{16\pi^4 T}\sum_{n=1}^{\infty}\frac{1}{n^3}\frac{b}{a}\left[a\cosh\left(\frac{an}{T}\right)K_1\left(\frac{bn}{T}\right) - b\sinh\left(\frac{an}{T}\right)K_2\left(\frac{bn}{T}\right)\right].
\end{aligned} \tag{8.43}$$

We made use of Eq.(8.41) to obtain the second equality, and the following relation for modified Bessel functions,

$$\frac{\partial K_n(x)}{\partial x} = -K_{n-1}(x) - \frac{nK_n(x)}{x}. \tag{8.44}$$

to obtain the final equality in Eq.(8.43).

By combining Eqs.(8.40)-(8.43) we find that the temperature-dependent contribution to the free energy from the charged pion modes can be written as,

$$\begin{aligned}
\Omega^T_{1,\pi^+} + \Omega^T_{1,\pi^-} &= -\frac{b^2T^2}{\pi^2}\sum_{n=1}^{\infty}\frac{K_2\left(\frac{bn}{T}\right)}{n^2}\cosh\left(\frac{an}{T}\right) \\
&-\frac{\mu_I^4\alpha^4}{128\pi^4 T}\sum_{n=1}^{\infty}\frac{1}{n^3}\frac{b}{a}\left[a\cosh\left(\frac{an}{T}\right)K_1\left(\frac{bn}{T}\right) - b\sinh\left(\frac{an}{T}\right)K_2\left(\frac{bn}{T}\right)\right] + O(\alpha^8).
\end{aligned} \tag{8.45}$$

We obtain the full temperature-dependence of the free energy Ω^T in the region of the phase-plane where $\alpha \ll 1$ and $T \ll m_\pi$ by adding Eq.(8.35) and Eq.(8.45). The result reads,

$$\begin{aligned}
\Omega^T_{1,\pi^0} + \Omega^T_{1,\pi^+} + \Omega^T_{1,\pi^-} &= -\frac{1}{2}\frac{m_3^2T^2}{\pi^2}\sum_{n=1}^{\infty}\frac{K_2\left(\frac{m_3 n}{T}\right)}{n^2} - \frac{b^2T^2}{\pi^2}\sum_{n=1}^{\infty}\frac{K_2\left(\frac{bn}{T}\right)}{n^2}\cosh\left(\frac{an}{T}\right) \\
&-\frac{\mu_I^4\alpha^4}{128\pi^4 T}\sum_{n=1}^{\infty}\frac{1}{n^3}\frac{b}{a}\left[a\cosh\left(\frac{an}{T}\right)K_1\left(\frac{bn}{T}\right) - b\sinh\left(\frac{an}{T}\right)K_2\left(\frac{bn}{T}\right)\right] + O(\alpha^8).
\end{aligned} \tag{8.46}$$

In Ref.[44] the temperature-independent part of the renormalized free energy is expanded in α up to $O(\alpha^4)$. Using Eq.(8.36) and Eq.(8.46) we may now do a similar expansion of the temperature-dependent part of Ω, and thereby extend the zero-temperature analysis from Ref.[44] into the (μ_I, T)-plane. This is precisely what we proceed to do in the following.

8.3 Landau functional

Our assumptions so far are that the effective order parameter is small $\alpha \ll 1$ and that the critical temperature is low $T \ll m_\pi$. To proceed with a consistent analytical expansion of Eq.(8.46), we first have to probe the low-temperature behavior of the theory. More specifically, we have to choose between one of the following approximations, $|b-a| \ll T \ll m_\pi$ and $T \ll |b-a| \ll m_\pi$. If neither of the approximations are justifiable in the relevant part of the phase plane, then we have to restrict our analysis to smaller subsets of the phase plane until one of the approximations can be justified.

It is useful to see the leading-order expansion of a and b in powers of α to get a clearer overview of our alternatives,

$$a = \mu_I - \frac{\mu_I}{2}\alpha^2 + \frac{\mu_I}{24}\alpha^4 + ..., \tag{8.47}$$

$$b = m_\pi + \frac{m_\pi}{4}\left(\frac{\mu_I^2 - m_\pi^2}{m_\pi^2}\right)\alpha^2 - \frac{m_\pi}{48}\left(\frac{4\mu_I^2 - m_\pi^2}{m_\pi^2}\right)\alpha^4 + ... \tag{8.48}$$

Adding the two equations above we find that $|b-a| = \mu_I - m_\pi + O(\alpha^2)$. Thus, $|b-a|$ effectively measures the difference in isospin chemical potential relative to the zero-temperature transition point $\mu_I = m_\pi$, when $\alpha \ll 1$. The two possible approximations are therefore equivalent to assuming that the phase-transition line is very steep $|b-a| \ll T$, or very flat $T \ll |b-a|$. LQCD simulations[27], various effective model results[36, 133, 134] and previously obtained χPT[48, 114] results all suggest that the phase-transition curve is very steep in the region where $T \ll m_\pi$. We will therefore consider the limit $|b-a| \ll T \ll m_\pi$ in the following.

The preceding assumptions justify the following approximation,

$$e^{-\frac{b}{T}}\cosh\left(\frac{a}{T}\right) \approx e^{-\frac{b}{T}}\sinh\left(\frac{a}{T}\right) \approx \frac{\exp\left\{-\frac{b-a}{T}\right\}}{2}. \tag{8.49}$$

When $T \ll b$ we may safely use the asymptotic expansion of K_2 given in Eq.(8.36). Combining the asymptotic expansion of K_2 with the approximation in Eq.(8.49) we obtain,

$$\begin{aligned} &-\frac{b^2T^2}{\pi^2}\sum_{n=1}^{\infty}\frac{K_2\left(\frac{bn}{T}\right)}{n^2}\cosh\left(\frac{an}{T}\right) = -\frac{1}{2}\sqrt{\frac{b^3T^5}{2\pi^3}}\sum_{n=1}^{\infty}\frac{\exp\left[-\frac{n}{T}(b-a)\right]}{n^{\frac{5}{2}}}\left[1+\frac{15}{8}\frac{T}{bn}+O\left(\frac{T^2}{m^2}\right)\right] \\ &= -\frac{1}{2}\sqrt{\frac{b^3T^5}{2\pi^3}}\left[\mathrm{Li}_{\frac{5}{2}}\left(e^{-\left(\frac{b-a}{T}\right)}\right)+\frac{15}{8}\frac{T}{b}\mathrm{Li}_{\frac{7}{2}}\left(e^{-\left(\frac{b-a}{T}\right)}\right)\right]+..., \end{aligned} \tag{8.50}$$

and

$$\begin{aligned} &-\frac{\mu_I^4\alpha^4}{128\pi^4T}\sum_{n=1}^{\infty}\frac{1}{n^3}\frac{b}{a}\left[a\cosh\left(\frac{an}{T}\right)K_1\left(\frac{bn}{T}\right)-b\sinh\left(\frac{an}{T}\right)K_2\left(\frac{bn}{T}\right)\right] = \\ &-\frac{\mu_I^4\alpha^4}{128\pi^4T}\sum_{n=1}^{\infty}\frac{1}{n^3}\frac{b}{a}\sqrt{\frac{\pi T}{8bn}}e^{-\left(\frac{b-a}{T}\right)n}\left[(a-b)+\frac{T}{bn}\left(\frac{3a}{8}-\frac{15b}{8}\right)\right] = \\ &\frac{\mu_I^4\alpha^4}{2048a\sqrt{2b\pi^7T}}\left[8b(b-a)\mathrm{Li}_{\frac{7}{2}}\left(e^{-\left(\frac{b-a}{T}\right)}\right)+3T(5b-a)\mathrm{Li}_{\frac{9}{2}}\left(e^{-\left(\frac{b-a}{T}\right)}\right)\right]. \end{aligned} \tag{8.51}$$

The polylogarithm functions in the last lines of Eqs.(8.50) and (8.51) are defined by their series expansions,

$$\mathrm{Li}_n(z) \equiv \sum_{k=1}^{\infty}\frac{z^k}{k^n}. \tag{8.52}$$

Comparing Eqs.(8.35),(8.46) and (8.50)-(8.51) we see that the neutral contribution $\Omega^T_{\pi^0}$ to the Landau functional is exponentially suppressed compared to $\Omega^T_{1,\pi^+} + \Omega^T_{1,\pi^-}$, and it can therefore be safely neglected in the following.

We can use the following series expansion of the polylogarithmic function $\mathrm{Li}_{\frac{n}{2}}(z)$ around $z = 1$,[11]

$$\mathrm{Li}_{\frac{n}{2}}(z) = \zeta\left(\frac{n}{2}\right) + \zeta\left(\frac{n}{2}-1\right)(z-1) + \frac{1}{2}\left[\zeta\left(\frac{n}{2}-2\right) - \zeta\left(\frac{n}{2}-1\right)\right](z-1)^2 + O\left((z-1)^3\right)$$
$$- i^n\Gamma\left(1-\frac{n}{2}\right)(z-1)^{\frac{n}{2}-1} + O\left((z-1)^{\frac{n}{2}}\right), \qquad z \in \mathbb{R}, \tag{8.53}$$

to expand the polylogarithmic functions $\mathrm{Li}_{\frac{n}{2}}(\exp\{-\left(\frac{b-a}{T}\right)\})$ occurring in Eqs.(8.50) and (8.51) in powers of $\frac{(b-a)}{T}$.

Eqs.(8.47)-(8.53) contain all the information we need to obtain an analytical expression for the temperature-dependent part of the effective Landau functional in Eq.(8.46). Since we disregard terms of order $O(\alpha^6)$ we may substitute $a = \mu_I$ and $b = m$ into Eq.(8.51),[12] and approximate the polylogarithmic functions $\mathrm{Li}_{\frac{n}{2}}(z)$ occuring in Eq.(8.51) by the leading-order term $\zeta\left(\frac{n}{2}\right)$ in Eq.(8.53).

In Appendix C.4 we expand Eq.(8.50) to fourth order in α and obtain,

$$\frac{1}{2}\sqrt{\frac{b^3T^5}{2\pi^3}}\left[\mathrm{Li}_{\frac{5}{2}}\left(e^{-\left(\frac{b-a}{T}\right)}\right) + \frac{15}{8}\frac{T}{b}\mathrm{Li}_{\frac{7}{2}}\left(e^{-\left(\frac{b-a}{T}\right)}\right)\right] \approx \frac{1}{2}\sqrt{\frac{m^3T^5}{2\pi^3}}\left[\mathrm{Li}_{\frac{5}{2}}\left(e^{-\left(\frac{b-a}{T}\right)}\right)\right]$$
$$\approx \frac{1}{2}\sqrt{\frac{m^3T^5}{2\pi^3}}\zeta\left(\frac{5}{2}\right) - \frac{\mu_I}{4}\sqrt{\frac{m^3T^3}{2\pi^3}}\zeta\left(\frac{3}{2}\right)\alpha^2 + \frac{\mu_I^2}{16}\sqrt{\frac{m^3T}{2\pi^3}}\left[\zeta\left(\frac{1}{2}\right) - \zeta\left(\frac{3}{2}\right)\right]\alpha^4$$
$$+ O\left(\alpha^6\right). \tag{8.54}$$

Adding Eqs.(8.51) and (8.54) we finally obtain the temperature-dependent contribution to the effective Landau functional,[13]

$$\Omega_T \approx -\frac{1}{2}\sqrt{\frac{m_\pi^3T^5}{2\pi^3}}\zeta\left(\frac{5}{2}\right) + \frac{\mu_I}{4}\sqrt{\frac{m_\pi^3T^3}{2\pi^3}}\zeta\left(\frac{3}{2}\right)\alpha^2 - \frac{\mu_I^2}{16}\sqrt{\frac{m_\pi^3T}{2\pi^3}}\left[\zeta\left(\frac{1}{2}\right) - \zeta\left(\frac{3}{2}\right)\right]\alpha^4$$
$$+ \frac{3\mu_I^3}{512}\sqrt{\frac{m_\pi T}{2\pi^7}}\zeta\left(\frac{9}{2}\right)\alpha^4 + O\left(\alpha^6\right). \tag{8.55}$$

We can now combine Eq.(8.55) with the temperature-independent contribution $\Omega_{T=0}$ obtained by Adhikari and Andersen in Ref.[44] to write down the full Landau functional,

$$\Omega = c_0 + c_2\alpha^2 + c_4\alpha^4 + O(\alpha^6), \tag{8.56}$$

[11] Here $\zeta(x)$ denotes the Riemann-Zeta function, which is ≥ 1 for $x \geq 1$.

[12] Which is equivalent to evaluating a and b at $\alpha = 0$.

[13] Using $mT \gg m(m-\mu_I)$ to see that the first term in the parentheses in Eq.(8.51) is much smaller than the second, and that $3T(5m-\mu_I) \approx 12Tm$.

whose coefficients c_2 and c_4 are given below,

$$c_2 = \frac{1}{2}m^2 f^2 \left[1 - \frac{m_\pi^2}{2(4\pi)^2 f^2}(\bar{l}_3 - 4\bar{l}_4)\right] - \frac{1}{2}f^2\mu_I^2 \left[1 + \frac{2m_\pi^2}{(4\pi)^2 f^2}\bar{l}_4\right] + \frac{\mu_I}{4}\sqrt{\frac{m_\pi^3 T^3}{2\pi^3}}\zeta\left(\frac{3}{2}\right), \tag{8.57}$$

$$\begin{aligned} c_4 = -\frac{1}{24}f^2 \Bigg\{ & (m^2 - 4\mu_I^2) - \frac{1}{2(4\pi)^2 f^2}\left[6\mu_I^2\sqrt{m_\pi^4 - \mu_I^4} - 10m_\pi^2\mu_I^2(3 - 4\bar{l}_4)\right. \\ & \left. + 4m_\pi^4\left(\frac{9}{4} + \bar{l}_3 - 4\bar{l}_4\right) + 8\mu_I^4\left(\frac{9}{4} - \bar{l}_1 - 2\bar{l}_2 + \frac{3}{2}\log\frac{\sqrt{m_\pi^2 - \mu_I^2} + \sqrt{m_\pi^2 + \mu_I^2}}{\sqrt{2}m_\pi}\right)\right]\Bigg\} \\ & - \frac{\mu_I^2}{16}\sqrt{\frac{m_\pi^3 T}{2\pi^3}}\left[\zeta\left(\frac{1}{2}\right) - \zeta\left(\frac{3}{2}\right)\right] + \frac{3\mu_I^3}{512}\sqrt{\frac{m_\pi T}{2\pi^7}}\zeta\left(\frac{9}{2}\right). \end{aligned} \tag{8.58}$$

The next-to-leading order relations in Eq.(3.35) and Eq.(3.52) lets us rewrite c_2 as,

$$c_2 = \frac{1}{2}f_\pi^2(m_\pi^2 - \mu_I^2) + \frac{\mu_I}{4}\sqrt{\frac{m_\pi^3 T^3}{2\pi^3}}\zeta\left(\frac{3}{2}\right), \tag{8.59}$$

which manifests the zero-temperature phase-transition at $\mu_I = m_\pi$.

We proceed to solve $c_2(\mu_I) = 0$ for the isospin chemical potential and obtain,

$$\mu_I^c(T) \approx m_\pi + \frac{1}{4f_\pi^2}\sqrt{\frac{m_\pi^3 T^3}{2\pi^3}}\zeta\left(\frac{3}{2}\right), \tag{8.60}$$

which is in agreement with the result obtained by Splittorff et al. in Ref.[48]. Thus, the analytical approximation suggests that the transition curve $\mu_I^c(T)$ should scale as $T^{\frac{3}{2}}$ for $(\mu_I - m_\pi) \ll T \ll m_\pi$.

The analytical approximation of the phase-transition curve in Eq.(8.60) is displayed by the black dashed line in Fig.8.2. The solid blue line in the figure shows the phase-transition curve obtained by He et al. in Ref.[36], where they use a mean-field flavor $SU(2)$ NJL model. The green shaded area marked with "LQCD" shows the phase-transition curve obtained on the lattice by Brandt et al. in Ref.[27]. The green bar separates the BEC phase from the normal phase at low temperatures and the BEC phase from QGP phase at high temperatures, as indicated in the figure. The phase-transition curve obtained on the lattice is almost vertical for temperatures up to ~ 150 MeV, and then suddenly flattens out to make the curve attain a scythe-like shape. We observe that the mean-field NJL phase-transition curve is in quite good agreement with LQCD data up to $T \approx 100$ MeV, and then starts to display a more pronounced temperature dependence.

The $T^{\frac{3}{2}}$ behavior of the low-temperature approximation is in quite good agreement with the NJL model result at very low temperatures. It is, however, not in very good agreement with the LQCD result in any part of the phase-plane. We pay no attention to the high-temperature behavior of the black curve, as the low-temperature approximation is doomed to fail long before we even get close to the deconfinement crossover.

We have included a plot of the assumptions underlying the analytical χPT calculation in Fig.8.3, to gain a deeper insight into the region of validity for the result in Eq.(8.60). The red curve shows the normalized critical temperature $\frac{T}{m_\pi}$ as a function of normalized isospin chemical potential, the blue curve shows $\frac{\mu_I - m_\pi}{T}$ as a function of normalized isospin chemical potential, and the horizontal black curve $y = 0.1$ is a suggestive cutoff for the validity of the assumptions. We observe that $(\mu_I - m_\pi) \ll T$ is a reasonable assumption when the isospin chemical potential is smaller than $\mu_I \approx 1.04 m_\pi$. The assumption that $T \ll m_\pi$ is, however, only seen to be somewhat satisfied when $\mu_I < 1.01 m_\pi$. The latter

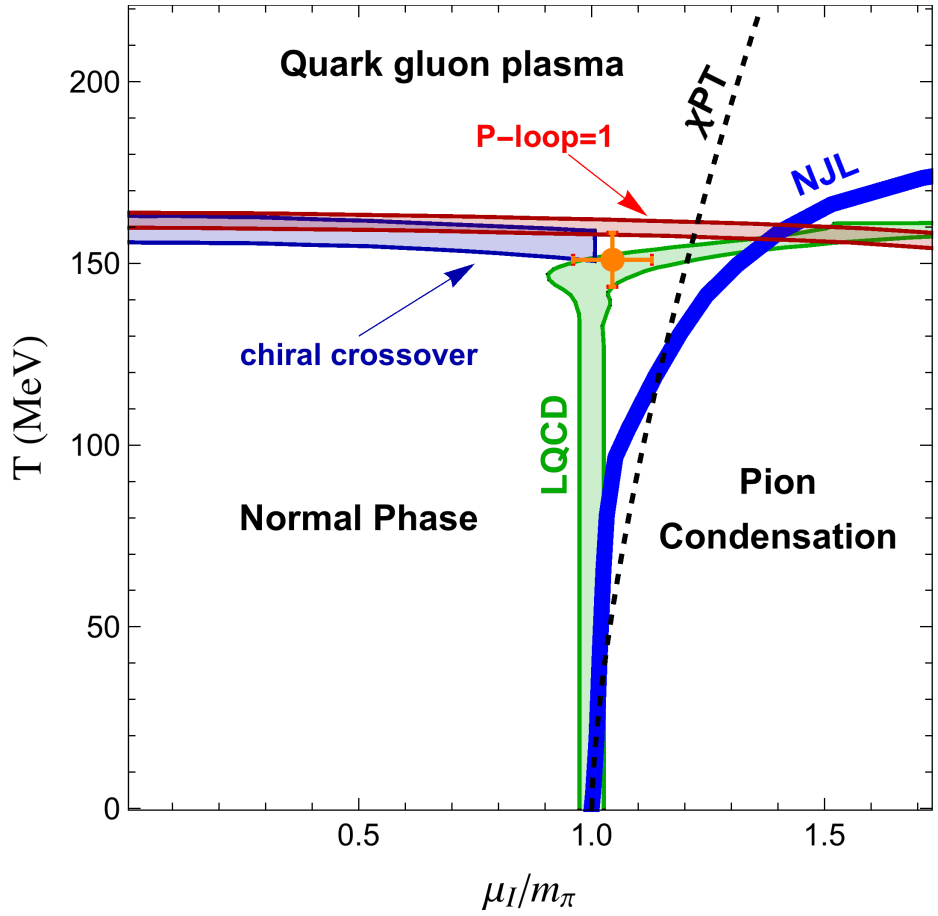

Figure 8.2: Isospin-temperature phase diagram for hadronic matter. The green shaded area marked with LQCD shows the second-order phase-transition curve obtained in (2+1)-flavor LQCD simulations by Brandt et al[27]. The solid blue line shows the mean-field flavor $SU(2)$ NJL-model result for the second-order phase-transition curve obtained in Ref.[36] by He et al. The black dashed line shows the analytical low-temperature χPT result in Eq.(8.60), see the text for more details. The shaded blue area is the chiral crossover transition, connecting (0 MeV, 160 MeV) to the triple point (orange dot with error bars) at approximately (140(10) MeV, 151(7) MeV). The chiral and BEC transitions coincide beyond this point[27]. The shaded red area indicates a probable deconfinement phase transition reported by Brandt et al, where they use the Polyakov loop as their measure for deconfinement. The interested reader is referred to Refs.[27] and [91] for further details about the phase diagram and the different curves. The figure is taken from Ref.[91] with the author's permission.

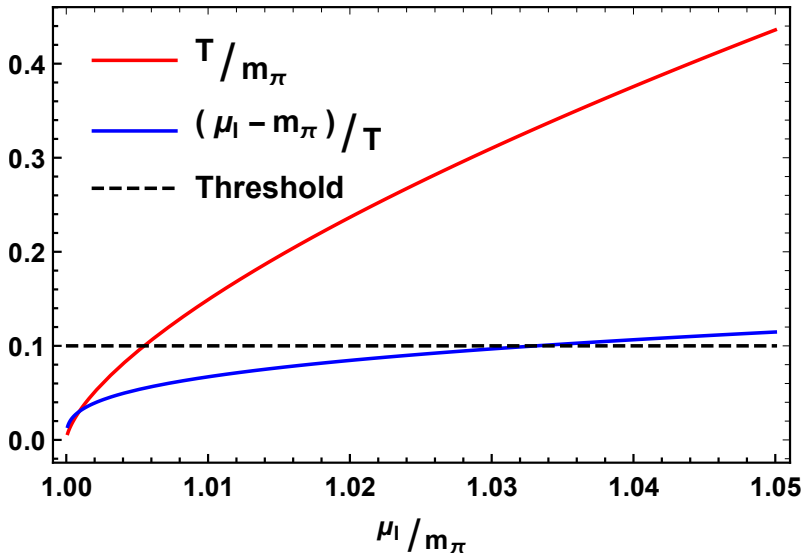

Figure 8.3: The figure shows the assumptions that we used to derive the analytical result for the phase-transition curve in Eq.(8.60). The red curve shows the normalized critical temperature $\frac{T}{m_\pi}$ as a function of normalized isospin chemical potential, and the blue curve shows $\frac{\mu_I - m_\pi}{T}$ as a function of normalized isospin chemical potential. The black dashed line provides a suggestive cutoff for the region of validity for the assumptions, see the text for details.

observation implies that the analytical approximation in Eq.(8.60) can only be justified for temperatures below 20 MeV.

Finally, inspired by Splittorf et al. we address the possibility of having a tricritical point, $(\mu_I^{\rm tri}, T^{\rm tri})$, which satisfies $c_2(\mu_I^{\rm tri}, T^{\rm tri}) = c_4(\mu_I^{\rm tri}, T^{\rm tri}) = 0$. Since μ_I^c scales as $T^{\frac{3}{2}}$, while the terms in the last line of Eq.(8.58) only scale as $\sqrt{T}$, we can perform a suggestive low-temperature estimation of the hypothetical tricritcal point by substituting $\mu_I = m_\pi$ into Eq.(8.58). Ignoring the second term in the last line of (8.58), which is small compared to the first term, we obtain the following estimation,

$$T^{\rm tri} \approx \frac{2\pi^3}{\zeta\left(\frac{1}{2}\right) - \zeta\left(\frac{3}{2}\right)} \left[\frac{2f^2m^2}{m_\pi^4} + \frac{1}{3(4\pi)^2}\left(-3 - 8\bar{l}_1 - 16\bar{l}_2 + 4\bar{l}_3 + 24\bar{l}_4\right)\right]^2 m_\pi \sim m_\pi. \tag{8.61}$$

The result in Eq.(8.61) suggests that *if* a tricritical point exists, then it should be located in a region of the phase-plane where the assumptions that we used to derive the analytical approximation are no longer valid. This conclusion is in agreement with LQCD data, which show no sign of a tricritical point.

8.4 Quark and Pion condensates

We will now return our focus to the full expression for the free energy given in Eq.(8.32) and use it to generate the expressions for the pion condensate and the quark condensate at finite temperature. We proceed to discuss the numerical approach that we employ to determine the BEC-transition curve and whether the interpretation of α as an effective order parameter is justifiable at finite temperature.

Pion condensate

The pion condensate at finite temperature can be decomposed into a sum of the temperature-independent contribution given in Eq.(7.27), and the temperature-dependent contribution $\langle\pi^+\rangle_T$ given by,

$$\langle\pi^+\rangle_T = \frac{1}{2}\frac{\partial\Omega_T}{\partial j}. \tag{8.62}$$

It follows from Eqs.(8.32)-(8.33) and Eq.(8.62) that the temperature-dependence of the pion condensate can be written on the following form,

$$\langle\pi^+\rangle_T = \frac{1}{2}\int_k \frac{\partial E_{\pi^0}}{\partial j} n_B(E_{\pi^0}) + \frac{1}{2}\int_k \frac{\partial E_{\pi^+}}{\partial j} n_B(E_{\pi^+}) + \frac{1}{2}\int_k \frac{\partial E_{\pi^-}}{\partial j} n_B(E_{\pi^-}), \tag{8.63}$$

where $n_B(x)$ denotes the Bose-Einstein factor,

$$n_B(x) \equiv \frac{1}{e^{\beta x} - 1}. \tag{8.64}$$

By first substituting the source-dependent masses given in Eqs.(7.11)-(7.13) into the expressions for the dispersion relations in Eqs.(4.27)-(4.28), and then differentiate the source-dependent dispersion relations with respect to j, we obtain,

$$\frac{\partial E_{\pi^0}}{\partial j} = \frac{B_0 \sin\alpha}{E_{\pi^0}}, \tag{8.65}$$

$$\frac{\partial E_{\pi^\pm}}{\partial j} = \frac{B_0 \sin\alpha}{E_{\pi^\pm}}\left[1 \pm \frac{m_{12}^2}{\sqrt{4k^2 m_{12}^2 + (m_1^2 + m_2^2 + m_{12}^2)^2 - 4m_1^2 m_2^2}}\right]. \tag{8.66}$$

The final expression for the temperature-dependent contribution to the pion condensate is obtained by substituting Eqs.(8.65)-(8.66) into Eq.(8.63). It follows that the pion condensate at finite temperature can be written as,

$$\langle\pi^+\rangle_{\mu_I,T} = \langle\pi^+\rangle_{\mu_I,0} + \frac{1}{2}B_0 \sin\alpha \left\{\int_k \frac{n_B\left(E_{\pi^+}\right)}{E_{\pi^+}}\left[1 + \frac{m_{12}^2}{\sqrt{4k^2 m_{12}^2 + (m_1^2 + m_2^2 + m_{12}^2)^2 - 4m_1^2 m_2^2}}\right]\right.$$
$$\left. + \int_k \frac{n_B\left(E_{\pi^-}\right)}{E_{\pi^-}}\left[1 - \frac{m_{12}^2}{\sqrt{4k^2 m_{12}^2 + (m_1^2 + m_2^2 + m_{12}^2)^2 - 4m_1^2 m_2^2}}\right] + \int_k \frac{n_B\left(E_{\pi^0}\right)}{E_{\pi^0}}\right\}, \tag{8.67}$$

where the expression for $\langle\pi^+\rangle_{\mu_I,0}$ is given in Eq.(7.27).

The onset of pion condensation at finite temperature is characterized by the order parameter in Eq.(8.67), whose magnitude changes from zero to nonzero at the onset. We observe that a sudden change in $\langle\pi^+\rangle_{\mu_I,T}$ can only be induced by a sudden change in α, as long as μ_I and T are smoothly varying variables. We also notice that $\langle\pi^+\rangle_{\mu_I,T}$ vanishes when $\alpha = 0$, while it is nonzero when α is nonzero. These observations justify the employment of α as an effective order parameter at finite temperature.

The parameter α is determined by minimizing the renormalized free energy Ω given in Eq.(8.33). The discussion in the preceding paragraph suggests that a change in $\alpha_{\rm gs}$ from zero to a finite value, where $\alpha_{\rm gs}$ is defined by,

$$\left.\frac{\partial\Omega}{\partial\alpha}\right|_{\alpha_{\rm gs}} = 0, \tag{8.68}$$

signals a transition from the normal phase to the BEC phase. Our numerical result for the transition curve is obtained by iterating over a range of values for T and μ_I for which we solve Eq.(8.68) and subsequently check whether the solution is zero or nonzero. More

specifically, we iterate over a list of values of T, and for each value of T we iterate over an ordered list of values of μ_I where the first element is smaller than or equal to the zero-temperature critical isospin chemical potential. The pair (μ_I, T) is acknowledged as a point on the phase-transition curve if the associated solution $\alpha_{\rm gs}$ is larger than a threshold value. The order of the phase-transition at (μ_I, T) is determined by checking whether $\alpha_{\rm gs}$ changes continuously or discontinuously from zero to a finite value as we increase the magnitude of the isospin chemical potential from $\mu_I - \epsilon$ to $\mu_I + \epsilon$, where $\epsilon \ll \mu_I$. The results are discussed in section 8.5.

Quark condensate

Similar to the pion condensate, the quark condensate may also be decomposed into a sum of a temperature-independent contribution and a temperature-dependent contribution, where the latter is given by,

$$\langle\bar{\psi}\psi\rangle_T = \frac{1}{2}\int_k \frac{\partial E_{\pi^0}}{\partial m_q} n_B(E_{\pi^0}) + \frac{1}{2}\int_k \frac{\partial E_{\pi^+}}{\partial m_q} n_B(E_{\pi^+}) + \frac{1}{2}\int_k \frac{\partial E_{\pi^-}}{\partial m_q} n_B(E_{\pi^-}). \tag{8.69}$$

Differentiating the source-dependent dispersion relations with respect to m_q, we obtain,

$$\frac{\partial E_{\pi^0}}{\partial m_q} = \frac{B_0 \cos\alpha}{E_{\pi^0}}, \tag{8.70}$$

$$\frac{\partial E_{\pi^\pm}}{\partial m_q} = \frac{B_0 \cos\alpha}{E_{\pi^\pm}} \left[1 \pm \frac{m_{12}^2}{\sqrt{4k^2 m_{12}^2 + (m_1^2 + m_2^2 + m_{12}^2)^2 - 4m_1^2 m_2^2}}\right]. \tag{8.71}$$

It follows from Eqs.(8.69)-(8.71) that the next-to-leading order result for the chiral condensate at finite temperature and isospin chemical potential can be written as,

$$\langle\bar{\psi}\psi\rangle_{\mu_I,T} = \langle\bar{\psi}\psi\rangle_{\mu_I,0} + \frac{1}{2}B_0\cos\alpha\left\{\int_k \frac{n_B\left(E_{\pi^+}\right)}{E_{\pi^+}}\left[1 + \frac{m_{12}^2}{\sqrt{4k^2 m_{12}^2 + (m_1^2 + m_2^2 + m_{12}^2)^2 - 4m_1^2 m_2^2}}\right]\right.$$
$$\left. + \int_k \frac{n_B\left(E_{\pi^-}\right)}{E_{\pi^-}}\left[1 - \frac{m_{12}^2}{\sqrt{4k^2 m_{12}^2 + (m_1^2 + m_2^2 + m_{12}^2)^2 - 4m_1^2 m_2^2}}\right] + \int_k \frac{n_B\left(E_{\pi^0}\right)}{E_{\pi^0}}\right\}, \tag{8.72}$$

where the expression for $\langle\bar{\psi}\psi\rangle_{\mu_I,0}$ is given in Eq.(7.29).

By comparing Eq.(8.67) with Eq.(8.72) we notice that the temperature dependent contributions to the chiral condensate and the pion condensate satisfy the tree-level relation,

$$\left\langle\pi^+\right\rangle_T \cos\alpha = \left\langle\bar{\psi}\psi\right\rangle_T \sin\alpha. \tag{8.73}$$

This allows us to extend the zero-temperature NLO relation in Eq.(7.35) to a finite-temperature NLO relation on the same form,

$$\langle\bar{\psi}\psi\rangle_{\mu_I,T} = \frac{\cos\alpha}{\sin\alpha}\langle\pi^+\rangle_{\mu_I,T} - 16h_1 B_0^2 m_u. \tag{8.74}$$

We observe that the magnitude of h_1 in Eq.(8.74) parametrizes how bad the tree-level relation

$$\sin\alpha\langle\bar{\psi}\psi\rangle_{\mu_I,T} = \cos\alpha\langle\pi^+\rangle_{\mu_I,T} \tag{8.75}$$

is broken at next-to-leading order.

8.5 Results: BEC transition and condensates

In this section, we present numerical results for the phase-transition curve $\mu_I^c(T)$ separating the normal phase from the BEC phase. We obtain the phase-transition curve by studying the behavior of the ansatz-parameter α, as discussed in the previous section. We compare our results with the analytical low-temperature approximation in Eq.(8.60), and with the NJL-model and LQCD results displayed in Fig.8.2.

In Fig.8.4 we plot data (red dots) from the full numerical calculation within χPT to next-to-leading order, along with the analytical approximation in Eq.(8.60). The results are in very good agreement when $T \leq 15$ MeV, while there is clear tension for temperatures higher than 20 MeV. This observation is consistent with our previous discussion concerning the validity of the underlying assumptions of Eq.(8.60), where we concluded that the analytical approximation only remains somewhat justifiable for temperatures lower than 20 MeV.

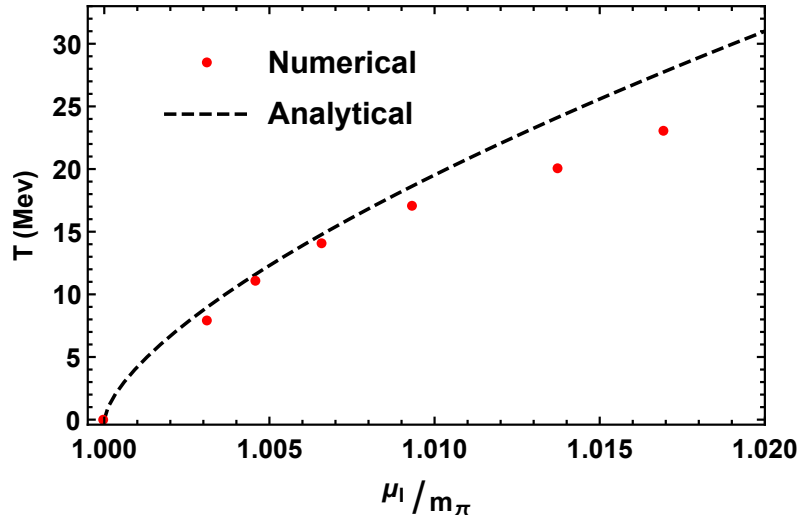

Figure 8.4: The figure shows the second-order phase-transition curve separating the normal phase from the BEC phase at low temperatures. The black dashed line is the analytical approximation derived from the effective Landau functional in section 8.3. The red dots are data from the numerical calculation of full χPT to next-to-leading order.

To arrange for a fair visual comparison between our numerical calculation and the results displayed in Fig.8.2, we plot our numerical data along with the analytical approximation in Fig.8.5, while using a layout that is very similar to the layout in Fig.8.2. The red dashed curve shows the numerical result, where we have used central values for the phenomenological parameters. The black dashed line displayed in Figs.8.2 and 8.5 are identical.

While the red and black curves in Fig.8.5 are indistinguishable at very low temperatures, we observe a much more prominent deflection in the red curve compared to the black curve at higher temperatures. This behavior is strikingly different from the NJL-model and LQCD results displayed in Fig.8.2. The deflection in the red curve looks somewhat similar to the deflection in the NJL-model result, with the deflection in the latter starting at $T \approx 100$ MeV, and the deflection in the former starting at $T \approx 20$ MeV. Apart from this, there does not seem to be any resemblance between our result and the established NJL-model and LQCD results for the phase-transition curve.

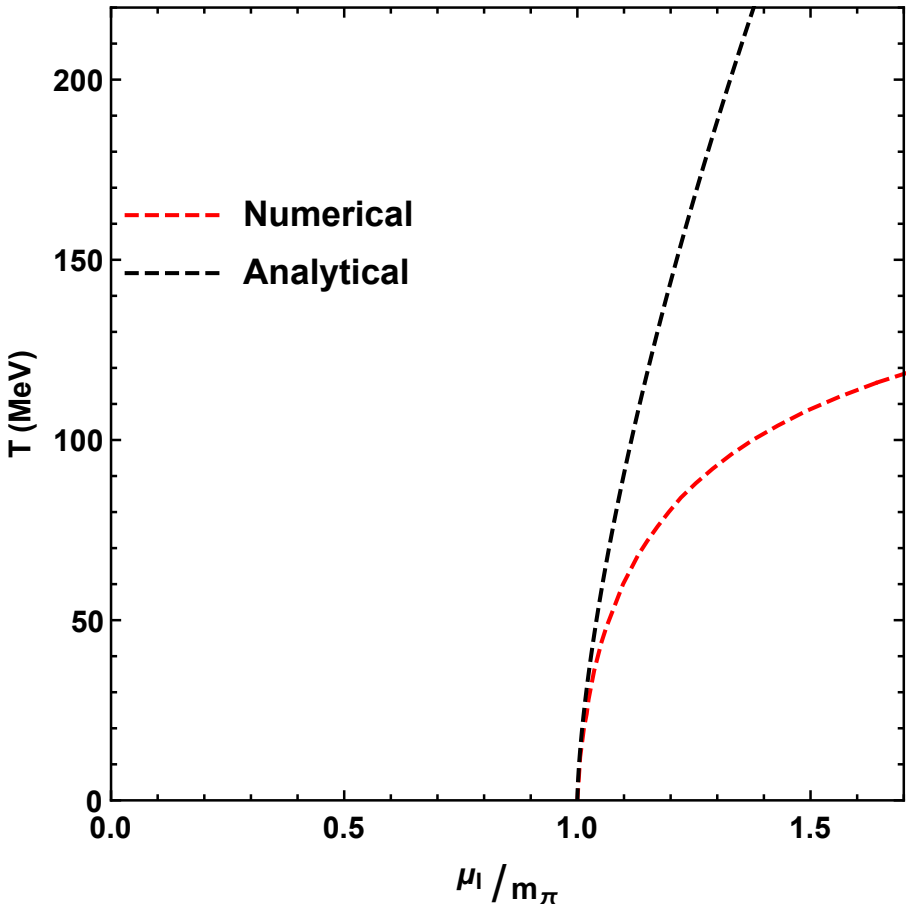

Figure 8.5: The figure shows the phase-transition curve separating the BEC phase from the normal phase at low temperatures and the BEC phase from the QGP phase at high temperatures. The black curve shows the analytical low-temperature approximation obtained by Splittorff et al. in Ref.[111]. The red curve shows the numerical result for full χPT to next-to-leading order. The layout of the figure is similar to the layout of Fig.8.2, see the text for further details.

Order of the phase-transition

Previously, we argued that the order of the phase transition can be determined by employing the solution to Eq.(8.68) $\alpha_{\rm gs}$ as an effective order parameter. We consider the region of the phase plane displayed in Fig.8.5 and find that $\alpha_{\rm gs}$ changes continuously from zero to nonzero as we cross the critical line, i.e., the red line in Fig.8.5. This behavior in $\alpha_{\rm gs}$ signals that the phase-transition from the normal phase to the BEC phase is of second order. Our findings are in agreement with the lattice study of Brandt et al., which unlike Splittorff et al., do *not* obtain a tricritical point where the phase transition changes from second to first order.

In Fig.8.6, we plot $\alpha_{\rm gs}$ as a function of the normalized isospin chemical potential while keeping the temperature fixed. We observe that although the curves evolve very differently at small isospin densities, they all seem to asymptote towards the same ground-state configuration at high values of μ_I. We also observe a discontinuity in $\alpha_{\rm gs}$ when $T = 100$ MeV (the green curve) and $T = 120$ MeV (the black curve) occurring inside the pion-condensed phase, which signals a discontinuous change in the ground-state configuration on the Goldstone manifold. The discontinuities in α propagate into the expressions for the pion condensate and the chiral condensate, which consequently become discontinuous at the same points in the pion-condensed phase.

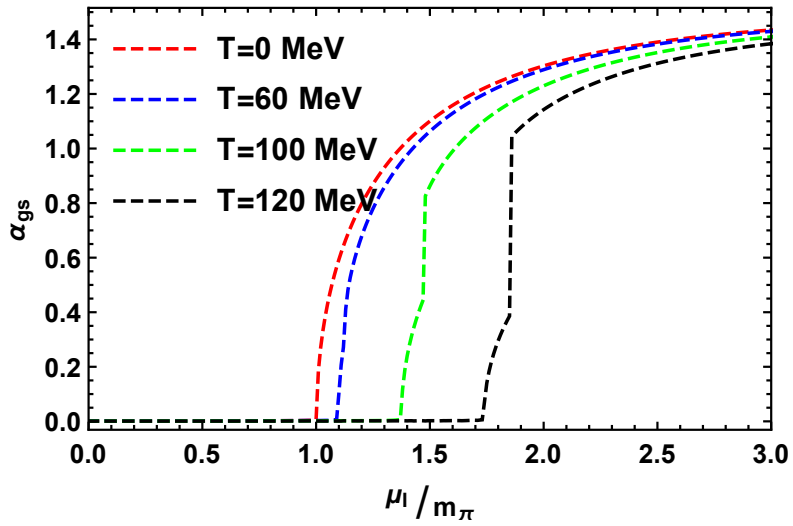

Figure 8.6: The figure shows $\alpha_{\rm gs}$ as a function of the normalized isospin chemical potential at fixed values for the temperature. The red line, the blue line, the green line and the black line shows $\alpha_{\rm gs}(\mu_I)$ for $T = 0$ MeV, $T = 60$ MeV, $T = 100$ MeV, and $T = 120$ MeV, respectively.

To obtain a better understanding of this phenomenon, we plot the free energy as a function of α at $T = 120$ MeV and with two different values for the normalized isospin chemical potential in Fig.8.7. The magnitude of μ_I in the left frame is slightly smaller than the isospin chemical potential μ_I^d, for which we observe a discontinuity in the black curve in Fig.8.6. Meanwhile, the magnitude of μ_I in the right frame is larger than μ_I^d.

We observe that there is a competition between two local minima in the free energy, which are indicated by red dots in Fig.8.7. The minimum to the left has evolved continuously from being located at $\alpha = 0$ in the normal phase to its current location on the α-axis in the pion-condensed phase. Increasing the isospin chemical potential causes another local minimum to appear, which is separated from the first one by a local maximum. When the magnitude of the isospin chemical potential reaches μ_I^d the new minimum becomes the global minimum, leading to a discontinuity in $\alpha_{\rm gs}$. This evolution is illustrated by

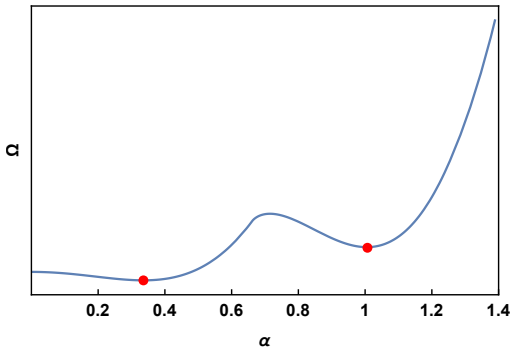

(a) The red dot to the left indicates the global minimum of the free energy as a function of α, while the red dot to the right indicates a local minimum.

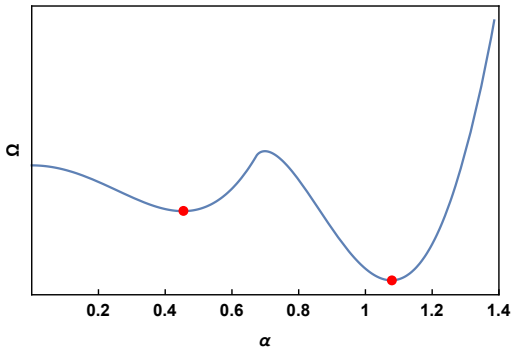

(b) The red dot to the left indicates a local minimum in the free energy as a function of α, while the red dot to the right indicates a global minimum.

Figure 8.7: The two panels display the free energy as a function of α at $T = 120$ MeV and $\mu_I = 1.82 m_\pi$ (left) and $\mu_I = 1.9 m_\pi$ (right). The red dots indicate local minima in the free energy.

the two panels in Fig. 8.7. The order of the phase transition is left unaffected since the discontinuity in $\alpha_{\rm gs}$ occurs while the minimum to the left is located at a finite value for α.

We have checked that cranking up the temperature eventually causes the local minimum to the right to become global while the local minimum to the left is still located at $\alpha = 0$, which makes the phase transition of first order. However, we do not discuss this any further because it does *not* occur in a region of the phase plane where the validity of χPT is expected to be reasonable.

8.5.1 Pion and quark condensates

In this section, we present results from our numerical calculations of $\Sigma_{\bar{\psi}\psi}$ and Σ_{π^+} at finite temperature and vanishing pionic source. The temperature-dependent contributions to the condensate deviations, $\Sigma_{\bar{\psi}\psi}$ and Σ_{π^+}, become increasingly oscillatory at higher temperatures. We have not been able to handle the oscillations entirely, which is evident in the plots. The issue is most significant in regions of the phase-plane where $\alpha_{\rm gs}$ vanishes. The results for Σ_{π^+} are therefore less affected than the results for $\Sigma_{\bar{\psi}\psi}$, since the magnitude of $\langle \pi^+ \rangle$ is damped by a factor of $\sin\alpha$. We will direct the following discussion towards the most stable regions of the phase plane, particularly when we discuss the results for $\Sigma_{\bar{\psi}\psi}$.

Quark-condensate deviation

In Fig.8.8, we plot $\Sigma_{\bar{\psi}\psi}$ as a function of normalized isospin chemical potential while keeping the temperature fixed. The values of T associated with the different curves are displayed in the figure. We notice that the magnitude of $\Sigma_{\bar{\psi}\psi}$ decreases as we crank up the temperature in the vacuum $\mu_I = 0$. This is consistent with the general expectation about a chiral crossover transition at high temperatures, where the magnitude of $\langle \bar{\psi}\psi \rangle$ is very small (and vanish entirely in the chiral limit $m_u \to 0$).

We observe that the magnitude of $\Sigma_{\bar{\psi}\psi}$ increases as we crank up the temperature in the high-density regime in Fig.8.8. Generally speaking, one would expect that thermal fluctuations should have the opposite effect on the magnitude of the chiral condensate, i.e., make it smaller. It is unclear why this is not the case here.

Even though the temperature dependence of $\Sigma_{\bar{\psi}\psi}$ in the high-density regime is unexpected, we observe that the differences between the curves in Fig.8.8 decrease as we go to very high values for the isospin chemical potential. This observation suggests that

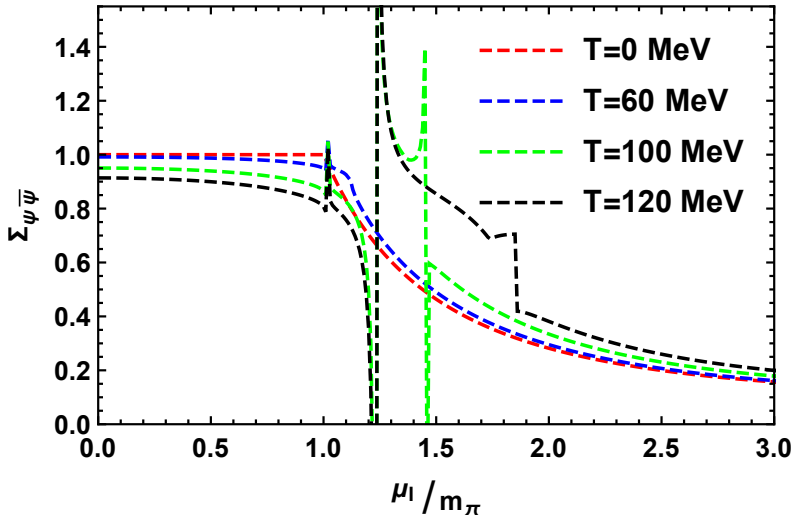

Figure 8.8: The figure shows $\Sigma_{\bar{\psi}\psi}$ as a function of the normalized isospin chemical potential at fixed values of the temperature. The red line, the blue line, the green line and the black line shows $\alpha_{\rm gs}(\mu_I)$ for $T = 0$ MeV, $T = 60$ MeV, $T = 100$ MeV, and $T = 120$ MeV, respectively.

finite-temperature effects become less important in the asymptotic (isospin) behavior of $\Sigma_{\bar{\psi}\psi}$.

Pion-condensate deviation

In Fig.8.9, we plot Σ_{π^+} as a function of the normalized isospin chemical potential while keeping the temperature fixed. The result for $T = 100$ MeV suffers from the same numerical problem as the $T = 100$ MeV result for $\Sigma_{\bar{\psi}\psi}$ in Fig.8.8, which cause the abrupt changes in the green curves around $\mu_I \approx 1.47 m_\pi$. Apart from this, we see that the numerical results for Σ_{π^+} are quite well behaved.

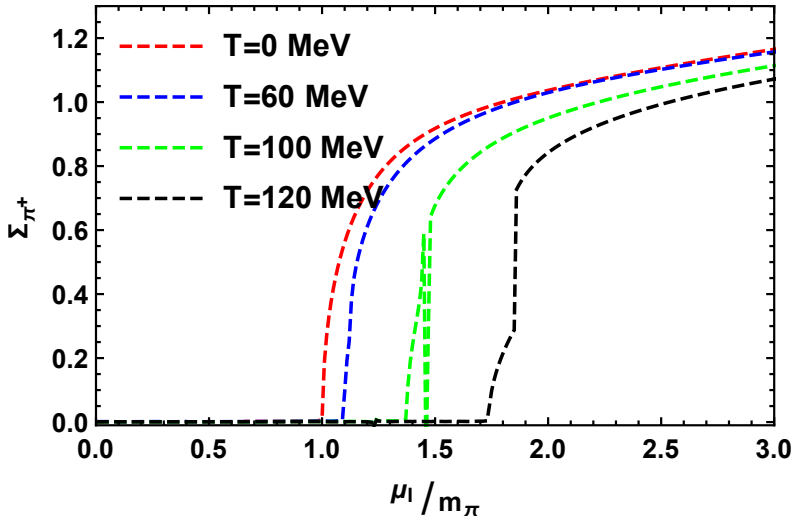

Figure 8.9: The figure shows Σ_{π^+} as a function of the normalized isospin chemical potential at fixed values of the temperature. The red line, the blue line, the green line and the black line show $\alpha_{\rm gs}(\mu_I)$ for $T = 0$ MeV, $T = 60$ MeV, $T = 100$ MeV, and $T = 120$ MeV, respectively.

The discontinuity in the ground state configuration $\alpha_{\rm gs}$ is recognized very clearly in

the result for Σ_{π^+} at $T = 120$ MeV (the black curve in Fig.8.9), which has a discontinuity at the same location as the black curve in Fig.8.6. It is harder to recognize the impact that the discontinuity in $\alpha_{\rm gs}$ at $T = 100$ MeV has on the result for Σ_{π^+} at $T = 100$ MeV, due to the numerical problem.

We observe that thermal fluctuations weaken the strength of the pion condensate throughout the region of consideration in Fig.8.9. We also observe that the magnitude of the pion condensate is increasing steadily as a function of μ_I at high isospin densities. Finite-temperature effects are still quite significant in this region, and we observe a nearly 10% difference between the red curve and the black curve at $\mu_I = 3m_\pi$.

A final remark on the chiral crossover

In Fig.8.8, we see that χPT at finite temperature and small isospin chemical potential, $\mu_I \ll m_\pi$, predicts the strength of the chiral condensate to become weaker as we crank up the temperature. This observation motivated us to look for signs of the chiral crossover in the regime where $\mu_I \ll m_\pi$.

The pseudo-critical temperature T_{pc} depends on the criteria that we use to detect the crossover transition. There are several different criteria that we may use, see for example Ref.[127] for a discussion, which may yield different results for T_{pc}, but all reduce to the same unique result in the chiral limit. Inspired by Brandt et al.'s choice, we decided to use $\partial_T^2 \Sigma_{\bar{\psi}\psi} = 0$ as our criterion. Our calculations of $\partial_T^2 \Sigma_{\bar{\psi}\psi}$ as a function of temperature displayed a rather constant behavior at high temperatures, showing no sign of a crossover.

Over 30 years ago, Gerber and Leutwyler[90] used finite temperature χPT to estimate the pseudo-critical temperature in the absence of chemical potentials, by performing a low-temperature expansion of the chiral condensate to three loops. To obtain numerical results they had to set a numerical value for $h_1^{\rm GL}$, which they estimated in two different ways; by using model arguments (see for example Appendix B in Ref.[22]), and by using large N_c arguments, see Ref.[90] for details. They obtained a pseudo-critical temperature $T_c \approx 190$ MeV for nonzero quark masses to three loops, and a one-loop result that was much higher. We performed the same analysis with our result for $\langle \bar{\psi}\psi \rangle$ in Eq.(8.72) and found that even changing the sign of $h_1^{\rm GL}$ and varying it over a large range of values, leads to results well above 200 MeV. These observations indicate that two-flavor χPT is unsuitable, at least to one loop, in the regime where the chiral crossover takes place.

Chapter 9

Conclusions and outlook

9.1 Summary

In this thesis, we have studied the chiral condensate and the pion condensate at finite isospin chemical potential within two-flavor chiral perturbation theory. We worked to next-to-leading order in the low-energy expansion and investigated the cases of zero and nonzero pionic source at vanishing temperature, and vanishing pionic source at finite temperature. We also studied the phase-transition curve between the normal phase and the BEC phase. Furthermore, we have discussed how to renormalize the quasi-particle masses in the pion-condensed phase to one loop and considered the neutral mode and the Goldstone mode in detail.

Quasi-particle masses

We identified all contributions to the self-energy of the neutral pion π^0 in the pion-condensed phase. We presented the expressions for the diagrams and discussed how to isolate the divergent contributions from the loop integrals. We also obtained the Feynman diagrams contributing to the self energy of the (rotated) π^+ field and showed that it is a massless Goldstone boson in the pion-condensed phase.

Condensates at zero temperature

We calculated the ground-state parameter α, the chiral condensate, and the pion condensate at nonzero values for the pionic source at zero temperature. We used our results to perform a qualitative comparison with recent (2+1)-flavor lattice QCD simulations and found that the agreement becomes significantly better when we include next-to-leading order corrections. Our results show that the rotation relation between the chiral condensate and the pion-condensate in the pion-condensed phase is broken at next-to-leading order.

We also performed a calculation of the chiral and pion condensates at vanishing pionic source. The results can gauge the accuracy of future LQCD simulations at vanishing pionic source, a calculation that is currently challenging to perform.

Condensates at finite temperature

We extended the analysis of the free energy, the chiral condensate, and the pion condensate to include finite-temperature effects. We performed calculations of the condensates while keeping the temperature fixed, and analyzed the temperature dependence of the chiral and the pion condensates. A complete analysis of the chiral condensate was not performed due to difficulties with the numerical evaluations. We found that the χPT results are much more sensitive to temperature fluctuations than the lattice results.

As we increased the temperature, we found a new type of behavior in the density evolution of the ground-state configuration. Instead of rotating smoothly on the Goldstone manifold in the pion-condensed phase, the evolution of the ground-state configuration changes discontinuously at some value for the isospin chemical potential at high temperatures. We showed that this behavior originates from the competition between two local minima in the free energy at high temperatures.

The BEC transition

We calculated the phase-transition curve between the normal and the BEC phases numerically by treating the ansatz-parameter α as an effective order parameter. We found that thermal fluctuations have a significant impact on the phase-transition curve. Our result is in good agreement with Splittorff et al.'s analytical low-temperature approximation in Ref.[48] for temperatures below 20 MeV. However, it is in very poor agreement with the $SU(2)$ NJL-model result of He et al. presented in Ref.[36], the $(2+1)$-flavor lattice QCD result of Brandt et al. presented in Ref.[27], the χM model result of Folkestad et al. presented in Ref.[133], and the Polyakov-loop quark-meson model result of Adhikari et al. presented in Ref.[134]. All of the abovementioned studies find that the phase transition is quite insensitive to thermal fluctuations for temperatures up to 100-160 MeV. Thus, finite-temperature χPT at next-to-leading order predicts a very different phase-transition curve between the normal and the BEC phases in the low-temperature regime, as well as the high-temperature regime, compared to LQCD, NJL-model, χM-model, and Polyakov-loop quark-meson model results.

9.2 Conclusion

We find that the rotated π^+ field is massless when $\mu_I \geq m_\pi$ at vanishing temperature, which provides a non-trivial check of the consistency of χPT in the pion-condensed phase beyond leading order. We obtain the chiral and pion condensates at finite pionic source and vanishing temperature in χPT to next-to-leading order, which are in good agreement with available lattice data. We also obtain the chiral and the pion condensates at vanishing pionic source and zero temperature, which can be used to gauge the quality of future LQCD calculations.

We find the agreement between LQCD and χPT at next-to-leading order to be significantly worse at finite temperature compraed to zero temperature. Our results for the phase-transition curve and the pion condensate disagree qualitatively with lattice results. The result for the phase-transition curve is also in poor agreement with effective model results.

9.3 Outlook

There are several ways to improve, continue, and extend the work presented in this thesis. In the following, we summarize some possibilities.

Possible improvements

There are several ways to improve the work presented in this thesis. One step would be to improve the numerical calculations of the chiral condensate at finite temperature. Another step would be to calculate the neutral pion mass in the pion-condensed phase using the correct value for α in the loop integrals. This would open up the possibility for a new quantitative comparison between LQCD and χPT beyond leading order in the pion-condensed phase.

Calculate the phase-transition curve using the Goldstone boson

One may calculate the thermal π^+ mass in the normal phase and use it to identify the phase-transition curve separating the normal and the BEC phases. The condition $m_{\pi^+} = 0$ should provide a curve in the (μ_I, T)-phase plane which coincides with the BEC-transition curve obtained in this thesis. Solving $m_{\pi^+} = 0$ for μ_I would therefore provide a non-trivial check of our result. We have already obtained the relevant diagrams and expressions for the self-energy of π^+, which are presented in Appendix D. The remaining steps are to calculate the thermal mass corrections from the loop propagators and implement the result numerically.

Calculations in the normal phase are considerably easier to perform than calculations in the pion-condensed phase, since α vanishes in the former phase. For this reason, we only propose to perform the analysis in the normal phase even though we should obtain the same result by performing the analysis in the pion-condensed phase, as long as the phase transition remains second order.

Include an external axial vector field

In Ref.[42] Brandt et al. calculate an axial vector condensate $\sigma_A = \frac{1}{2}(\bar{u}\gamma_0\gamma_5 d + \bar{d}\gamma_0\gamma_5 u)$ on the lattice. By including the external axial vector field a^0 in the χPT Lagrangian, see Eq.(2.28), we may generate the axial vector condensate at finite isospin density and compare results with the lattice. The tree-level calculation has been performed by Brauner et al. in Ref.[135], but next-to-leading order corrections have not been considered yet. We may also do this calculation for three-flavor χPT, which opens the possibility for a new comparison between two-flavor χPT, three-flavor χPT and lattice QCD in the pion-condensed phase.

To perform a fair comparison between two-flavor and three-flavor χPT we may consider the large-m_s limit,[1] where three-flavor results should reduce to two-flavor results with modified LECs. The large-m_s limit allows us to use three-flavor LECs in the two-flavor result and thereby avoid an unfair comparison due to the difference in precision and uncertainty of two-flavor and three-flavor LECs. This procedure was first employed by Adhikari et al. in Ref.[45] to fairly compare pressure, isospin density and energy density results between two-flavor χPT, three-flavor χPT and LQCD.

[1] Here m_s denotes the strange-quark mass.

Appendices

Appendix A

Conventions

- We use the Einstein summation convention, where repeated indices are summed over unless otherwise stated.
- We employ natural units, where the reduced Planck constant $\hbar$, the Boltzmann constant k_B and the speed of light c are all set to unity, $\hbar = k_B = c = 1$.
- We choose the Minkowski metric signature $g_{\mu\nu}$ =diag$(1, -1, -1, -1)$.
- We write n-momentum integrals[1] in the $\overline{\text{MS}}$ scheme in $d = n - 2\epsilon$ dimensions at zero temperature as,

$$\int_k \equiv \Big(\frac{e^\gamma \Lambda^2}{4\pi}\Big)^\epsilon \int \frac{d^d k}{(2\pi)^d}. \tag{A.1}$$

- We write sum-integrals at finite temperature as,

$$\frac{1}{\beta} \sum_{n=-\infty}^{\infty} \int_k \equiv \sum\!\!\!\!\!\!\int_K . \tag{A.2}$$

[1] n is set to four when we integrate over four-momentum and it is set to three when we integrate over spatial momentum.

Appendix B

Derivations of $\mathcal{L}_2$ and $\mathcal{L}_4$

In this Appendix we expand the χPT Lagrangian at nonzero isospin chemical potential in the pion-fields π_i.

We will be using the following parametrization of fluctuations around the ground state on the Goldstone manifold,

$$\Sigma = A_\alpha(U\Sigma_0 U)A_\alpha, \tag{B.1}$$

where,

$$A_\alpha = \cos\frac{\alpha}{2} + i\tau_1 \sin\frac{\alpha}{2}, \tag{B.2}$$

$$\Sigma_0 = \mathbb{1}, \tag{B.3}$$

$$U = \exp\left(i\frac{\pi_a\tau_a}{2f}\right). \tag{B.4}$$

In the calculations that follow we make frequent use of the following trace relations,

$$\begin{aligned}
&\mathrm{Tr}(\tau_a\tau_b) = 2\delta_{ab},\\
&\mathrm{Tr}(\tau_a\tau_b\tau_c) = 2i\epsilon_{abc},\\
&\mathrm{Tr}(\tau_a\tau_b\tau_c\tau_d) = 2(\delta_{ab}\delta_{cd} - \delta_{ac}\delta_{bd} + \delta_{ad}\delta_{bc}),\\
&\mathrm{Tr}(\tau_a\tau_b\tau_c\tau_d\tau_e) = 2i[\epsilon_{cde}\delta_{ab} + \epsilon_{abx}(\delta_{xc}\delta_{de} - \delta_{xd}\delta_{ce} + \delta_{xe}\delta_{cd})],
\end{aligned}$$

which are easily derived from the (anti)commutation relations below,

$$\begin{aligned}
\left[\frac{\tau_a}{2}, \frac{\tau_b}{2}\right] &= i\epsilon_{abc}\frac{\tau_c}{2},\\
\left\{\frac{\tau_a}{2}, \frac{\tau_b}{2}\right\} &= \frac{1}{2}\delta_{ab}.
\end{aligned}$$

B.1 The LO Lagrangian

In this section we expand the LO Lagrangian to quartic order in the pion fields. The LO Lagrangian was expanded to quadratic order in the pion fields in Ref.[Project thesis], and the following derivation of the non-interaction terms is based on that work. The derivation of the interaction terms at leading order, and the next-to-leading order terms are not based on previous work.

The χPT Lagrangian at finite isospin chemical potential to order p^2 reads,

$$\mathcal{L}_2 = \frac{f^2}{4}\,\mathrm{Tr}\left[\nabla^\mu\Sigma^\dagger\nabla_\mu\Sigma\right] + \frac{f^2m^2}{4}\,\mathrm{Tr}\left[\Sigma + \Sigma^\dagger\right], \tag{B.5}$$

where the covariant derivatives are defined as,

$$\nabla_\mu \Sigma = \partial_\mu \Sigma - i[v_\mu, \Sigma], \tag{B.6}$$

$$\nabla_\mu \Sigma^\dagger = \partial_\mu \Sigma^\dagger - i[v_\mu, \Sigma^\dagger], \tag{B.7}$$

where $v_\mu = \delta_{\mu 0}\mu_I \frac{\tau_3}{2}$.

Non-interaction terms

We begin by expanding Eq.(B.1) to quadratic order in the pion fields,

$$\Sigma = \Big(\cos\frac{\alpha}{2} + i\tau_1 \sin\frac{\alpha}{2}\Big)\left(1 + \frac{i}{f}\pi_a\tau_a - \frac{1}{2f^2}\pi_a\tau_a\pi_b\tau_b + ...\right)\Big(\cos\frac{\alpha}{2} + i\tau_1\sin\frac{\alpha}{2}\Big), \tag{B.8}$$

which gives,

$$\begin{aligned}\Sigma = \cos\alpha + i\sin\alpha\tau_1 + \frac{i\pi_a}{f}\cos^2\frac{\alpha}{2}\tau_a - \frac{i\pi_a}{f}\sin^2\frac{\alpha}{2}(2\delta_{a1}\tau_1 - \tau_a) - \frac{\pi_a}{f}\sin\alpha\delta_{a1} \\ - \frac{\pi_a\pi_a}{2f^2}\cos^2\frac{\alpha}{2} + \frac{\pi_a\pi_a}{2f^2}\sin^2\frac{\alpha}{2} - \frac{i\pi_a\pi_a}{2f^2}\sin\alpha\tau_1.\end{aligned} \tag{B.9}$$

The static term in the leading-order Lagrangian is easily obtained from Eq.(B.9), and reads,

$$\frac{f^2m^2}{4}\mathrm{Tr}\Big(\Sigma + \Sigma^\dagger\Big) = f^2m^2\cos\alpha - m^2 f\sin\alpha\pi_1 - \frac{m^2}{2}\cos\alpha(\pi_1^2 + \pi_2^2 + \pi_3^2). \tag{B.10}$$

The kinetic term $\nabla^\mu\Sigma^\dagger\nabla_\mu\Sigma$ can be expanded as,

$$\nabla^\mu\Sigma^\dagger\nabla_\mu\Sigma = \partial^\mu\Sigma^\dagger\partial_\mu\Sigma - i\{(\partial^\mu\Sigma^\dagger)[v_\mu,\Sigma] - \mathrm{h.c}\} + [v^\mu,\Sigma]^\dagger[v_\mu,\Sigma], \tag{B.11}$$

where h.c denotes the Hermitian conjugate. We observe from Eq.(B.11) that it will be easy to obtain the expression for $\nabla^\mu\Sigma^\dagger\nabla_\mu\Sigma$ once we have the appropriate expressions for $\partial_\mu\Sigma$ and $[v_\mu,\Sigma]$.[1] We use this observation in the following.

Differentiating Eq.(B.9) with respect to x^μ yields,

$$\begin{aligned}\partial_\mu\Sigma = \frac{i\partial_\mu\pi_a}{f}\Big[\cos^2\frac{\alpha}{2}\tau_a - \sin^2\frac{\alpha}{2}(2\delta_{a1}\tau_1 - \tau_a) + i\sin\alpha\delta_{a1}\Big] \\ + \frac{\partial_\mu(\pi_a\pi_a)}{2f^2}\Big[-\cos^2\frac{\alpha}{2} + \sin^2\frac{\alpha}{2} - i\sin\alpha\tau_1\Big],\end{aligned} \tag{B.12}$$

where the first line is linear in the pion fields and the second line is quadratic in the pion fields. Using Eq.(B.12) we obtain,

$$\frac{f^2}{4}\mathrm{Tr}\Big(\partial^\mu\Sigma^\dagger\partial_\mu\Sigma\Big) = \frac{1}{2}\partial^\mu\pi_a\partial_\mu\pi_a. \tag{B.13}$$

This is just the canonical kinetic term that we obtain in the limit of vanishing isospin chemical potential $\mu_I = 0$.

It follows from Eq.(B.9) that $[v_\mu,\Sigma]$ can be expanded as,

$$\begin{aligned}[v_\mu,\Sigma] = -\delta_{\mu0}\mu_I\sin\alpha\tau_2 + \delta_{\mu0}\frac{\mu_I}{f}\cos^2\frac{\alpha}{2}(\pi_2\tau_1 - \pi_1\tau_2) \\ + 2\delta_{\mu0}\frac{\mu_I\pi_1}{f}\sin^2\frac{\alpha}{2}\tau_2 - i\delta_{\mu0}\frac{\mu_I\pi_a\pi_a}{2f^2}\sin\alpha\tau_2 + ...\end{aligned} \tag{B.14}$$

[1] We will refer to these constituents as the *building blocks*.

We use this expansion to obtain,

$$\mathrm{Tr}\{[v^\mu,\Sigma]^\dagger[v_\mu,\Sigma]\} = \frac{2}{f^2}\mu_I^2\cos(2\alpha)\pi_1^2 + \frac{2}{f^2}\mu_I^2\cos^2\alpha\pi_2^2 - \frac{2}{f^2}\mu_I^2\sin^2\alpha\pi_3^2 + 2\mu_I^2\sin^2\alpha + \frac{4\mu_I^2}{f}\cos\alpha\sin\alpha\pi_1. \tag{B.15}$$

By combining the expansions in Eq.(B.12) and Eq.(B.14) we obtain,

$$-i\,\mathrm{Tr}\{(\partial^\mu\Sigma^\dagger)[v_\mu,\Sigma] - \mathrm{h.c}\} = \frac{4}{f}\mu_I\sin\alpha\partial_0\pi_2 + \frac{4}{f^2}\mu_I\cos\alpha(\pi_1\partial_0\pi_2 - \pi_2\partial_0\pi_1). \tag{B.16}$$

Finally, by combining Eqs.(B.11), (B.13), (B.15) and (B.16) we obtain the leading-order kinetic term to quadratic order in the pion fields,

$$\frac{f^2}{4}\,\mathrm{Tr}\Big[\nabla^\mu\Sigma^\dagger\nabla_\mu\Sigma\Big] = \frac{1}{2}\partial^\mu\pi_a\partial_\mu\pi_a + f\mu_I\sin\alpha\partial_0\pi_2 + \mu_I\cos\alpha(\pi_1\partial_0\pi_2 - \pi_2\partial_0\pi_1) + \frac{1}{2}\mu_I^2\cos(2\alpha)\pi_1^2 + \frac{1}{2}\mu_I^2\cos^2\alpha\pi_2^2 - \frac{1}{2}\mu_I^2\sin^2\alpha\pi_3^2 + \frac{1}{2}f^2\mu_I^2\sin^2\alpha + f\mu_I^2\cos\alpha\sin\alpha\pi_1. \tag{B.17}$$

The terms in the leading-order Lagrangian $\mathcal{L}_2$ can be written on the conventional form $\mathcal{L}_2 = \mathcal{L}_2^{\mathrm{static}} + \mathcal{L}_2^{\mathrm{linear}} + \mathcal{L}_2^{\mathrm{quadratic}} + ...$ By adding Eq.(B.10) and Eq.(B.17) we obtain,

$$\mathcal{L}_2^{\mathrm{static}} = f^2m^2\cos\alpha + \frac{1}{2}f^2\mu_I^2\sin^2\alpha, \tag{B.18}$$

$$\mathcal{L}_2^{\mathrm{linear}} = f(-m^2\sin\alpha + \mu_I^2\cos\alpha\sin\alpha)\pi_1 + f\mu_I\sin\alpha\partial_0\pi_2, \tag{B.19}$$

$$\mathcal{L}_2^{\mathrm{quadratic}} = \frac{1}{2}\partial^\mu\pi_a\partial_\mu\pi_a + \mu_I\cos\alpha(\pi_1\partial_0\pi_2 - \pi_2\partial_0\pi_1) - \frac{1}{2}(m^2\cos\alpha - \mu_I^2\cos2\alpha)\pi_1^2 - \frac{1}{2}(m^2\cos\alpha - \mu_I^2\cos^2\alpha)\pi_2^2 - \frac{1}{2}(m^2\cos\alpha + \mu_I^2\sin^2\alpha)\pi_3^2. \tag{B.20}$$

Interaction terms

To obtain the cubic and quartic interaction terms from the leading-order Lagrangian, we first need to expand Eq.(B.8) to quartic order in the pion fields. The relevant contribution from Eq.(B.8) reads,

$$\left(\cos\frac{\alpha}{2} + i\tau_1\sin\frac{\alpha}{2}\right)\left(-\frac{i}{6f^3}\pi_a\pi_b\pi_c\tau_a\tau_b\tau_c + \frac{1}{24f^4}\pi_a\pi_b\pi_c\pi_d\tau_a\tau_b\tau_c\tau_d\right)\left(\cos\frac{\alpha}{2} + i\tau_1\sin\frac{\alpha}{2}\right),$$

which is equivalent to,

$$-\frac{i\cos\alpha}{6f^3}\pi_a\pi_a\pi_b\tau_b + \frac{\cos\alpha}{24f^4}\pi_a\pi_a\pi_b\pi_b + \frac{\sin\alpha}{6f^3}\pi_a\pi_a\pi_1 + \frac{i\sin\alpha}{24f^4}\pi_a\pi_a\pi_b\pi_b. \tag{B.21}$$

This expansion leads to the following contribution from the static part of the Lagrangian,

$$\frac{f^2m^2}{4}\,\mathrm{Tr}\Big(\Sigma+\Sigma^\dagger\Big)^{\mathrm{cubic}} = \frac{m^2\sin\alpha}{6f}\pi_1\pi_a\pi_a, \tag{B.22}$$

$$\frac{f^2m^2}{4}\,\mathrm{Tr}\Big(\Sigma+\Sigma^\dagger\Big)^{\mathrm{quartic}} = \frac{m^2\cos\alpha}{24f^2}\pi_a\pi_a\pi_b\pi_b. \tag{B.23}$$

In order to obtain the contribution from the kinetic part of the Lagrangian, we have to expand $\partial_\mu\Sigma$ and $[v_\mu,\Sigma]$ to cubic and to quartic order in the pion fields, respectively. The result can be written as,

$$\partial_\mu\Sigma^{\text{cubic}} = \frac{1}{6f^3}\partial_\mu(\pi_a\pi_a\pi_c)\left(-i\cos\alpha\tau_c + \sin\alpha\delta_{1c}\right), \tag{B.24}$$

$$[v_\mu,\Sigma]^{\text{cubic}} = -i\delta_{\mu 0}\frac{\mu_I}{12f^3}\cos\alpha\pi_a\pi_a\pi_c[\tau_3,\tau_c], \tag{B.25}$$

$$[v_\mu,\Sigma]^{\text{quartic}} = i\delta_{\mu 0}\frac{\mu_I}{24f^4}\sin\alpha\pi_a\pi_a\pi_b\pi_b\tau_2. \tag{B.26}$$

By combining the expressions above with the expressions in Eq.(B.12) and Eq.(B.14), we obtain the following equalities,

$$\text{Tr}\{\partial^\mu\Sigma^\dagger\partial_\mu\Sigma\}^{\text{cubic}} = 0, \tag{B.27}$$

$$\text{Tr}\{\partial^\mu\Sigma^\dagger\partial_\mu\Sigma\}^{\text{quartic}} = \frac{2}{3f^4}\left[\pi_a\pi_b\partial^\mu\pi_a\partial_\mu\pi_b - \pi_a\pi_a\partial^\mu\pi_b\partial_\mu\pi_b\right], \tag{B.28}$$

$$-i\,\text{Tr}\{(\partial^\mu\Sigma^\dagger)[v_\mu,\Sigma] - \text{h.c}\}^{\text{cubic}} = -\frac{4\mu_I\sin\alpha}{f^3}\left(\pi_1^2\partial_0\pi_2 + \pi_3^2\partial_0\pi_2\right), \tag{B.29}$$

$$-i\,\text{Tr}\{(\partial^\mu\Sigma^\dagger)[v_\mu,\Sigma] - \text{h.c}\}^{\text{quartic}} = -\frac{4\mu_I\cos\alpha}{3f^4}\pi_a\pi_a\left(\pi_1\partial_0\pi_2 - \pi_2\partial_0\pi_1\right), \tag{B.30}$$

$$\text{Tr}\{[v^\mu,\Sigma]^\dagger[v_\mu,\Sigma]\}^{\text{cubic}} = -\frac{8\mu_I^2}{3f^3}\sin\alpha\cos\alpha\pi_1\pi_a\pi_a \tag{B.31}$$

$$\text{Tr}\{[v^\mu,\Sigma]^\dagger[v_\mu,\Sigma]\}^{\text{quartic}} = -\frac{2\mu_I^2}{3f^4}\pi_a\pi_a\left(\pi_1^2\cos(2\alpha) + \cos^2\alpha\pi_2^2 - \sin^2\alpha\pi_3^2\right). \tag{B.32}$$

We combine the equations above with Eq.(B.11) to obtain the kinetic part of the Lagrangian, which we add to Eqs.(B.22)-(B.23), to obtain the final result for $\mathcal{L}_2^{\text{cubic}}$ and $\mathcal{L}_2^{\text{quartic}}$, which reads,

$$\mathcal{L}_2^{\text{cubic}} = \frac{(m^2 - 4\mu_I^2\cos\alpha)\sin\alpha}{6f}\pi_1\pi_a\pi_a - \frac{\mu_I\sin\alpha}{f}[\pi_1^2\partial_0\pi_2 + \pi_3^2\partial_0\pi_2], \tag{B.33}$$

$$\begin{aligned}\mathcal{L}_2^{\text{quartic}} &= \frac{1}{24f^2}\pi_a\pi_a[(m^2\cos\alpha - 4\mu_I^2\cos 2\alpha)\pi_1^2 + (m^2\cos\alpha - 4\mu_I^2\cos^2\alpha)\pi_2^2 \\ &+ (m^2\cos\alpha + 4\mu_I^2\sin^2\alpha)\pi_3^2] - \frac{\mu_I\cos\alpha}{3f^2}\pi_a\pi_a(\pi_1\partial_0\pi_2 - \pi_2\partial_0\pi_1) \\ &+ \frac{1}{6f^2}\left[\pi_a\pi_b\partial^\mu\pi_a\partial_\mu\pi_b - \pi_a\pi_a\partial^\mu\pi_b\partial_\mu\pi_b\right].\end{aligned} \tag{B.34}$$

B.2 The NLO Lagrangian

In this section we expand the order-p^4 Lagrangian to quadratic order in the pion fields. If we ignore the WZW terms, then the two-flavor Lagrangian at order-p^4 consists of ten terms [22], with bare coupling constants $l_1 - l_7$ and $h_1 - h_3$. The terms that are relevant to us in this thesis, can be written as follows,

$$\begin{aligned}\mathcal{L}_4 &= \frac{1}{4}l_1(\text{Tr}[\nabla_\mu\Sigma^\dagger\nabla^\mu\Sigma])^2 + \frac{1}{4}l_2\text{Tr}[\nabla_\mu\Sigma^\dagger\nabla_\nu\Sigma]\text{Tr}[\nabla^\mu\Sigma^\dagger\nabla^\nu\Sigma] \\ &+ \frac{1}{16}(l_3+l_4)m^4(\text{Tr}[\Sigma+\Sigma^\dagger])^2 + \frac{1}{8}l_4m^2\text{Tr}[\nabla_\mu\Sigma^\dagger\nabla^\mu\Sigma]\text{Tr}[\Sigma+\Sigma^\dagger] + h_1\,\text{Tr}\big[m^4\big],\end{aligned} \tag{B.35}$$

where we have used the notation in Ref.[90]. Here h_1 is a contact term which in the present context only contributes to the vacuum energy.

The relevant terms in $\mathcal{L}_4$ are obtained by appropriate combinations of $\mathrm{Tr}[\Sigma+\Sigma^\dagger]$, $\mathrm{Tr}[\nabla_\mu\Sigma^\dagger\nabla^\mu\Sigma]$ and $\mathrm{Tr}[\nabla_\mu\Sigma^\dagger\nabla_\nu\Sigma]$. The first two expressions are given up to quadratic order in Eq.(B.10) and Eq.(B.17), respectively. The last expression is obtained from the following set of equations,

$$\begin{aligned}
&\mathrm{Tr}[\nabla_\mu\Sigma^\dagger\nabla_\nu\Sigma] = \mathrm{Tr}[\partial_\mu\Sigma^\dagger\partial_\nu\Sigma] - i\mathrm{Tr}\left[\partial_\mu\Sigma[v_\nu,\Sigma^\dagger] + [v_\mu,\Sigma^\dagger]\partial_\nu\Sigma\right] \\
&+ \mathrm{Tr}\{[v_\mu,\Sigma]^\dagger[v_\nu,\Sigma]\}, \qquad\qquad (B.36)\\
&\mathrm{Tr}[\partial_\mu\Sigma^\dagger\partial_\nu\Sigma] = \frac{2}{f^2}\partial_\mu\pi_a\partial_\nu\pi_a, \qquad\qquad (B.37)\\
&-i\mathrm{Tr}\left[\partial_\mu\Sigma[v_\nu,\Sigma^\dagger] + [v_\mu,\Sigma^\dagger]\partial_\nu\Sigma^\dagger\right] = \frac{2\delta_{\nu0}}{f}\mu_I\sin\alpha\partial_\mu\pi_2 \\
&+ \frac{2\delta_{\nu0}}{f^2}\mu_I\cos\alpha(\pi_1\partial_\mu\pi_2 - \pi_2\partial_\mu\pi_1) + \mu\leftrightarrow\nu, \qquad\qquad (B.38)\\
&\mathrm{Tr}\{[v_\mu,\Sigma]^\dagger[v_\nu,\Sigma]\} = \delta_{\mu0}\delta_{\nu0}\Big(\frac{2}{f^2}\mu_I^2\cos(2\alpha)\pi_1^2 + \frac{2}{f^2}\mu_I^2\cos^2\alpha\pi_2^2 \\
&- \frac{2}{f^2}\mu_I^2\sin^2\alpha\pi_3^2 + 2\mu_I^2\sin^2\alpha + \frac{4\mu_I^2}{f}\cos\alpha\sin\alpha\pi_1\Big). \qquad\qquad (B.39)
\end{aligned}$$

The static terms in the NLO Lagrangian $\mathcal{L}_4^{\mathrm{static}}$ are obtained by substituting the static parts of $\mathrm{Tr}\big[\nabla^\mu\Sigma^\dagger\nabla_\mu\Sigma\big]$ and $\mathrm{Tr}\big(\Sigma+\Sigma^\dagger\big)$ into Eq.(B.35),

$$\mathcal{L}_4^{\mathrm{static}} = (l_1+l_2)\mu_I^4\sin^4\alpha + l_4m^2\mu_I^2\cos\alpha\sin^2\alpha + (l_3+l_4)m^4\cos^2\alpha + 2h_1m^4. \qquad (B.40)$$

By substituting Eq.(B.10), (B.17), and (B.37)-(B.39) appropriately into Eq.(B.35) we obtain the relevant linear and quadratic terms at next-to-leading order,[2]

$$\begin{aligned}
\mathcal{L}_4^{\mathrm{linear}} &= \left[4\,(l_1+l_2)\,\frac{\mu_I^4}{f}\sin^3\alpha\cos\alpha + l_4\frac{m^2\mu_I^2}{f}\left(2\sin\alpha - 3\sin^2\alpha\right) - (l_3+l_4)\,\frac{m^4}{f}\sin2\alpha\right]\pi_1 \\
&+ \left[4\,(l_1+l_2)\,\frac{\mu_I^3}{f}\sin^3\alpha + l_4\frac{m^2\mu_I}{f}\sin2\alpha\right]\partial_0\pi_2, \qquad (B.41)
\end{aligned}$$

and

$$\begin{aligned}
\mathcal{L}_4^{\mathrm{quadratic}} &= (l_1+l_2)\frac{2\mu_I^4\sin^2\alpha}{f^2}\left[(1+2\cos(2\alpha))\pi_1^2 + \cos^2\alpha\pi_2^2 - \sin^2\alpha\pi_3^2\right] \\
&+ l_1\frac{4\mu_I^2\sin^2\alpha}{f^2}(\partial_0\pi_2)^2 + l_2\frac{2\mu_I^2\sin^2\alpha}{f^2}(\partial_0\pi_2)^2 + (l_1+l_2)\frac{4\mu_I^3\sin\alpha\sin(2\alpha)}{f^2}\left[\pi_1\partial_0\pi_2 - \pi_2\partial_0\pi_1\right] \\
&+ l_1\frac{2\mu_I^2}{f^2}\sin^2\alpha(\partial_\mu\pi_a)(\partial^\mu\pi_a) + l_2\frac{2\mu_I^2}{f^2}\sin^2\alpha(\partial_0\pi_a)^2 + l_2\frac{2\mu_I^2}{f^2}\sin^2\alpha(\partial_\mu\pi_2)(\partial^\mu\pi_2) \\
&- (l_3+l_4)\frac{m^4}{f^2}\left[\cos(2\alpha)\pi_1^2 + \cos^2\alpha(\pi_2^2+\pi_3^2)\right] - l_4\frac{m^2\mu_I}{f^2}(\cos^2\alpha + \cos(2\alpha))(\pi_2\partial_0\pi_1 - \pi_1\partial_0\pi_2) \\
&+ l_4\frac{m^2\mu_I^2\cos\alpha}{f^2}\left[(-5+9\cos(2\alpha))\pi_1^2 + (1+3\cos(2\alpha))\pi_2^2 - 6\sin^2\alpha\pi_3^2\right] \\
&+ l_4\frac{m^2\cos\alpha}{f^2}(\partial_\mu\pi_a)(\partial^\mu\pi_a). \qquad (B.42)
\end{aligned}$$

[2]We have used partial integration, and Stokes's theorem to write the terms on this particular form.

B.3 The LO Lagrangian at finite pionic source

In this section we expand the leading-order Lagrangian at finite pionic source j to quadratic order in the pion fields. The inclusion of the pionic source modifies Eq.(B.5) to,

$$\mathcal{L}_2 = \frac{f^2}{4}\,\mathrm{Tr}\left[\nabla^\mu\Sigma^\dagger\nabla_\mu\Sigma\right] + \frac{f^2}{4}\,\mathrm{Tr}\left[\chi^\dagger\Sigma + \Sigma^\dagger\chi\right], \tag{B.43}$$

where $\chi = 2B_0 m_q + 2iB_0 j\tau_1$ and the covariant derivative is the same as in Eq.(B.6). Using $2B_0 m_q = m^2$ we rewrite the Lagrangian to

$$\mathcal{L}_2 = \mathcal{L}_2^0 - iB_0 j\frac{f^2}{2}\,\mathrm{Tr}\left[\tau_1\Sigma - \Sigma^\dagger\tau_1\right], \tag{B.44}$$

where $\mathcal{L}_2^0$ denotes the leading-order Lagrangian at zero pionic sources given in Eq.(B.5). Using Eq.(B.8) and (anti)commutation relations between Pauli matrices we rewrite the second term in Eq.(B.44) as,

$$-iB_0 j\frac{f^2}{2}\,\mathrm{Tr}\left[\tau_1\Sigma - \Sigma^\dagger\tau_1\right] = 2B_0 j\left(f^2\sin\alpha + f\cos\alpha\pi_1 - \frac{1}{2}\sin\alpha\pi_a\pi_a\right). \tag{B.45}$$

Combining Eq.(B.44) and Eq.(B.45) with Eqs.(B.18)-(B.20) we obtain,

$$\mathcal{L}_2^{\text{static}} = 2B_0 f^2(m_q\cos\alpha + j\sin\alpha) + \frac{1}{2}f^2\mu_I^2\sin^2\alpha, \tag{B.46}$$

$$\mathcal{L}_2^{\text{linear}} = f(\mu_I^2\cos\alpha\sin\alpha + 2B_0 j\cos\alpha - 2B_0 m_q\sin\alpha)\pi_1 + f\mu_I\sin\alpha\partial_0\pi_2, \tag{B.47}$$

$$\begin{aligned}\mathcal{L}_2^{\text{quadratic}} &= \frac{1}{2}\partial^\mu\pi_a\partial_\mu\pi_a + \mu_I\cos\alpha(\pi_1\partial_0\pi_2 - \pi_2\partial_0\pi_1) - \frac{1}{2}\left(-\mu_I^2\cos 2\alpha\right.\\ &\left.+2B_0 m_q\cos\alpha + 2B_0 j\sin\alpha\right)\pi_1^2 - \frac{1}{2}\left(-\mu_I^2\cos^2\alpha + 2B_0 m_q\cos\alpha + 2B_0 j\sin\alpha\right)\pi_2^2\\ &- \frac{1}{2}\left(\mu_I^2\sin^2\alpha + 2B_0 m_q\cos\alpha + 2B_0 j\sin\alpha\right)\pi_3^2.\end{aligned} \tag{B.48}$$

B.4 $\mathcal{L}_4^{\text{static}}$ at finite pionic source

Since we are only interested in the static part of the Lagrangian at next-to-leading order we start by performing the following substitution,

$$m^2\,\mathrm{Tr}\left[\Sigma + \Sigma^\dagger\right] \to 8B_0(m_q\cos\alpha + j\sin\alpha), \tag{B.49}$$

into Eq.(B.35). Running through the arguments that led to Eq.(B.40) yields the following result for the static Lagrangian at next-to-leading order at finite pionic source,

$$\begin{aligned}\mathcal{L}_4^{\text{static}} &= (l_1 + l_2)\,\mu_I^4\sin^4\alpha + 2l_4 B_0\mu_I^2\sin^2\alpha\,(m_q\cos\alpha + j\sin\alpha)\\ &+ 4\,(l_3 + l_4)\,B_0^2\,(m_q\cos\alpha + j\sin\alpha)^2 + 8h_1 B_0^2(m_q^2 + j^2).\end{aligned} \tag{B.50}$$

Appendix C

Additional Derivations

C.1 Renormalizing the one-point function

In this section we renormalize the π_1 one-point function Γ^1 to next-to-leading order. We will be denoting the $O(p^{2+2n})$ contribution to the one-point function by Γ^1_n.

The tree-level contribution to the one-point function is obtained from Eq.(4.16), and reads,

$$\Gamma^1_0 = if(-m^2 \sin\alpha + \mu_I^2 \cos\alpha \sin\alpha). \tag{C.1}$$

Minimizing the leading-order free energy Ω_0, given by Eq.(4.49), with respect to α gives,

$$\frac{\partial \Omega_0}{\partial \alpha} = m^2 \sin\alpha - \mu_I^2 \cos\alpha \sin\alpha = 0. \tag{C.2}$$

Comparing Eq.(C.1) with Eq.(C.2), we obtain,

$$\Gamma^1_0 = -\frac{i}{f}\frac{\partial \Omega_0}{\partial \alpha}, \tag{C.3}$$

so the one-point function vanishes at tree level.

The next-to-leading order contributions to the one-point function are obtained from Eqs.(4.19) and (4.41), and are represented diagrammatically in Fig.C.1. We denote the sum of the diagrams in the figure by Γ^1_1.

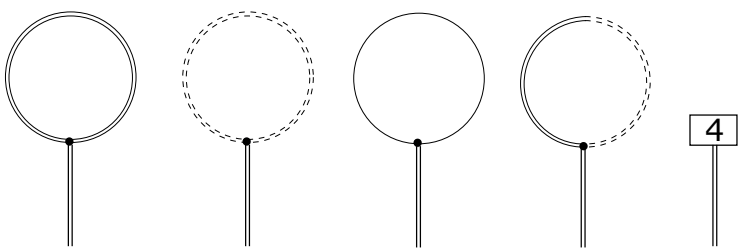

Figure C.1: Diagrams contributing to the one-point function at next-to-leading order. The first four diagrams are one-loop corrections derived from $\mathcal{L}_2^{\text{quartic}}$, and the last diagram is derived from $\mathcal{L}_4^{\text{linear}}$.

The sum of the diagrams (written in the order that they appear in Fig.C.1) reads,

$$\Gamma_1^1 = \frac{(4\mu_I^2\cos\alpha - m^2)\sin\alpha}{6f}\left[3\int_k \frac{k^2-m_2^2}{(k_0^2-E_{\pi^+}^2)(k_0^2-E_{\pi^-}^2)} + \int_k \frac{k^2-m_1^2}{(k_0^2-E_{\pi^+}^2)(k_0^2-E_{\pi^-}^2)} + \int_k \frac{1}{k^2-m_3^2}\right] - \frac{2m_{12}\mu_I\sin\alpha}{f}\int_k \frac{k_0^2}{(k_0^2-E_{\pi^+}^2)(k_0^2-E_{\pi^-}^2)} + \frac{i}{f}\Big[4\,(l_1+l_2)\,\mu_I^4\sin^3\alpha\cos\alpha + l_4 m^2\mu_I^2\left(2\sin\alpha - 3\sin^3\alpha\right) - (l_3+l_4)\,m^4\sin 2\alpha\Big]. \tag{C.4}$$

We notice from Eq.(C.1) and Eq.(C.4) that the one-point function $\Gamma^1 = \Gamma_1^1 + \Gamma_0^1$ is proportional to $\sin\alpha$, and therefore vanishes in the normal phase. We now proceed to show that the one-point function also vanishes in the BEC phase.

The next-to-leading order contribution to the free energy, Ω_1, can be written as,

$$\Omega_1 = \Omega_1^{\text{loop}} + \Omega_1^{\text{static}} = \frac{1}{2}(-i)\int_k \log\left(-k^2+m_3^2\right) + \frac{1}{2}(-i)\int_k \log\left[\left(-k^2+m_1^2\right)\left(-k^2+m_2^2\right) - k_0^2 m_{12}^2\right] - (l_1+l_2)\mu_I^4\sin^4\alpha - l_4 m^2\mu_I^2\cos\alpha\sin^2\alpha - (l_3+l_4)m^4\cos^2\alpha. \tag{C.5}$$

Comparing Eqs.(C.4) and (C.5) it is easy to see that the contribution to the one-point function arising from $\mathcal{L}_4^{\text{linear}}$ can be written as,

$$\Gamma_{\text{linear}}^1 = -\frac{i}{f}\frac{\partial\Omega_1^{\text{static}}}{\partial\alpha}. \tag{C.6}$$

We can rewrite the one-loop diagrams in Eq.(C.4) as,

$$\frac{(4\mu_I^2\cos\alpha - m^2)\sin\alpha}{2f}\int_k \frac{k^2-m_2^2}{(k_0^2-E_{\pi^+}^2)(k_0^2-E_{\pi^-}^2)} = \frac{1}{2f}\int_k \frac{(k^2-m_2^2)\frac{\partial m_1^2}{\partial\alpha}}{(k_0^2-E_{\pi^+}^2)(k_0^2-E_{\pi^-}^2)}, \tag{C.7}$$

$$\frac{(4\mu_I^2\cos\alpha - m^2)\sin\alpha}{6f}\int_k \frac{k^2-m_1^2}{(k_0^2-E_{\pi^+}^2)(k_0^2-E_{\pi^-}^2)} = \frac{1}{2f}\int_k \frac{(k^2-m_1^2)\frac{\partial m_2^2}{\partial\alpha}}{(k_0^2-E_{\pi^+}^2)(k_0^2-E_{\pi^-}^2)} - \frac{\sin\alpha}{3f}(\mu_I^2\cos\alpha - m^2)\int_k \frac{k^2-m_1^2}{(k_0^2-E_{\pi^+}^2)(k_0^2-E_{\pi^-}^2)}, \tag{C.8}$$

$$\frac{(4\mu_I^2\cos\alpha - m^2)\sin\alpha}{6f}\int_k \frac{1}{k^2-m_3^2} = \frac{1}{2f^2}\int_k \frac{\frac{\partial m_3^2}{\partial\alpha}}{k^2-m_3^2} - \frac{\sin\alpha}{3f}(\mu_I^2\cos\alpha - m^2)\int_k \frac{1}{k^2-m_3^2}, \tag{C.9}$$

$$-\frac{2m_{12}\mu_I\sin\alpha}{f}\int_k \frac{k_0^2}{(k_0^2-E_{\pi^+}^2)(k_0^2-E_{\pi^-}^2)} = \frac{1}{2f}\int_k \frac{k_0^2\frac{\partial m_{12}^2}{\partial\alpha}}{(k_0^2-E_{\pi^+}^2)(k_0^2-E_{\pi^-}^2)}. \tag{C.10}$$

By comparing the expressions above with the expression for Ω_1^{loop} in Eq.(C.5), we find that the sum of Eqs.(C.7)-(C.10), which we denote by Γ_{loop}^1, can be written on the following form,

$$\Gamma_{\text{loop}}^1 = -\frac{i}{f}\frac{\partial\Omega_1^{\text{loop}}}{\partial\alpha} - \frac{\sin\alpha}{3f}(\mu_I^2\cos\alpha - m^2)\left[\int_k \frac{k^2-m_1^2}{(k_0^2-E_{\pi^+}^2)(k_0^2-E_{\pi^-}^2)} + \int_k \frac{1}{k^2-m_3^2}\right]. \tag{C.11}$$

Adding Eqs.(C.3), (C.6) and (C.11) we obtain,

$$\Gamma^1 = -\frac{i}{f}\frac{\partial\Omega}{\partial\alpha} - \frac{\sin\alpha}{3f}(\mu_I^2\cos\alpha - m^2)\left[\int_k \frac{k^2-m_1^2}{(k_0^2-E_{\pi^+}^2)(k_0^2-E_{\pi^-}^2)} + \int_k \frac{1}{k^2-m_3^2}\right], \tag{C.12}$$

where Ω denotes the free-energy to next-to-leading order.

We have so far overlooked the fact that we have to evaluate vertex factors in one-loop diagrams at the tree-level minimum $\cos\alpha = \frac{m^2}{\mu_I^2}$, in order to work consistently to next-to-leading order[44]. This means that one-loop contributions that can be written on the following form,

$$\sim (\mu_I^2 \cos\alpha - m^2)X, \tag{C.13}$$

where the $(\mu_I^2 \cos\alpha - m^2)$-factor arises from vertices, and X is a one-loop integral, only have non-vanishing NNLO contributions in the pion-condensed phase. Thus, to working order Eq.(C.12) reduces to the following in the BEC phase,

$$\Gamma^1 = -\frac{i}{f}\frac{\partial\Omega}{\partial\alpha} = 0, \tag{C.14}$$

where the last equality is the EoM for Ω.

The tadpole diagrams contributing to the quasi-particle masses m_{π^0}, m_{π^+} and m_{π^-} are proportional to the one-point function Γ^1. Since we just showed that Γ^1 vanishes to working order, we conclude that the tadpole diagrams vanish as well.

C.2 $\Sigma_{22}(0)$ in the BEC phase

In this section we evaluate Σ_{22} at $p^2 = p_0 = 0$. The three diagrams in the third line of Fig.[D.2], whose expressions are given by Eqs.(D.21)-(D.23), vanishes in this limit. The sum of the remaining diagrams can be organized into the following form,

$$\begin{aligned}
\Sigma_{22}(0) &= -\frac{1}{3f^2}(-i)\int_k \frac{(k^2-m_1^2)(k^2-m_2^2) - m_{12}^2 k_0^2}{(k_0^2 - E_{\pi^+}^2)(k_0^2 - E_{\pi^-}^2)} \\
&- \frac{(m^2 - \mu_I^2\cos\alpha)\cos\alpha}{3f^2}(-i)\int_k \frac{k^2 - m_2^2}{(k_0^2 - E_{\pi^+}^2)(k_0^2 - E_{\pi^-}^2)} + \\
&(-i)\int_k \frac{1}{(k_0^2 - E_{\pi^+}^2)(k_0^2 - E_{\pi^-}^2)}\left[\frac{2k^2}{3f^2}(m^2\cos\alpha - 4\mu_I^2\cos^2\alpha) + \frac{m_{12}^2}{f^2}k_0^2\right. \\
&\left. - \left(\frac{m_1^2}{2f^2} + \frac{m_2^2}{6f^2}\right)\left(m^2\cos\alpha - 4\mu_I^2\cos^2\alpha\right) - \frac{(m^2 - 4\mu_I^2\cos\alpha)^2\sin^2\alpha}{(3f)^2}\right] \\
&+ \Sigma_{22(4\pi)}^{\pi_3}(0) + \Sigma_{22(2\pi)}^{\pi_2\pi_2}(0),
\end{aligned} \tag{C.15}$$

where,

$$\Sigma_{22(4\pi)}^{\pi_3}(0) = -\frac{1}{6f^2}(m^2\cos\alpha + 2\mu_I^2\cos^2\alpha)(-i)\int_k \frac{1}{k^2 - m_3^2}, \tag{C.16}$$

$$\begin{aligned}
\Sigma_{22(2\pi)}^{\pi_2\pi_2}(0) &= -4(l_1+l_2)\frac{\mu_I^4\sin^2\alpha\cos^2\alpha}{f^2} - l_4\frac{m^2\mu_I^2\cos\alpha}{2f^2}(1+3\cos 2\alpha) \\
&+ 2(l_3+l_4)\frac{m^4\cos^2\alpha}{f^2}.
\end{aligned} \tag{C.17}$$

The integrand in the first line of Eq.(C.15) is one, so that integral vanishes in dimensional regularization. The term in the second line of Eq.(C.15) is zero at next-to-leading order, as we discussed in the paragraph leading to Eq.(C.13) in Appendix C.1. Comparing Eq.(C.17) to the expression for the static part of the free energy at next-to-leading order in Eq.(4.50), it is easy to see that,

$$\Sigma_{22(2\pi)}^{\pi_2\pi_2}(0) = \frac{1}{f^2}\frac{\cos\alpha}{\sin\alpha}\frac{\partial\Omega_1^{\text{static}}}{\partial\alpha} \tag{C.18}$$

The remaing terms in Eq.(C.15) can be rewritten as follows,

$$\frac{2(m^2\cos\alpha-4\mu_I^2\cos^2\alpha)}{3f^2}(-i)\int_k\frac{k^2}{(k_0^2-E_{\pi^+}^2)(k_0^2-E_{\pi^-}^2)}=-\frac{1}{2f^2}\left(\frac{\cos\alpha}{\sin\alpha}\right)(-i)\Big[\int_k\frac{k^2\left(\frac{\partial m_1^2}{\partial\alpha}+\frac{\partial m_2^2}{\partial\alpha}\right)}{(k_0^2-E_{\pi^+}^2)(k_0^2-E_{\pi^-}^2)}\Big]-\frac{\cos\alpha}{3f^2}(m^2-\mu_I^2\cos\alpha)(-i)\int_k\frac{k^2}{(k_0^2-E_{\pi^+}^2)(k_0^2-E_{\pi^-}^2)},\tag{C.19}$$

$$\frac{m_{12}^2}{f^2}(-i)\int_k\frac{k_0^2}{(k_0^2-E_{\pi^+}^2)(k_0^2-E_{\pi^-}^2)}=-\frac{1}{2f^2}\left(\frac{\cos\alpha}{\sin\alpha}\right)(-i)\int_k\frac{k_0^2\frac{\partial m_{12}^2}{\partial\alpha}}{(k_0^2-E_{\pi^+}^2)(k_0^2-E_{\pi^-}^2)},\tag{C.20}$$

$$-\left[\left(\frac{m_1^2}{2f^2}+\frac{m_2^2}{6f^2}\right)(m^2\cos\alpha-4\mu_I^2\cos^2\alpha)+\frac{(m^2-4\mu_I^2\cos\alpha)^2\sin^2\alpha}{(3f)^2}\right](-i)\int_k\frac{1}{(k_0^2-E_{\pi^+}^2)(k_0^2-E_{\pi^-}^2)}=\frac{(-i)}{2f^2}\int_k\frac{1}{(k_0^2-E_{\pi^+}^2)(k_0^2-E_{\pi^-}^2)}\left\{\left[m_2^2\frac{\partial m_1^2}{\partial\alpha}+m_1^2\frac{\partial m_2^2}{\partial\alpha}\right]\left(\frac{\cos\alpha}{\sin\alpha}\right)+\frac{2}{3}(\mu_I^2\cos\alpha-m^2)\left[(\mu_I^2\cos\alpha-m^2)\left(\cos\alpha-\frac{1}{3}\right)-2\mu_I^2\cos\alpha\right]\right\},\tag{C.21}$$

$$-\frac{1}{6f^2}(m^2\cos\alpha+2\mu_I^2\cos^2\alpha)(-i)\int_k\frac{1}{k^2-m_3^2}=-\frac{1}{2f^2}\left(\frac{\cos\alpha}{\sin\alpha}\right)(-i)\int_k\frac{\frac{\partial m_3^2}{\partial\alpha}}{(k_0^2-E_{\pi^+}^2)(k_0^2-E_{\pi^-}^2)}+\frac{2\cos\alpha}{3f^2}\left(\mu_I^2\cos\alpha-m^2\right)(-i)\int_k\frac{1}{k^2-m_3^2}.\tag{C.22}$$

Adding Eqs.(C.18)-(C.22), and comparing the right-hand sides of Eqs.(C.19)-(C.22) to $\frac{\partial\Omega_1^{\text{loop}}}{\partial\alpha}$, we obtain,

$$\Sigma_{22}(0)=\frac{1}{f^2}\left(\frac{\cos\alpha}{\sin\alpha}\right)\frac{\partial\Omega_1}{\partial\alpha}+...\tag{C.23}$$

where the omitted terms can be written on the same form as Eq.(C.13), and therefore vanishes at NLO. Thus, to working order it is correct to write,

$$\Sigma_{22}(0)=\frac{1}{f^2}\left(\frac{\cos\alpha}{\sin\alpha}\right)\frac{\partial\Omega_1}{\partial\alpha}.\tag{C.24}$$

C.3 Manipulation of sum-integrals

The author was not able to find a full derivation of how to get from Eq.(8.33) to Eq.(8.34) in the literature, and has therefore included one here. We will, for the sake of generality, perform the derivation at a finite spatial volume $V=L_xL_yL_z$. Evaluating the infinite-volume limit of the result will lead us to Eq.(8.34).

The sum-integral that we wish to evaluate, which we will denote by $\Pi(m)$, reduces to the following sum,

$$\Pi(m)=\frac{1}{\beta V}\sum_{l\in\mathbb{Z}}\log\big(k^2+m^2\big),\tag{C.25}$$

at finite volume. The finite volume and temperature-momentum $k = (k_0, k_i)$ is given by $k_0 = \frac{2\pi l_0}{\beta}$ and $k_i = \frac{2\pi l_i}{L_i}$.

The logarithm on right hand side of Eq.(C.25) can be expressed as,

$$\ln\left(k^2 + m^2\right) = -\frac{\partial}{\partial\alpha}\frac{1}{(k^2+m^2)^\alpha}\Big|_{\alpha=0}. \tag{C.26}$$

We will need the Poisson sum formula in the following,

$$\sum_{k'\in\mathbb{Z}} g(k') = \sum_{n'\in\mathbb{Z}} \mathcal{F}\{g(k)\} = \sum_{n'\in\mathbb{Z}} \int d^d x g(x) e^{-2\pi i x n'}, \tag{C.27}$$

where $\mathcal{F}\{g(k)\}$ denotes the Fourier transform of the function $g(k)$. The sums are four dimensional, where n' and k' denotes $n' = (n'_0, n'_1, n'_2, n'_3)$ and $k' = (k'_0, k'_1, k'_2, k'_3)$, respectively, with $n'_i, k'_i \in \mathbb{Z}$. By choosing a new set of variables $n = (\beta n'_0, L_i n'_i)$ and $k = (\frac{2\pi k'_0}{\beta}, \frac{2\pi k'_i}{L_i})$, we may rewrite Eq.(C.27) as

$$\frac{1}{\beta V}\sum_k f(k) = \sum_n \int \frac{d^d x}{(2\pi)^d} f(x) e^{-ixn} = \sum_n \int_x f(x) e^{-ixn}, \tag{C.28}$$

where $f(x) = g\left(\frac{\beta x_0}{2\pi}, \frac{L_i x_i}{2\pi}\right)$. Notice that the sums are now over "frequencies" and *not* $\mathbb{Z}$. By combining Eqs.(C.25), (C.26) and (C.28) we obtain,

$$\Pi(m) = -\frac{\partial}{\partial\alpha}\sum_n \int_k \frac{e^{-ikn}}{(k^2+m^2)^\alpha}\Big|_{\alpha=0}. \tag{C.29}$$

We rewrite the denominator as

$$\frac{1}{(k^2+m^2)^\alpha} = \frac{1}{\Gamma(\alpha)}\int_0^\infty dt t^{\alpha-1} e^{-t(k^2+m^2)}, \tag{C.30}$$

so the momentum integral becomes Gaussian,

$$\Pi(m) = -\frac{\partial}{\partial\alpha}\sum_n \int_0^\infty dt \int_k \frac{t^{\alpha-1}}{\Gamma(\alpha)} e^{-t(k-\frac{in}{2t})^2 - \frac{n^2}{4t} - tm^2}. \tag{C.31}$$

Evaluating the momentum integral, and the derivative with respect to α, using

$$\lim_{\alpha\to 0}\left\{-\frac{\partial}{\partial\alpha}\frac{t^\alpha - 1}{\Gamma(\alpha)}\right\} = -\frac{1}{t}, \tag{C.32}$$

we obtain,

$$\Pi(m) = -\sum_n \int_0^\infty \frac{e^{-tm^2}}{(4\pi)^{\frac{d}{2}} t^{\frac{d}{2}+1}} e^{-\frac{n^2}{4t}} dt, \tag{C.33}$$

which is the finite-volume result. Taking the infinite-volume limit $V \to \infty$ we obtain,

$$\begin{aligned}\Pi(m) &= \sum\!\!\!\!\!\!\int_K \log\left(\omega_n^2 + \vec{k}^2 + m^2\right) = -\sum_{n_0}\int_0^\infty \frac{dt e^{-tm^2}}{(4\pi)^{\frac{d}{2}} t^{\frac{d}{2}+1}} e^{-\frac{n_0^2}{4t}} \\ &= -\sum_{n\in\mathbb{Z}}\int_0^\infty \frac{dt e^{-tm^2}}{(4\pi)^{\frac{d}{2}} t^{\frac{d}{2}+1}} e^{-\frac{n^2}{4T^2 t}}.\end{aligned} \tag{C.34}$$

We denote the temperature-independent part of Π arising from the $n = 0$ term in Eq.(C.34) by Π_0, and the remaining temperature-dependent part by Π_T. Integrating over t in the temperature-independent part Π_0 yields,

$$\Pi_0(m) = -\int_0^\infty \frac{dte^{-tm^2}}{(4\pi)^{\frac{d}{2}} t^{\frac{d}{2}+1}} = -\frac{\Gamma\left(-\frac{d}{2}\right) m^2}{(4\pi)^{\frac{d}{2}}}, \tag{C.35}$$

which is equivalent to what we found in Eq.(4.57) in four dimensions. Comparing the temperature-dependent part,

$$\Pi_T(m) = -2\sum_{n=1}^{\infty}\int_0^\infty \frac{dte^{-tm^2}}{(4\pi)^{\frac{d}{2}} t^{\frac{d}{2}+1}} e^{-\frac{n^2}{4T^2 t}}, \tag{C.36}$$

to the following integral representation of the modified Bessel function $K_v(z)$,

$$K_v(z) = \frac{1}{2}\left(\frac{1}{2}z\right)^v \int_0^\infty \frac{dt}{t^{v+1}} e^{-t-\frac{z^2}{4t}}, \tag{C.37}$$

we obtain,

$$\Pi_T(m) = \frac{2^{2+\frac{d}{2}}}{(4\pi)^{\frac{d}{2}}}(m^2)^{d/4}\sum_{n=1}^{\infty}\left(\frac{T^2}{n^2}\right)^{\frac{d}{4}} K_{\frac{d}{2}}\left(\frac{mn}{T}\right). \tag{C.38}$$

If we specialize to $d = 4$ dimensions, then the temperature-dependence of Π becomes,

$$\Pi_T(m) = -\frac{16m^2T^2}{(4\pi)^2}\sum_{n=1}^{\infty}\frac{K_2\left(\frac{mn}{T}\right)}{n^2}. \tag{C.39}$$

A small twist

The procedure above can be generalized quite easily to sums on the following form,

$$\Pi_\pm = \frac{1}{\beta V}\sum_k \log[(k_0 \pm ia)^2 + k_i k_i + b^2], \tag{C.40}$$

where a and b are independent of k. This leads to a result similar to Eq.(C.31), but with the exponential replaced by,

$$\exp\left\{-t(k_i - \frac{in_i}{2t})^2 - \frac{n_i^2}{4t} - ik_0n_0 - t(k_0 \pm ia)^2 - tb^2\right\}. \tag{C.41}$$

The integration over spatial momentum remains unaffected by this change, while the integration over k_0 produces a different result than the one in Eq.(C.33). If we substitute $k_0 \to k_0 \mp ia$, then the exponential becomes,

$$\exp\left\{-t\left(k - \frac{in}{2t}\right)^2 - \frac{n^2}{4t} \pm n_0 a - tb^2\right\}. \tag{C.42}$$

Comparing this expression to Eqs.(C.31) and (C.33), we find that,

$$\Pi_\pm = -\sum_n \int_0^\infty \frac{e^{-tb^2}e^{\pm an_0}}{(4\pi)^{\frac{d}{2}} t^{\frac{d}{2}+1}} e^{-\frac{n^2}{4t}} dt, \tag{C.43}$$

In the expansion of the free energy in α we encounter sum-integrals, which take the following form at finite volume,

$$\Pi = \sum_k \log[(k_0+ia)^2 + k_i k_i + b^2][(k_0-ia)^2 + k_i k_i + b^2]. \tag{C.44}$$

Comparing Eq.(C.44) with Eq.(C.40) and Eq.(C.43) we see that,

$$\Pi = -2\sum_n \int_0^\infty \cosh(an_0)\frac{e^{-tb^2}e^{-\frac{n^2}{4t}}}{(4\pi)^{\frac{d}{2}}t^{\frac{d}{2}+1}}dt. \tag{C.45}$$

which in the infinite-volume limit $V \to \infty$ reduces to the following,

$$\Pi = \sum\!\!\!\!\!\!\int_K \log[(k_0+ia)^2 + \vec{k}^2 + b^2][(k_0-ia)^2 + \vec{k}^2 + b^2] =$$
$$-2\sum_{n\in\mathbb{Z}} \cosh\Big(\frac{an}{T}\Big)\int_0^\infty \frac{e^{-tb^2}e^{-\frac{n^2}{4T^2t}}}{(4\pi)^{\frac{d}{2}}t^{\frac{d}{2}+1}}dt. \tag{C.46}$$

The t-dependence in the expression above is similar to the t-dependence in Eq.(C.34), which implies that the temperature-dependent part can be written as,

$$\Pi_{\mathrm{T}} = \frac{2^{2+\frac{d}{2}}}{(4\pi)^{\frac{d}{2}}}(b^2)^{d/4}\sum_{n=1}^\infty \left(\frac{T^2}{n^2}\right)^{\frac{d}{4}} K_{\frac{d}{2}}\left(\frac{bn}{T}\right) 2\cosh\Big(\frac{an}{T}\Big). \tag{C.47}$$

Specializing to $d=4$ dimensions we finally get,

$$\Pi_{\mathrm{T}} = -\frac{32b^2T^2}{(4\pi)^2}\sum_{n=1}^\infty \frac{K_2\left(\frac{bn}{T}\right)}{n^2}\cosh\Big(\frac{an}{T}\Big). \tag{C.48}$$

C.4 Additional calculations

In this section we elaborate on how we get from Eq.(8.50) to Eq.(8.55), when we derive the Landau functional in the text.

Using the expansions of a and b in α, see Eqs.(8.47)-(8.48) for details, we obtain,

$$\frac{b-a}{T} = -\frac{\mu_I - m}{T} + \frac{1}{2T}\left[\mu_I + \frac{m}{2}\left(\frac{\mu_I^2-m^2}{m^2}\right)\right]\alpha^2 - \frac{1}{24T}\left[\frac{m}{2}\left(\frac{4\mu_I^2-m^2}{m^2}\right) - \mu_I\right]\alpha^4$$
$$+ O(\alpha^6) \approx -\frac{\mu_I - m}{T} + \frac{\mu_I}{2T}\alpha^2 - \frac{1}{48T}\left[\frac{4\mu_I^2-m^2}{m} - 2\mu_I\right]\alpha^4 + O(\alpha^6). \tag{C.49}$$

We notice that the coefficient in front of α^2 is much bigger than the constant term, and much bigger than the coefficient in front of α^4.

It follows immediately from (8.48) that,

$$b^{\frac{3}{2}} \approx m^{\frac{3}{2}}\left[1 + \frac{3}{8}\left(\frac{\mu_I^2-m^2}{m^2}\right)\alpha^2 - \frac{1}{128}\left(\frac{4\mu_I^2-m^2}{m^2}\right)\alpha^4\right] + O(\alpha^6). \tag{C.50}$$

We notice that the coefficient in front of α^2 is much smaller than $m^{\frac{3}{2}}$, and also much smaller than the coefficient in front of α^2 in Eq.(C.49).

Using the expansion of the polylogarithm around $z=1$, given in (8.53), we obtain the following approximations,

$$\mathrm{Li}_{\frac{5}{2}}\left(e^{-\left(\frac{b-a}{T}\right)}\right) \approx \zeta\left(\frac{5}{2}\right) - \zeta\left(\frac{3}{2}\right)\left(\frac{b-a}{T}\right) + \frac{1}{2}\left[\zeta\left(\frac{1}{2}\right) - \zeta\left(\frac{3}{2}\right)\right]\left(\frac{b-a}{T}\right)^2$$
$$-\Gamma\left(-\frac{3}{2}\right)\left(\frac{b-a}{T}\right)^{\frac{3}{2}} + O\left(\alpha^6\right), \tag{C.51}$$

and,

$$\frac{T}{b}\mathrm{Li}_{\frac{7}{2}}\left(e^{-\left(\frac{b-a}{T}\right)}\right) \approx \frac{T}{m}\left[1-\frac{1}{4}\left(\frac{\mu_I^2-m^2}{m^2}\right)\alpha^2+\frac{1}{48}\left(\frac{4\mu_I^2-m^2}{m^2}\right)\alpha^4\right]\times$$
$$\left\{\zeta\left(\frac{7}{2}\right)-\zeta\left(\frac{5}{2}\right)\left(\frac{b-a}{T}\right)+\frac{1}{2}\left[\zeta\left(\frac{3}{2}\right)-\zeta\left(\frac{5}{2}\right)\right]\left(\frac{b-a}{T}\right)^2\right\}+O\left(\alpha^6\right). \tag{C.52}$$

By comparing the expansions above, in particular the magnitude of the different coefficients, we conclude that,

$$\frac{1}{2}\sqrt{\frac{b^3T^5}{2\pi^3}}\left[\mathrm{Li}_{\frac{5}{2}}\left(e^{-\left(\frac{b-a}{T}\right)}\right)+\frac{15}{8}\frac{T}{b}\mathrm{Li}_{\frac{7}{2}}\left(e^{-\left(\frac{b-a}{T}\right)}\right)\right] \approx \frac{1}{2}\sqrt{\frac{m^3T^5}{2\pi^3}}\left[\mathrm{Li}_{\frac{5}{2}}\left(e^{-\left(\frac{b-a}{T}\right)}\right)\right]$$
$$\approx \frac{1}{2}\sqrt{\frac{m^3T^5}{2\pi^3}}\zeta\left(\frac{5}{2}\right)-\frac{\mu_I}{4}\sqrt{\frac{m^3T^3}{2\pi^3}}\zeta\left(\frac{3}{2}\right)\alpha^2+\frac{\mu_I^2}{16}\sqrt{\frac{m^3T}{2\pi^3}}\left[\zeta\left(\frac{1}{2}\right)-\zeta\left(\frac{3}{2}\right)\right]\alpha^4$$
$$+O\left(\alpha^6\right). \tag{C.53}$$

Appendix D

Charged mass eigenstates

In this appendix we present the Feynman diagrams that contribute to Σ_{11} and Σ_{22}.

D.1 Σ_{11}

$$-i\Sigma_{11}(p^2,p_0) = -i\Big[\Sigma^{\pi_1}_{11(4\pi)}(p^2,p_0) + \Sigma^{\pi_2}_{11(4\pi)}(p^2,p_0) + \Sigma^{\pi_3}_{11(4\pi)}(p^2,p_0) + \Sigma^{\pi_1\pi_2}_{11(4\pi)}(p^2,p_0) + \Sigma^{\pi_1\pi_1}_{11(3\pi)}(p^2,p_0) + \Sigma^{\pi_2\pi_2}_{11(3\pi)}(p^2,p_0) + \Sigma^{\pi_3\pi_3}_{11(3\pi)}(p^2,p_0) + \Sigma^{\pi_1\pi_2}_{11(3\pi)}(p^2,p_0) + \Sigma^{(\pi_1\pi_2)\pi_1}_{11(3\pi)}(p^2,p_0) + \Sigma^{(\pi_1\pi_2)\pi_2}_{11(3\pi)}(p^2,p_0) + \Sigma^{(\pi_1\pi_2)(\pi_2\pi_1)}_{11(3\pi)}(p^2,p_0) + \Sigma^{(\pi_1\pi_2)(\pi_1\pi_2)}_{11(3\pi)}(p^2,p_0) + \Sigma^{\pi_1\pi_1}_{11(2\pi)}(p^2,p_0)\Big] \tag{D.1}$$

4-vertex diagrams

$$\Sigma^{\pi_1}_{11(4\pi)} = \frac{1}{2f^2}\left(m^2\cos\alpha - 4\mu_I^2\cos 2\alpha\right)(-i)\int_k \frac{k^2-m_2^2}{(k_0^2-E^2_{\pi^+})(k_0^2-E^2_{\pi^-})}, \tag{D.2}$$

$$\Sigma^{\pi_2}_{11(4\pi)} = \frac{1}{6f^2}\left(m^2\cos\alpha - 4\mu_I^2\cos^2\alpha + 2\mu_I^2\sin^2\alpha - 2p^2\right)(-i)\int_k \frac{k^2-m_1^2}{(k_0^2-E^2_{\pi^+})(k_0^2-E^2_{\pi^-})} - \frac{1}{3f^2}(-i)\int_k \frac{k^2(k^2-m_1^2)}{(k_0^2-E^2_{\pi^+})(k_0^2-E^2_{\pi^-})}, \tag{D.3}$$

$$\Sigma^{\pi_3}_{11(4\pi)} = \frac{1}{6f^2}\left(m^2\cos\alpha - 2\mu_I^2\cos^2\alpha + 4\mu_I^2\sin^2\alpha - 2p^2\right)(-i)\int_k \frac{1}{k^2-m_3^2} - \frac{1}{3f^2}(-i)\int_k \frac{k^2}{k^2-m_3^2}, \tag{D.4}$$

$$\Sigma^{\pi_1\pi_2}_{11(4\pi)} = \frac{8\mu_I\cos\alpha}{3f^2}m_{12}(-i)\int_k \frac{k_0^2}{(k_0^2-E^2_{\pi^+})(k_0^2-E^2_{\pi^-})}, \tag{D.5}$$

3-vertex diagrams

$$\Sigma^{\pi_1\pi_1}_{11(3\pi)} = -\frac{(m^2-4\mu_I^2\cos\alpha)^2\sin^2\alpha}{2f^2}(-i)\int_k \frac{(k^2-m_2^2)(q^2-m_2^2)}{(k_0^2-E^2_{\pi^+})(k_0^2-E^2_{\pi^-})(q_0^2-E^2_{\pi^+})(q_0^2-E^2_{\pi^-})}, \tag{D.6}$$

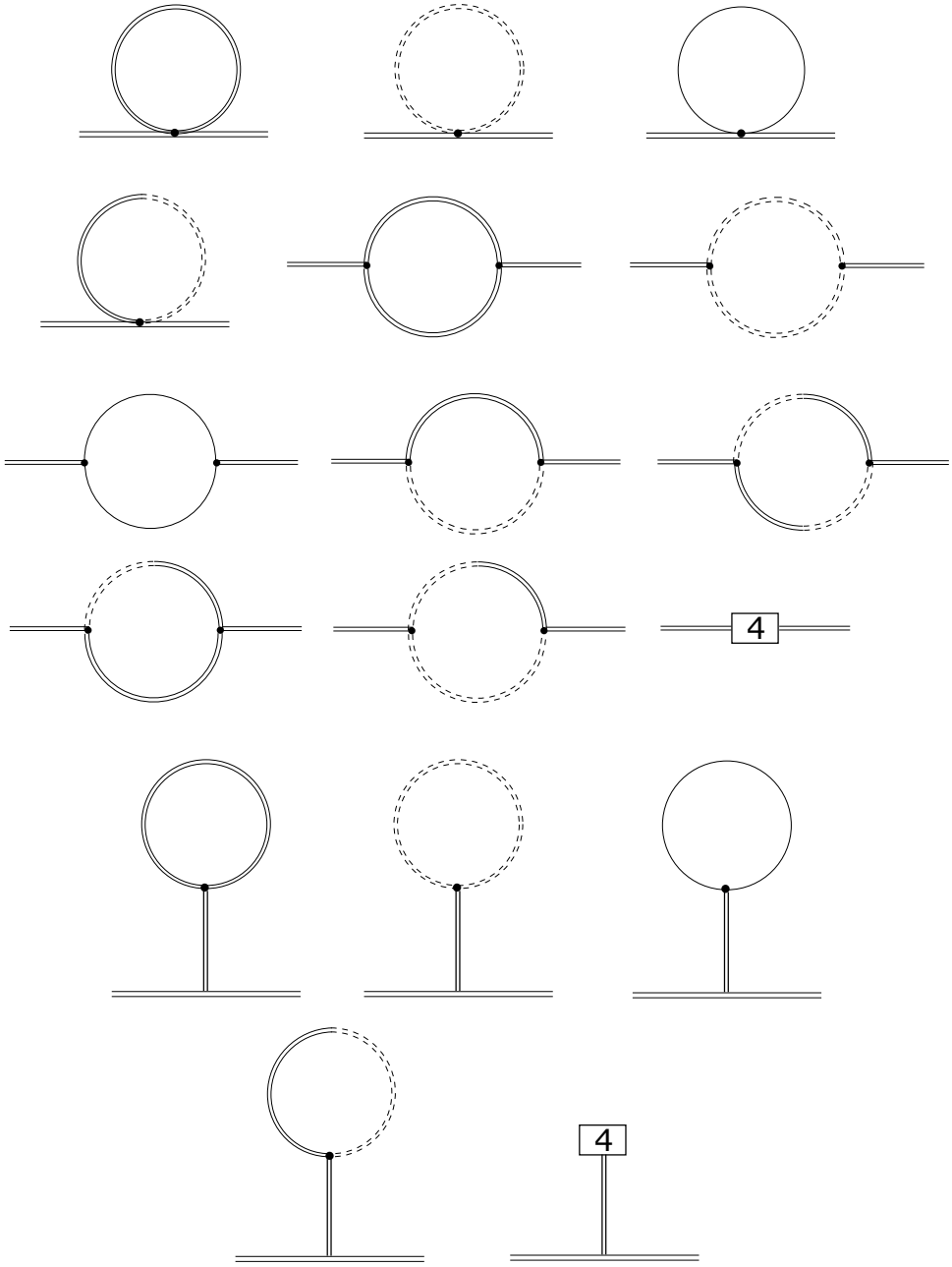

Figure D.1: π_1 self-energy diagrams at $O(p^4)$. The first four diagrams are one-loop corrections derived from $\mathcal{L}_2^{\text{quartic}}$, the next eight diagrams are one-loop corrections derived from $\mathcal{L}_2^{\text{cubic}}$, and the last diagram in the fourth line is derived from $\mathcal{L}_4^{\text{quadratic}}$. The tadpole diagrams vanishes, since the one-point function is zero, as explained in Appendix C.1.

$$\Sigma^{\pi_2\pi_2}_{11(3\pi)} = -\frac{(m^2-4\mu_I^2\cos\alpha)^2\sin^2\alpha}{18f^2}(-i)\int_k \frac{(k^2-m_1^2)(q^2-m_1^2)}{(k_0^2-E^2_{\pi^+})(k_0^2-E^2_{\pi^-})(q_0^2-E^2_{\pi^+})(q_0^2-E^2_{\pi^-})}, \tag{D.7}$$

$$\Sigma^{\pi_3\pi_3}_{11(3\pi)} = -\frac{(m^2-4\mu_I^2\cos\alpha)^2\sin^2\alpha}{18f^2}(-i)\int_k \frac{1}{(k^2-m_3^2)(q^2-m_3^2)}, \tag{D.8}$$

$$\Sigma^{\pi_1\pi_2}_{11(3\pi)} = -\frac{4\mu_I^2\sin^2\alpha}{f^2}(-i)\int_k \frac{k_0^2(k^2-m_1^2)(q^2-m_2^2)}{(k_0^2-E^2_{\pi^+})(k_0^2-E^2_{\pi^-})(q_0^2-E^2_{\pi^+})(q_0^2-E^2_{\pi^-})}, \tag{D.9}$$

$$\Sigma^{(\pi_1\pi_2)\pi_1}_{11(3\pi)} = -2m_{12}\frac{(m^2-4\mu_I^2\cos\alpha)\mu_I\sin^2\alpha}{f^2}(-i)\int_k \frac{k_0^2(q^2-m_2^2)}{(k_0^2-E^2_{\pi^+})(k_0^2-E^2_{\pi^-})(q_0^2-E^2_{\pi^+})(q_0^2-E^2_{\pi^-})}, \tag{D.10}$$

$$\Sigma^{(\pi_1\pi_2)\pi_2}_{11(3\pi)} = 2m_{12}\frac{(m^2-4\mu_I^2\cos\alpha)\mu_I\sin^2\alpha}{3f^2}(-i)\int_k \frac{k_0q_0(q^2-m_1^2)}{(k_0^2-E^2_{\pi^+})(k_0^2-E^2_{\pi^-})(q_0^2-E^2_{\pi^+})(q_0^2-E^2_{\pi^-})}, \tag{D.11}$$

$$\Sigma^{(\pi_1\pi_2)(\pi_2\pi_1)}_{11(3\pi)} = -\frac{4\mu_I^2\sin^2\alpha}{f^2}m_{12}^2(-i)\int_k \frac{k_0^2q_0^2}{(k_0^2-E^2_{\pi^+})(k_0^2-E^2_{\pi^-})(q_0^2-E^2_{\pi^+})(q_0^2-E^2_{\pi^-})}, \tag{D.12}$$

$$\Sigma^{(\pi_1\pi_2)(\pi_1\pi_2)}_{11(3\pi)} = \frac{(m^2-4\mu_I^2\cos\alpha)^2\sin^2\alpha}{6f^2}m_{12}^2(-i)\int_k \frac{k_0q_0}{(k_0^2-E^2_{\pi^+})(k_0^2-E^2_{\pi^-})(q_0^2-E^2_{\pi^+})(q_0^2-E^2_{\pi^-})}, \tag{D.13}$$

Counterterms

$$\begin{aligned}\Sigma^{\pi_1\pi_1}_{11(2\pi)} &= -\frac{(l_1+l_2)}{f^2}\left[3m_{12}^2m_1^2-4m_1^4\right]-\frac{l_4}{f^2}\left[-\frac{1}{8}m_{12}^4+\frac{7}{4}m_{12}^2m_1^2\right]\\ &+\frac{l_3+l_4}{f^2}\left[\frac{1}{8}m_{12}^4-\frac{1}{2}m_{12}^2m_1^2\right]-\frac{l_1}{f^2}4m_1^2p^2-\frac{l_2}{f^2}4m_1^2p_0^2-\frac{l_4}{f^2}\frac{1}{2}m_{12}^2p^2.\end{aligned} \tag{D.14}$$

D.2 Σ_{22}

The expressions associated with the self-energy diagrams displayed in Fig.[D.2] are listed below.

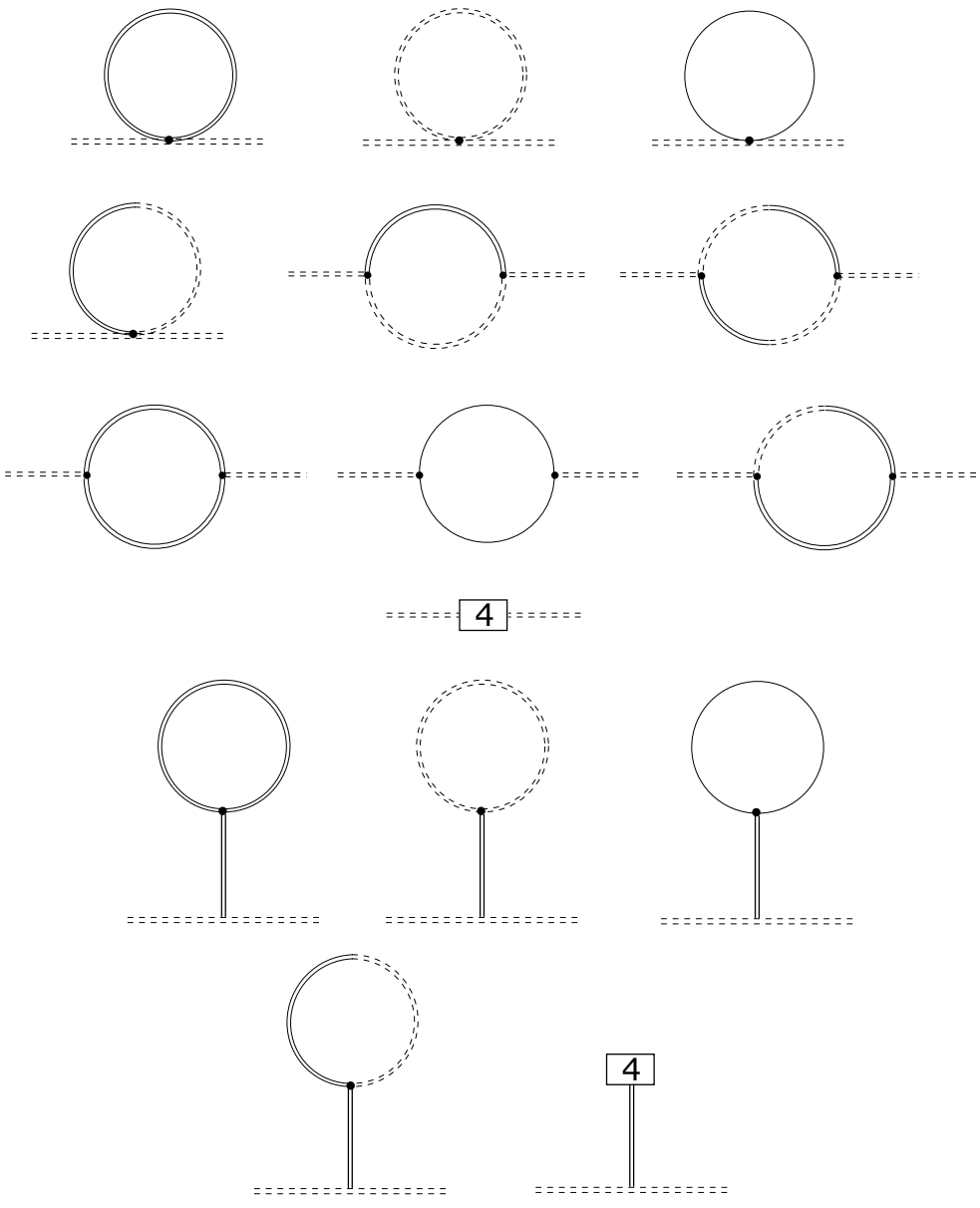

Figure D.2: π_2 self-energy diagrams at $O(p^4)$. The first four diagrams are one-loop corrections derived from $\mathcal{L}_2^{\text{quartic}}$, the next five diagrams are one-loop corrections derived from $\mathcal{L}_2^{\text{cubic}}$, and the diagram in the fourth line is derived from $\mathcal{L}_4^{\text{quadratic}}$. The tadpole diagrams vanishes, since the one-point function is zero, as explained in Appendix C.1.

4-vertex diagrams

$$\Sigma^{\pi_1}_{22(4\pi)} = \frac{1}{6f^2}\left(m^2\cos\alpha - 4\mu_I^2\cos^2\alpha + 2\mu_I^2\sin^2\alpha - 2p^2\right)(-i)\int_k \frac{k^2-m_2^2}{(k_0^2-E^2_{\pi^+})(k_0^2-E^2_{\pi^-})} - \frac{1}{3f^2}(-i)\int_k \frac{k^2(k^2-m_2^2)}{(k_0^2-E^2_{\pi^+})(k_0^2-E^2_{\pi^-})} \tag{D.15}$$

$$\Sigma^{\pi_2}_{22(4\pi)} = \frac{1}{2f^2}\left(m^2\cos\alpha - 4\mu_I^2\cos^2\alpha\right)(-i)\int_k \frac{k^2-m_1^2}{(k_0^2-E^2_{\pi^+})(k_0^2-E^2_{\pi^-})} \tag{D.16}$$

$$\Sigma^{\pi_3}_{22(4\pi)} = \frac{1}{6f^2}(m^2\cos\alpha - 2\mu_I^2\cos(2\alpha) - 2p^2)(-i)\int_k \frac{1}{k^2-m_3^2} - \frac{1}{3f^2}(-i)\int_k \frac{k^2}{k^2-m_3^2} \tag{D.17}$$

$$\Sigma^{\pi_1\pi_2}_{22(4\pi)} = \frac{8\mu_I\cos\alpha}{3f^2}m_{12}(-i)\int_k \frac{k_0^2}{(k_0^2-E^2_{\pi^+})(k_0^2-E^2_{\pi^-})} \tag{D.18}$$

3-vertex diagrams

$$\Sigma^{\pi_1\pi_2}_{22(3\pi)} = -\frac{(m^2-4\mu_I^2\cos\alpha)^2\sin^2\alpha}{(3f)^2}(-i)\int_k \frac{(k^2-m_2^2)(q^2-m_1^2)}{(k_0^2-E^2_{\pi^+})(k_0^2-E^2_{\pi^-})(q_0^2-E^2_{\pi^+})(q_0^2-E^2_{\pi^-})} \tag{D.19}$$

$$\Sigma^{(\pi_1\pi_2)(\pi_2\pi_1)}_{22(3\pi)} = -\frac{(m^2-4\mu_I^2\cos\alpha)^2\sin^2\alpha}{(3f)^2}m_{12}^2(-i)\int_k \frac{k_0q_0}{(k_0^2-E^2_{\pi^+})(k_0^2-E^2_{\pi^-})(q_0^2-E^2_{\pi^+})(q_0^2-E^2_{\pi^-})} \tag{D.20}$$

$$\Sigma^{\pi_1\pi_1}_{22(3\pi)} = -\frac{2\mu_I^2\sin^2\alpha}{f^2}p_0^2(-i)\int_k \frac{(k^2-m_2^2)(q^2-m_2^2)}{(k_0^2-E^2_{\pi^+})(k_0^2-E^2_{\pi^-})(q_0^2-E^2_{\pi^+})(q_0^2-E^2_{\pi^-})} \tag{D.21}$$

$$\Sigma^{\pi_3\pi_3}_{22(3\pi)} = -\frac{2\mu_I^2\sin^2\alpha}{f^2}p_0^2(-i)\int_k \frac{1}{(k^2-m_3^2)(q^2-m_3^2)} \tag{D.22}$$

$$\Sigma^{(\pi_2\pi_1)\pi_1}_{22(3\pi)} = \frac{2\mu_I(m^2-4\mu_I^2\cos\alpha)\sin^2\alpha}{3f^2}m_{12}p_0(-i)\int_k \frac{k_0(q^2-m_2^2)}{(k_0^2-E^2_{\pi^+})(k_0^2-E^2_{\pi^-})(q_0^2-E^2_{\pi^+})(q_0^2-E^2_{\pi^-})} \tag{D.23}$$

Counterterms

$$\Sigma^{\pi_2\pi_2}_{22(2\pi)} = -4(l_1+l_2)\frac{\mu_I^4\sin^2\alpha\cos^2\alpha}{f^2} - l_4\frac{m^2\mu_I^2\cos\alpha}{2f^2}(1+3\cos 2\alpha) + 2(l_3+l_4)\frac{m^4\cos^2\alpha}{f^2} - 4(l_1+l_2)\frac{\mu_I^2\sin^2\alpha}{f^2}p^2 - 8(l_1+l_2)\frac{\mu_I^2\sin^2\alpha}{f^2}p_0^2 - 2l_4\frac{m^2\cos\alpha}{f^2}p^2 \tag{D.24}$$

Appendix E

Integrals

In this Appendix we use dimensional regularization to evaluate a set of integrals that is sufficient to determine the divergent part of Σ_{33}. We begin by describing how the integrals arise in the calculation of Σ_{33}. We proceed to calculate a master integral in dimensional regularization, which we make frequent use of in the derivations. We then present a set of integrals that are sufficient to determine the divergent part of Σ_{33}. Finally, we evaluate a set of integrals that are sufficient to determine Σ_{33} in the limit where $\cos\alpha = \frac{m_\pi^2}{\mu_I^2}$, which we use in chapter 5.

In order to renormalize the quasi-particle masses we need to isolate the divergent parts of the self-energy diagrams. The following series expansion is used to isolate the divergent parts of the loop integrals,

$$\frac{1}{(k_0^2 - E_{\pi^+}^2)(k_0^2 - E_{\pi^-}^2)} = \frac{1}{(k_0^2 - E_1^2)(k_0^2 - E_2^2)} + \frac{m_{12}^2 k_0^2}{(k_0^2 - E_1^2)^2(k_0^2 - E_2^2)^2} + \frac{m_{12}^4 k_0^4}{(k_0^2 - E_1^2)^3(k_0^2 - E_2^2)^3} + ... \tag{E.1}$$

It is rather straightforward to evaluate the integrals on the right-hand-side of the expansion above by using Feynman parametrization. The price we have to pay is that the integrals over the Feynman parameters can become highly non trivial.

We will make use of the following notation in this Appendix,

$$\begin{aligned} q &\equiv p - k, \\ E_1 &\equiv \vec{k}^2 + m_1^2, \\ E_2 &\equiv \vec{k}^2 + m_2^2. \end{aligned}$$

E.1 A master integral

In this section we evaluate the following Euclidean integral,

$$\int \frac{d^d l}{(2\pi)^d} \frac{l^{2s}}{(l^2 + \Delta)^n}. \tag{E.2}$$

This integral, along with the following replacements,[1]

$$l^\mu l^\nu \longleftrightarrow \frac{l^2}{d} g^{\mu\nu}, \tag{E.3}$$

$$l^\mu l^\nu l^\rho l^\sigma \longleftrightarrow \frac{(l^2)^2}{d(d+2)} (g^{\mu\nu} g^{\rho\sigma} + g^{\mu\rho} g^{\nu\sigma} + g^{\mu\sigma} g^{\nu\rho}), \tag{E.4}$$

[1] These replacements inside the integral are allowed by symmetry, and the formulas are easily verified by contracting both sides with the metric tensor.

will be sufficient to isolate the divergent parts of the integrals that follow in the next section.

The integral in Eq.(E.2) with $s = 0$ or $s = 1$ is commonly used as an illustration of how calculations in dimensional regularization work. The general case rely on the same techniques, and we calculate it in the following.

The integral in Eq.(E.2) can be written as,

$$\int \frac{d^d l}{(2\pi)^d} \frac{l^{2s}}{(l^2+\Delta)^n} = \int \frac{d\Omega_d}{(2\pi)^d} \int dl \frac{l^{2s+d-1}}{(l^2+\Delta)^n}, \tag{E.5}$$

where Ω_d denotes the surface area of a d-dimensional unit sphere,

$$\int \Omega_d = \frac{2\pi^{\frac{d}{2}}}{\Gamma\left(\frac{d}{2}\right)}. \tag{E.6}$$

The second factor in Eq.(E.5) is,

$$\int dl \frac{l^{2s+d-1}}{(l^2+\Delta)^n} = \frac{1}{2}\int dl^2 \frac{(l^2)^{s-1+\frac{d}{2}}}{(l^2+\Delta)^n} = \frac{1}{2}\left(\frac{1}{\Delta}\right)^{n-s-\frac{d}{2}} \int_0^1 dx x^{n-s-\frac{d}{2}-1}(1-x)^{s+\frac{d}{2}-1}, \tag{E.7}$$

where we performed the substitution $x = \frac{\Delta}{l^2+\Delta}$ in the second line. Using the definition of the Beta function,

$$\int_0^1 dx x^{\alpha-1}(1-x)^{\beta-1} = B(\alpha,\beta) = \frac{\Gamma(\alpha)\Gamma(\beta)}{\Gamma(\alpha+\beta)}, \tag{E.8}$$

we rewrite Eq.(E.7) as,

$$\frac{1}{2}\left(\frac{1}{\Delta}\right)^{n-s-\frac{d}{2}} \int_0^1 dx x^{n-s-\frac{d}{2}-1}(1-x)^{s+\frac{d}{2}-1} = \frac{1}{2}\left(\frac{1}{\Delta}\right)^{n-s-\frac{d}{2}} \frac{\Gamma\left(n-s-\frac{d}{2}\right)\Gamma\left(s+\frac{d}{2}\right)}{\Gamma(n)}. \tag{E.9}$$

The final result for the master integral is,

$$\int \frac{d^d l}{(2\pi)^d} \frac{l^{2s}}{(l^2+\Delta)^n} = \frac{1}{(4\pi)^{\frac{d}{2}}}\left(\frac{1}{\Delta}\right)^{n-s-\frac{d}{2}} \frac{\Gamma\left(n-s-\frac{d}{2}\right)}{\Gamma(n)} \frac{\frac{d}{2}(s+\frac{d}{2}-1)!}{\frac{d}{2}!}, \tag{E.10}$$

where we used that,

$$\frac{\Gamma(a+b)}{\Gamma(a)} = \frac{a(a+b-1)!}{a!}. \tag{E.11}$$

Wick-rotating back to Minkowski space, we obtain the following result,

$$\int \frac{d^d k}{(2\pi)^d} \frac{k^{2s}}{(k^2-\Delta)^n} = \frac{(-1)^{n+s} i}{(4\pi)^{\frac{d}{2}}}\left(\frac{1}{\Delta}\right)^{n-s-\frac{d}{2}} \frac{\Gamma\left(n-s-\frac{d}{2}\right)}{\Gamma(n)} \frac{\frac{d}{2}(s+\frac{d}{2}-1)!}{\frac{d}{2}!}, \tag{E.12}$$

or equivalently,

$$\int \frac{d^d k}{(2\pi)^d} \frac{k^{2s}}{(k^2-\Delta)^n} = \frac{(-1)^{n+s} i}{(4\pi)^{\frac{d}{2}}}\left(\frac{1}{\Delta}\right)^{n-s-\frac{d}{2}} \frac{\Gamma\left(n-s-\frac{d}{2}\right)\Gamma\left(s+\frac{d}{2}\right)}{\Gamma(n)\Gamma\left(\frac{d}{2}\right)}. \tag{E.13}$$

Combining Eq.(E.13) with Eqs.(E.3)-(E.4) we obtain some useful special cases,

$$\int \frac{d^dk}{(2\pi)^d}\frac{1}{(k^2-\Delta)^n} = \frac{(-1)^n i}{(4\pi)^{d/2}}\frac{\Gamma(n-\frac{d}{2})}{\Gamma(n)}\left(\frac{1}{\Delta}\right)^{n-\frac{d}{2}}, \tag{E.14}$$

$$\int \frac{d^dk}{(2\pi)^d}\frac{k^\mu k^\nu}{(k^2-\Delta)^n} = \frac{(-1)^{n-1} i}{(4\pi)^{d/2}}\frac{g^{\mu\nu}}{2}\frac{\Gamma(n-\frac{d}{2}-1)}{\Gamma(n)}\left(\frac{1}{\Delta}\right)^{n-\frac{d}{2}-1}, \tag{E.15}$$

$$\int \frac{d^dk}{(2\pi)^d}\frac{k^\mu k^\nu k^\rho k^\sigma}{(k^2-\Delta)^n} = \frac{(-1)^n i}{(4\pi)^{d/2}}\frac{\Gamma(n-\frac{d}{2}-2)}{\Gamma(n)}\left(\frac{1}{\Delta}\right)^{n-\frac{d}{2}-2}\times\frac{1}{4}(g^{\mu\nu}g^{\rho\sigma}+g^{\mu\rho}g^{\nu\sigma}+g^{\mu\sigma}g^{\nu\rho}). \tag{E.16}$$

E.2 Integrals in Σ_{33}

In this section we present all the dimensionally regularized integrals that are needed to renormalize the neutral-pion mass. We begin by presenting all the relevant integrals where we treat α as a free parameter. We proceed to present the integrals that we used in the calculation in chapter 5 where we fixed α by using the tree-level relation $\cos\alpha = \frac{m_\pi^2}{\mu_I^2}$.[2]

4-vertex loop integrals

$$\int_k \frac{1}{k^2-m_1^2} = \frac{im_1^2}{(4\pi)^2}\left[\frac{1}{\epsilon}+1+\log\frac{\Lambda^2}{m_1^2}\right], \tag{E.17}$$

$$\int_k \frac{k^2}{k^2-m_1^2} = \frac{im_1^4}{(4\pi)^2}\left[\frac{1}{\epsilon}+1+\log\frac{\Lambda^2}{m_1^2}\right], \tag{E.18}$$

$$\int_k \frac{k_0^2}{(k^2-m_1^2)(k^2-m_2^2)} = \frac{i}{4(4\pi)^2}\left[(m_1^2+m_2^2)\left(\frac{1}{\epsilon}+\frac{3}{2}\right)+\frac{m_1^4}{m_1^2-m_2^2}\log\frac{\Lambda^2}{m_1^2}-\frac{m_2^4}{m_1^2-m_2^2}\log\frac{\Lambda^2}{m_2^2}\right], \tag{E.19}$$

$$\int_k \frac{k_0^2}{(k^2-m_1^2)^2(k^2-m_2^2)} = \frac{i}{4(4\pi)^2}\left[\frac{1}{\epsilon}+\frac{1}{2}+\frac{m_2^2(m_2^2-m_1^2)}{(m_1^2-m_2^2)^2}+\frac{m_1^2(m_1^2-2m_2^2)}{(m_1^2-m_2^2)^2}\log\frac{\Lambda^2}{m_1^2}+\frac{m_2^4}{(m_1^2-m_2^2)^2}\log\frac{\Lambda^2}{m_2^2}\right], \tag{E.20}$$

$$\int_k \frac{k_0^2k^2}{(k^2-m_1^2)^2(k^2-m_2^2)} = \frac{i}{4(4\pi)^2}\left[(2m_1^2+m_2^2)\left(\frac{1}{\epsilon}+\frac{2}{3}\right)+\frac{2m_1^6}{3(m_1^2-m_2^2)^2}-\frac{3m_1^4m_2^2}{2(m_1^2-m_2^2)^2}+\frac{5m_2^6}{6(m_1^2-m_2^2)^2}+\frac{2m_1^6-3m_1^4m_2^2}{(m_1^2-m_2^2)^2}\log\frac{\Lambda^2}{m_1^2}+\frac{m_2^6}{(m_1^2-m_2^2)^2}\log\frac{\Lambda^2}{m_2^2}\right], \tag{E.21}$$

$$\int_k \frac{k_0^4}{(k^2-m_1^2)^2(k^2-m_2^2)^2} = \frac{i}{8(4\pi)^2}\left\{\frac{1}{\epsilon}+\frac{1}{6(m_1^2-m_2^2)^3}\left[5(m_1^6-m_2^6)-27m_1^2m_2^2(m_1^2-m_2^2)+6m_1^4(m_1^2-3m_2^2)\log\frac{\Lambda^2}{m_1^2}-6m_2^4(m_2^2-3m_1^2)\log\frac{\Lambda^2}{m_2^2}\right]\right\}, \tag{E.22}$$

[2]The tree-level relation for α should not be used in the loop integrals, as we have mentioned many times already. However, we have decided to these integrals as well for the sake of completeness.

$$\int_k \frac{k_0^4 k^2}{(k^2-m_1^2)^3(k^2-m_2^2)^2} = \frac{3}{8(4\pi)^2}\int dxdy\delta(x+y-1)x^2y\left(\frac{4}{\epsilon}-1+4\log\frac{\Lambda^2}{m_1^2x+m_2^2y}\right) \tag{E.23}$$

3-vertex loop integrals at $p^2 = m_3^2$

$$\int_k \frac{1}{(q^2-m_3^2)(k^2-m_1^2)} = \frac{i}{(4\pi)^2}\left[\frac{1}{\epsilon}-\int_0^1 dx\Theta(1-x)\Theta(x)\log\left[m_1^2(1-x)+m_3^2x^2\right]\right], \tag{E.24}$$

$$\int_k \frac{k_0^2}{(q^2-m_3^2)(k^2-m_2^2)} = \frac{i}{2(4\pi)^2}\int\left[(\Delta+2p_0^2x^2)\left(\frac{1}{\epsilon}+\log\frac{\Lambda^2}{\Delta}\right)+\Delta\right]\delta(x+y-1)dxdy, \tag{E.25}$$

where $\Delta \equiv m_3^2x^2+m_2^2y$.

$$\int_k \frac{k_0^2}{(q^2-m_3^2)(k^2-m_1^2)(k^2-m_2^2)} = \frac{i}{2(4\pi)^2}\int\delta(x+y+z-1)\left[\frac{1}{\epsilon}-\frac{2p_0^2x^2}{\Delta}+\log\frac{\Lambda^2}{\Delta}\right]dxdydz, \qquad \text{where} \quad \Delta \equiv m_3^2x^2+m_1^2y+m_2^2z. \tag{E.26}$$

$$\int_k \frac{k_0^4}{(q^2-m_3^2)(k^2-m_1^2)(k^2-m_2^2)^2} = \frac{i}{(4\pi)^2}\int\delta(x+y+z-1)z\left[\frac{3}{4}\left(\frac{1}{\epsilon}+\log\frac{\Lambda^2}{\Delta}\right)-\frac{3p_0^2x^2}{\Delta}+\frac{p_0^4x^4}{\Delta^2}\right]dxdydz, \qquad \text{where} \quad \Delta \equiv m_3^2x^2+m_1^2y+m_2^2z. \tag{E.27}$$

4-vertex loop integrals at $\cos\alpha = \frac{m_\pi^2}{\mu_I^2}$

$$\int_k \frac{k^2-m_2^2}{(k_0^2-E_1^2)(k_0^2-E_2^2)} = \frac{im_1^2}{(4\pi^2)}\left[\frac{1}{\epsilon}+1+\log\frac{\Lambda^2}{m_1^2}\right], \tag{E.28}$$

$$\int_k \frac{k_0^2(k^2-m_2^2)}{(k_0^2-E_1^2)^2(k_0^2-E_2^2)^2} = \frac{i}{4(4\pi)^2}\left[\frac{1}{\epsilon}+\frac{1}{2}+\log\frac{\Lambda^2}{m_1^2}\right], \tag{E.29}$$

$$\int_k \frac{k^2(k^2-m_2^2)}{(k_0^2-E_1^2)(k_0^2-E_2^2)} = \frac{im_1^4}{(4\pi)^2}\left[\frac{1}{\epsilon}+1+\log\frac{\Lambda^2}{m_1^2}\right], \tag{E.30}$$

$$\int_k \frac{k_0^2k^2(k^2-m_2^2)}{(k_0^2-E_1^2)^2(k_0^2-E_2^2)^2} = \frac{im_1^2}{2(4\pi)^2}\left[\frac{1}{\epsilon}+1+\log\frac{\Lambda^2}{m_1^2}\right], \tag{E.31}$$

$$\int_k \frac{k_0^4k^2(k^2-m_2^2)}{(k_0^2-E_1^2)^3(k_0^2-E_2^2)^3} = \frac{i}{8(4\pi)^2}\left[\frac{1}{\epsilon}+\frac{1}{3}+\log\frac{\Lambda^2}{m_1^2}\right], \tag{E.32}$$

$$\int_k \frac{k^2 - m_1^2}{(k_0^2 - E_1^2)(k_0^2 - E_2^2)} = 0, \tag{E.33}$$

$$\int_k \frac{k_0^2(k^2 - m_1^2)}{(k_0^2 - E_1^2)^2(k_0^2 - E_2^2)^2} = \frac{i}{4(4\pi)^2}\left[\frac{1}{\epsilon} + \frac{3}{2} + \log\frac{\Lambda^2}{m_1^2}\right], \tag{E.34}$$

$$\int_k \frac{k^2(k^2 - m_1^2)}{(k_0^2 - E_1^2)(k_0^2 - E_2^2)} = 0, \tag{E.35}$$

$$\int_k \frac{k_0^2 k^2(k^2 - m_1^2)}{(k_0^2 - E_1^2)^2(k_0^2 - E_2^2)^2} = \frac{i m_1^2}{4(4\pi)^2}\left[\frac{1}{\epsilon} + \frac{3}{2} + \log\frac{\Lambda^2}{m_1^2}\right], \tag{E.36}$$

$$\int_k \frac{k_0^4 k^2(k^2 - m_1^2)}{(k_0^2 - E_1^2)^3(k_0^2 - E_2^2)^3} = \frac{i}{8(4\pi)^2}\left[\frac{1}{\epsilon} + \frac{5}{6} + \log\frac{\Lambda^2}{m_1^2}\right], \tag{E.37}$$

$$\int_k \frac{1}{k^2 - m_3^2} = \frac{i m_3^2}{(4\pi)^2}\left[\frac{1}{\epsilon} + 1 + \log\frac{\Lambda^2}{m_3^2}\right] \tag{E.38}$$

$$\int_k \frac{k_0^2}{(k_0^2 - E_1^2)(k_0^2 - E_2^2)} = \frac{i m_1^2}{4(4\pi)^2}\left[\frac{1}{\epsilon} + \frac{3}{2} + \log\frac{\Lambda^2}{m_1^2}\right] \tag{E.39}$$

$$\int_k \frac{k_0^4}{(k_0^2 - E_1^2)^2(k_0^2 - E_2^2)^2} = \frac{i}{8(4\pi)^2}\left[\frac{1}{\epsilon} + \frac{5}{6} + \log\frac{\Lambda^2}{m_1^2}\right] \tag{E.40}$$

3-vertex loop integrals when $\cos\alpha = \frac{m_\pi^2}{\mu_I^2}$ and $p^2 = m_3^2$

$$\int_k \frac{1}{(q^2 - m_3^2)(k^2 - m_1^2)} = \frac{i}{(4\pi)^2}\left[\frac{1}{\epsilon} - \int_0^1 dx \Theta(1-x)\Theta(x)\log\left[m_1^2(1-x) + m_3^2 x^2\right]\right] \tag{E.41}$$

$$\int_k \frac{k_0^2}{[q^2 - m_3^2]k^2} = \frac{i}{(4\pi)^2}\left[\left(\frac{m_3^2}{4} - \frac{p^2}{12}\right)\left(\frac{1}{\epsilon} + \frac{5}{3} - \log\frac{\Lambda^2}{m_3^2}\right) + \frac{p_0^2}{3}\left(\frac{1}{\epsilon} + \frac{2}{3} + \log\frac{\Lambda^2}{m_3^2}\right)\right], \tag{E.42}$$

$$\int_k \frac{k_0^4}{(q^2 - m_3^2)(k^2 - m_1^2)k^4} = \frac{i}{2(4\pi)^2}\left[\frac{1}{4\epsilon} - \int_0^1 dy \int_0^{1-y} dx \Theta[1-x-y, x+y]\left(-\frac{3y}{2}\log\frac{\Lambda^2}{\Delta} + 6\frac{yx^2}{\Delta}p_0^2 - 2\frac{yx^4}{\Delta^2}p_0^4\right)\right], \tag{E.43}$$

where $\Delta \equiv m_3^2 x^2 + m_1^2 y$.

$$\int_k \frac{k_0^2}{k^2(k^2 - m_1^2)(q^2 - m_3^2)} = \frac{i}{(4\pi)^2}\left[\frac{1}{4\epsilon} - \frac{p_0^2}{m_1^2}\int_0^1 x^2 \log\left(\frac{m_1^2 - m_1^2 x + m_3^2 x^2}{m_3^2 x^2}\right)dx + \frac{1}{2}\int_0^1 dy \int_0^{1-y} \Theta[1-x-y, x+y]\log\frac{\Lambda^2}{m_1^2 x + m_3^2 y^2}dx\right] \tag{E.44}$$

Appendix F

Code

In the following we provide the Mathematica routines used to minimize the free energy, obtain the BEC transition curve and compute the chiral condensate and the pion condensate. The code used for plotting is voluminous and not included.

Masses

```
mj[a_, j_, m_] := (m) Cos[a] + (j) Sin[a];
mjbar[a_, j_, m_] := (m) Sin[a] - (j) Cos[a];
m1[a_, uI_, j_, m_, B_] := Sqrt[2 (B) mj[a, j, m] - uI^2 Cos[2 a]];
m2[a_, uI_, j_, m_, B_] := Sqrt[2 (B) mj[a, j, m] - uI^2 Cos[a]^2];
m3[a_, uI_, j_, m_, B_] := Sqrt[2 (B) mj[a, j, m] + uI^2 Sin[a]^2];
m12[a_, uI_] := 2 (uI) Cos[a];
m1b[a_, uI_, j_, m_, B_] := m3[a, uI, j, m, B];
m2b[a_, j_, m_, B_] := Sqrt[2 B (mj[a, j, m])];
```

Spectrum

```
Ep[p_, a_, uI_, j_, m_, B_] :=
 Sqrt[p^2 + 1/2 (m1[a, uI, j, m, B]^2 + m2[a, uI, j, m, B]^2 + m12[a, uI]^2) +
    1/2 Sqrt[4 p^2 m12[a, uI]^2 + (m1[a, uI, j, m, B]^2 + m2[a, uI, j, m, B]^2 + m12[a, uI]^2)^2 -
       4 m1[a, uI, j, m, B]^2 m2[a, uI, j, m, B]^2]]
Em[p_, a_, uI_, j_, m_, B_] := Sqrt[p^2 +
    1/2 (m1[a, uI, j, m, B]^2 + m2[a, uI, j, m, B]^2 + m12[a, uI]^2) -
    1/2 Sqrt[4 p^2 m12[a, uI]^2 + (m1[a, uI, j, m, B]^2 + m2[a, uI, j, m, B]^2 + m12[a, uI]^2)^2 -
       4 m1[a, uI, j, m, B]^2 m2[a, uI, j, m, B]^2]]
E1[p_, a_, uI_, j_, m_, B_] := Sqrt[p^2 + m1b[a, uI, j, m, B]^2]
E2[p_, a_, uI_, j_, m_, B_] := Sqrt[p^2 + m2b[a, j, m, B]^2]
```

Implementation of Free energy at zero temperature

Ftree

```
Vtreej[a_, uI_, j_, m_, B_] := -2 f^2 (B) mj[a, j, m] - 1 / 2 f^2 uI^2 Sin[a]^2
```

F1

```
VloopminusVfinj[a_, uI_, j_, m_, B_] :=
 -1 / ((4 Pi)^2) (3 / 2 - l3b + 4 l4b + Log[(2 B (m)) / (m2b[a, j, m, B]^2)] +
     2 Log[(2 B (m)) / (m3[a, uI, j, m, B]^2)]) (B^2 mj[a, j, m]^2) -
  1 / ((4 Pi)^2) (1 + 2 l4b + 2 Log[(2 B (m)) / (m3[a, uI, j, m, B]^2)])
   (B (mj[a, j, m]) uI^2 Sin[a]^2) - 1 / (2 (4 Pi)^2)
   (1 / 2 + 1 / 3 l1b + 2 / 3 l2b + Log[(2 B (m)) / (m3[a, uI, j, m, B]^2)]) (uI^4 (Sin[a]^4))
```

Ffin

```
integrandj[p_, a_, uI_, j_, m_, B_] :=
  1/2 4 π p^2 / (2 π)^3 ((Ep[p, a, uI, j, m, B] + Em[p, a, uI, j, m, B]) -
     (E1[p, a, uI, j, m, B] + E2[p, a, uI, j, m, B]));
Vfinj[a_, uI_, j_, m_, B_] := NIntegrate[integrandj[mp x, a, uI, j, m, B],
   {x, 0, 400}, WorkingPrecision → 14, PrecisionGoal → 10, AccuracyGoal → 10];
```

Ftot

```
V1loopj[a_, uI_, j_, m_, B_] :=
  Vtreej[a, uI, j, m, B] + VloopminusVfinj[a, uI, j, m, B] + Vfinj[a, uI, j, m, B];
```

Implementation of condensates at zero temperature

```
QuarkIntegrand[p_, a_, uI_, j_, m_, B_] :=
  1/4 4 π p^2 / (2 π)^3 (B (Cos[a])) (1 / (Ep[p, a, uI, j, m, B]) (1 + m12[a, uI]^2 /
        (Sqrt[4 p^2 m12[a, uI]^2 + (m1[a, uI, j, m, B]^2 + m2[a, uI, j, m, B]^2 +
              m12[a, uI]^2)^2 - 4 m1[a, uI, j, m, B]^2 × m2[a, uI, j, m, B]^2])) +
    1 / (Em[p, a, uI, j, m, B]) (1 - m12[a, uI]^2 / (Sqrt[4 p^2 m12[a, uI]^2 +
          (m1[a, uI, j, m, B]^2 + m2[a, uI, j, m, B]^2 + m12[a, uI]^2)^2 -
          4 m1[a, uI, j, m, B]^2 × m2[a, uI, j, m, B]^2])) -
    1 / (Sqrt[p^2 + m1b[a, uI, j, m, B]^2]) - 1 / (Sqrt[p^2 + m2b[a, j, m, B]^2]));

PionIntegrand[p_, a_, uI_, j_, m_, B_] :=
  1/4 4 π p^2 / (2 π)^3 (B (Sin[a])) (1 / Ep[p, a, uI, j, m, B] (1 + m12[a, uI]^2 /
        (Sqrt[4 p^2 m12[a, uI]^2 + (m1[a, uI, j, m, B]^2 + m2[a, uI, j, m, B]^2 +
              m12[a, uI]^2)^2 - 4 m1[a, uI, j, m, B]^2 × m2[a, uI, j, m, B]^2])) +
    1 / (Em[p, a, uI, j, m, B]) (1 - m12[a, uI]^2 / (Sqrt[4 p^2 m12[a, uI]^2 +
          (m1[a, uI, j, m, B]^2 + m2[a, uI, j, m, B]^2 + m12[a, uI]^2)^2 -
```

| 3

```
        4 m1[a, uI, j, m, B]^2 × m2[a, uI, j, m, B]^2])) -
    1 / (Sqrt[p^2 + m1b[a, uI, j, m, B]^2]) - 1 / (Sqrt[p^2 + m2b[a, j, m, B]^2]));

quarkFin[a_, uI_, j_, m_, B_] := NIntegrate[QuarkIntegrand[x, a, uI, j, m, B],
   {x, 0, 400 mp}, WorkingPrecision → 14, PrecisionGoal → 10, AccuracyGoal → 10];
pionFin[a_, uI_, j_, m_, B_] := NIntegrate[PionIntegrand[x, a, uI, j, m, B],
   {x, 0, 400 mp}, WorkingPrecision → 14, PrecisionGoal → 10, AccuracyGoal → 10];

PCondminusPCondFin[a_, uI_, j_, m_, B_] :=
  -f^2 (B) Sin[a] (1 + 1 / (4 Pi)^2 (-l3b + 4 l4b + Log[2 B (m) / (m2b[a, j, m, B]^2)] +
        2 Log[2 B (m) / (m3[a, uI, j, m, B]^2)]) B (mj[a, j, m]) / f^2 +
     1 / (4 Pi)^2 (l4b + Log[2 B (m) / (m3[a, uI, j, m, B]^2)]) uI^2 Sin[a]^2 / f^2);
QCondminusQCondFin[a_, uI_, j_, m_, B_] := - (B) Cos[a]
   (f^2 + 1 / (4 Pi)^2 (-l3b + 4 l4b + Log[2 B (m) / (m2b[a, j, m, B]^2)] +
        2 Log[2 B (m) / (m3[a, uI, j, m, B]^2)]) B (mj[a, j, m]) +
     1 / (4 Pi)^2 (l4b + Log[2 B (m) / (m3[a, uI, j, m, B]^2)]) uI^2 Sin[a]^2);
```

Adjust j here

```
javg = 0;
```

Find Minimum for avg values and build condensates at zero temperature

```
l1b = -0.4; l2b = 4.3; l3b = 2.9; l4b = 4.4;
mp = 131;
fp = 128 / √2 ;
m = 3.47;
f = 84.93420736769619;
mpn = 132.48844729503415;
B = (mpn)^2 / (2 m);
bLO = (mp)^2 / (2 m);

agslistLO = {};
agslist = {};
mulist = Table[x, {x, 0, 3.05 mp, 2}];
pionCondensateList = {};
quarkCondensateList = {};
pionCondensateListLO = {};
quarkCondensateListLO = {};
Print[ProgressIndicator[Dynamic[i / Length[mulist]]],
 " ", Dynamic[i / Length[mulist] // N]]
For[i = 1, i < (Length[mulist] + 1), i++,
  mu = mulist[[i]];
  LOMin = a /. Last[
```

```
    FindMinimum[{-2 bLO (mj[a, javg, m]) - 1/2 mu^2 Sin[a]^2, a ≥ 0, a ≤ π/2}, {a}]];
  sol = Table[{a, Re[V1loopj[a, mu, javg, m, B]]}, {a, 0, π/2, 1/100 π/2}] // Quiet;
  solf = Interpolation[sol];
  min = a /. Last[FindMinimum[{solf[a], a ≥ 0, a ≤ π/2}, {a}]];
  PCondVal = -2 m/(mp^2 fp^2)
     (PCondminusPCondFin[min, mu, javg, m, B] + Re[pionFin[min, mu, javg, m, B]]);
  QCondVal = -2 m/(mp^2 fp^2) (QCondminusQCondFin[min, mu, javg, m, B] +
       Re[quarkFin[min, mu, javg, m, B]] - QCondminusQCondFin[0, 0, 0, m, B]) + 1;

  AppendTo[agslist, {mu/mp, min}];
  AppendTo[pionCondensateList, {mu/mp, PCondVal}];
  AppendTo[quarkCondensateList, {mu/mp, QCondVal}];
  AppendTo[pionCondensateListLO,
   {mu/mp, -2 m/(mp^2 fp^2) (-fp^2 bLO (Sin[LOMin]))}];
  AppendTo[quarkCondensateListLO,
   {mu/mp, -2 m/(mp^2 fp^2) (-fp^2 bLO (Cos[LOMin]) + fp^2 bLO) + 1}];
  AppendTo[agslistLO, {mu/mp, LOMin}]
  (*Print[mu];*)] // Quiet
```

Find Minimum for high values and build condensates at zero temperature

```
l1b = -0.4 + 0.6; l2b = 4.3 + 0.1; l3b = 2.9 + 2.4; l4b = 4.4 + 0.2;
mpn = 136.9060408108898;
f = 86.53625497704442;
mp = 131 + 3;
fp = (128 + 3)/√2;
B = (mpn)^2/(2 m); bLO = (mp)^2/(2 m);

agslisthigh = {};
mulist = Table[x, {x, 0, 3.05 mp, 2}];
pionCondensateListhigh = {};
quarkCondensateListhigh = {};
Print[ProgressIndicator[Dynamic[i/Length[mulist]]],
 " ", Dynamic[i/Length[mulist] // N]]
For[i = 1, i < (Length[mulist] + 1), i++,
  mu = mulist[[i]];
  sol = Table[{a, Re[V1loopj[a, mu, javg, m, B]]}, {a, 0, π/2, 1/100 π/2}] // Quiet;
  solf = Interpolation[sol];
  min = a /. Last[FindMinimum[{solf[a], a ≥ 0, a ≤ π/2}, {a}]];
  PCondVal = -2 m/(mp^2 fp^2)
     (PCondminusPCondFin[min, mu, javg, m, B] + Re[pionFin[min, mu, javg, m, B]]);
  QCondVal = -2 m/(mp^2 fp^2) (QCondminusQCondFin[min, mu, javg, m, B] +
       Re[quarkFin[min, mu, javg, m, B]] - QCondminusQCondFin[0, 0, 0, m, B]) + 1;
```

```
  AppendTo[agslisthigh, {mu / mp, min}];
  AppendTo[pionCondensateListhigh, {mu / mp, PCondVal}];
  AppendTo[quarkCondensateListhigh, {mu / mp, QCondVal}]
  (*Print[mu];*)] // Quiet
```

Find Minimum for low values and build condensates at zero temperature

```
l1b = -0.4 - 0.6; l2b = 4.3 - 0.1; l3b = 2.9 - 2.4; l4b = 4.4 - 0.2;
mpn = 128.24085879566127;
f = 83.29281307565242;
mp = 131 - 3;
fp = (128 - 3) / Sqrt[2];
B = (mpn)^2 / (2 m);
bLO = (mp)^2 / (2 m);

agslistlow = {};
mulist = Table[x, {x, 0, 3.05 mp, 2}];
pionCondensateListlow = {};
quarkCondensateListlow = {};
Print[ProgressIndicator[Dynamic[i / Length[mulist]]],
 " ", Dynamic[i / Length[mulist] // N]]
For[i = 1, i < (Length[mulist] + 1), i++,
  mu = mulist[[i]];
  sol = Table[{a, Re[V1loopj[a, mu, javg, m, B]]}, {a, 0, Pi/2, 1/100 Pi/2}] // Quiet;
  solf = Interpolation[sol];
  min = a /. Last[FindMinimum[{solf[a], a ≥ 0, a ≤ Pi/2}, {a}]];
  PCondVal = -2 m / (mp^2 fp^2)
    (PCondminusPCondFin[min, mu, javg, m, B] + Re[pionFin[min, mu, javg, m, B]]);
  QCondVal = -2 m / (mp^2 fp^2) (QCondminusQCondFin[min, mu, javg, m, B] +
      Re[quarkFin[min, mu, javg, m, B]] - QCondminusQCondFin[0, 0, 0, m, B]) + 1;

  AppendTo[agslistlow, {mu / mp, min}];
  AppendTo[pionCondensateListlow, {mu / mp, PCondVal}];
  AppendTo[quarkCondensateListlow, {mu / mp, QCondVal}]
  (*Print[mu];*)] // Quiet
```

Finite temperature

```
nB[E_, T_] := 1 / (Exp[E / T] - 1)
```

F_T

```
temperatureIntegrand[p_, a_, uI_, j_, m_, B_, T_] :=
  4 π p^2 / (2 π)^3 T (Log[1 - Exp[- (E0[p, a, uI, j, m, B]) / T]] + Log[
      1 - Exp[- (Ep[p, a, uI, j, m, B]) / T]] + Log[1 - Exp[- (Em[p, a, uI, j, m, B]) / T]]);

VTemp[a_, uI_, j_, m_, B_, T_] :=
  Re[NIntegrate[temperatureIntegrand[(x), a, uI, j, m, B, T], {x, 0, 100 mp},
    WorkingPrecision → 20, PrecisionGoal → 20, AccuracyGoal → 20, MaxRecursion → 35]];
```

F_total

```
VtotjT[a_, uI_, j_, m_, B_, T_] := Re[Vtreej[a, uI, j, m, B] +
    VloopminusVfinj[a, uI, j, m, B] + Vfinj[a, uI, j, m, B] + VTemp[a, uI, j, m, B, T]];
```

parameters

```
l1b = -0.4; l2b = 4.3; l3b = 2.9; l4b = 4.4;
mp = 131;
fp = 128 / √2 ;
m = 3.47;
f = 84.93420736769619;
mpn = 132.48844729503415;
B = (mpn) ^2 / (2 m);
bLO = (mp) ^2 / (2 m);
mp = 1;  f = f / 131;
fp = fp / 131;
```

| 7

Obtain bec transition curve

```
mulist = Table[x, {x, mp, 3 mp, 0.002 mp}];
temperaturelist = Table[x, {x, 8, 129, 4}];
becList = {{1, 0}};
threshold = 0.05;
Print[ProgressIndicator[Dynamic[t/Length[temperaturelist]]],
 " ", Dynamic[t/Length[temperaturelist] // N]]
Print[ProgressIndicator[Dynamic[i/Length[mulist]]], " ", Dynamic[i/Length[mulist] // N]]
For[t = 1, t < (Length[temperaturelist] + 1), t++,
  T = temperaturelist[[t]];
  For[i = 1, i < (Length[mulist] + 1), i++,
   mu = mulist[[i]];
   sol =
    Table[{a, VtotjT[a, mu, 0, m/131, B/131, T/131]}, {a, 0, π/5, 1/100 π/5}] // Quiet;
   solf = Interpolation[sol];
   min = a /. Last[FindMinimum[{solf[a], a ≥ 0, a ≤ π/5}, {a, 0}]];
   If[min > threshold, AppendTo[becList, {mu, (T)}]];
   If[Length[becList] == t + 1, Break[]];
  ]] // Quiet
```

Implementation of finite temperature condensates

```
QuarkIntegrandTemperature[p_, a_, uI_, j_, m_, B_, T_] :=
  1/2 (4 π p^2)/(2 π)^3 (B (Cos[a])) (nB[Ep[p, a, uI, j, m, B], T] / (Ep[p, a, uI, j, m, B])
      (1 + m12[a, uI]^2 / (Sqrt[4 p^2 m12[a, uI]^2 +
            (m1[a, uI, j, m, B]^2 + m2[a, uI, j, m, B]^2 + m12[a, uI]^2)^2 -
            4 m1[a, uI, j, m, B]^2 × m2[a, uI, j, m, B]^2])) +
     nB[Em[p, a, uI, j, m, B], T] / (Em[p, a, uI, j, m, B]) (1 - m12[a, uI]^2 /
         (Sqrt[4 p^2 m12[a, uI]^2 + (m1[a, uI, j, m, B]^2 + m2[a, uI, j, m, B]^2 +
               m12[a, uI]^2)^2 - 4 m1[a, uI, j, m, B]^2 × m2[a, uI, j, m, B]^2])) +
     nB[E0[p, a, uI, j, m, B], T] / (E0[p, a, uI, j, m, B]));


PionIntegrandTemperature[p_, a_, uI_, j_, m_, B_, T_] :=
  1/2 (4 π p^2)/(2 π)^3 (B (Sin[a])) (nB[Ep[p, a, uI, j, m, B], T] / (Ep[p, a, uI, j, m, B])
      (1 + m12[a, uI]^2 / (Sqrt[4 p^2 m12[a, uI]^2 +
            (m1[a, uI, j, m, B]^2 + m2[a, uI, j, m, B]^2 + m12[a, uI]^2)^2 -
            4 m1[a, uI, j, m, B]^2 × m2[a, uI, j, m, B]^2])) +
     nB[Em[p, a, uI, j, m, B], T] / (Em[p, a, uI, j, m, B]) (1 - m12[a, uI]^2 /
         (Sqrt[4 p^2 m12[a, uI]^2 + (m1[a, uI, j, m, B]^2 + m2[a, uI, j, m, B]^2 +
               m12[a, uI]^2)^2 - 4 m1[a, uI, j, m, B]^2 × m2[a, uI, j, m, B]^2])) +
     nB[E0[p, a, uI, j, m, B], T] / (E0[p, a, uI, j, m, B]));
```

```
quarkFinTemp[a_, uI_, j_, m_, B_, T_] :=
  NIntegrate[QuarkIntegrandTemperature[x, a, uI, j, m, B, T], {x, 0, 100 mp},
   WorkingPrecision → 9, PrecisionGoal → 6, AccuracyGoal → 6, MaxRecursion → 4];

pionFinTemp[a_, uI_, j_, m_, B_, T_] :=
  NIntegrate[PionIntegrandTemperature[x, a, uI, j, m, B, T], {x, 0, 100 mp},
   WorkingPrecision → 10, PrecisionGoal → 10, AccuracyGoal → 10, MaxRecursion → 4];

PionCondT[a_, uI_, j_, m_, B_, T_] :=
  Re[pionFinTemp[a, uI, j, m, B, T] + pionFin[a, uI, j, m, B]] +
   PCondminusPCondFin[a, uI, j, m, B];
QuarkCondT[a_, uI_, j_, m_, B_, T_] :=
  Re[quarkFinTemp[a, uI, j, m, B, T] + quarkFin[a, uI, j, m, B]] +
   QCondminusQCondFin[a, uI, j, m, B];
PionCond0T[a_, uI_, j_, m_, B_] := Re[pionFin[a, uI, j, m, B]] +
   PCondminusPCondFin[a, uI, j, m, B];
QuarkCond0T[a_, uI_, j_, m_, B_] := Re[quarkFin[a, uI, j, m, B]] +
   QCondminusQCondFin[a, uI, j, m, B];
```

Generate condensates for 0, 60, 100, 120 MeV

```
mp = 1;
mulist = Table[x, {x, mp, 3.06 mp, 0.01 mp}];
pionCondensateList0 = {};
quarkCondensateList0 = {};
pionCondensateList60 = {};
quarkCondensateList60 = {};
pionCondensateList100 = {};
quarkCondensateList100 = {};
pionCondensateList120 = {};
quarkCondensateList120 = {};
minlist0 = {};
minlist60 = {};
minlist100 = {};
minlist120 = {};

Print[ProgressIndicator[Dynamic[i/Length[mulist]]], " ", Dynamic[i/Length[mulist] // N]]

For[i = 1, i < (Length[mulist] + 1), i++,
  mu = mulist[[i]];
  sol0 = Table[{a, Vtotj[a, mu, 0, m/131, B/131]}, {a, 0, π/2, 1/100 π/2}] // Quiet;
  solf0 = Interpolation[sol0];
  min0 = a /. Last[FindMinimum[{solf0[a], a ≥ 0, a ≤ π/2}, {a, 0}]];
  AppendTo[minlist0, {mu, min0}];
  AppendTo[pionCondensateList0,
   {mu, -2 m/(131)/(mp^2 fp^2) (PionCond0T[min0, mu, 0, m/131, B/131])}];
  AppendTo[quarkCondensateList0,
   {mu, -2 m/(131)/(mp^2 fp^2) (QuarkCond0T[min0, mu, 0, m/131, B/131] -
       QCondminusQCondFin[0, 0, 0, m/131, B/131]) + 1}];

  sol60 =
```

```
 Table[{a, VtotjT[a, mu, 0, m/131, B/131, 60/131]}, {a, 0, π/2, 1/100 π/2}] // Quiet;
solf60 = Interpolation[sol60];
min60 = a /. Last[FindMinimum[{solf60[a], a ≥ 0, a ≤ π/2}, {a}]];
AppendTo[minlist60, {mu, min60}];
AppendTo[pionCondensateList60,
 {mu, -2 (m/131) / (mp^2 fp^2) (PionCondT[min60, mu, 0, m/131, B/131, 60/131])}];
AppendTo[quarkCondensateList60,
 {mu, -2 (m/131) / (mp^2 fp^2) (QuarkCondT[min60, mu, 0, m/131, B/131, 60/131] -
      QCondminusQCondFin[0, 0, 0, m/131, B/131]) + 1}];

sol120 =
 Table[{a, VtotjT[a, mu, 0, m/131, B/131, 120/131]}, {a, 0, π/2, 1/100 π/2}] // Quiet;
solf120 = Interpolation[sol120];
min120first = a /. Last[FindMinimum[{solf120[a], a ≥ 0, a ≤ π/2}, {a, 0}]];
min120firstvalue = FindMinimum[{solf120[a], a ≥ 0, a ≤ π/2}, {a, 0}][[1]];
min120second = a /. Last[FindMinimum[{solf120[a], a ≥ 0, a ≤ π/2}, {a, 1.5}]];
min120secondvalue = FindMinimum[{solf120[a], a ≥ 0, a ≤ π/2}, {a, 1.5}][[1]];
min120 = If[min120secondvalue < min120firstvalue, min120second, min120first];
AppendTo[minlist120, {mu, min120}];
AppendTo[pionCondensateList120, {mu,
  -2 (m/131) / (mp^2 fp^2) (PionCondT[min120, mu, 0, m/131, B/131, 120/131])}];
AppendTo[quarkCondensateList120,
 {mu, -2 (m/131) / (mp^2 fp^2) (QuarkCondT[min120, mu, 0, m/131, B/131, 120/131] -
      QCondminusQCondFin[0, 0, 0, m/131, B/131]) + 1}];
sol100 = Table[{a, VtotjT[a, mu, 0, m/131, B/131, 100/131]},
   {a, 0, π/2, 1/100 π/2}] // Quiet;
solf100 = Interpolation[sol100];
min100first = a /. Last[FindMinimum[{solf100[a], a ≥ 0, a ≤ π/2}, {a, 0}]];
min100firstvalue = FindMinimum[{solf100[a], a ≥ 0, a ≤ π/2}, {a, 0}][[1]];
min100second = a /. Last[FindMinimum[{solf100[a], a ≥ 0, a ≤ π/2}, {a, 1.5}]];
min100secondvalue = FindMinimum[{solf100[a], a ≥ 0, a ≤ π/2}, {a, 1.5}][[1]];
min100 = If[min100secondvalue < min100firstvalue, min100second, min100first];
AppendTo[minlist100, {mu, min100}];
AppendTo[pionCondensateList100, {mu,
  -2 (m/131) / (mp^2 fp^2) (PionCondT[min100, mu, 0, m/131, B/131, 100/131])}];
AppendTo[quarkCondensateList100,
 {mu, -2 (m/131) / (mp^2 fp^2) (QuarkCondT[min100, mu, 0, m/131, B/131, 100/131] -
      QCondminusQCondFin[0, 0, 0, m/131, B/131]) + 1}];
] //
Quiet
```

Bibliography

[1] H. Fritzsch, M. Gell-Mann, and H. Leutwyler, "Advantages of the Color Octet Gluon Picture", Phys. Lett. **47B**, 365–368 (1973).

[2] D. J. Gross and F. Wilczek, "Ultraviolet Behavior of Non-Abelian Gauge Theories", Phys. Rev. Lett. **30**, 1343–1346 (1973).

[3] H. D. Politzer, "Reliable Perturbative Results for Strong Interactions?", Phys. Rev. Lett. **30**, 1346–1349 (1973).

[4] K. Fukushima and T. Hatsuda, "The phase diagram of dense QCD", Reports on Progress in Physics **74**, 014001 (2010).

[5] K. Rajagopal and F. Wilczek, "The condensed matter physics of QCD", At The Frontier of Particle Physics, 2061–2151 (2001).

[6] S. Borsányi, Z. Fodor, C. Hoelbling, S. D. Katz, S. Krieg, C. Ratti, and K. K. Szabó, "Is there still any Tc mystery in lattice QCD? Results with physical masses in the continuum limit III", Journal of High Energy Physics **2010** (2010).

[7] K. Adcox et al., "Formation of dense partonic matter in relativistic nucleus–nucleus collisions at RHIC: Experimental evaluation by the PHENIX Collaboration", Nuclear Physics A **757**, 184–283 (2005).

[8] J. Adams et al., "Experimental and theoretical challenges in the search for the quark–gluon plasma: The STAR Collaboration's critical assessment of the evidence from RHIC collisions", Nuclear Physics A **757**, 102–183 (2005).

[9] B. Back et al., "The PHOBOS perspective on discoveries at RHIC", Nucl. Phys. A **757**, 28–101 (2005).

[10] M. G. Alford, K. Rajagopal, and F. Wilczek, "QCD at finite baryon density: Nucleon droplets and color superconductivity", Phys. Lett. B **422**, 247–256 (1998).

[11] M. G. Alford, K. Rajagopal, and F. Wilczek, "Color flavor locking and chiral symmetry breaking in high density QCD", Nucl. Phys. B **537**, 443–458 (1999).

[12] M. G. Alford, A. Schmitt, K. Rajagopal, and T. Schäfer, "Color superconductivity in dense quark matter", Rev. Mod. Phys. **80**, 1455–1515 (2008).

[13] S. P. Jordan, K. S. M. Lee, and J. Preskill, "Quantum Algorithms for Quantum Field Theories", Science **336**, 1130–1133 (2012).

[14] G. Aarts, "Introductory lectures on lattice QCD at nonzero baryon number", Journal of Physics: Conference Series **706**, 022004 (2016).

[15] P. de Forcrand and O. Philipsen, "The QCD phase diagram for small densities from imaginary chemical potential", Nucl. Phys. B **642**, 290–306 (2002).

[16] C. R. Allton, S. Ejiri, S. J. Hands, O. Kaczmarek, F. Karsch, E. Laermann, C. Schmidt, and L. Scorzato, "QCD thermal phase transition in the presence of a small chemical potential", Phys. Rev. D **66**, 074507 (2002).

[17] Y. Nambu and G. Jona-Lasinio, "Dynamical Model of Elementary Particles Based on an Analogy with Superconductivity. I", Phys. Rev. **122**, 345–358 (1961).

[18] M. Gell-Mann and M. Levy, "The axial vector current in beta decay", Nuovo Cim. **16**, 705 (1960).

[19] M. Gell-Mann, "A Schematic Model of Baryons and Mesons", Phys. Lett. **8**, 214–215 (1964).

[20] K. Fukushima, "Chiral effective model with the Polyakov loop", Physics Letters B **591**, 277–284 (2004).

[21] S. Weinberg, "Phenomenological Lagrangians", Physica A: Statistical Mechanics and its Applications **96**, 327–340 (1979).

[22] J. Gasser and H. Leutwyler, "Chiral perturbation theory to one loop", Annals of Physics **158**, 142–210 (1984).

[23] J. Gasser and H. Leutwyler, "Chiral perturbation theory: Expansions in the mass of the strange quark", Nuclear Physics B **250**, 465–516 (1985).

[24] M. Alford, A. Kapustin, and F. Wilczek, "Imaginary chemical potential and finite fermion density on the lattice", Physical Review D **59** (1999).

[25] D. T. Son and M. A. Stephanov, "QCD at Finite Isospin Density", Physical Review Letters **86**, 592–595 (2001).

[26] J. Bardeen, L. N. Cooper, and J. R. Schrieffer, "Microscopic theory of superconductivity", Phys. Rev. **106**, 162 (1957).

[27] B. B. Brandt, G. Endrődi, and S. Schmalzbauer, "QCD phase diagram for nonzero isospin-asymmetry", Physical Review D **97** (2018).

[28] K. Splittorff, D. T. Son, and M. A. Stephanov, "QCD-like theories at finite baryon and isospin density", Phys. Rev. D **64**, 016003 (2001).

[29] M. Loewe and C. Villavicencio, "Thermal pions at a finite isospin chemical potential", Physical Review D **67** (2003).

[30] S. Carignano, L. Lepori, A. Mammarella, M. Mannarelli, and G. Pagliaroli, "Scrutinizing the pion condensed phase", The European Physical Journal A **53**, 35 (2017).

[31] J. O. Andersen, N. Haque, M. G. Mustafa, and M. Strickland, "Three-loop hard-thermal-loop perturbation theory thermodynamics at finite temperature and finite baryonic and isospin chemical potential", Physical Review D **93** (2016).

[32] E. E. Svanes and J. O. Andersen, "Functional renormalization group at finite density and Bose condensation", Nuclear Physics A **857**, 16–28 (2011).

[33] D. Toublan and J. Kogut, "Isospin chemical potential and the QCD phase diagram at nonzero temperature and baryon chemical potential", Physics Letters B **564**, 212–216 (2003).

[34] M. Frank, M. Buballa, and M. Oertel, "Flavor-mixing effects on the QCD phase diagram at non-vanishing isospin chemical potential: one or two phase transitions?", Physics Letters B **562**, 221–226 (2003).

[35] A. Barducci, R. Casalbuoni, G. Pettini, and L. Ravagli, "Calculation of the QCD phase diagram at finite temperature, and baryon and isospin chemical potentials", Physical Review D **69** (2004).

[36] L. He, M. Jin, and P. Zhuang, "Pion superfluidity and meson properties at finite isospin density", Phys. Rev. D **71**, 116001 (2005).

[37] H. Ueda, T. Z. Nakano, A. Ohnishi, M. Ruggieri, and K. Sumiyoshi, "QCD phase diagram at finite baryon and isospin chemical potentials in the Polyakov loop extended quark meson model with vector interaction", Phys. Rev. D **88**, 074006 (2013).

[38] H. Mao, N. Petropoulos, S. Shu, and W.-Q. Zhao, "The linear sigma model at a finite isospin chemical potential", Journal of Physics G: Nuclear and Particle Physics **32**, 2187–2198 (2006).

[39] B. Klein, D. Toublan, and J. J. M. Verbaarschot, "QCD phase diagram at nonzero temperature, baryon, and isospin chemical potentials in random matrix theory", Physical Review D **68** (2003).

[40] D. Albrecht and J. Erlich, "Pion condensation in holographic QCD", Physical Review D **82** (2010).

[41] B. B. Brandt and G. Endrodi, *QCD phase diagram with isospin chemical potential*, 2016.

[42] B. Brandt, G. Endrodi, E. Fraga, M. Hippert, J. Schaffner-Bielich, and S. Schmalzbauer, "New class of compact stars: Pion stars", Physical Review D **98** (2018).

[43] B. Brandt, F. Cuteri, G. Endrődi, and S. Schmalzbauer, "The Dirac spectrum and the BEC-BCS crossover in QCD at nonzero isospin asymmetry", Particles **3**, 80–86 (2020).

[44] P. Adhikari, J. O. Andersen, and P. Kneschke, "Two-flavor chiral perturbation theory at nonzero isospin: Pion condensation at zero temperature", (2019).

[45] P. Adhikari and J. O. Andersen, *Pion and kaon condensation at zero temperature in three-flavor PT at nonzero isospin and strange chemical potentials at next-to-leading order*, 2019.

[46] P. Adhikari and J. O. Andersen, "QCD at finite isospin density: chiral perturbation theory confronts lattice data", Phys. Lett. B **804**, 135352 (2020).

[47] P. Adhikari and J. O. Andersen, "Quark and pion condensates at finite isospin density in chiral perturbation theory", (2020).

[48] K. Splittorff, D. Toublan, and J. Verbaarschot, "Thermodynamics of chiral symmetry at low densities", Nuclear Physics B **639**, 524–548 (2002).

[49] M. E. Peskin and D. V. Schroeder, *An Introduction to quantum field theory* (Addison-Wesley, Reading, USA, 1995).

[50] Weinberg, Steven, "Non-Abelian Gauge Theories of the Strong Interactions", Phys. Rev. Lett. **31**, 494–497 (1973).

[51] C. Patrignani et al., "Review of Particle Physics", Chin. Phys. **C40**, 100001 (2016).

[52] W. J. Marciano and H. Pagels, "Quantum Chromodynamics: A Review", Phys. Rept. **36**, 137 (1978).

[53] S. Scherer, "Introduction to chiral perturbation theory", Adv. Nucl. Phys. **27**, 277 (2003).

[54] M. Srednicki, *Quantum field theory* (Cambridge University Press, 2007).

[55] M. D. Schwartz, *Quantum Field Theory and the Standard Model* (Cambridge University Press, 2014).

[56] E. Noether, "Invariant variation problems", Transport Theory and Statistical Physics **1**, 186–207 (1971).

[57] S. L. Adler and W. A. Bardeen, "Absence of Higher-Order Corrections in the Anomalous Axial-Vector Divergence Equation", Phys. Rev. **182**, 1517–1536 (1969).

[58] S. L. Adler, "Axial-Vector Vertex in Spinor Electrodynamics", Phys. Rev. **177**, 2426–2438 (1969).

[59] M. Gell-Mann, "The Eightfold Way: A Theory of strong interaction symmetry", (1961).

[60] C. Vafa and E. Witten, "Restrictions on Symmetry Breaking in Vector-Like Gauge Theories", Nucl. Phys. B **234**, 173–188 (1984).

[61] M. Gell-Mann, "Symmetries of Baryons and Mesons", Phys. Rev. **125**, 1067–1084 (1962).

[62] M. Gell-Mann, "The symmetry group of vector and axial vector currents", Physics Physique Fizika **1**, 63–75 (1964).

[63] S. Weinberg, "Pion Scattering Lengths", Phys. Rev. Lett. **17**, 616–621 (1966).

[64] S. L. Adler, "Consistency Conditions on the Strong Interactions Implied by a Partially Conserved Axial-Vector Current", Phys. Rev. **137**, B1022–B1033 (1965).

[65] S. Weinberg, "Precise Relations between the Spectra of Vector and Axial-Vector Mesons", Phys. Rev. Lett. **18**, 507–509 (1967).

[66] A. Pich, *Effective field theory*, 1998.

[67] A. V. Manohar, "Effective field theories", Lecture Notes in Physics, 311–362.

[68] D. B. Kaplan, *Five lectures on effective field theory*, 2005.

[69] G. Ecker, *Effective field theories*, 2005.

[70] I. Z. Rothstein, *Tasi lectures on effective field theories*, 2003.

[71] H. Georgi, "Effective field theory", Ann. Rev. Nucl. Part. Sci. **43**, 209–252 (1993).

[72] S. Weinberg, *Effective Field Theory, Past and Future*, 2009.

[73] E. D'Hoker and S. Weinberg, "General effective actions", Physical Review D **50**, R6050–R6053 (1994).

[74] H. Leutwyler, "On the Foundations of Chiral Perturbation Theory", Annals of Physics **235**, 165–203 (1994).

[75] J. Wess and B. Zumino, "Consequences of anomalous Ward identities", Phys. Lett. **37B**, 95–97 (1971).

[76] E. Witten, "Global Aspects of Current Algebra", Nucl. Phys. **B223**, 422–432 (1983).

[77] J. Bijnens, "Chiral perturbation theory beyond one loop", Progress in Particle and Nuclear Physics **58**, 521–586 (2007).

[78] A. Zee, *Quantum field theory in a nutshell* (Princeton University Press, 2010).

[79] A. Manohar and H. Georgi, "Chiral Quarks and the Nonrelativistic Quark Model", Nucl. Phys. **B234**, 189–212 (1984).

[80] H. Georgi, *Weak Interactions and Modern Particle Theory* (1984).

[81] H. W. Fearing and S. Scherer, "Extension of the chiral perturbation theory meson Lagrangian to order p^6", Phys. Rev. D **53**, 315–348 (1996).

[82] S. Weinberg, "Nonlinear Realizations of Chiral Symmetry", Phys. Rev. **166**, 1568–1577 (1968).

[83] S. Coleman, J. Wess, and B. Zumino, "Structure of Phenomenological Lagrangians. I", Phys. Rev. **177**, 2239–2247 (1969).

[84] A. Balachandran, G. Marmo, B. Skagerstam, and A. Stern, *Classical topology and quantum states chapter 12.2* (World Scientific, 1991).

[85] M. Gell-Mann, R. J. Oakes, and B. Renner, "Behavior of Current Divergences under $SU(3) \times SU(3)$", Phys. Rev. **175**, 2195–2199 (1968).

[86] H. Georgi, "On-shell effective field theory", Nucl. Phys. **B361**, 339–350 (1991).

[87] C. G. Knetter, "Effective Lagrangians with higher derivatives and equations of motion", Phys. Rev. D **49**, 6709–6719 (1994).

[88] C. Arzt, "Reduced effective Lagrangians", Physics Letters B **342**, 189–195 (1995).

[89] R. Kaiser, "Anomalies and the WZW term of two-flavor QCD", Physical Review D **63** (2001).

[90] P. Gerber and H. Leutwyler, "Hadrons Below the Chiral Phase Transition", Nucl. Phys. **B321**, 387–429 (1989).

[91] M. Mannarelli, "Meson Condensation", Particles **2**, 411–443 (2019).

[92] J. B. Kogut and D. Toublan, "QCD at small nonzero quark chemical potentials", Phys. Rev. D **64**, 034007 (2001).

[93] J. B. Kogut and D. K. Sinclair, "Quenched lattice QCD at finite isospin density and related theories", Physical Review D **66** (2002).

[94] M. Mojahed, "Chiral perturbation theory at nonzero isospin density", Unpublished project (2019).

[95] J. Bijnens, G. Colangelo, and G. Ecker, "Renormalization of Chiral Perturbation Theory to Order p6", Annals of Physics **280**, 100–139 (2000).

[96] G. 'tHooft, "Dimensional regularization and the renormalization group", Nuclear Physics B **61**, 455–468 (1973).

[97] K. Knopp and F. Bagemihl, *Theory of functions*, Theory of Functions v. 2 (Dover publications, 1945).

[98] G. Leibbrandt, "Introduction to the Technique of Dimensional Regularization", Rev. Mod. Phys. **47**, 849 (1975).

[99] J. F. Ashmore, "On renormalization and complex space-time dimensions", Comm. Math. Phys. **29**, 177–187 (1973).

[100] G. Passarino and M. J. G. Veltman, "One Loop Corrections for e+ e- Annihilation Into mu+ mu- in the Weinberg Model", Nucl. Phys. **B160**, 151–207 (1979).

[101] H. Nastase, *Introduction to Quantum Field Theory* (Cambridge University Press, 2019).

[102] S. Weinberg, *The Quantum theory of fields. Vol. 1: Foundations* (Cambridge University Press, 2005).

[103] D. Capper and G. Leibbrandt, "On a conjecture by 't Hooft and Veltman", Journal of Mathematical Physics **15** (1974).

[104] S. Coleman, "There are no Goldstone bosons in two dimensions", Comm. Math. Phys. **31**, 259–264 (1973).

[105] G. Colangelo, J. Gasser, and H. Leutwyler, "$\pi\pi$ scattering", Nuclear Physics B **603**, 125–179 (2001).

[106] J. Bijnens and N. H. Truedsson, "The pion mass and decay constant at three loops in two-flavour chiral perturbation theory", Journal of High Energy Physics **2017** (2017).

[107] J. Gasser and H. Leutwyler, "Thermodynamics of chiral symmetry", Physics Letters B **188**, 477–481 (1987).

[108] H. Lehmann, K. Symanzik, and W. Zimmermann, "Zur formulierung quantisierter feldtheorien", Il Nuovo Cimento (1955-1965) **1**, 205–225 (1955).

[109] D. T. Son and M. A. Stephanov, "QCD at a Finite isospin density: From the pion to quark-antiquark condensation", Physics of Atomic Nuclei **64**, 834–842 (2001).

[110] A. Mammarella and M. Mannarelli, "Intriguing aspects of meson condensation", Physical Review D **92** (2015).

[111] K. Splittorff, D. Toublan, and J. Verbaarschot, "QCD with two colors at finite baryon density at next-to-leading order", Nuclear Physics B **620**, 290–314 (2002).

[112] M. Kachelriess, *Quantum Fields*, Oxford Graduate Texts (Oxford University Press, 2017).

[113] T. D. Cohen, "Functional Integrals for QCD at Nonzero Chemical Potential and Zero Density", Physical Review Letters **91** (2003).

[114] M. Loewe and C. Villavicencio, "Thermal pion masses in the second phase:$|\mu_I| > m_\pi$", Physical Review D **70** (2004).

[115] T. Xia, L. He, and P. Zhuang, "Three-flavor Nambu–Jona-Lasinio model at finite isospin chemical potential", Physical Review D **88** (2013).

[116] M. Jamin, "Flavour-symmetry breaking of the quark condensate and chiral corrections to the Gell-Mann–Oakes–Renner relation", Physics Letters B **538**, 71–76 (2002).

[117] Ecker, Gerhard and Gasser, Jürg and Pich, Antonio and De Rafael, Eduardo, "The role of resonances in chiral perturbation theory", Nuclear Physics B **321**, 311–342 (1989).

[118] S. Durr, Z. Fodor, C. Hoelbling, S. Katz, S. Krieg, T. Kurth, L. Lellouch, T. Lippert, K. Szabo, and G. Vulvert, "Lattice QCD at the physical point: light quark masses", Phys. Lett. B **701**, 265–268 (2011).

[119] M. Gyulassy and L. McLerran, "New forms of QCD matter discovered at RHIC", Nuclear Physics A **750**, 30–63 (2005).

[120] M. L. Bellac, *Thermal Field Theory*, Cambridge Monographs on Mathematical Physics (Cambridge University Press, Mar. 2011).

[121] J. I. Kapusta and C. Gale, *Finite-temperature field theory: principles and applications*, 2nd ed., Cambridge Monographs on Mathematical Physics (Cambridge University Press, 2006).

[122] A. Fetter and J. Walecka, *Quantum theory of many-particle system*, Vol. 25 (Jan. 2003).

[123] L. Landau, "On the theory of phase transitions", Zh. Eksp. Teor. Fiz. **7**, 19–32 (1937).

[124] A. Bazavov, T. Bhattacharya, M. Cheng, C. DeTar, H.-T. Ding, S. Gottlieb, R. Gupta, P. Hegde, U. M. Heller, F. Karsch, and et al., "Chiral and deconfinement aspects of the QCD transition", Physical Review D **85** (2012).

[125] T. Bhattacharya, M. I. Buchoff, N. H. Christ, H.-T. Ding, R. Gupta, C. Jung, F. Karsch, Z. Lin, R. D. Mawhinney, G. McGlynn, S. Mukherjee, D. Murphy, P. Petreczky, D. Renfrew, C. Schroeder, R. A. Soltz, P. M. Vranas, and H. Yin, "QCD Phase Transition with Chiral Quarks and Physical Quark Masses", Phys. Rev. Lett. **113**, 082001 (2014).

[126] Y. Aoki, G. Endrődi, Z. Fodor, S. D. Katz, and K. K. Szabó, "The order of the quantum chromodynamics transition predicted by the standard model of particle physics", Nature **443**, 675–678 (2006).

[127] A. Bazavov, H.-T. Ding, P. Hegde, O. Kaczmarek, F. Karsch, N. Karthik, E. Laermann, A. Lahiri, R. Larsen, S.-T. Li, S. Mukherjee, H. Ohno, P. Petreczky, H. Sandmeyer, C. Schmidt, S. Sharma, and P. Steinbrecher, "Chiral crossover in QCD at zero and non-zero chemical potentials", Physics Letters B **795**, 15–21 (2019).

[128] M. Stephanov, K. Rajagopal, and E. Shuryak, "Signatures of the Tricritical Point in QCD", Physical Review Letters **81**, 4816–4819 (1998).

[129] M. A. Halasz, A. D. Jackson, R. E. Shrock, M. A. Stephanov, and J. J. M. Verbaarschot, "Phase diagram of QCD", Physical Review D **58** (1998).

[130] L. Dolan and R. Jackiw, "Symmetry behavior at finite temperature", Phys. Rev. D **9**, 3320–3341 (1974).

[131] M. Laine and A. Vuorinen, "Basics of thermal field theory", Lecture Notes in Physics (2016).

[132] M. Abramowitz, *Handbook of Mathematical Functions, With Formulas, Graphs, and Mathematical Tables* (Dover Publications, Inc., USA, 1974).

[133] A. Folkestad and J. O. Andersen, "Thermodynamics and phase diagrams of Polyakov-loop extended chiral models", Phys. Rev. D **99**, 054006 (2019).

[134] P. Adhikari, J. O. Andersen, and P. Kneschke, "Pion condensation and phase diagram in the Polyakov-loop quark-meson model", Phys. Rev. D **98**, 074016 (2018).

[135] T. Brauner and X.-G. Huang, "Vector meson condensation in a pion superfluid", Physical Review D **94** (2016).

Mojahed, Martin Aria

Chiral perturbation theory at finite isospin density

NTNU
Norwegian University of
Science and Technology